General Disclaimer

One or more of the Following Statements may affect this Document

- This document has been reproduced from the best copy furnished by the organizational source. It is being released in the interest of making available as much information as possible.

- This document may contain data, which exceeds the sheet parameters. It was furnished in this condition by the organizational source and is the best copy available.

- This document may contain tone-on-tone or color graphs, charts and/or pictures, which have been reproduced in black and white.

- This document is paginated as submitted by the original source.

- Portions of this document are not fully legible due to the historical nature of some of the material. However, it is the best reproduction available from the original submission.

FEBRUARY 1968

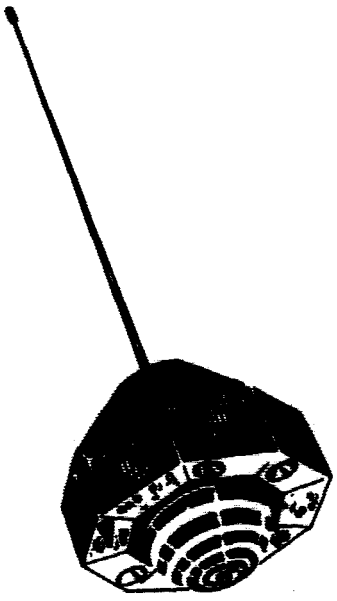

PROCEEDINGS OF THE GEOS PROGRAM REVIEW MEETING 12 - 14 DECEMBER 1967

VOLUME III

TRACKING INTERCOMPARISON TESTS WITH GEOS -I

BY

GODDARD SPACE FLIGHT CENTER

GREENBELT, MARYLAND

EDITED BY:

CSI INCORPORATED
communications & systems, incorporated
6565 Arlington Boulevard, Post Office Box 530, Falls Church, Virginia 22046

NATIONAL AERONAUTICS AND SPACE ADMINISTRATION

PROCEEDINGS OF THE GEOS PROGRAM REVIEW MEETING

12-14 December 1967
NASA Headquarters
400 Maryland Avenue, SW
Washington, D. C.

Volume III

Tracking Intercomparison Tests with GEOS-I

by

Goddard Space Flight Center
Greenbelt, Maryland

Edited by Communications & Systems, Incorporated
6565 Arlington Boulevard, Falls Church, Virginia

February 1968

LIST OF TECHNICAL PAPERS

FOREWARD

Volume III of the proceedings of the GEOS Program Review Meeting held at NASA Headquarters on 12-14 December 1967, presents the results to date of the Goddard Space Flight Center tracking intercomparison tests conducted with GEOS-I. This volume is composed of a series of technical papers prepared by various investigators at GSFC on the tracking intercomparisons conducted using the optical and electronic subsystems on the GEOS-I spacecraft which was launched into orbit on 6 November 1965 from the Eastern Test Range at Cape Kennedy, Florida.

John Berbert, Principal Investigator

GEOS A SHORT ARC OPTICAL SURVEY OF A SIXTEEN STATION MID-NORTH AMERICAN NET

By

Duane C. Brown
D. Brown Associates, Inc.
P.O. Drawer 550
Melbourne, Florida 32901

Prepared For

GEOS PROGRAM REVIEW MEETING
NASA Headquarters, Washington, D.C.
12-14 December 1967

NASA CONTRACT NO. NAS 5-9938

GEOS A Short Arc Optical Survey of a Sixteen Station Mid-North American Net

A simultaneous adjustment of 16 camera sites in and about North America was performed by means of the GEOS Data Adjustment Program (GDAP) . The program was exercised in the multi-pass or NEO-EMBET (N Epoch Orbital-Error Model Best Estimate of Trajectory) mode in which the initial conditions for a total of 24 selected orbits were recovered simultaneously with the coordinates of the optical tracking stations.

Ground traces of the observed portions of the various satellite passes relative to the camera sites are presented in Figure 1. Each heavy dot along a given ground trace indicates a separate group of seven flashes that was successfully observed by at least one station. Each line radiating from a given station indicates the direction to a group of flashes observed by the station. The observed numbers of flashes per station per pass are summarized in Table 1.

Detailed observational coverage for four specific passes is indicated Figures 2a, 2b, 2c, 2d. As many as seven, well-spaced groups of flashes were observed on some passes (the more typical number is four to five). Some stations by virtue of reorientation of the cameras, observed as many as four separate groups of flashes on a single pass, i.e., Grand Forks on Pass 1705 (Figure 2b). In general, the adopted observational philosophy required the maximum practicable exercise of each station on each observable pass.

Two separate reductions were performed. In both reductions the origin of the net was arbitrarily established at the camera site at Goddard, the coordinates of Goddard on the Cape Canaveral Datum being held fixed. The reductions were performed on two different computers (the CDC 3100 and the CDC 3800) and identical results were obtained on all runs. The total computing time (3 iterations) for each adjustment was 6 hours on the CDC 3100 and 20 minutes on the CDC 3800.

In Reduction 1, the coordinates of the following four stations on the Cape Canaveral Datum were subjected to a priori constraints of 5 meters (one sigma) in

longitude and height and 3 meters (one sigma) is latitude: Hunter, Semmes, Jupiter, Homestead. All other stations were subjected to a priori constraints of 100 meters (one sigma) in all three coordinates.

In Reduction 2, the one sigma a priori constraints on Hunter, Semmes, Jupiter and Homestead were relaxed to 100 meters. Here, no worthwhile scale for the optical reduction was made available from the existing survey; any worthwhile scale therefore had to be derived as a by-product of the exercise of short arc dynamic constraints.

In both Reductions 1 and 2 the given coordinates of the tracking stations were transformed to the Mercury Datum (Fischer Spheroid) prior to the adjustment in order to minimize dynamic errors induced by the displacement of the center of mass of the earth relative to the center of the spheroid. After completion of the adjustment, the new coordinates of the stations were transformed back into their original datums (NAD and CCD).

Key results of the adjustments are presented in Table 2 and in Figures 3 and 4. In Table 2 the corrections to the original survey in terms of local east (ΔE), north (ΔN) and up (ΔU) components are presented together with the standard deviations of the final coordinates. The standard deviations are based on the propagation of an observational standard deviation of one second of arc for declination and normalized right ascension (i.e., rt. ascen. x cosine decl.).

The grand rms closure of triangulation turned out to be 1.5 and 1.4 seconds of arc for Reductions 1 and 2, respectively. This is only slightly greater than the grand rms of 1.2 seconds of arc obtained from the analysis of residuals obtained from the least squares fitting of second degree polynomials to the raw observations.

A result of major importance in Table 2 is that the standard deviations from Reduction 2 are only slightly greater than those from Reduction 1. This demonstrates effectiveness of short arc dynamic scaling and shows that neither measured baselines nor electronic ranging is directly necessary to optical surveying; scale, potentially accurate to about one part in one million, can be imparted through the exercise of

short arc dynamic constraints.

The horizontal adjustments from Reduction 1 to the original survey are presented graphically in Figure 3a. The residual vectors are resolved into radial and tangential components relative to the origin at Goddard. The differences between the CCD and NAD coordinates of Goddard are known to be

$$\Delta\varphi = 0''.573 \text{ (CCD-NAD)}(\Delta N \approx 18\text{m}),$$
$$\Delta\lambda = -0''.098 \text{ (CCD-NAD)}(\Delta E \approx -2\text{m}).$$

In Figure 3b those stations referred to the NAD are displaced by the above $\Delta\varphi$, $\Delta\lambda$, and the resulting new displacement vectors are plotted (no adjustment is applied to those stations on the CCD). The significance of these results will be more apparent in the light of the results from Reduction 2.

Figures 4a and 4b are based on Reduction 2 and correspond to Figures 3a and 3b for Reduction 1. The striking feature of Figure 4b is the strongly radial character of the displacements of almost all of the NAD stations toward the origin at Goddard (the sole exception being Bedford). On the other hand, the radial displacements of the CCD stations Semmes and Homestead are small (2 to 3 meters) and both have sizeable tangential components suggestive of an azimuthal rotation of perhaps 2 seconds of arc (Hunter is not plotted in these figures because its given coordinates are suspect and require clarification). The tangential components of the NAD stations, by contrast, are generally small and not suggestive of an azimuthal rotation. It is especially noteworthy that the radial displacements of the CCD stations do not contradict the dynamically derived scale.

Because of the radial character of the displacements of the NAD stations in Figure 4b, an arbitrary scale factor of 1.000005 was applied to all NAD stations (this amounts to a change in scale of 1:200,000, a figure consistent with what one might reasonably expect for NAD stations). The results from this rescaling are presented in Figure 4c. Here, the vectors for all NAD stations, except Bedford, are markedly reduced. In particular, those for the western US become virtually random.

In view of the results obtained, the GEOS A short arc optical survey can only be described as outstandingly successful. Thus far, it has incorporated only a small fraction of the available optical data. Enough GEOS A plate reductions have already been performed to permit the above adjustment to be roughly duplicated about three times over; when plates yet to be reduced are considered, a fivefold duplication of the adjustment appears possible. In the immediate future (30 to 60 days), attention is being directed towards incorporating into the adjustment fourteen additional passes selected specifically to strengthen the peripheral stations. The observational coverage of these passes is indicated in Table 3. A revised version of Figure 1 reflecting the inclusion of these additional passes is provided in Figure 5.

The present reduction provides a survey accurate generally to about 3 to 5 meters that is suitable as an interim survey for GEOS A short arc tracking intercomparisons. The one sigma accuracies of the stronger of the optically established reference orbits are on the order of 1.5 to 2.5 meters in position and .007 m/sec in velocity. Such reference orbits will permit a much more precise evaluation of electronic trackers than has hitherto been possible.

When essentially all of the geodetically productive observations from GEOS A have been incorporated into the adjustment (this should be accomplished within about six months), accuracies on the order of one to two meters are to be expected in all three coordinates for those stations in the interior net and accuracies on the order of two to three meters are to be expected for those stations on the periphery. Moreover, the net will be expanded to embrace a total of about twenty-five stations. Although, by and large, the directional residuals from the adjustment are acceptably random, in future reductions each group of flashes from a given station will be considered to be subject to unknown biases having means of zero and standard deviations of 0.5 seconds of arc (the observations were treated as unbiased in the reductions presented above).

Figure 1. Ground Traces of Satellite Passes Employed in Reduction.

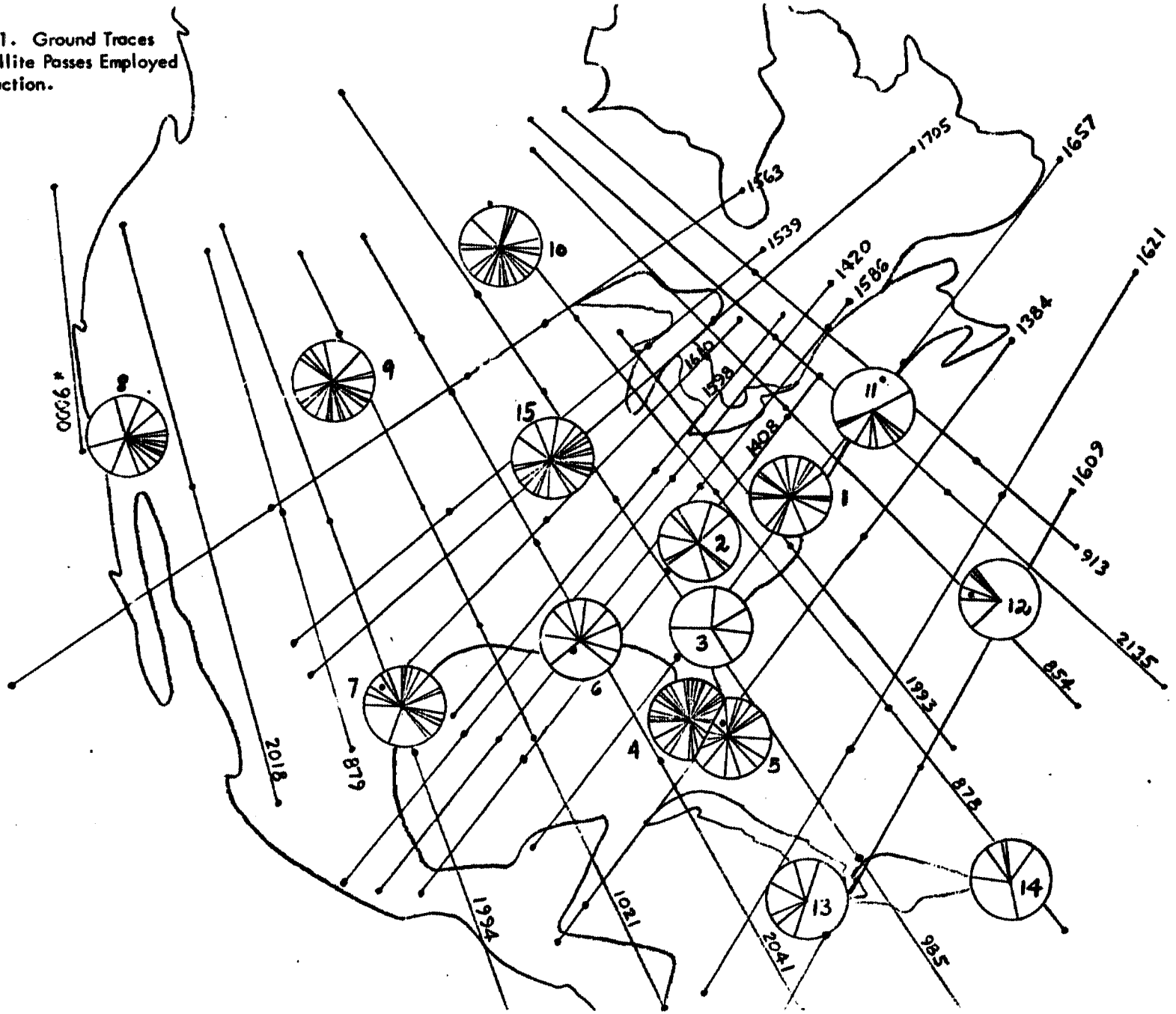

TABLE 1. SUMMARY OF OBSERVATIONAL COVERAGE (FLASHES/STATION/PASS)

ORBIT	G S F	B P O	J U 4	J U P	F T M	H O M	B E D	B E R	C O L	D E N	E D I	G F O	J A M	M O J	P U R	R C S	S E M	C H Y	G R V	H U N		
*9000										14				14								
1657	13								20							7						
1539					21						13			14								
913	7	13										14										
2018										20		14		7								
1598			6		17				17							20						
1993					14	14			14								21					
1420								3		6	14		5				6					
1408								6	14	12	13											
1610	7				14		6					13			*14							
1384	20		20		7						14											
1586	14				28				14	7			7									
1563	7								14	20	19			21								
1994					14	7			21	13			7	7								
879					7	7			7	6		13		13								
1609	14				28	6	12						7			14						
1705	14								21	21	7	28		14								
2135	7				7			6	7			7			7					9		
1621			14		19	7	20	7			6		14									
1021					14					14	14	14					14			5		
854					12	5	6	5				10			6		5					
78			3			14	7		14	4		13			7	7				5		
2041	6		14		12	14	12			7	14	14		14								
985		7			14	7		4	12		14	19			14	4	12			7		
TOTAL Observ.	109	00	57		226	81	63	31	175	141	28	159	40	104	84	63	88			28		523

Figure 2a. Optical Coverage, Orbit 985.

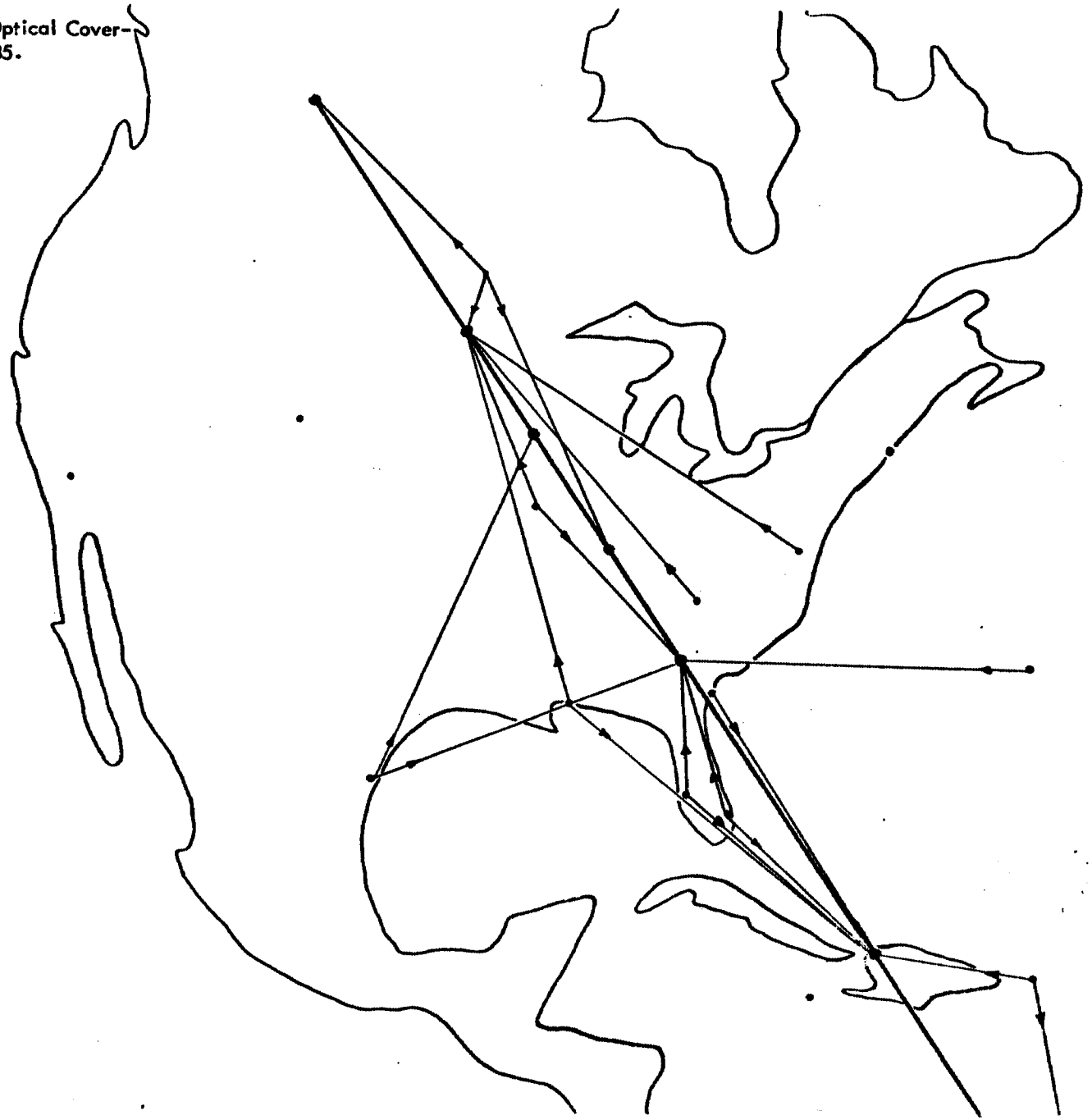

Figure 2b. Optical Coverage, Orbit 1705.

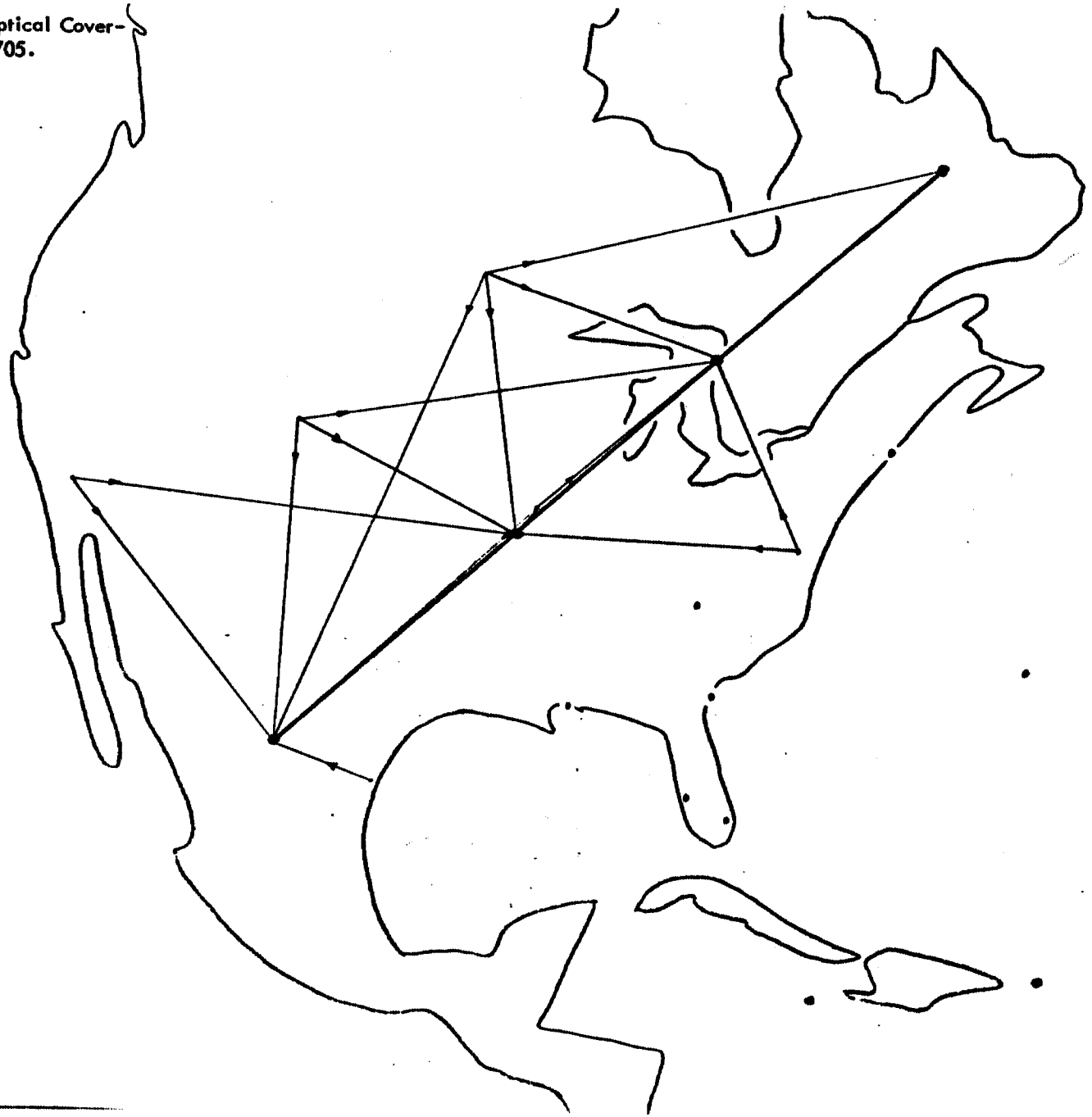

Figure 2c. Optical Coverage, Orbit 1621.

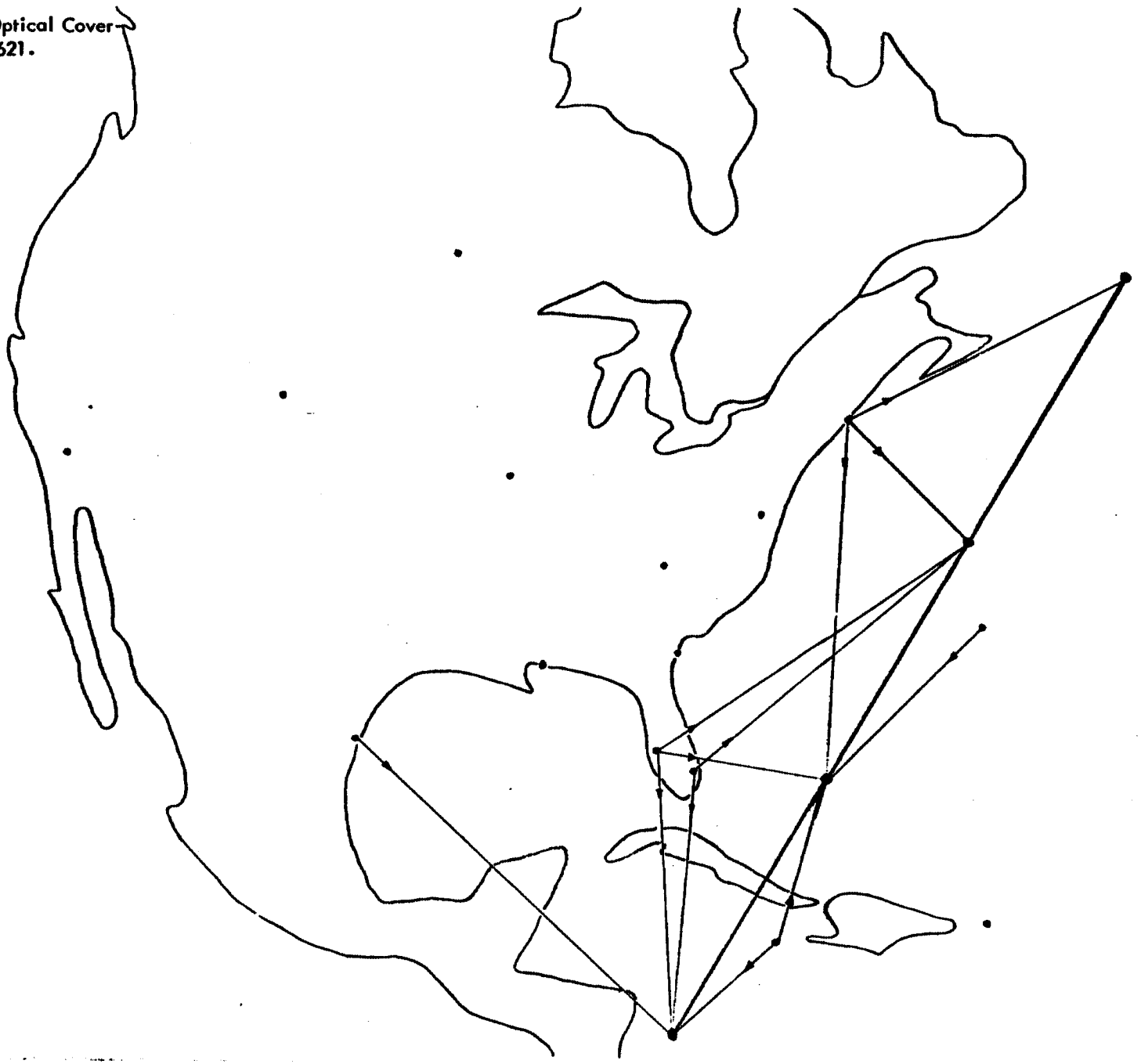

Figure 2d. Optical Coverage, Orbit 1994.

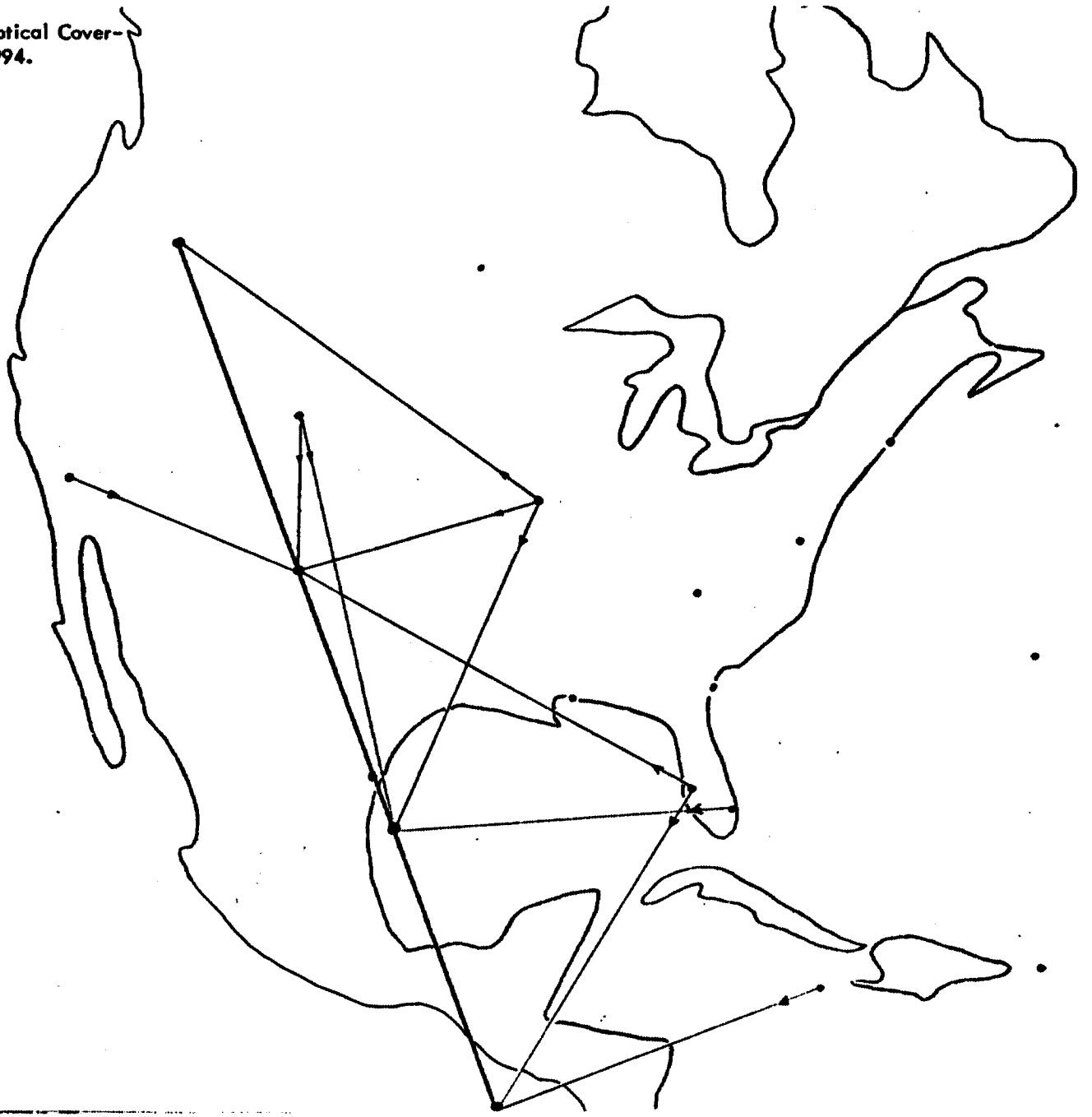

TABLE 2 KEY RESULTS OF GEOS-A SHORT ARC SURVEY

STATION	Reduction 1						Reduction 2					
	Adjustment			Standard Deviation			Adjustment			Standard Deviation		
	ΔE	ΔN	ΔU	σ_E	σ_N	σ_U	ΔE	ΔN	ΔU	σ_E	σ_N	σ_U
Goddard	0.0m	0.0m	0.0m	0.0m	0.0m	0.0m	0.0m	0.0m	0.0m	0.0m	0.0m	0.0m
Rosman, N. C.	9.2	-1.6	13.8	3.2	2.7	3.9	9.2	-6.4	9.3	3.4	3.1	4.1
Jupiter, Florida	0.4	0.3	0.8	2.6*	1.6*	3.1*	1.8	-8.7	0.6	3.3	3.9	4.3
Fort Myers, Florida	5.0	2.7	8.1	2.0	1.8	2.5	7.7	-5.9	7.2	2.5	3.4	3.1
Homestead, Florida	7.8	1.6	5.6	2.2	1.6	2.7	11.6	-6.8	6.4	2.9	3.9	3.6
Semmes, Alabama	4.6	-3.6	-5.5	2.3*	1.6*	3.0*	10.8	-18.3	-8.3	4.1	3.6	4.1
Edinburg, Texas	9.6	2.0	19.7	3.3	2.4	3.4	9.6	-8.5	18.4	4.5	4.1	3.8
Mohave, California	26.7	-4.3	0.2	5.6	2.4	4.1	22.8	-11.2	-2.1	7.3	3.4	4.5
Denver, Colorado	24.5	-10.1	6.3	3.8	2.1	3.3	22.9	-15.4	2.5	5.2	2.5	3.6
E. Grand Fork, Minn.	14.5	-20.6	9.9	3.0	2.7	2.1	14.8	-22.4	5.7	4.0	2.8	3.4
Bedford, Mass.	-10.5	8.0	4.3	3.1	3.0	3.8	-6.8	3.4	3.0	3.4	3.2	4.1
Bermuda	6.2	0.3	10.9	5.0	3.7	4.8	11.2	-7.8	9.3	5.3	4.4	5.1
Jamica	5.2	16.1	16.8	3.3	4.1	5.1	8.9	5.6	18.0	3.6	5.8	5.5
Puerto Rico	1.7	3.8	-32.6	3.5	3.7	4.8	5.0	-7.9	-30.1	3.9	5.4	5.4
Hunter, Florida	-1.3	-0.9	-4.2	2.2*	1.0*	3.1*	1.4	-17.2	-8.8	3.4	3.8	4.4
Columbia, Missouri	10.9	-17.7	6.4	2.7	1.9	2.7	11.3	-22.9	3.1	3.5	2.2	3.0

*Coordinates subjected to tight apriori constraints in Reduction 1.

Figure 3a. Vector Plot of Station Adjustments (Reduction 1).

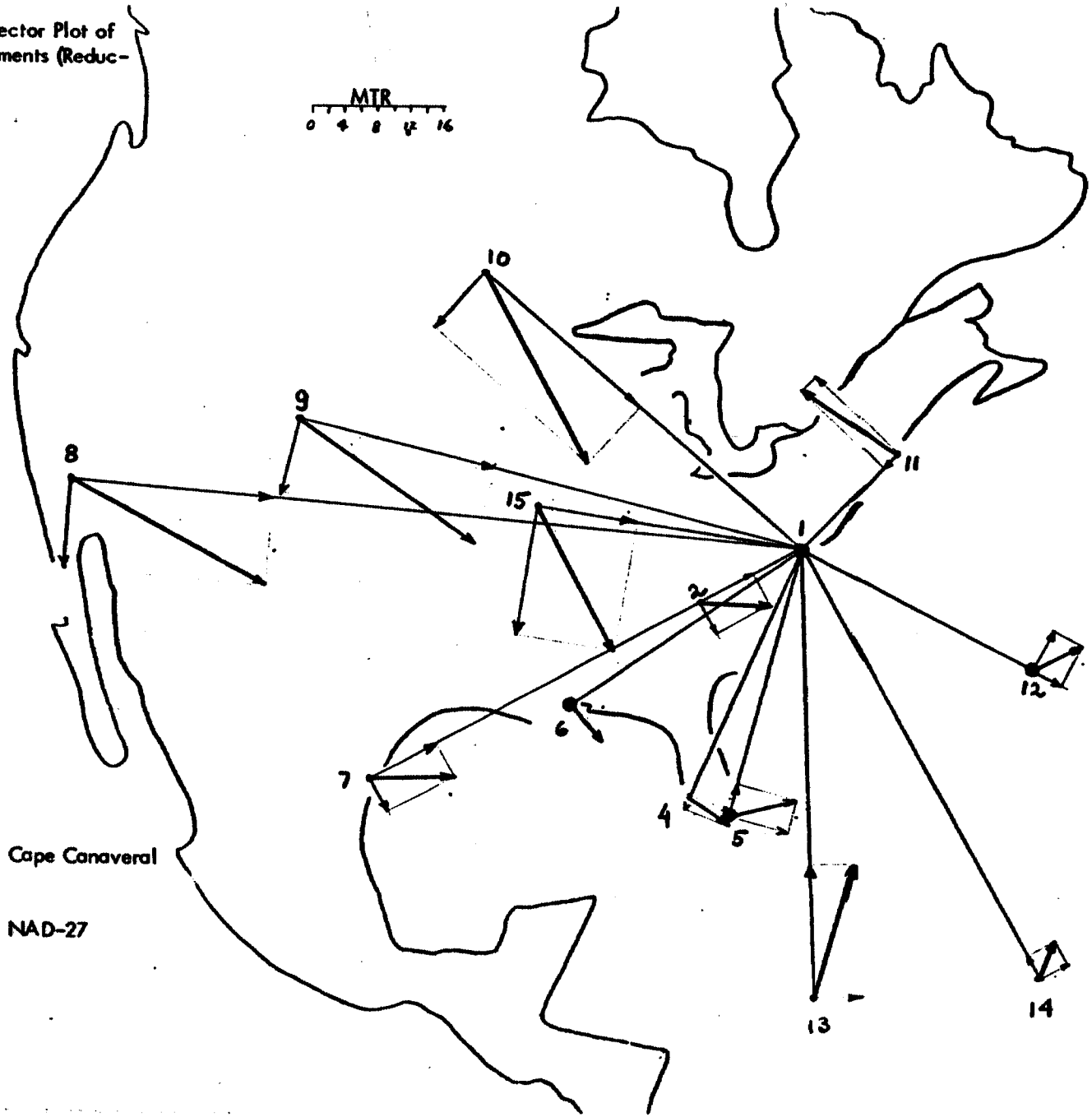

● Stations on Cape Canaveral Datum.

• Stations on NAD-27

Figure 4a. Vector Plot of Station Adjustments (Reduction 2).

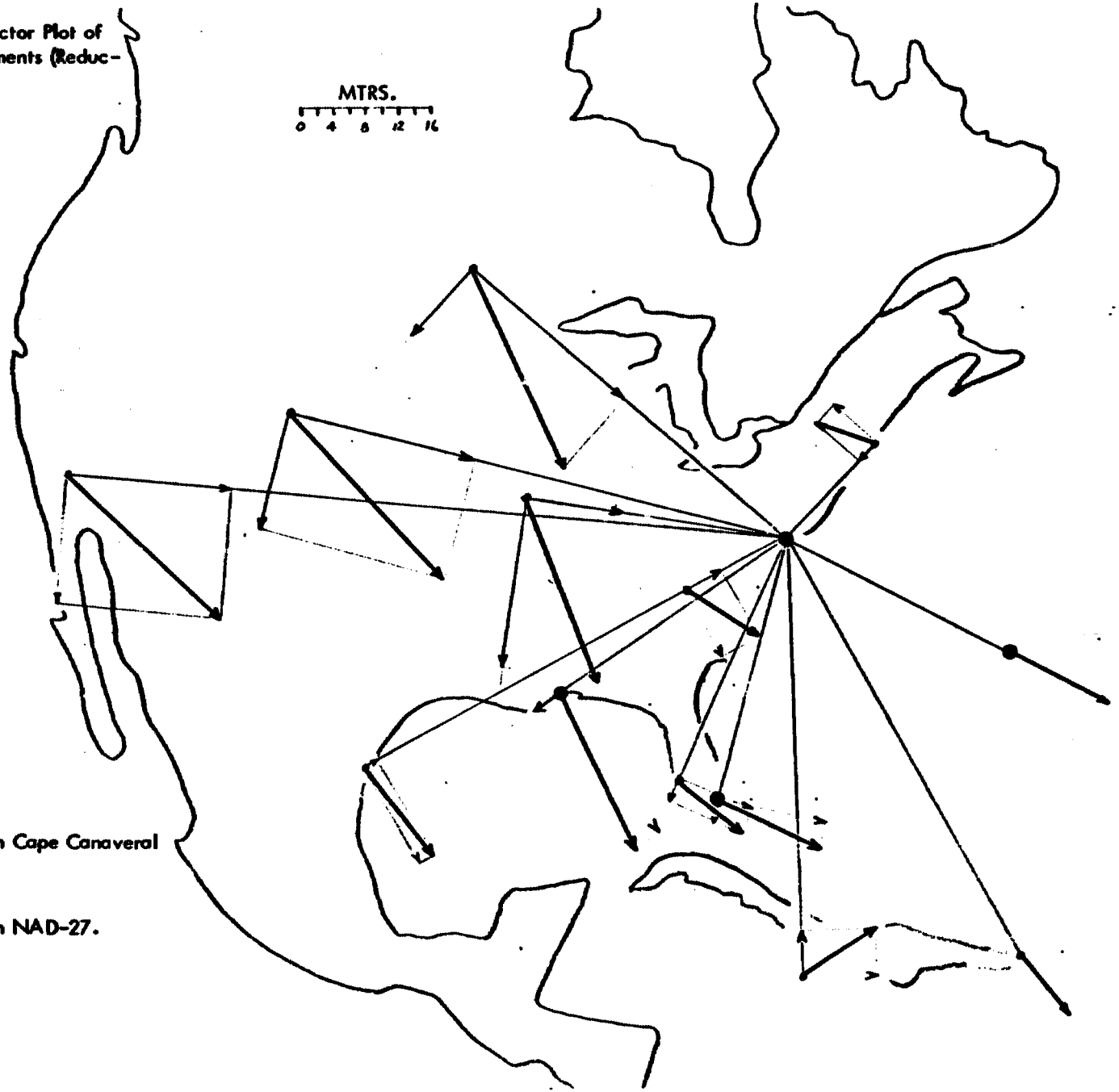

Figure 4b. Repeat of Figure 4a with NAD Stations displaced by CCD minus NAD coordinates of Goddard.

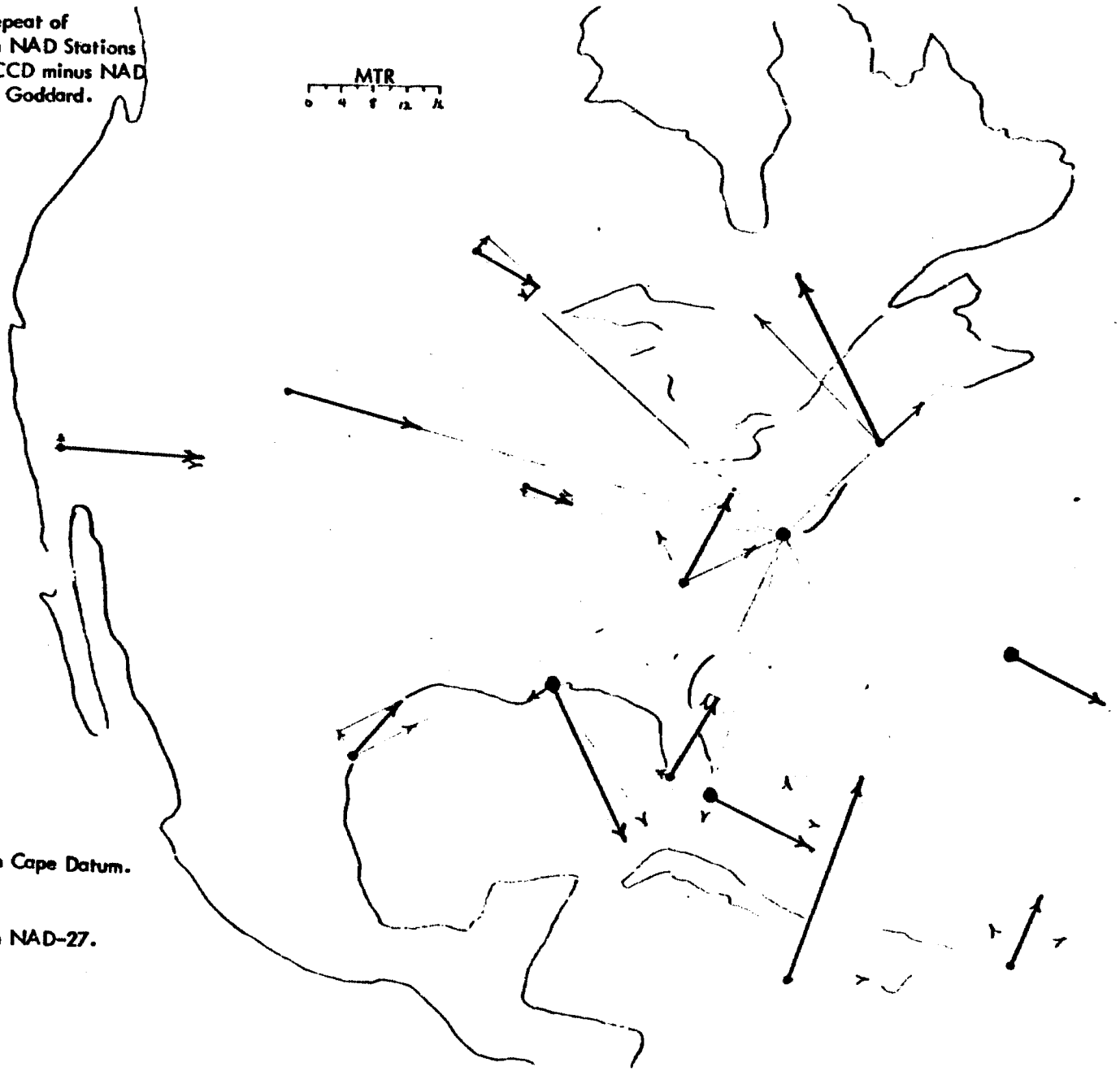

● Stations on Cape Datum.

. Stations on NAD-27.

Figure 4c. Repeat of Figure 4b scale adjusted by +1:200,000 for NAD Stations.

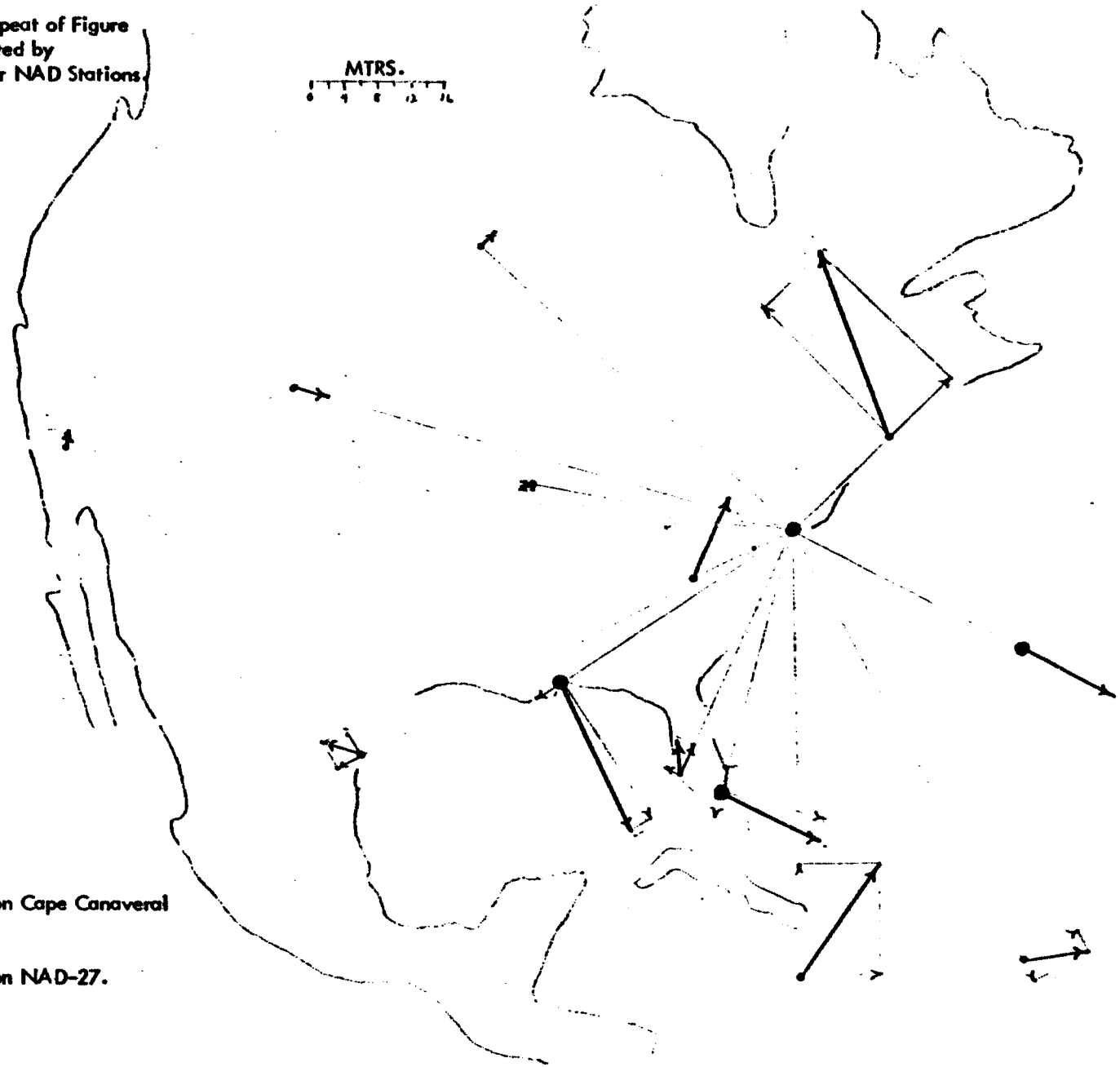

TABLE 3. OBSERVATIONAL COVERAGE OF SUPPLEMENTARY PASSES

Orbit	Time	GSF	BPO	JU4	JUP	FTM	HOM	BED	BER	COL	DEN	EDI	GFO	JAM	MOJ	PUR	ROS	SEM	HUN	Total
9003*	12-15-65 0024					14			11											25
831	1-15-66 0454	6	7	7		14				19		14								67
1502	3-12-66 0536			14	11			7						14			7			53
1597	3-20-66 0406	12		7	3	7	14		13							13	7		6	62
1682	3-27-66 0547									21	5		20				6			52
1835	4-09-66 0125			14		14	13										7		14	62
1838	4-09-66 0600		7						7	7							14			35
1898	4-14-66 0818			6		14			21				7	7		21	14			90
1934	4-17-66 0833	21												14	7		21	14		77
2017	4-24-66 0653					21					14		21			14	18			88
2088	4-30-66 0526			5		14			7				7	6					14	53
2278	5-16-66 0217		7			20								14		21				62
9001*	7-05-66 0848										21	14	21		21					77
9002*	7-11-66 0506		14						21			14	7	14		7				77
	Total Observations	39	35	53	14	118	27	7	80	47	40	42	83	69	28	76	94	14	14	900

Figure 5. Ground Traces of Extended Net Designed to Strengthen Peripheral Stations.

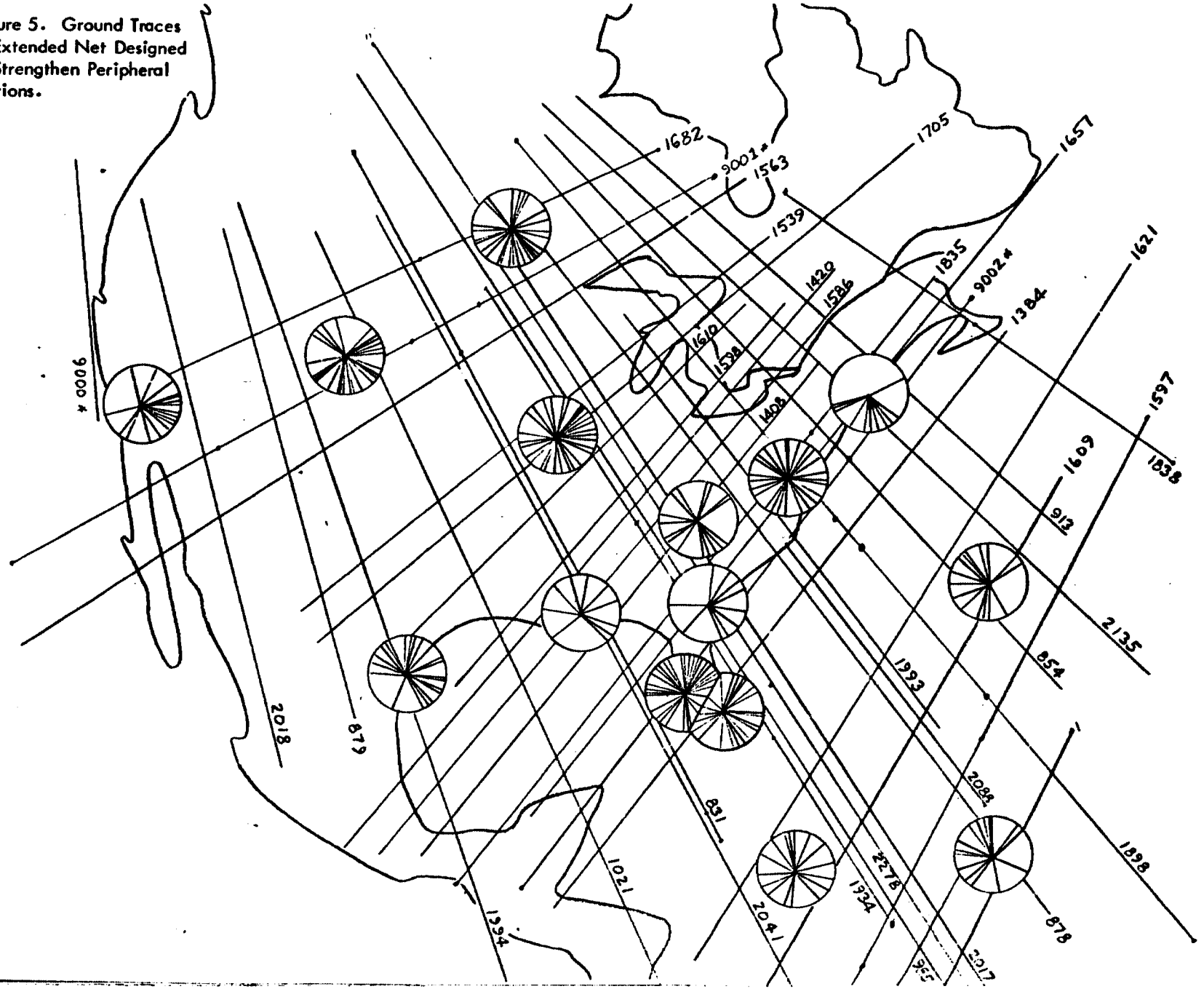

VARIATIONS IN THE MATHEMATICAL MODELING FOR GEOS-A

By:

J. G. Hartwell

D. BROWN ASSOCIATES, INC.
Post Office Drawer 550
Melbourne, Florida 32901

under

NASA CONTRACT NO. NAS5-9938

VARIATIONS IN THE MATHEMATICAL MODELING FOR GEOS-A

ABSTRACT

An investigation was made to determine the effects on the orbit of GEOS-A when certain minor variations were introduced in the differential equations describing the motion of the satellite. In particular, for various short and intermediate arc experiments involving the GEOS-A satellite, the effects of: variation in geopotential coefficients, uncertainties in the coordinates of earth's center of mass, and luni-solar perturbations were analyzed.

VARIATIONS IN THE MATHEMATICAL MODELING FOR GEOS-A

INTRODUCTION

The simulations presented below were performed in order to observe the effects on the orbit of GEOS-A when certain minor variations are introduced in the differential equations describing the motion of this satellite. In particular, for various short and intermediate arc experiments, the following effects are analyzed.

i. Variations in geopotential coefficients as determined by certain principal investigators.

ii. Effects of uncertainties in the coordinates of the earth's center of mass.

iii. Effects of neglecting perturbing accelerations of the sun and moon.

The main reasons for performing the simulations reported here were to determine the characteristics of the mathematical model required for the successful completion of the various GEOS-A short arc experiments and to acquire some preliminary insight into the characteristics required of the mathematical model for the GEOS-A intermediate arc experiments.

RESULTS

In the simulations which follow, the following procedures were usually adopted: Two orbits are integrated whose initial conditions are identical and characteristic of GEOS-A, but whose mathematical modeling is slightly different. One of these orbits will be designated as a reference orbit. The raw differences in position coordinates along the two orbits will be treated as observations to see if an adjustment, in the sense of least

squares, of the initial conditions only on the second orbit can accommodate the differences in the mathematical modeling. In general, the graphs show the differences in coordinates along the orbit before and after the least square adjustment.

i. Variations in Geopotential Coefficients.

Figures 1, 2, and 3 indicate the effects on the orbit when independent sets of geopotential coefficients are used. The reference orbit has a geopotential function defined by the SAO L-3 coefficients but truncated at seventh degree and seventh order. The other orbit's geopotential function is defined by the NWL 5E-6 coefficients. The time span of interest is 1000 seconds, or about one seventh of a revolution of GEOS-A. Maximum position residuals in meters are -8, +3, and +6 in X, Y, and Z, respectively, before the adjustment. After the least squares adjustment, the maximum position residuals are +1, +1, and +1 meters in X, Y, and Z.

Figures 4, 5, and 6 represent more of the same thing. The time span of interest is still 1000 seconds and the reference orbit's potential function is defined, as before, by the truncated SAO L-3 set. The potential function of the other orbit contained only Kozai's zonal harmonics truncated at fourth degree. All sectional, tesseral, and other zonal harmonic coefficients were set to zero. Maximum residuals of (-20, +4, +6) meters in (X, Y, Z) are observed before the adjustment. Maximum residuals of (-4, +1, -.5) meters in (X, Y, Z) are seen after the adjustment.

Figures 7, 8, 9 and 10 indicate the effects of variations in geopotential coefficients when the time span of interest is extended to cover longer arcs. The geopotential function of the reference orbit is still defined by the truncated SAO L-3 set. The NWL 5E-6 coefficients are used for the geopotential function of the other orbit. Only the effects on the X position coordinate are given, those for Y and Z being essentially the same. Figure 7 shows the X residuals in position over three revolutions before the least squares adjustment. Peak to peak residuals of 40 to -100 meters are noted. Figure 8 indicates little improvement in the residuals after the least squares adjustment. Peak to peak residuals of 35 to -100 meters

still exist. Figure 9 is indicative of the results of this investigation if the time span is reduced to two revolutions. Peak to peak residuals of 30 to -90 meters are still seen after the least square adjustment. The results of truncating this experiment after one revolution are to be seen in Figure 10. Nevertheless, peak to peak residuals of -40 to +40 meters are still to be observed.

In the event that we are somewhat high-handed in our treatment of the SAO L-3 set of potential coefficients, part of the foregoing procedure was repeated using the complete SAO L-3 geopotential function. The potential function for the other orbit was defined by the NWL 5E-6 set of coefficients. Figures 11, 12, and 13 are a plot of the position residuals in meters in X, Y, and Z, respectively. The overall character of the curves in these three figures suggest that a least squares adjustment of the initial conditions only will not remove these residuals and, therefore, no such adjustment was attempted.

ii. Effects of Uncertainties in the Coordinates of the Earth's Center of Mass.

Figures 14, 15, and 16 indicate the effects on the orbit when the center of mass is displaced slightly from the origin. In these simulations, the center of mass of the reference orbit is displaced +31.89 meters in each coordinate with respect to the origin. For the other orbit, the assumption is made that the center of mass is at the origin. A least squares adjustment of the latter orbit's initial conditions is made and the differences in positions before and after the adjustment is exhibited. Maximum position residuals in meters of (-2.5, +2.5, +20.0) in (X, Y, Z) are indicated before the adjustment. After the adjustment, maximum position residuals of (-1.5, -1.1, +4.0) meters are to be observed in (X, Y, Z). The time span of interest is 1000 seconds or about one seventh of a revolution of GEOS-A.

Figures 17, 18, and 19 represent two simulations with identical results. The situation is exactly the same as above. However, in the first of the two instances under discussion now, only the center of mass was allowed to adjust. It is to be observed that the residuals were effectively reduced to zero. For the second simulation, both the center of mass and the initial conditions were allowed to adjust. Since the initial conditions were already correct, they should not and did not change.

In Figure 20, some indication of the theoretical separability of errors in position and velocity from errors in coordinates of the earth's mass center is presented. In this simulation, the center of mass for the reference orbit is still displaced from the origin by +31.89 meters in each coordinate. Additionally, the initial coordinates of position of the other orbit are in error by +50 meters with respect to the origin. Moreover, the initial velocities are in error by +.1 meters per second in each coordinate. Only the results for the X coordinate are shown, those for Y and Z being essentially the same. The time span is still 1000 seconds and before the adjustment a maximum position residual of -160 meters can be seen. After the adjustment, these residuals have been reduced to zero.

iii. Effects of Neglecting Perturbing Acceleration of the Sun and Moon.

Figures 21, 22, and 23 indicate the effects of the perturbing accelerations from the sun and moon on the orbit of GEOS-A, over a time span of one day. The reference orbit is subject to the effects of earth, moon and sun while the other orbit is subject only to the effects of the earth. It can be observed that the maximum residuals in meters are (-13, -28, -35) in (X, Y, Z). After the least squares adjustment, the peak to peak residuals appear to be (+8 to -7, +12 to -12, +15 to -15) meters in (X, Y, Z).

CONCLUSIONS

The successful completion of various experiments using short arc orbital constraints does not appear to be sensitive to current variations in geopotential coefficients as determined by various principal investigators. For some tasks, the use of zonal harmonics only through fourth degree will be adequate. Non-conservative forces and extraterrestrial perturbations may be neglected.

A high quality determination of sensor site locations may be quite sensitive to uncertainties in the coordinates of the earth's center of mass. If the station locations are referred to a datum whose origin does not coincide with the center of mass of the earth, then the first order coefficients of the geopotential should be carried as appropriately constrained parameters.

The results obtained using different sets of geopotential coefficients for intermediate arc experiments is somewhat discomforting. The SAO set of coefficients is a more recent and more complete set than is the NWL set. It is possible that more recent determinations of the geopotential by NWL might produce more favorable comparisons.

The perturbing effects of the sun and moon should appear in the orbital differential equations for intermediate arc experiments. No investigations have been carried out to see if radiation pressure and drag need to be considered for GEOS-A. Naturally, if the coordinates of the center of mass should be carried as constrained parameters for short arc experiments, they must also be carried in intermediate arc experiments.

FIGURE 1. Least Squares Adjustment of Initial Conditions to Accomodate NWL 5E-6 Geopotential Coefficients to SAO L-3 Geopotential Coefficients. Residuals In X Position Coordinates.

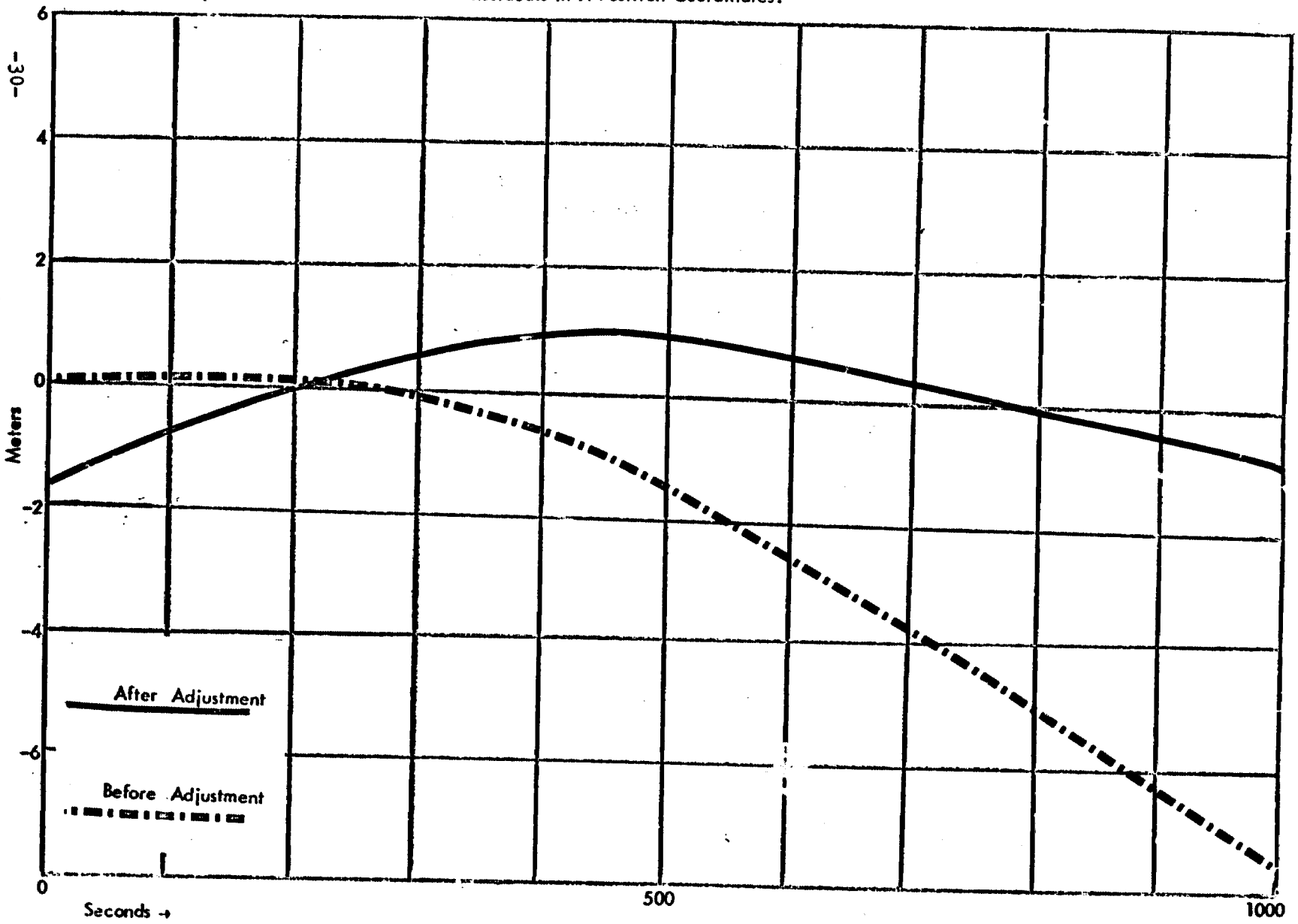

FIGURE 2. Least Squares Adjustment of Initial Conditions to Accomodate NWL 5E-6 Geopotential Coefficients to SAO L-3 Geopotential Coefficients. Residuals In Y Position Coordinates.

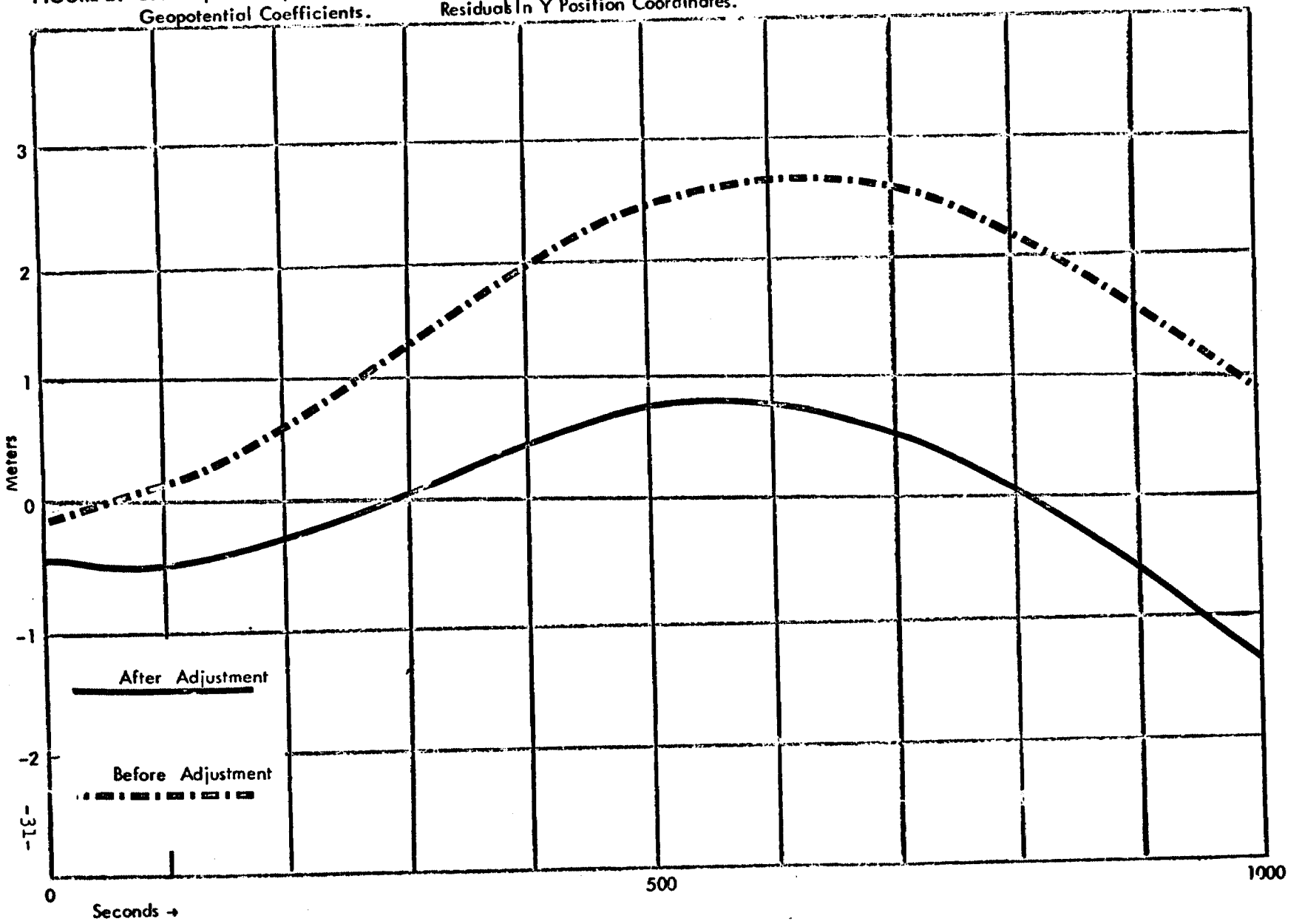

FIGURE 3. Least Squares Adjustment of Initial Conditions to Accomodate NWL 5E-6 Geopotential Coefficients to SAO L-3 Geopotential Coefficients. Residuals In Z Position Coordinates.

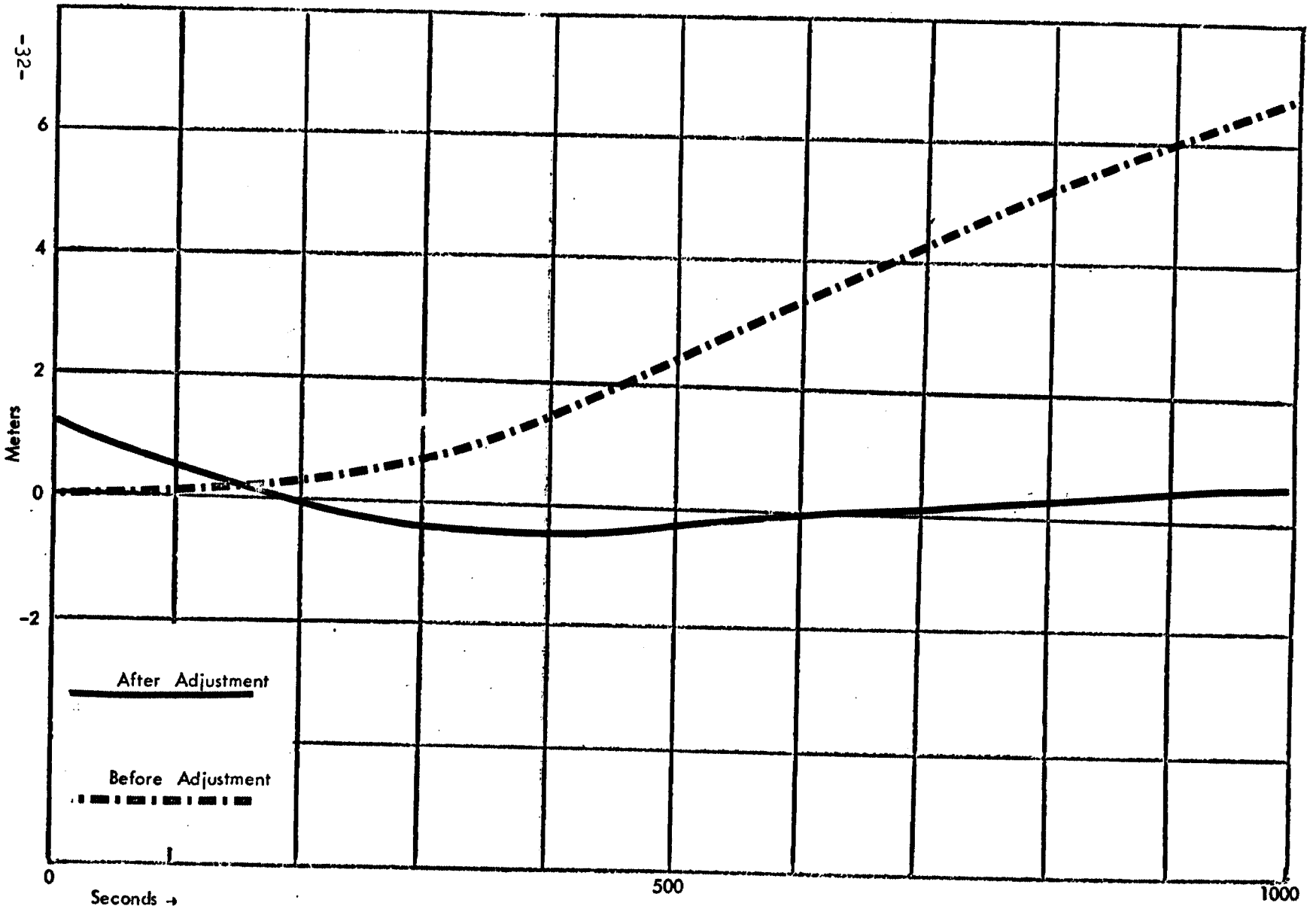

FIGURE 4. Least Squares Adjustment of Initial Conditions to Accomodate Kozai's Zonals Through Fourth Degree to SAO L-3 Geopotential Coefficients. Residuals In X Position Coordinates.

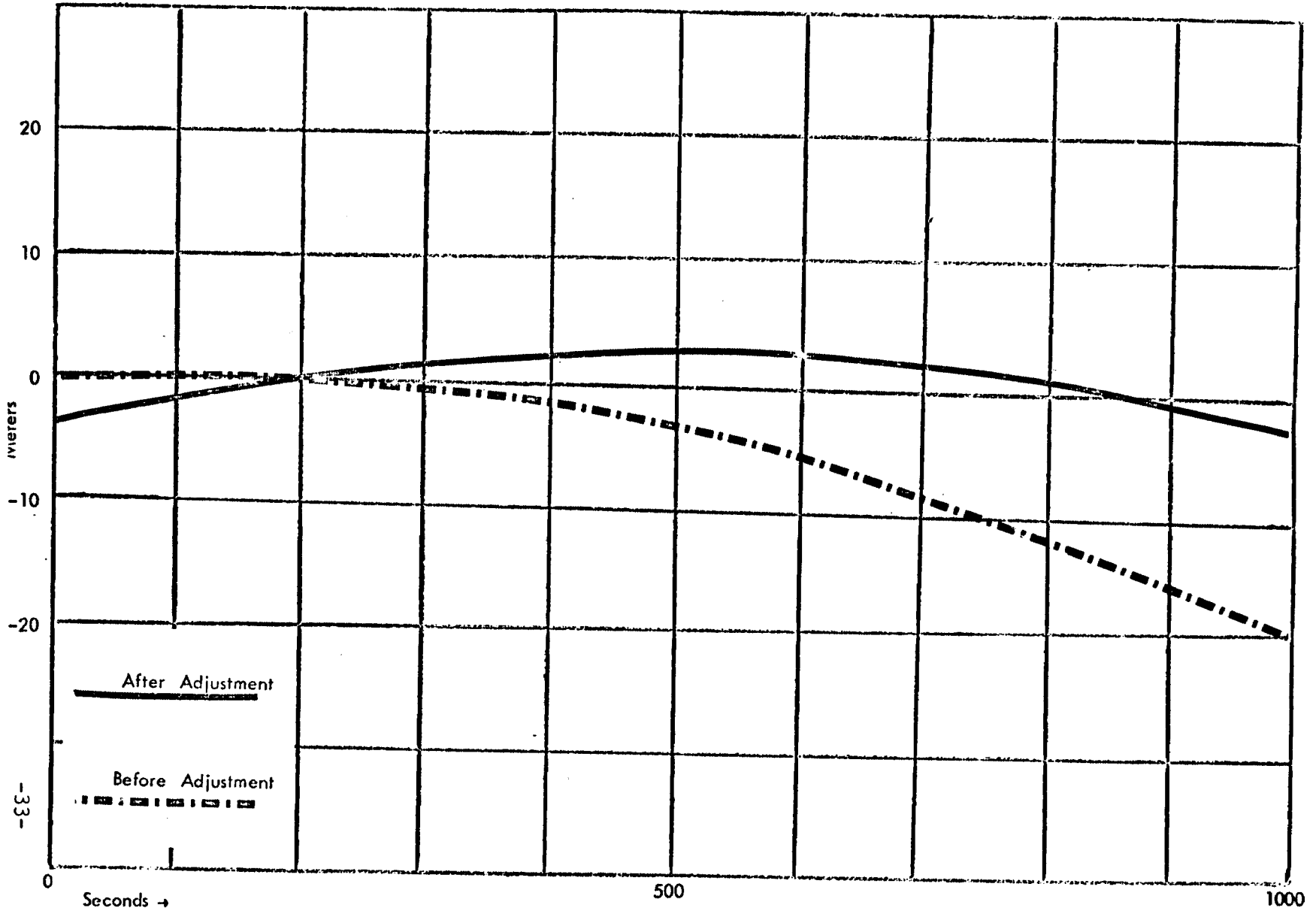

FIGURE 5. Least Squares Adjustment of Initial Conditions To Accomodate Kozai's Zonals Through Fourth Degree To SAO L-3 Geopotential Coefficients. Residuals In Y Position Coordinates.

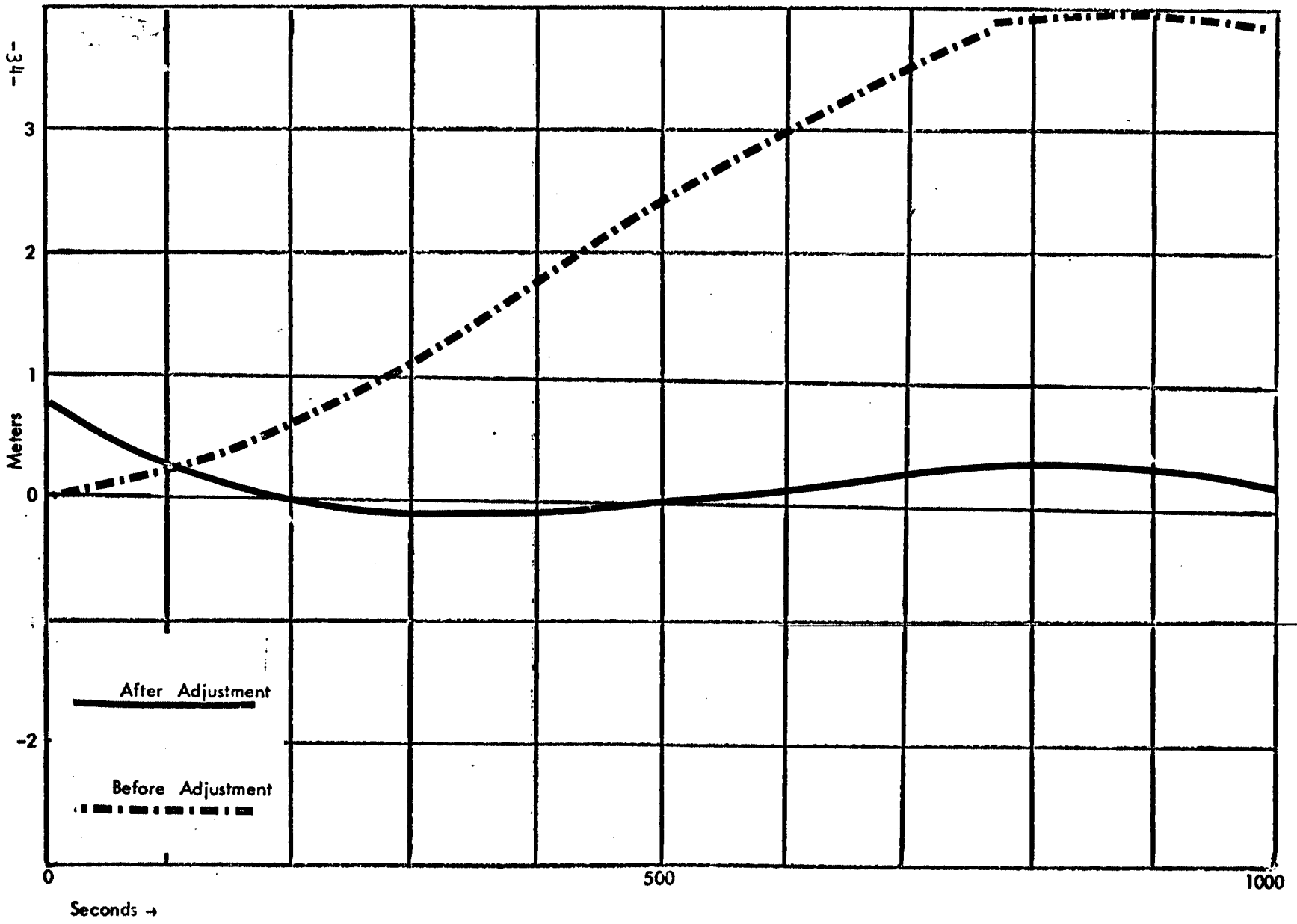

FIGURE 6. Least Squares Adjustment of Initial Conditions to Accomodate Kozai's Zonals Through Fourth Degree to SAO L-3 Geopotential Coefficients. Residuals In Z Position Coordinates.

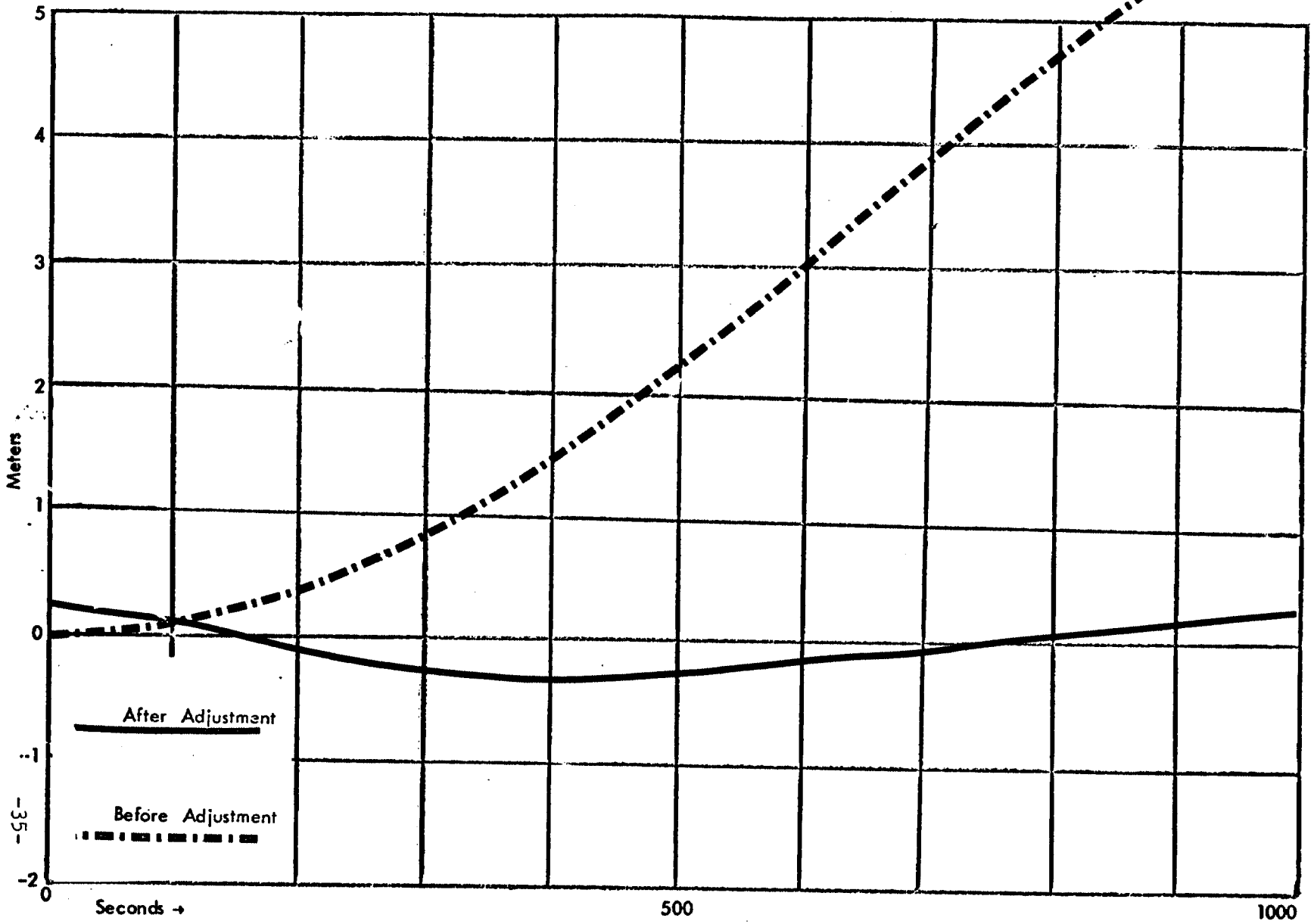

FIGURE 7. Residuals In X Position Coordinates Over Three Revolutions of GEOS A Satellite Resulting From Differences in NWL 5E-6 And SAO L-3 Geopotential Coefficients. Before Least Squares Adjustment Of Initial Conditions.

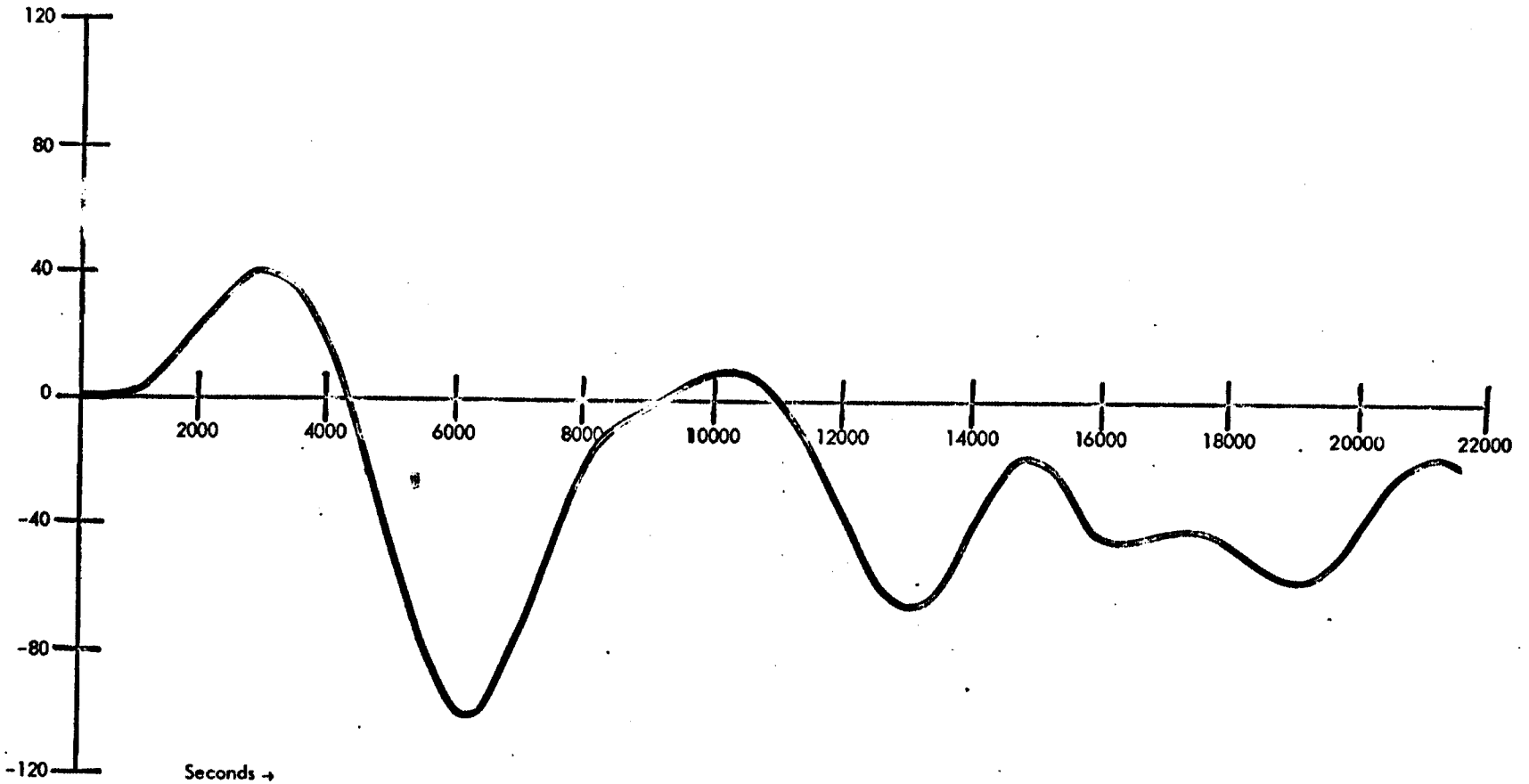

FIGURE 8. Residuals In X Position Coordinates Over Three Revolutions of GEOS A Satellite Resulting From Differences In NWL 5E-6 And SAO L-3 Geopotential Coefficie After Least Squares Adjustment Of Initial Conditions.

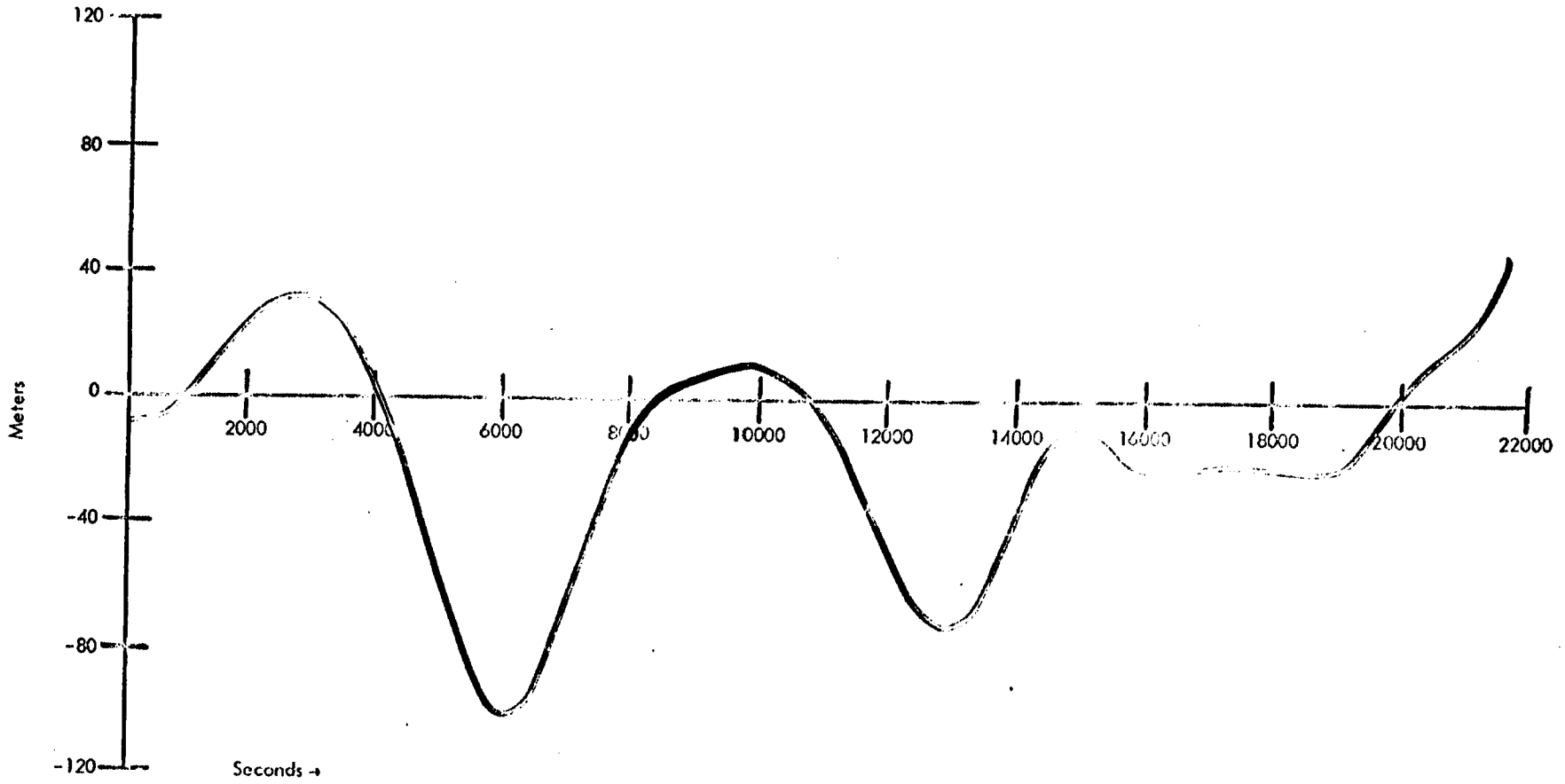

FIGURE 9. Residuals In X Position Coordinates Over Two Revolutions Of GEOS A Satellite. Resulting From Differences In NWL 5E-6 And SAO L-3 Geopotential Coefficients. After Least Squares Adjustment Of Initial Conditions.

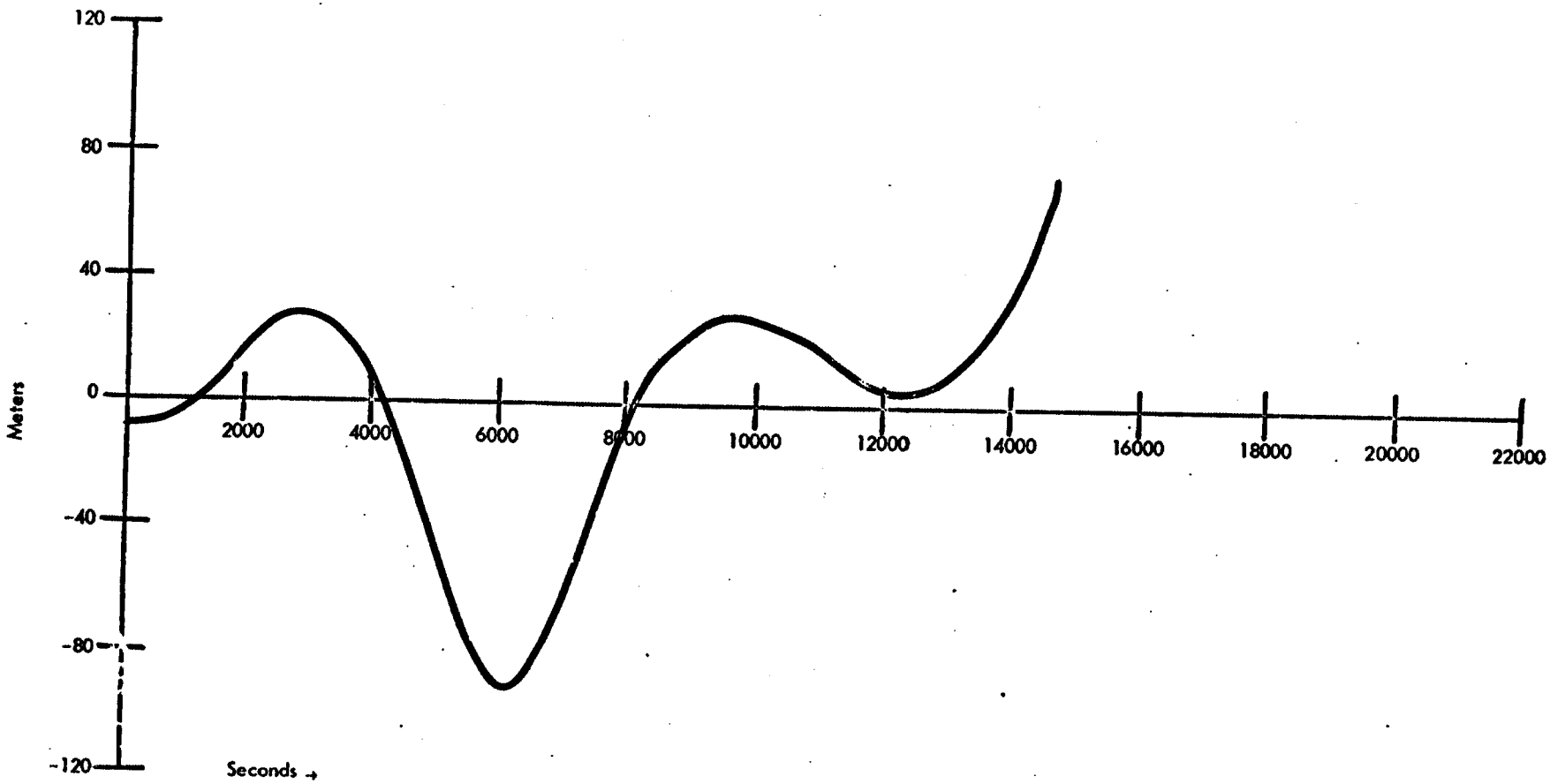

FIGURE 10. Residuals In X Position Coordinates Over One Revolution Of GEOS A Satellite Resulting From Differences In NWL 5E-6 And SAO L-3 Geopotential Coefficients. After Least Squares Adjustment Of Initial Conditions.

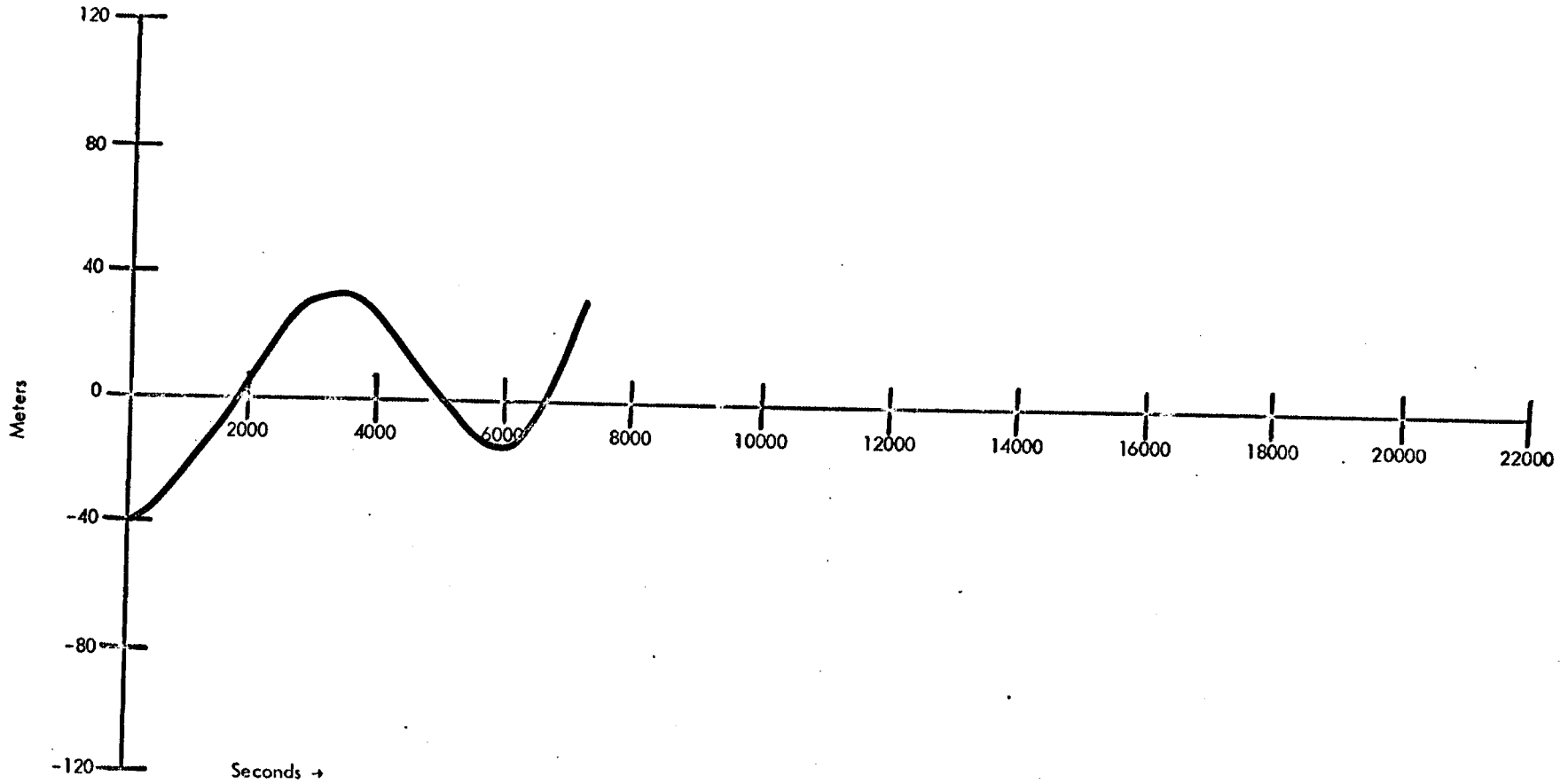

FIGURE 11. Residuals in X Position Coordinates Over Three Revolutions of GEOS A Satellite Resulting From Differences in NWL 5E-6 And Complete SAO L-3 Geopotential Coefficients. No Least Squares Adjustment Attempted.

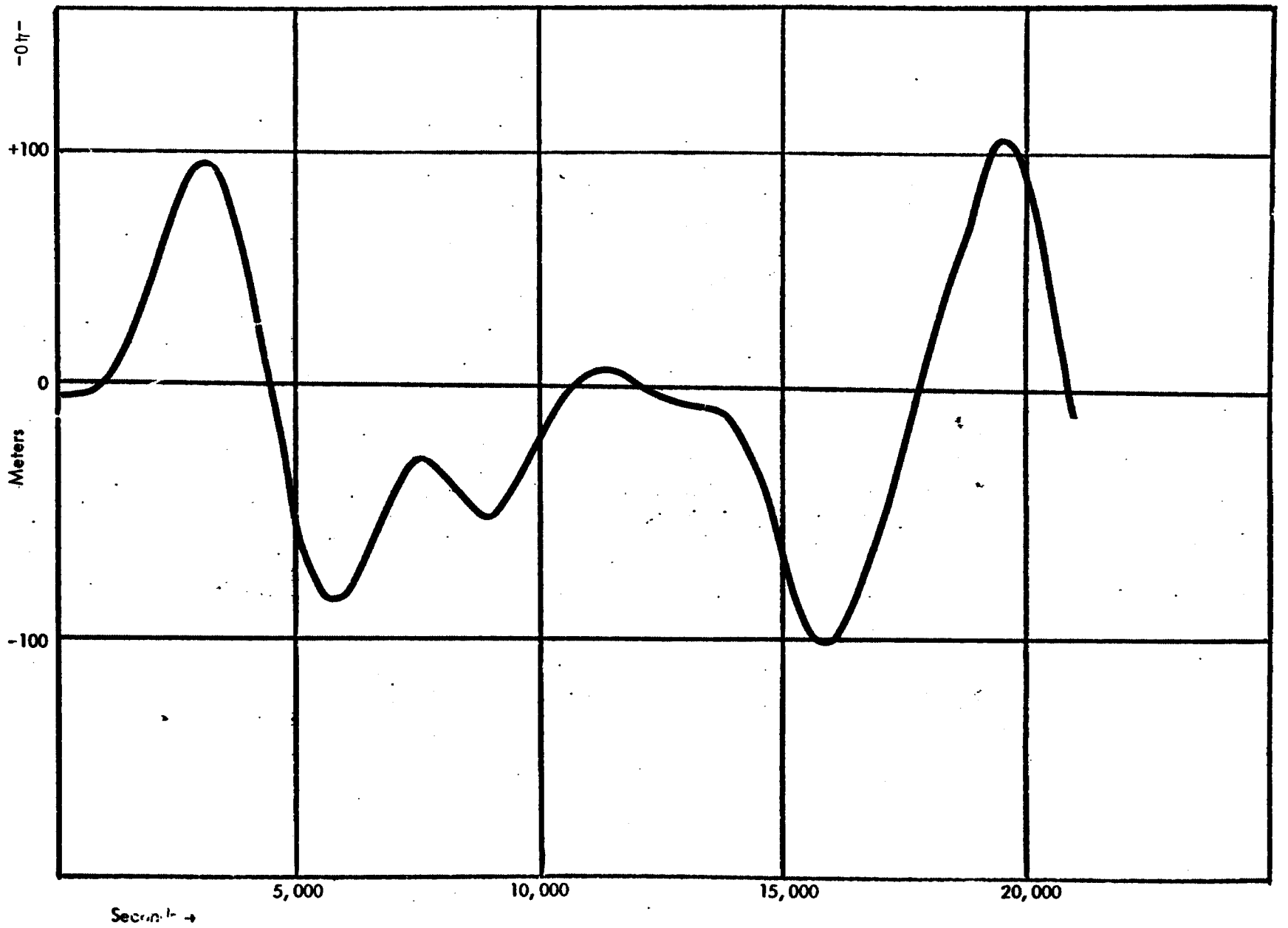

FIGURE 12. Residuals In Y Position Coordinate Over Three Revolutions of GEOS A Satellite Resulting From Differences in NWL 5-6E And Complete SAO L-3 Geopotential Coefficients. No Least Squares Adjustment Attempted.

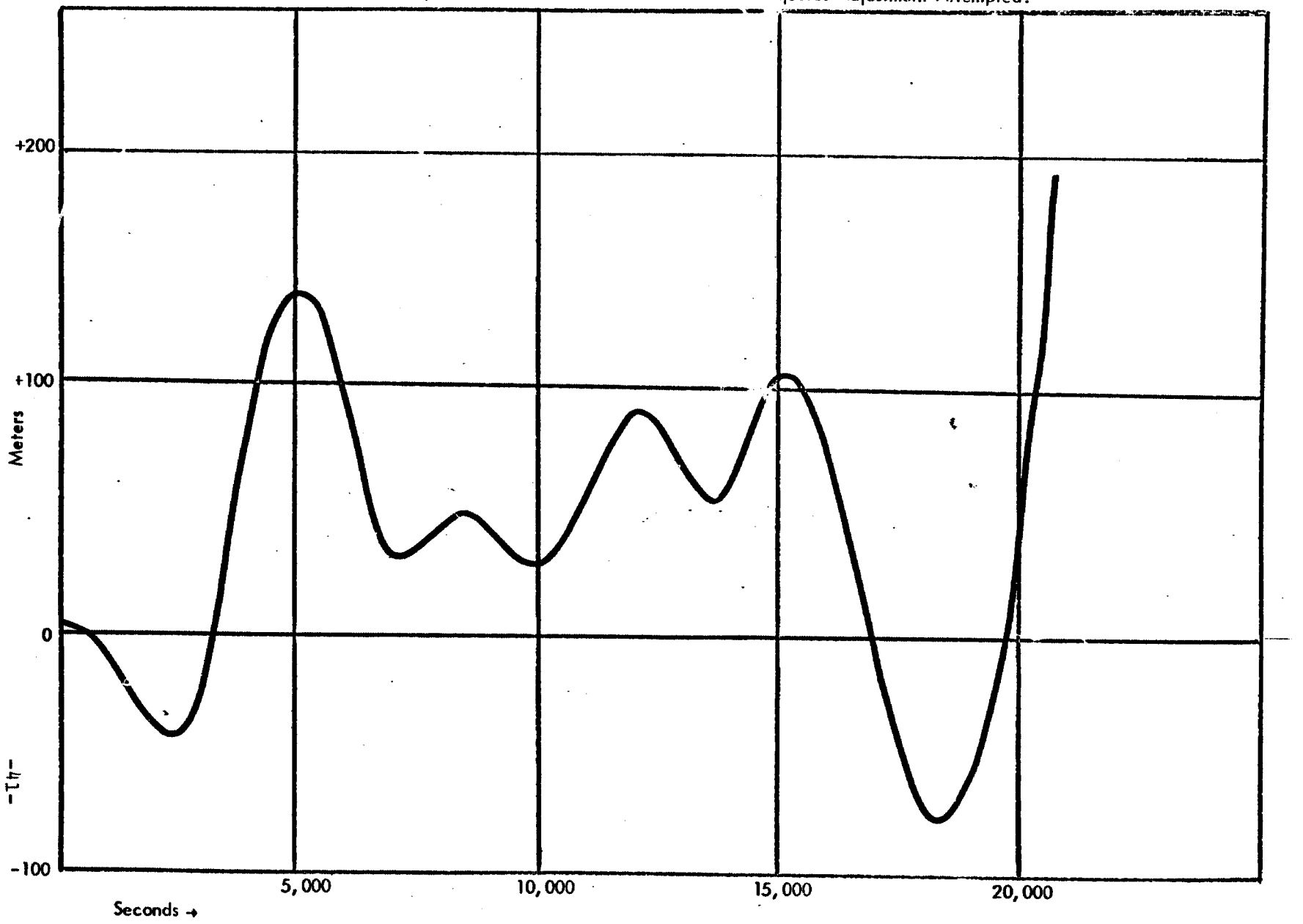

FIGURE 13. Residuals In Z Position Coordinates Over Three Revolutions of GEOS A Satellite Resulting From Differences in NWL 5-6E And Complete SAO L-3 Geopotential Coefficients. No Least Squares Adjustment Attempted.

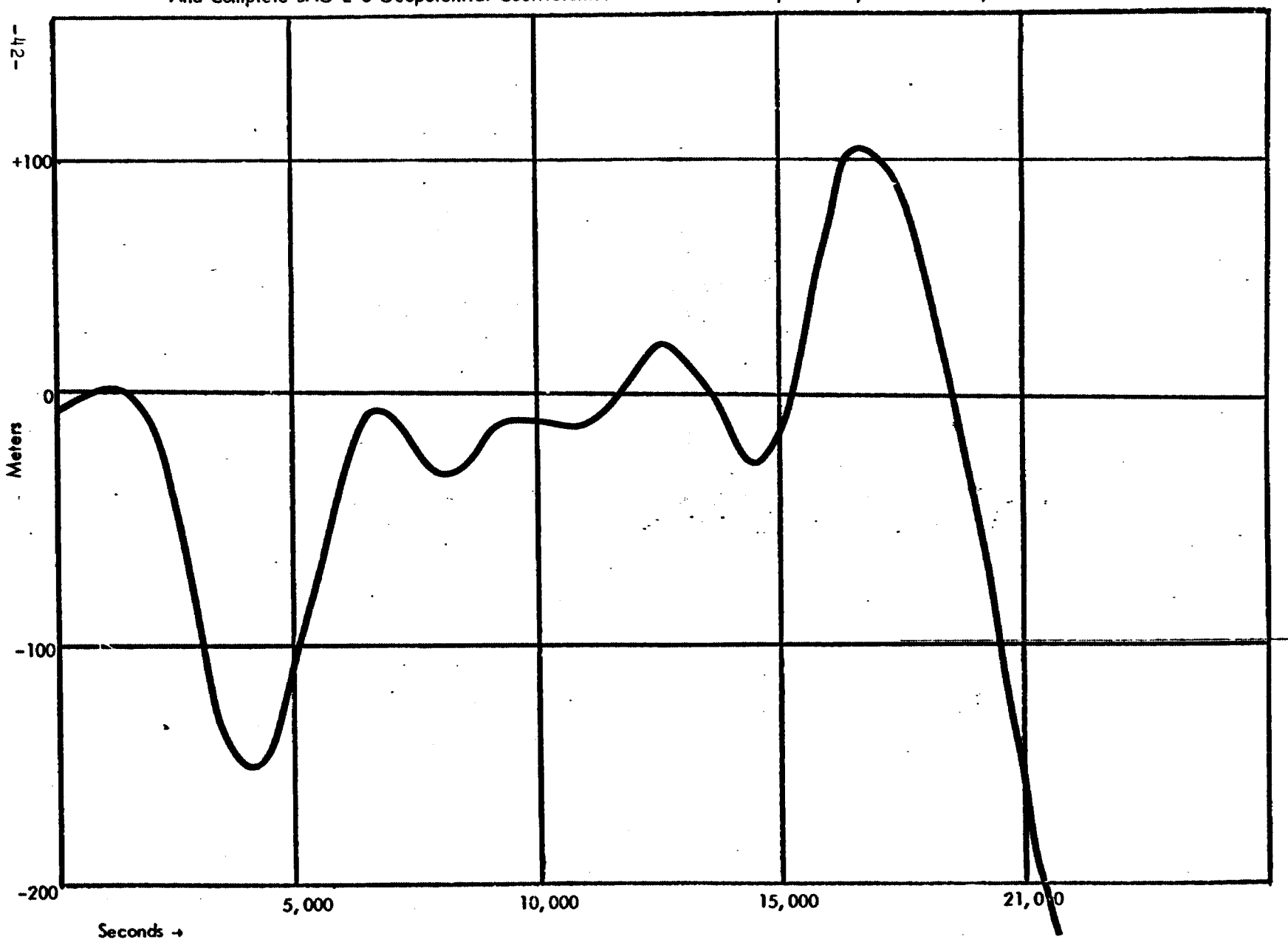

FIGURE 14. Least Squares Adjustment of Initial Conditions to Compensate for Location of Center of Mass Not At The Origin. Residuals In X Position Coordinates.

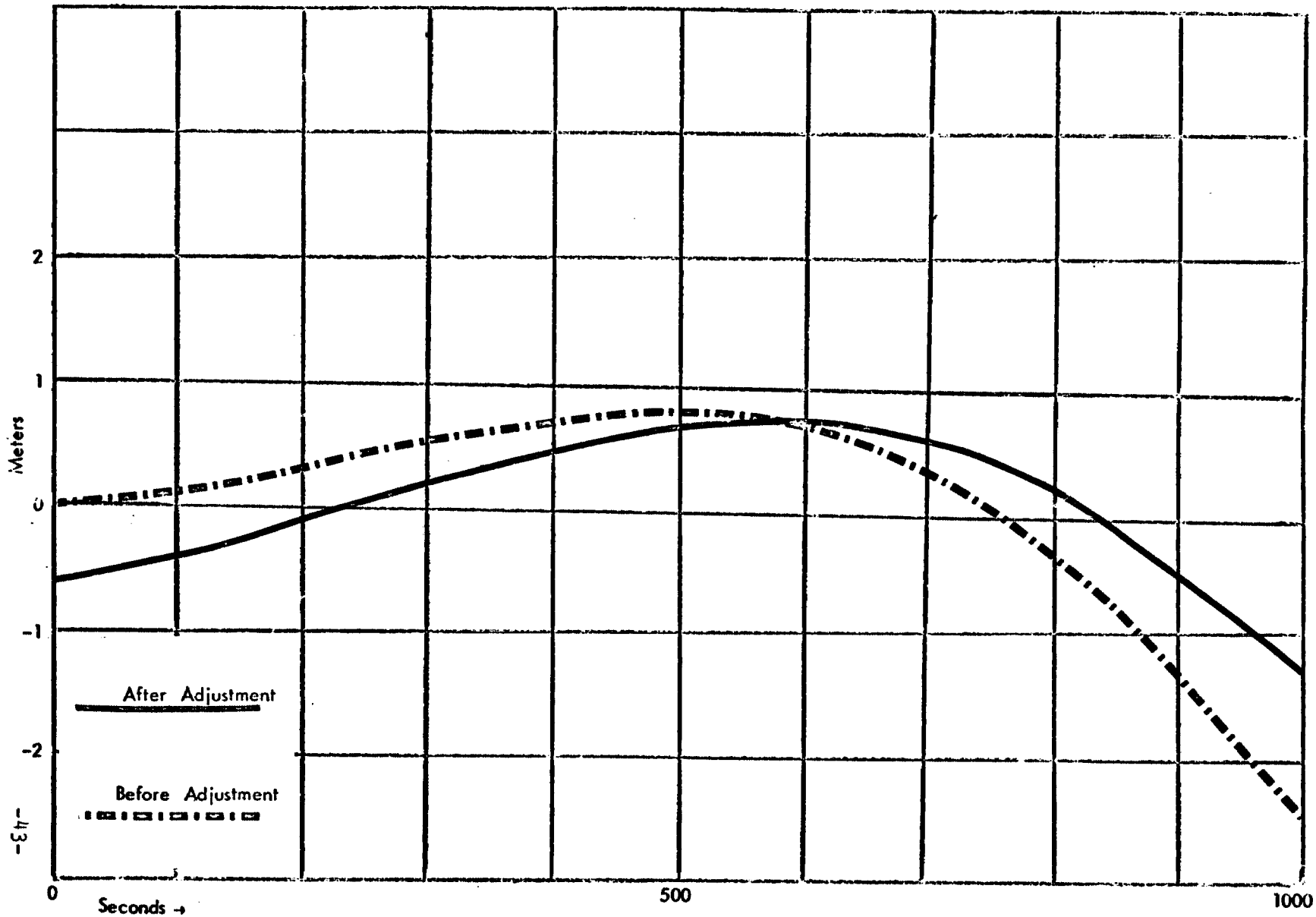

FIGURE 15. Least Squares Adjustment of Initial Conditions to Compensate for Location of Center of Mass Not At The Origin. Residuals In Y Position Coordinates.

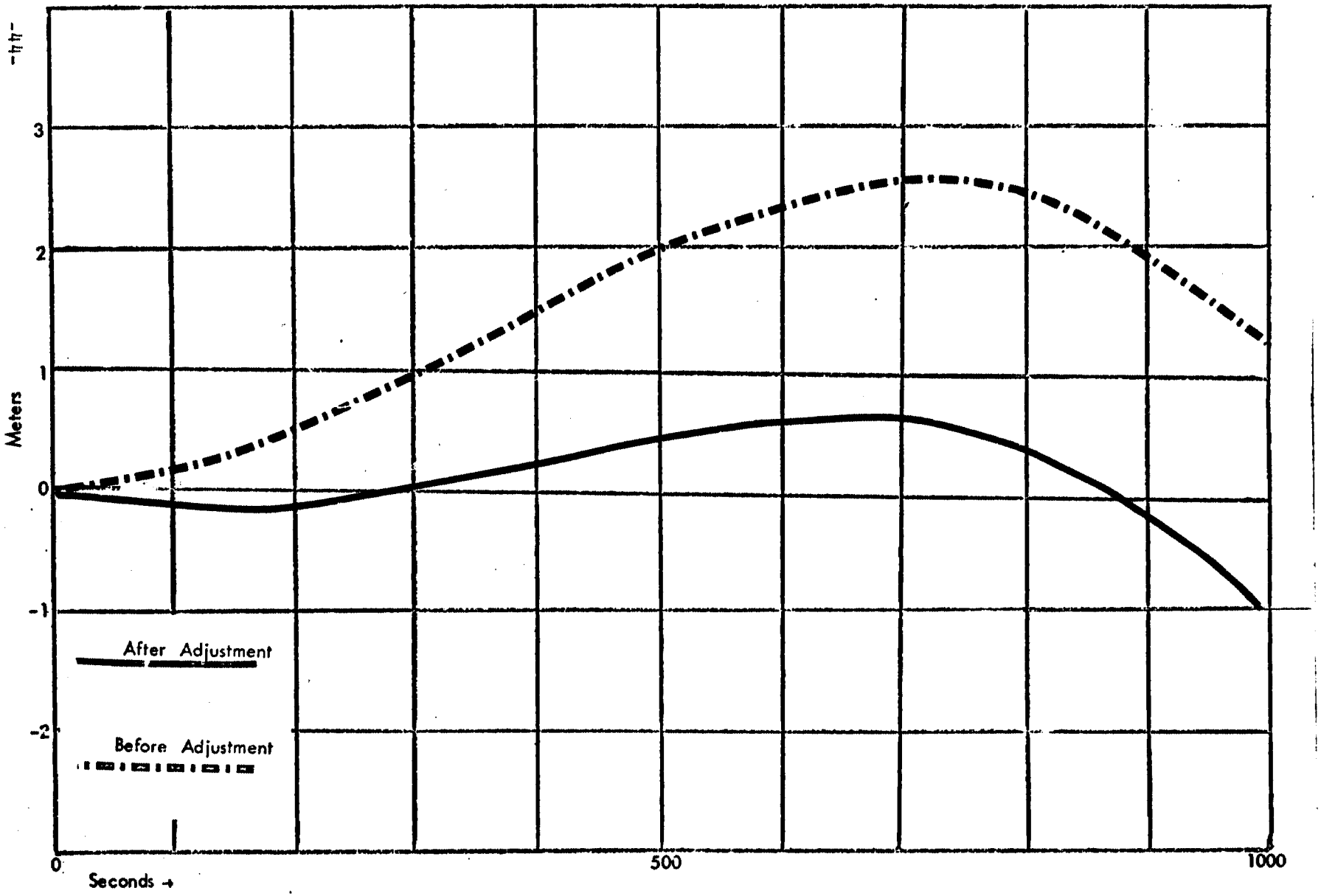

FIGURE 16. Least Squares Adjustment of Initial Conditions to Compensate for Location of Coordinates of Center of Mass Not At The Origin. Residuals In Z Position Coordinates.

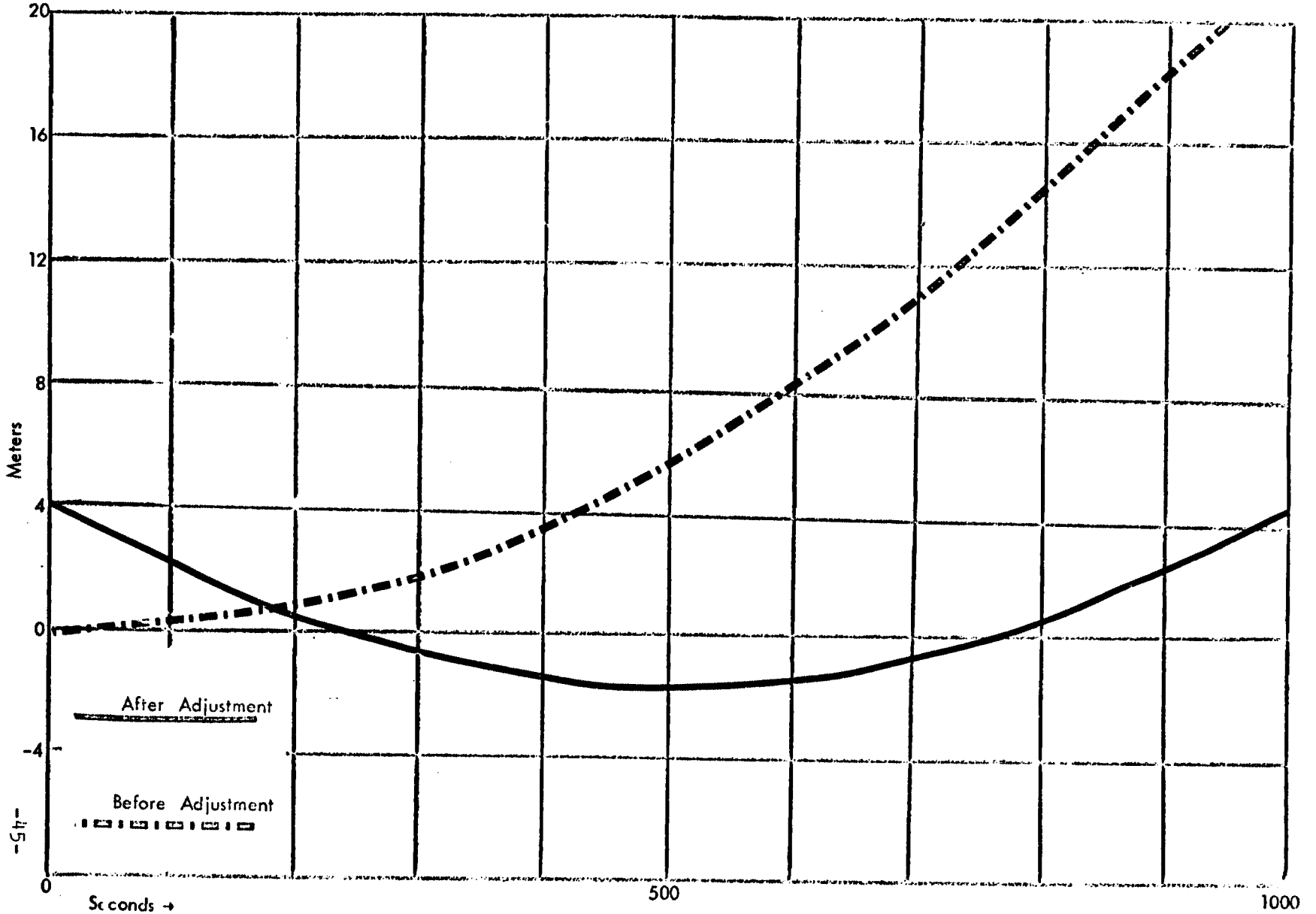

FIGURE 17. Least Squares Adjustment of Coordinates of Center of Mass When Center of Mass Is Not At The Origin. Residuals In X Position Coordinates.

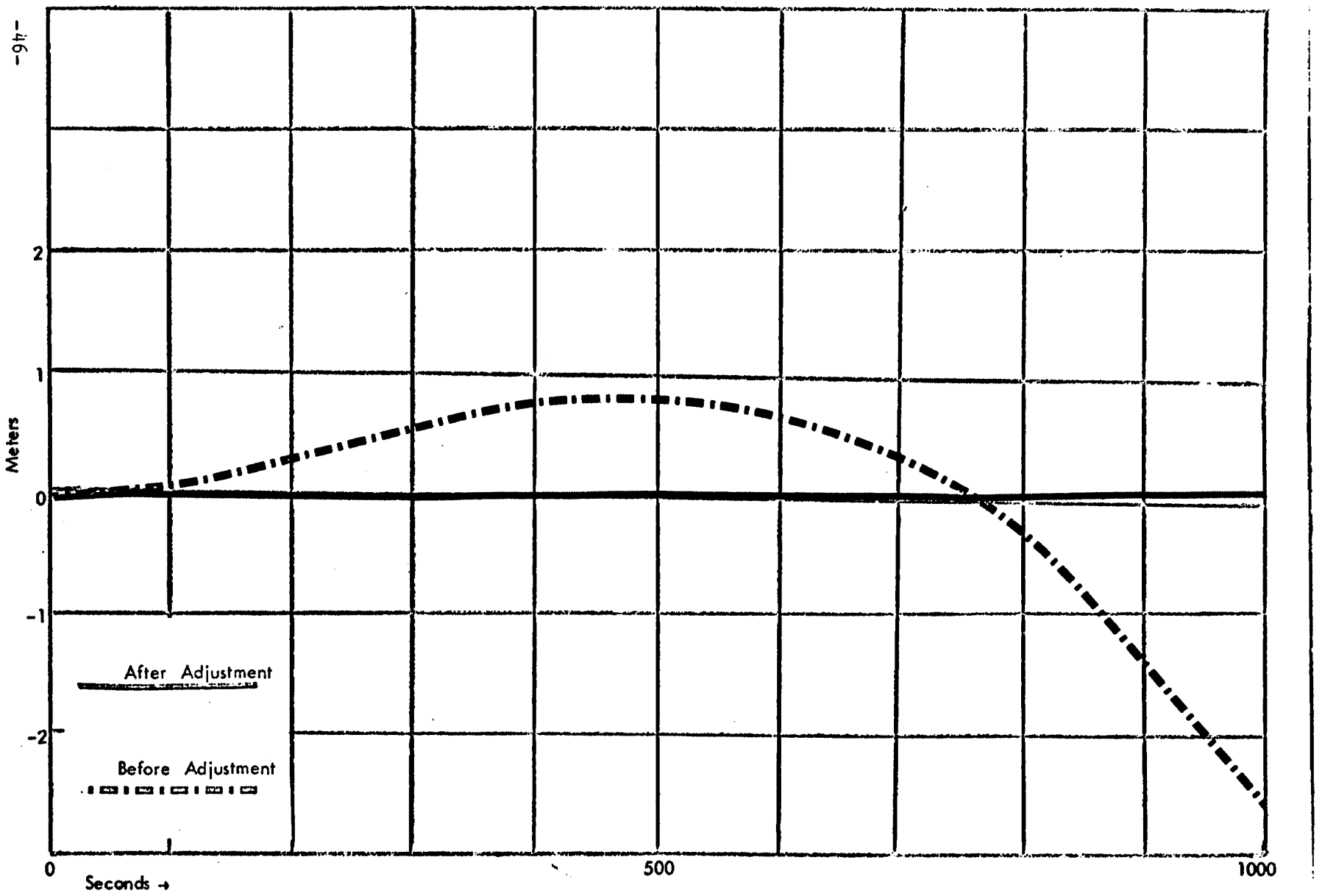

FIGURE 18. Least Squares Adjustment of Coordinates of Center of Mass When Center of Mass Is Not At The Origin. Residuals In Y Position Coordinates.

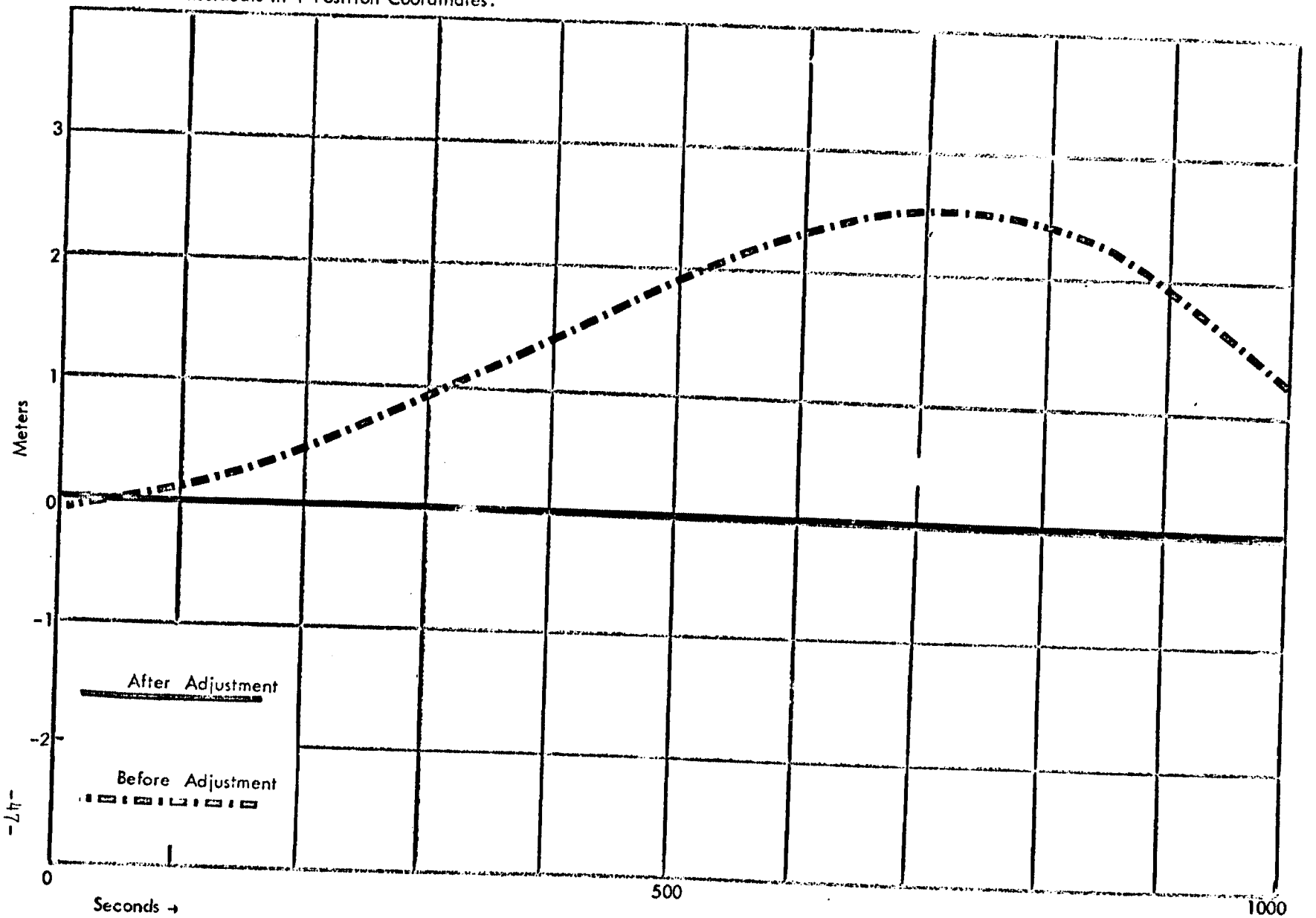

FIGURE 19. Least Squares Adjustment of Coordinates of Center of Mass When Center of Mass Is Not At The Origin. Residuals In Z Position Coordinates.

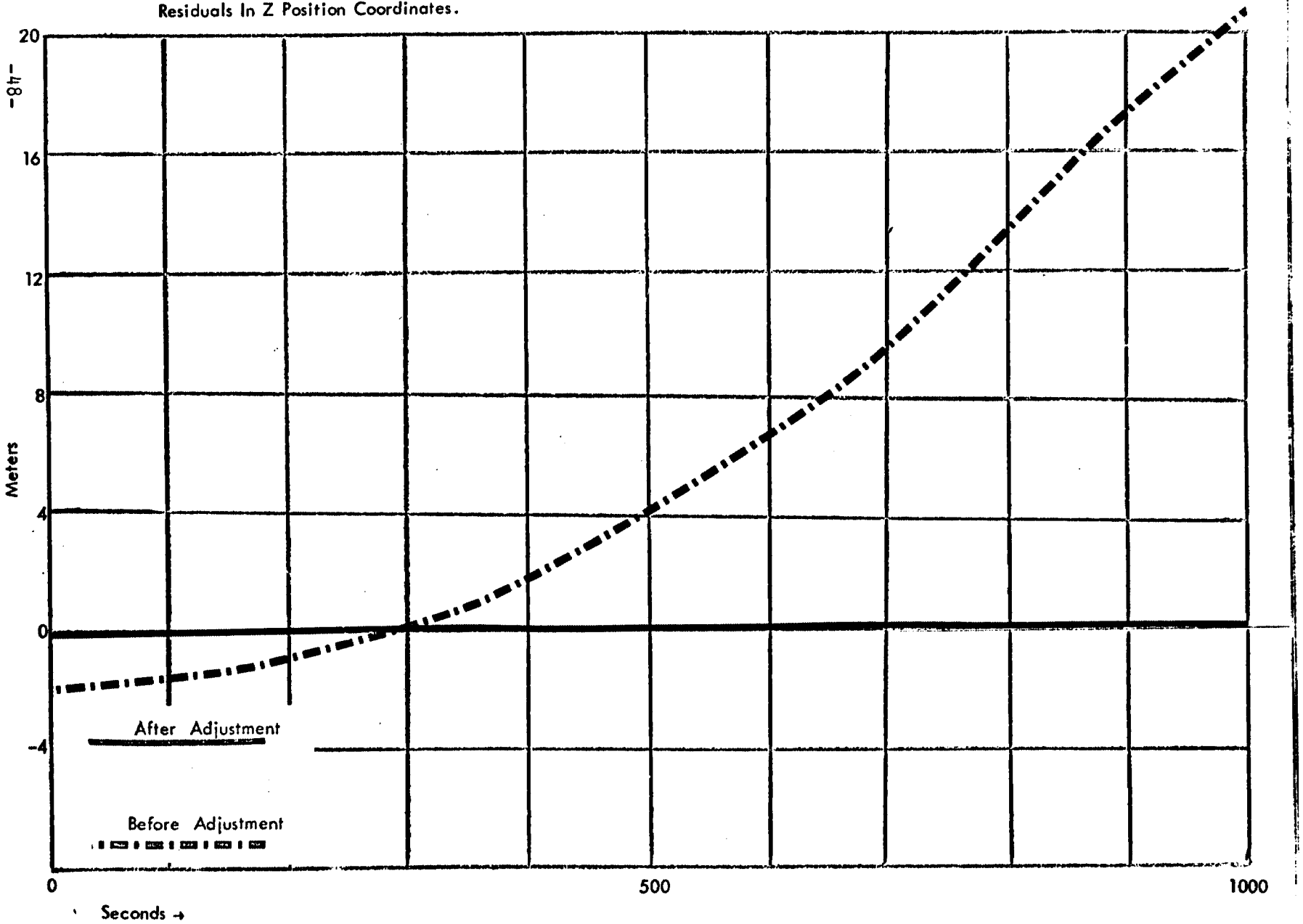

FIGURE 20. Simultaneous Least Squares Adjustment of Wrong Initial Conditions And Wrong Coordinates of Center of Mass. Residuals In X Position Coordinates.

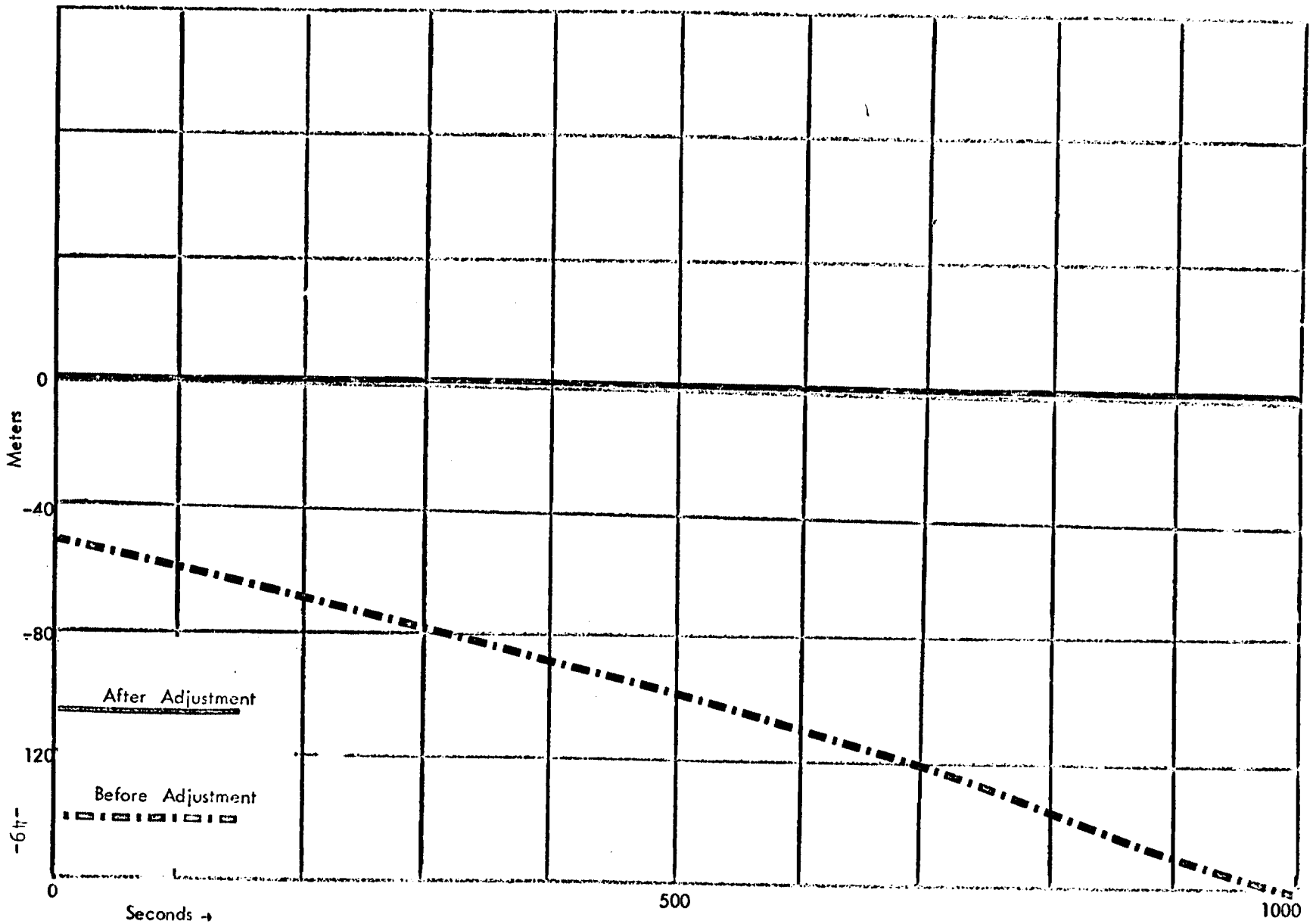

FIGURE 21. Least Squares Adjustment of Initial Conditions to Compensate For Neglecting Perturbing Acceleration of Sun And Moon. Residuals In X Position Coordinates.

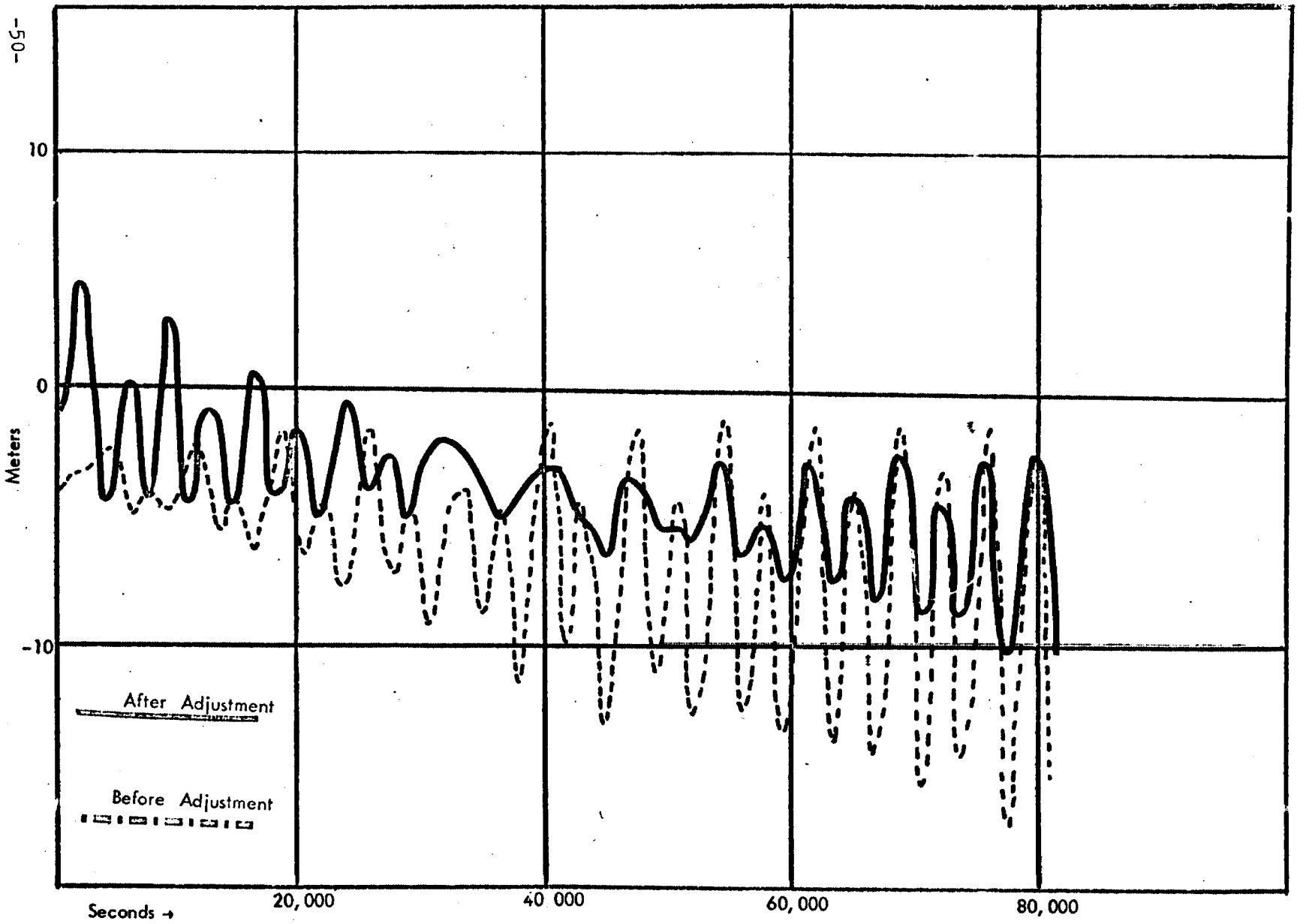

FIGURE 22. Least Squares Adjustment of Initial Conditions to Compensate For Neglecting Perturbing Accelerations of Sun And Moon. Residuals In Y Position Coordinates.

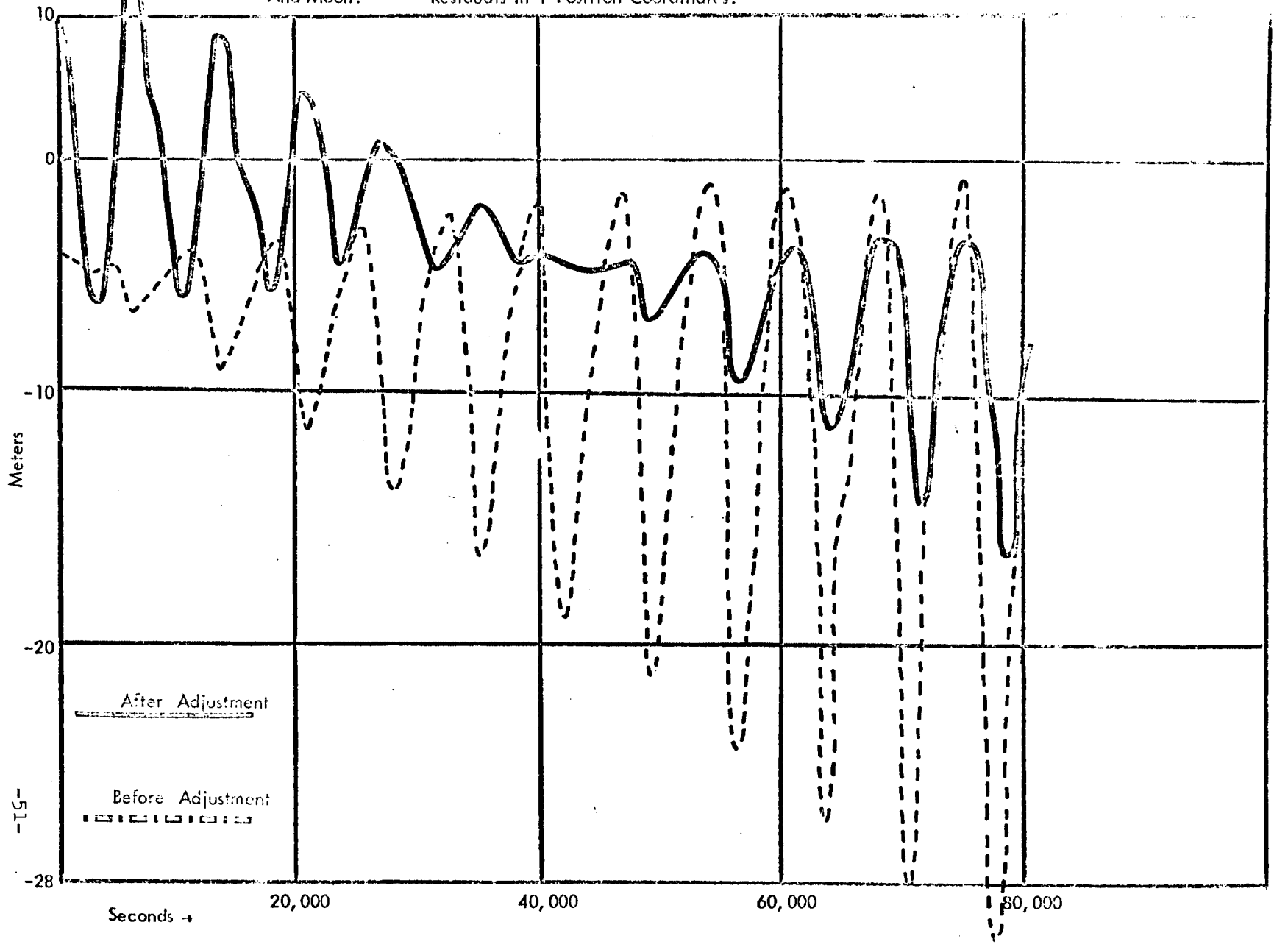

FIGURE 23. Least Squares Adjustment of Initial Conditions to Compensate For Neglecting Perturbing Accelerations of Sun And Moon. Residuals In Z Position Coordinates.

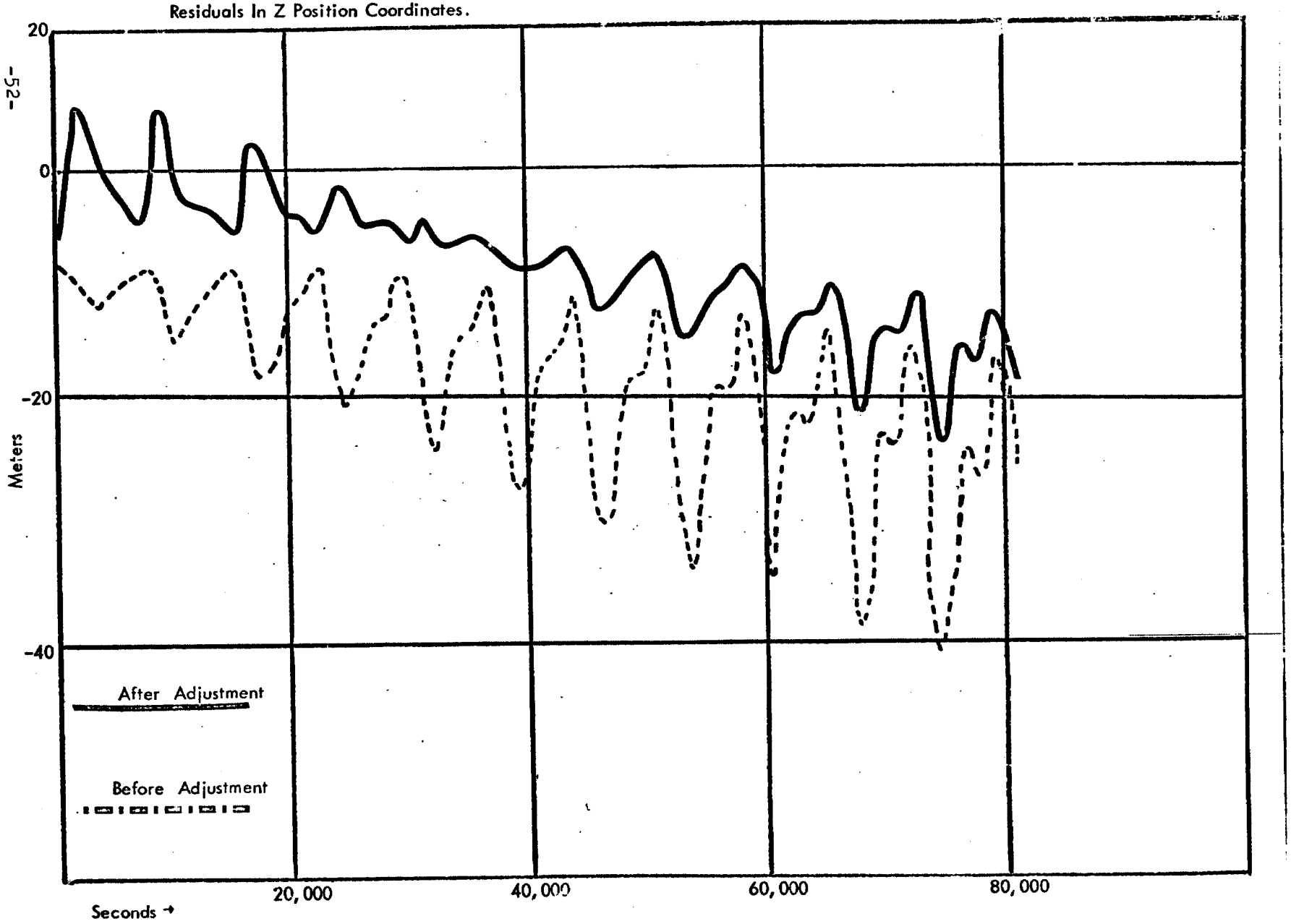

GEODETIC DATA ADJUSTMENT PROGRAM

Paper Presented at the GEOS Review Board Dec. 12-14

By: J. J. Lynn

D. Brown Associates, Inc.
P.O. Drawer 550
Melbourne, Florida 32901

under

NASA CONTRACT NO. NAS 5-9938

GDAP

GDAP, (Geodetic Data Adjustment Program) has been developed by D. Brown Associates, under contract to GSFC for the purpose of reduction and analysis of Geos satellite data. This is an error model adjustment program designed to solve a wide variety of problems belonging to the class of minimum variance statistical estimation. The problem formulation is restricted to problems pertaining to the tracking targets moving relative to some fixed coordinate frame and possibly subject to dynamic constraints imposed by the differential equations of motion due to gravitational force. This class is further restricted to those containing observations in coordinate systems commonly known as range, azimuth, elevation, topocentric right ascension, topocentric declination, direction cosines, range rage azimuth rate, and elevation rate. Statistical information associated with the observations as well as with various other parameters entering into the description of the trajectory data may be entered into the program and processed rigorously subject to certain statistical assumptions. The fundamental assumptions are that the data observations contain random error and systematic error and that the random error has zero mean and contains no cross or serial correlation with errors on other observational data sets.

To be more specific, the problems generally solved by this program can be described as adjustment of multiple sets of tracking observations to determine the geometric position (as a function of time) of a satellite, or the determination of its orbital elements at some arbitrarily chosen epoch. Various other parameters necessary to describe systematic errors which are included in the observational data sets may be estimated. These systematic error model parameters include uncertainties in the location or survey of the tracking instrument, zero set error, timing error, tropospheric refraction errors, scale error, phase drift error, and errors in the positions of the satellite, or in its orbital elements at a given epoch in the case of dynamic constraints.

The program contains many options for various usages. Input observations may be of various types previously described. The program can operate in three general modes: a geometric mode which solves by means of intersections of rays and surfaces, for the

sequence of positions of the staellite; a dynamic mode which solves for the position and velocity of the target at an epoch; and a simulation mode which generates and adjusts aritifical data in either of the two proceeding modes for error propagation studies. Two general forms of problem organization may be employed by the program. The first form which has been know as the EMBET (Error Model Best Estimate of Trajectory) is a single pass form which allows estimation of a set of discrete trajectory points (geometric mode) or of a single set of orbital elements (dynamic mode) along with the error model coefficients to be recovered. An advanced form known as the NEO EMBET from (N-Epoch Orbital EMBET) allows the estimation of the orbital parameters and error model coefficients peculiar to any number of satellite passes over a combination of tracking sites. The NEO EMBET form of solution employs a partitioning algorithm which allows reuse of the computer memory for generation of normal equation solutions for sequential passes, while preserving those portions of the normal equations which apply to all passes. It is by means of this partitioning algorithm of the patterned normal equation matrix into submatrices that the solution of an unlimited problem is made both practical and efficient even on a relatively small computer.

In the course of investigating results from the various tracking instrumentation on the Geos I Satellite , numerous GDAP reductions of four (4) early passes from January 1966 were performed.

At this time, we wish to report some of the results obtained when comparing some of the data obtained by the tracking systems with data from optical instrumentation sources. For the purpose of this intercomparisons, short arc reference orbits based on optical data only were computed. The discrepancies between these reference orbits and the data detained from the radio tracking systems, in the form of measurement residuals, were examined.

The following residuals were noted when no refraction or any other corrections (other than ambiguous) were applied.

	ORBIT 665		ORBIT 677		
HOMSR	65	21	55	22	meters
FTSWR	-	-	67	18	
GRESR	82	25	66	17	
HERSR	62	22	56	15	
ROSGR	46	21	29	12	m/sec.
ROSGD	.017	.06	.015	.013	
APLTD	.062	.13	.109	.10	
LACTD	-	-	-.054	.11	

The cameras used for the reference orbit:

677: SEM PC-1000, HUN PC-1000, JUP PC-1000, JU40 MOTS, JU24 MOTS, MOJM, DENM

665: HUN PC-1000, HOM PC-1000, FTM MOTS, DEN MOTS

orbits were good to 6 meters in pos, 2-3 m/sec in velocity at epoch.

Same further analysis of the available SECOR data indicated the possibility that the given value for the ionospheric refraction correction may be in error by some constant bias. It was then decided to apply a mathematical model to account for ionospheric refraction errors in the SECOR range data, and to also augment the error models to include a zero set and timing error coefficients. The results of these reductions resulted in much smaller SECOR and RARR residuals. In some instances however, a certain systematic trend was still apparent.

Some typical values for the residuals resulting from these reductions ranged from 2 meters RMS and no systematic trend, (in SECOR data), to an RMS value of 12 meters with a pronounced slope on one of the passes examined.

Typical residuals for the RARR system ranged from 10 to 20 meters with an average value of 12 meters for range and about 1 to 2 cm/sec for the range rate. (random in nature) Some constant bias was also indiacated to exist in the range RARR data. This varied from -7 to +23 meters on the four (4) passes in question. A scale or frequency error of 15 ppm was indicated in the range rate data.

Similar reductions were also performed on two other orbits obtained after March 1966. These two (2) orbits were nos. 1408 and 1994.

Secor Range residuals obtained in these two (2) reductions in a short arc orbital mode using optical data for a reference orbit, were examined, both before and after the application of ionospheric refraction corrections as given by the SECOR 2 frequency method. Again there is a strong indication that the given value for ionospheric correction contains a systematic constant bias error. The use of a regression model to recover and remove this possible bias resulted in random range residuals of 2 to 5 meters RMS.

A possible reason for the existence of this constant bias may be due to mis-interpretation of the station reported calibration figures-this should be investigated further.

I would like to point out that in the reduction of SECOR data. ambiguities which are multiples of 256 meters, have been removed prior to subjecting this data to the above comparisons. These ambituities appear in the data presented to us and could present problems if not accounted for properly, especially values of $\pm$ 256 meters.

LASER/GRARR COLLOCATION EXPERIMENT

by

P. A. Maresca

Radio Corporation of America Service Company
9430 Lanham-Severn Road
Scabrook, Maryland 20801

under

NASA CONTRACT NO. NAS5-10600

NAME: Paul A. Maresca

DATE: 13, December 1967

SUBJECT: Geodetic Investigation at GSFC

LASER/GRARR COLLOCATION EXPERIMENT

As part of the Geodetic Earth Orbiting Satellite-I (GEOS-I) Observations Systems intercomparison investigation, several groups of tests were conducted from July 1966 through November 1966 at Rosman, North Carolina. These tests consisted of side-by-side tracking of the GEOS-I spacecraft by the Goddard Range and Range Rate (GRARR) system and the Goddard Laser tracking system. The primary purpose of the collocated tracking was the comparison of the accuracy of the two systems involved. A by product of the intercomparison was the determination of the effectiveness of the Laser as a calibration instrument for electronic tracking systems.

During the five month period in which the Laser was located at Rosman, seventeen satellite passes were tracked by the Laser to be used in the intercomparison. There are several reasons why only seventeen passes were taken. Foremost was the fact that during many of the passes the satellite was not illuminated by the sun while the station was in darkness which was necessary for tracking by the prototype Laser used at Rosman. The weather was an important factor since acquisition and tracking of the satellite was impossible during periods of heavy cloud cover.

Of the seventeen passes, ten were found acceptable for the intercomparison investigation. The procedure used in analyzing the data was to smooth the Laser data using the GEOS Data Adjustment Program (GDAP). This yielded a standard error estimate for the Laser range data and a reference orbit at the selected time of epoch in the form of a cartesian position and velocity vector. Then using the measured GRARR data and the Laser determined orbital elements, GDAP solved for the range zero set error and the range timing error and calculated the standard error estimates for the range and the range measurements. Since the error model capabilities on the version of GDAP used in this analysis were limited, the final set of residuals from GDAP were used as input to a sequential least squares regression program in order to investigate more extensive error models for both range and range rate.

For the GRARR range measurements the average bias error at Rosman was found to be -5.3±2.5 meters. The average timing error was -2.1±1.2 milliseconds. It should be noted that all GRARR passes used in the intercomparison were taken on the high frequency channel and the bias and timing error presented here are representative only of data taken on this channel. A somewhat larger bias seems to be present for data taken on the low frequency channel.

After removal of the bias and timing error from the range data the root mean square (RMS) error of the measurements was 6.8 meters. This is approximately equal to the specified noise inherent in the system. More elaborate error models were fit to the range residuals but in all cases the reduction in RMS was negligible. It was concluded that an error model consisting of a bias term and a timing error term was sufficient to describe the systematic error in the range measurements.

Concerning the large range timing error, it should be pointed out that what is referred to herein as a timing error is simply, for range measurements, the value of the coefficient of range rate in the range error model. This coefficient has the units of seconds of time but since the Laser was synchronized to the GRARR timing pulse to within 100 microseconds it could not have been a true error in timing. Since this large apparent timing error could not be explained as a true timing error or by effects at the ground station, an investigation was initiated into the characteristics of the narrow-band filter which causes most of the time delay of the signal in the GRARR S-band transponder aboard the spacecraft. The results of that investigation will be reported later in this paper.

In order to thoroughly examine various range rate error models three passes were chosen for concentrated analysis. The average RMS value for these three passes was 2.6 cm/sec. A number of error models were fit to the range rate residuals from each of the three passes. The error models were formulated by combining terms whose coefficients represented the following errors: ground transmitter frequency error, range rate timing error, range rate servo lag error, transponder delay error and range rate refraction error. A range rate timing error of -0.2 milliseconds appeared consistently. A large but fairly consistent ground transmitter frequency error of approximately 10 parts per million or 22.7 KHz was noted. About 25 percent of this error has been noted as an actual frequency drift at the ground station. Because of the magnitude of the remaining error, the transmitter frequency error is probably a combination of other systematic effects which have not been isolated. The only other consistent and significant error model term appeared to be what is called the transponder delay term. This is the coefficient of the product of the range rate and range acceleration. The

range rate servo lag error was negligible for all passes while the range rate refraction error term was inconsistent from pass to pass and highly correllated with the transmitter frequency error. The range rate error model consisting of terms representing a timing error, a transmitter frequency error and a transponder delay error reduced the range rate RMS to 1 cm/sec and was considered the most acceptable.

The RMS value for the Laser range measurements was 1.8 meters. A Chi-square test of normality was run on selected passes and none of them were found to be significantly non-normal, and if any systematic effects were present they were negligible. From the intercomparison experiment it appears that Laser defined orbits can be used to detect systematic errors in both range and range rate to 2 meters and 1 cm/sec respectively.

In an effort to find the cause of the apparent range timing error in the GRARR system, the narrow-band filter in the GRARR S-band transponder was modeled. Modeling the filter consists of describing the electrical network with a set of differential equations. This is usually done in a network analysis program such as the Electronic Circuit Analysis Program (ECAP) used in this analysis. When using ECAP, it is necessary only to specify the values of the circuit elements, the circuit topology and the type of analysis desired (AC, DC or transcient).

During the preprocessing of the GRARR range data a correction is applied for the time delay of the signal-through the filter. This correction is in the form of a non-linear curve representing time delay versus doppler frequency. An hypothesis was put forth in a previous document entitled "Intercomparison of Collocated Laser Optical and GRARR Radio Ranging System Tracks on GEOS-I" that a shift of the time delay curve caused by variations in transponder components aboard the spacecraft was the major cause of what appeared to be a range timing error in the orbital fits of the GRARR data. The analysis of the filter was to determine whether or not changes in values of the elements of the filter from their initial valued due to lift-off vibration, solar radiation, aging, etc. could cause such a shift.

The first step in the analysis was to obtain initial values of the circuit elements that matched as closely as possible their actual physical values. Since many of the values associated with filter elements were determined during the module bench test, only approximate or limiting values were available from the schematic diagram of the circuit. Therefore, a number of computer runs were necessary using ECAP to approximate the theoretical amplitude response curve as was done in the actual alignment procedure. The bench test procedure for filter alignment was followed wherever possible. The amplitude response obtained from the model

circuit at the center frequency of 1.4MHz was within 0.01 percent of the theorectical value while at ±40KHz, which is approximately the operating region of GEOS-I, the difference was 10.0 percent.

After obtaining a satisfactory set of elements, an analysis of the effect of perturbations in the values of the circuit elements on the time delay of a signal through the filter was conducted. Each element was perturbed from its initial value by an amount felt to be indicative of changes which could occur on board the spacecraft. The inductors were varied ±2.0 percent, the capacitors ±0.1 percent and the resistors ±0.2 percent. Plots of the time delay versus frequency were made and the results studied.

Changes of ±0.1 percent and ±0.2 percent in the capacitors and resistors respectively, produced negligible effects in the time delay of the simulated signal through the filter. It should be noted that perturbations much greater than those mentioned previously were introduced in the capacitors and resistors in the course of the investigation without appreciably effecting the delay. However, significant changes were observed in the time delay characteristic of the filter when the values of certain inductors were perturbed from their initial values.

A single stage of the two stage filter used in the S-band transponder has three inductors. It was found that changing the values of two of the inductors had a significant effect on the time delay while the effect of varying the third was negligible. When one of the two significant inductors was decreased 2.0 percent in value the time delay curve was shifted in the positive direction along the frequency axis approximately 5KHz while a 2.0 percent decrease in the second, shifted the curve in the same direction 10KHz. In both cases an increase of 2.0 percent shifted the curve in the negative direction. For the first inductor the shift was about 2KHz while the shift for the second was 8KHz. When both inductors were perturbed simultaneously by ±2.0 percent the shifts were in the same direction as described previously. For a 2.0 percent decrease in value the shift was 13KHz and for a 2.0 percent increase the shift was 10KHz.

These results indicate that changes in the values of circuit elements, especially inductors, can cause a shift in the transponder delay curve. If such a shift occurs and is not taken into account in the preprocessing of GRARR range data, the effect in an orbital fit using the data would be an apparent range timing error. The magnitude of the shifts caused by ±2.0 percent perturbations in the circuit inductors does not fully account for the -2.1 millisecond range timing error noted in the intercomparison investigation but it is felt that changes greater than ±2.0 percent could conceivably occur in the inductor values during the life of GEOS-I.

GRAVITY MODEL COMPARISON USING GEOS-I LONG ARC ORBITAL SOLUTIONS

Francis J. Lerch
James G. Marsh

Mission and Trajectory Determination Branch
Mission and Trajectory Analysis Division
Tracking and Data Systems Directorate

GODDARD SPACE FLIGHT CENTER

Brian O'Neill

Wolf Research and Development Corporation
Applied Sciences Department
College Park, Maryland

under

NASA CONTRACT NAS5-9756

December 1967

Goddard Space Flight Center
Greenbelt, Maryland

SUMMARY

This report presents some of the results obtained from satellite tracking data using three different sets of coefficients in the mathematical model that describes the earth's gravitational field. The results were not intended to be used as a definitive evaluation of the different coefficients but as an assessment of the effects that different coefficients, station coordinates, and earth parameters that have been published, have on orbital geodetic results.

The orbital solutions were primarily estimated from optical tracking data from the GEOS-I satellite, taken by five major geodetic optical tracking networks. The networks and camera types consisted of the SAO Baker-Nunn, GSFC STADAN and SPEOPT MOTS 40" and 24", USAF PC-1000, and the US C&GS BC-4. The three sets of gravity coefficients used were the SAO M-1 set, APL 3.5 set, and the NWL 5E-6 set. The semi-major axis, gravitational constant, and flattening consistent with each set of coefficients were also used. The station coordinates used were referenced to the SAO C-5 standard earth as no other complete set of optical station coordinates were available.

Several long arc orbital analyses were completed using each set of coefficients and the results were compared. Orbits were fitted to two overlapping data sets; the arc lengths of these orbits were 5-1/2 days and 1 day. The orbital solutions obtained with each set of coefficients were compared. Furthermore, the trajectory differences were computed, and the along track differences were as great as 400 meters for the 5-1/2 day arc and 200 meters for the 1 day arc.

Two estimates of the coordinates for the Goddard Range and Range Rate station in Tananarive, Madagascar were obtained from independent data sets using each set of coefficients. Only the SAO M-1 set produced two estimates that were consistent; they differed by only 5 meters.

These comparisons serve to reinforce what was intuitively obvious -- that for long arc geodetic work, the most complete set of gravity coefficients together with consistent station coordinates should be used.

TABLE OF CONTENTS

APPENDICES

1.0 INTRODUCTION

This report presents some results that have been obtained from satellite tracking data using three different sets of coefficients in the mathematical model that describes the earth's gravitational field. These comparisons were not intended as an evaluation of the coefficients but as an assessment of the effects of using the different sets in order to choose the most suitable available set of gravity coefficients and station coordinates for long arc (greater than 6 revolutions) geodetic purposes.

These results were obtained using the orbit determination program NONAME [1], and the orbital solutions were estimated from optical tracking data taken from the GEOS-I satellite. The NONAME program uses a mathematical function based on Legendre polynomials to approximate the earth's gravitational field [Appendix A-1]. Several sets of coefficients for these polynomials have been published; three of these sets were used for this work; they are:

1. The SAO M-1 Set [2],

2. The APL 3.5 Set [3],

3. The NWL 5E-6 Set [4].

These are summarized in Table II.

For the purposes of these comparisons, the semi-major axis, gravitational constant, and flattening that are consistent with each set of coefficients were used. These are summarized in Table I. The station coordinates were unchanged and were referenced to the SAO C-5 standard earth [Appendix A-3], this was because no other complete set of coordinates for the optical tracking stations was available.

The use of only the one set of station coordinates prevents these results being used as any sort of definitive evaluation of these sets of gravity coefficients. It should be noted, however,that the ellipsoids defined by the parameters in Table I are very similar; thus the station coordinates, if they are fairly accurately determined with reference to the center of mass, as the SAO C-5 coordinates are generally accepted to be, should not introduce any large differences in the results.

Several long arc analyses were completed using each set of coefficients in turn, and the results have been compared; these are discussed in some detail in Sections 3.0 - 6.0.

2.0 DESCRIPTION OF THE EARTH'S GRAVITATIONAL FIELD

The earth's geopotential can be approximated by the following mathematical model:

$$u = \frac{GM}{r}\left\{1 + \sum_{n=2}^{k}\sum_{m=0}^{n}\left(\frac{a}{r}\right)^n P_n^m\left(\sin\phi\right)\left[C_{nm}\cos m\lambda + S_{nm}\sin m\lambda\right]\right\} \quad (1)$$

where

G is the universal gravitational constant,

M is the mass of the earth,

r is the geocentric satellite distance,

a is the earth's mean equatorial radius,

ϕ is the sub-satellite latitude,

λ is the sub-satellite east longitude,

$P_m^n\left(\sin\phi\right)$ are the associated Legendre polynomials of degree n and order m,

and

C_{nm}, S_{nm} are the denormalized gravitational coefficients.

The geopotential formulated in this manner can be converted into gravitational accelerations in inertial coordinates (x, y, z) as follows:

$$\ddot{x}_o = \frac{\partial u}{\partial r}\frac{\partial r}{\partial x} + \frac{\partial u}{\partial \phi}\frac{\partial \phi}{\partial x} + \frac{\partial u}{\partial \lambda}\frac{\partial \lambda}{\partial u} ,$$

where the subscript "o" denotes accelerations due to the earth's gravitational field. Similar expressions hold for y_o and z_o. The NONAME program uses a model in this form to compute the accelerations due to the earth's gravitational field.

The three different sets of harmonic coefficients (normalized) and associated earth parameters used in this analysis are shown in Tables I and II. The SAO M-1 is the largest set with a total of 122 coefficients; the APL 3.5 set has 84 coefficients and the NWL 5E-6 set has 64. Of these three sets, only the SAO M-1 set has GEOS-I resonant terms (harmonics of order 12).

The SAO M-1 set was determined using optical observations from a number of satellites, and the other two sets were determined from Doppler observations, again from a number of satellites.

The geopotential formulated in this manner can be converted into gravitational accelerations in inertial coordinates (x, y, z) as follows:

$$\ddot{x}_{\oplus} = \frac{\partial u}{\partial r}\frac{\partial r}{\partial x} + \frac{\partial u}{\partial \phi}\frac{\partial \phi}{\partial x} + \frac{\partial u}{\partial \lambda}\frac{\partial \lambda}{\partial u} ,$$

where the subscript "$\oplus$" denotes accelerations due to the earth's gravitational field.

Similar expressions hold for $\ddot{y}_{\oplus}$ and $\ddot{z}_{\oplus}$.

The NONAME program uses a model of this form to compute the accelerations due to the earth's gravitational field.

TABLE I

PARAMETERS FOR THE EARTH'S ELLIPSOID

PARAMETER \ MODEL	SAO M-1	APL 3.5	NWL 5E-6
GRAVITATIONAL CONSTANT (KM^3/SEC^2)	3.986032 x 10"	3.986075 x 10"	3.9860542 x 10"
SEMI-MAJOR AXIS (KM)	6378.165	6378.166	6378.165
FLATTENING	$\frac{1.}{298.25}$	$\frac{1.}{298.30}$	$\frac{1.}{298.25}$

TABLE II

HARMONIC COEFFICIENTS (NORMALIZED)

		SAO M1		APL 3.5		NWL 5E-6	
n	m	$\bar{C} \times 10^6$	$\bar{S} \times 10^6$	$\bar{C} \times 10^6$	$\bar{S} \times 10^6$	$\bar{C} \times 10^6$	$\bar{S} \times 10^6$
2	0	-484.1735		-484.198		-484.194	
2	1					0.016	0.062
2	2	2.379	-1.351	2.381	-1.198	2.446	-1.519
3	0	0.9623		1.011		0.984	
3	1	1.936	0.266	1.84	0.215	2.148	0.274
3	2	0.734	-0.538	1.219	-0.6791	0.978	-0.906
3	3	0.561	1.620	0.6609	0.9795	0.585	1.625
4	0	0.5497		0.467		0.507	
4	1	-0.572	-0.469	-0.5624	-0.4403	-0.495	-0.575
4	2	0.330	0.661	0.4179	0.4438	0.274	0.671
4	3	0.851	-0.190	0.8464	0.007062	1.030	-0.247
4	4	-0.053	0.230	-0.2106	0.1898	-0.413	0.336
5	0	0.0633		0.084		0.045	
5	1	-0.079	-0.103	0.1370	-0.1669	0.032	-0.119
5	2	0.631	-0.232	0.2684	-0.3379	0.637	-0.328
5	3	-0.520	0.007	0.09131	0.1035	-0.389	-0.124
5	4	-0.265	0.064	-0.4884	-0.260	-0.549	0.148
5	5	0.156	-0.592	-0.03358	-0.6686	0.215	-0.594

TABLE II (cont'd)

		SAO M1		APL 3.5		NWL 5E-6	
n	m	$\bar{C} \times 10^6$	$\bar{S} \times 10^6$	$\bar{C} \times 10^6$	$\bar{S} \times 10^6$	$\bar{C} \times 10^6$	$\bar{S} \times 10^6$
6	0	-0.1792		-0.103		-0.219	
6	1	-0.047	-0.027	-0.0002093	0.1009	-0.085	0.192
6	2	0.069	-0.366	-0.1610	-0.1555	0.129	-0.457
6	3	-0.054	0.031	0.5303	0.05111	-0.020	-0.134
6	4	-0.044	-0.518	-0.3069	-0.5087	-0.193	-0.316
6	5	-0.313	-0.458	-0.18	-0.5091	-0.093	-0.786
6	6	-0.040	-0.155	0.01434	-0.2316	-0.324	-0.360
7	0	0.0860		0.153		0.105	
7	1	0.197	0.156	0.1261	0.09355	0.331	0.083
7	2	0.364	0.163	0.4586	0.05998	0.350	-0.195
7	3	0.250	0.018	0.3938	-0.2067	0.323	0.045
7	4	-0.152	-0.102	-0.1368	0.0004798	-0.467	-0.244
7	5	0.076	0.054	-0.05682	-0.1871	0.055	0.021
7	6	-0.209	0.063	-0.4552	0.758	-0.477	-0.244
7	7	0.055	0.096	0.08840	-0.1443		
8	0	0.0655		0.170			
8	1	-0.075	0.065	-0.1481	-0.04843		
8	2	0.026	0.039	0.09472	-0.03764		
8	3	-0.037	0.004	-0.05497	0.2168		
8	4	-0.212	-0.012	-0.06901	0.03761		

TABLE II (cont'd)

n	m	SAO M1		APL 3.5		NWL 5E-6	
		$\bar{C} \times 10^6$	$\bar{S} \times 10^6$	$\bar{C} \times 10^6$	$\bar{S} \times 10^6$	$\bar{C} \times 10^6$	$\bar{S} \times 10^6$
8	5	-0.053	0.118	0.08040	-0.002495		
8	6	-0.017	0.318	-0.02193	0.6658		
8	7	-0.0087	0.031	0.1697	-0.07009		
8	8	-0.248	0.102	-0.1457	0.09424		
9	0	0.0122		0.041			
9	1	0.117	0.012				
9	2	-0.0040	0.035				
10	00	0.0118					
10	01	0.105	-0.126				
10	02	-0.105	-0.042				
10	03	-0.065	0.030				
10	04	-0.074	-0.111				
11	00	-0.0630		0.104			
11	01	-0.053	0.015				

TABLE II (cont'd)

		SAO M1		APL 3.5		NWL 5E-6	
n	m	$\bar{C} \times 10^6$	$\bar{S} \times 10^6$	$\bar{C} \times 10^6$	$\bar{S} \times 10^6$	$\bar{C} \times 10^6$	$\bar{S} \times 10^6$
12	00	0.0714		0.062			
12	01	-0.163	-0.071				
12	02	-0.103	-0.0051				
12	12	-0.031	0.0008				
13	00	0.0219					
13	12	-0.059	0.050				
13	13	-0.059	0.077	-0.4689	0.04748	-0.03	0.11
14	00	-0.0332					
14	01	-0.015	0.0053				
14	11	0.0002	-0.0001				
14	12	0.094	-0.028				
14	14	-0.014	-0.003	-0.06368	-0.037		
15	09	-0.0009	-0.0018				
15	12	-0.0619	0.0578				
15	13	-0.058	-0.046			-0.06	-0.06
15	14	0.0043	-0.0211	0.00087843	-0.0101	0.01	-0.03

3.0 DIFFERENCES IN ORBITAL SOLUTIONS

Orbits were fitted to two data sets from the first week in January 1966, and the arc lengths of these orbits were 5 1/2 days and 1 day. The 5 1/2 day arc covered the period from 01 hrs GMT on December 31, 1965 to 06 hrs, January 5, 1966, and the data set consisted of 1057 optical observations. The 1 day arc covered the period from 06 hrs, January 2, 1966, to 08 hrs, January 3, 1966, and the data was a subset of the 5 1/2 day arc data set and consisted of 444 optical observations. These data sets are summarized in Table III.

The root mean squares of the observations about the orbital solutions were computed and these are shown in Table IV . The rms values were lower for the orbits fitted using the SAO M-1 set for both arcs. The differences between the observed measurements and values computed from the orbital solutions were computed and plotted on histograms; these are shown in Figure 1-4. These figures clearly indicate that the orbital solution obtained with the SAO M-1 set of coefficients fits the data sets better than the other solutions. The right ascension residuals shown in these figures have been multiplied by the cosine of the corresponding declination measurement in order to make them homoscedastic.

TABLE III

SUMMARY OF OPTICAL MEASUREMENTS BY STATION

NETWORK	STATION	CAMERA TYPE	NO. OF OBSERVATIONS	
			5 1/2 DAY ARC	1 DAY ARC
SAO	1ORGAN	BAKER-NUNN	2	
	1JUPTR	BAKER-NUNN	26	26
	1NATOL	BAKER-NUNN	8	2
	OSLONR	BAKER-NUNN	4	
	AUSBAK	BAKER-NUNN	4	
	1SHRAZ	BAKER-NUNN	2	2
	1SPAIN	BAKER-NUNN	6	
	1TOKYO	BAKER-NUNN	12	4
	1VILDO	BAKER-NUNN	2	
	1MAUID	BAKER-NUNN	2	
	AGASS1	GEODETIC 36"	10	
	TOTAL:		78	34
SPEOPT	1COLBA	MOTS 40"	164	71
	1JUM40	MOTS 40"	22	16
	1BERMD	MOTS 40"	84	36
	1PUR10	MOTS 40"	14	
	1DENVR	MOTS 40"	70	14
	1JUM24	MOTS 24"	26	24
	TOTAL:		380	158
STADAN	1FTMYR	MOTS 40"	82	54
	1BPOIN	MOTS 40"	53	
	1GFORK	MOTS 40"	26	9
	1MOJAV	MOTS 40"	25	25
	TOTAL:		186	91

TABLE III(cont'd)

NETWORK	STATION	CAMERA TYPE	NO. OF OBSERVATIONS	
			5 1/2 DAY ARC	1 DAY ARC
USAF	HUNTER	PC-1000	59	47
	SWANIS	PC-1000	14	14
	GRDTRK	PC-1000	7	
	ANTIGA	PC-1000	26	
	SEMMES	PC-1000	60	36
	CURACO	PC-1000	40	26
	HOMEST	PC-1000	94	24
	JUPRAF	PC-1000	17	17
	BEDFRD	PC-1000	22	
	ABERDN	PC-1000	74	
	TOTAL:		413	164

TABLE IV

ROOT MEAN SQUARES ABOUT THE ORBITAL SOLUTION

ARC LENGTH	R.M.S. OF FIT (SECS OF ARC)		
	SAO M-1	APL 3.5	NWL 5E-6
5 1/2 day	3.08	11.14	11.01
1 day	2.33	2.50	4.54

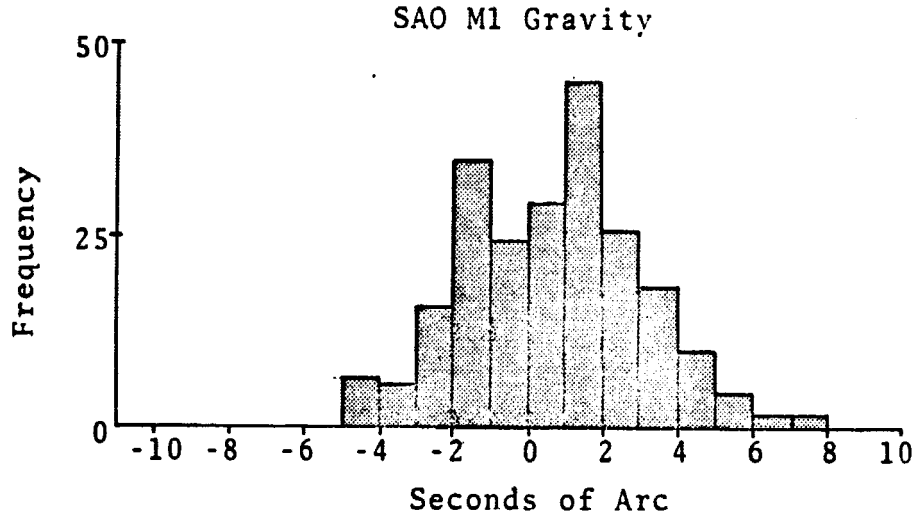
SAO M1 Gravity
50
25
0
Frequency
-10 -8 -6 -4 -2 0 2 4 6 8 10
Seconds of Arc

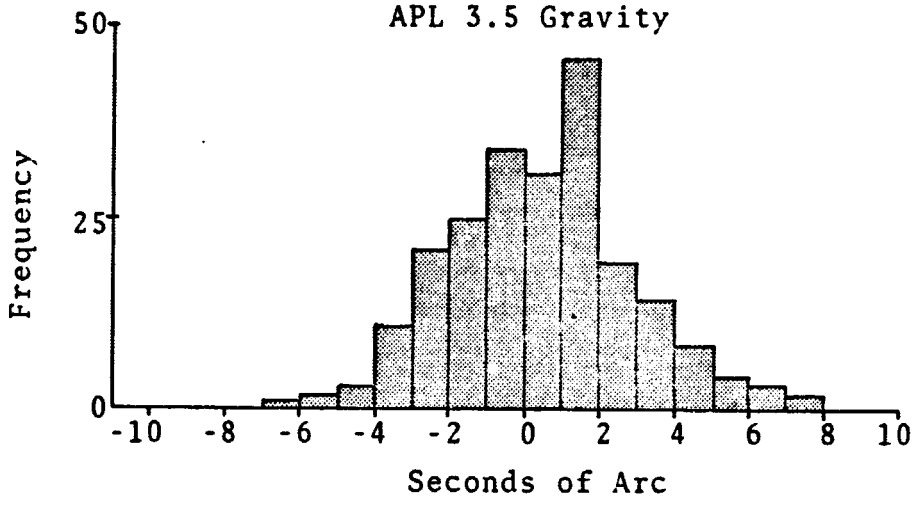
APL 3.5 Gravity
50
25
0
Frequency
-10 -8 -6 -4 -2 0 2 4 6 8 10
Seconds of Arc

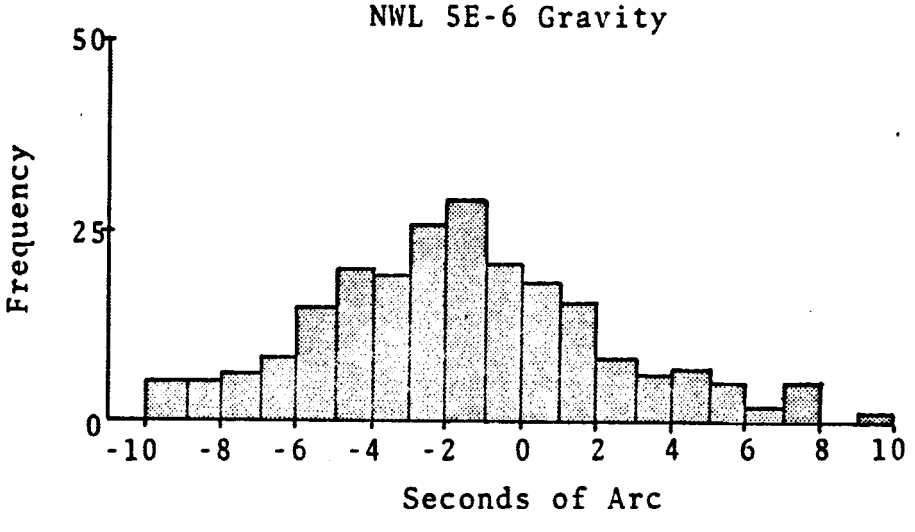
NWL 5E-6 Gravity
50
25
0
Frequency
-10 -8 -6 -4 -2 0 2 4 6 8 10
Seconds of Arc

FIG. 1

Declination Residuals from 1 Day Arc

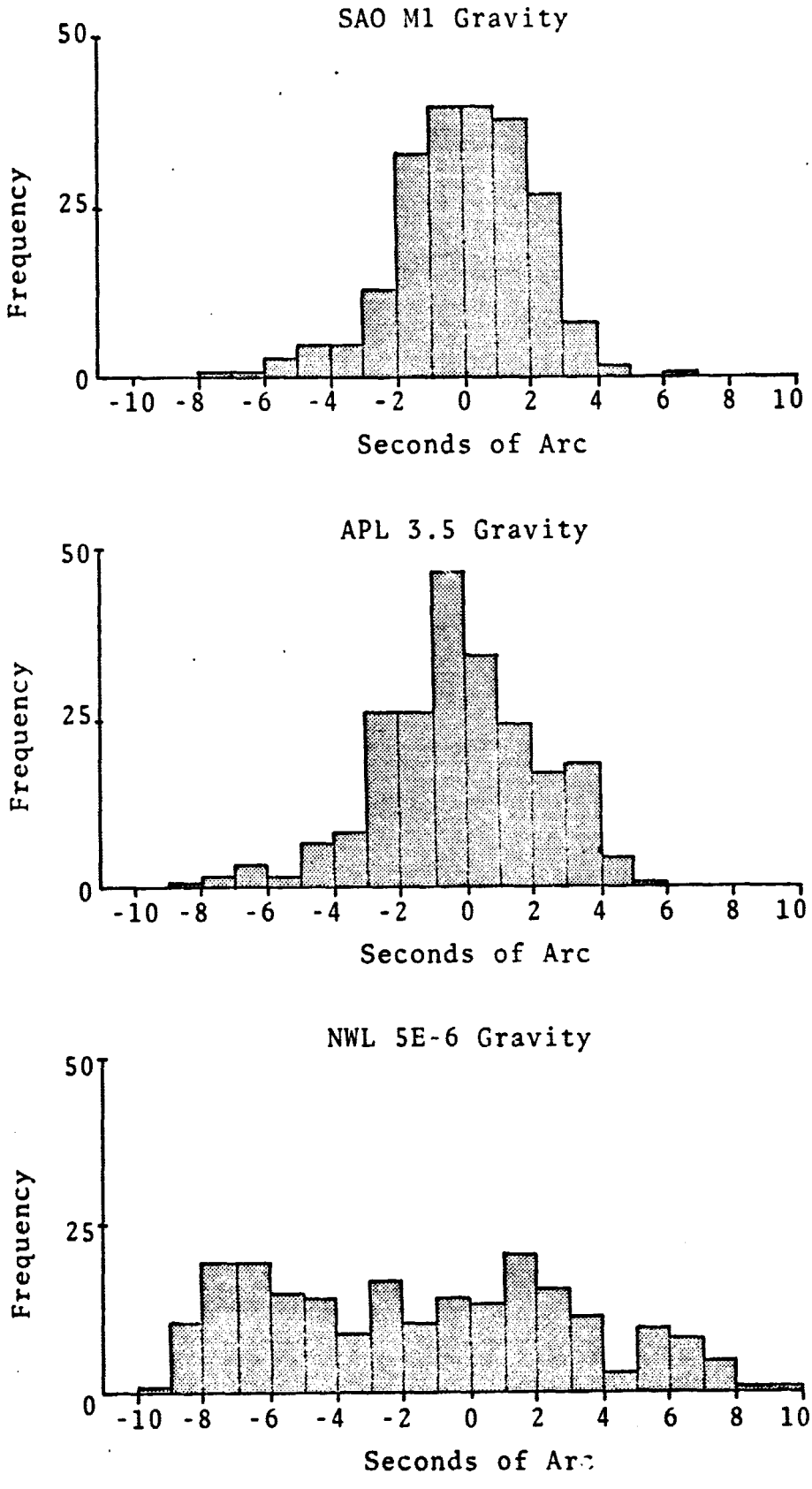

FIG. 2

Right Ascension Residuals from $5\frac{1}{2}$ Day Arc

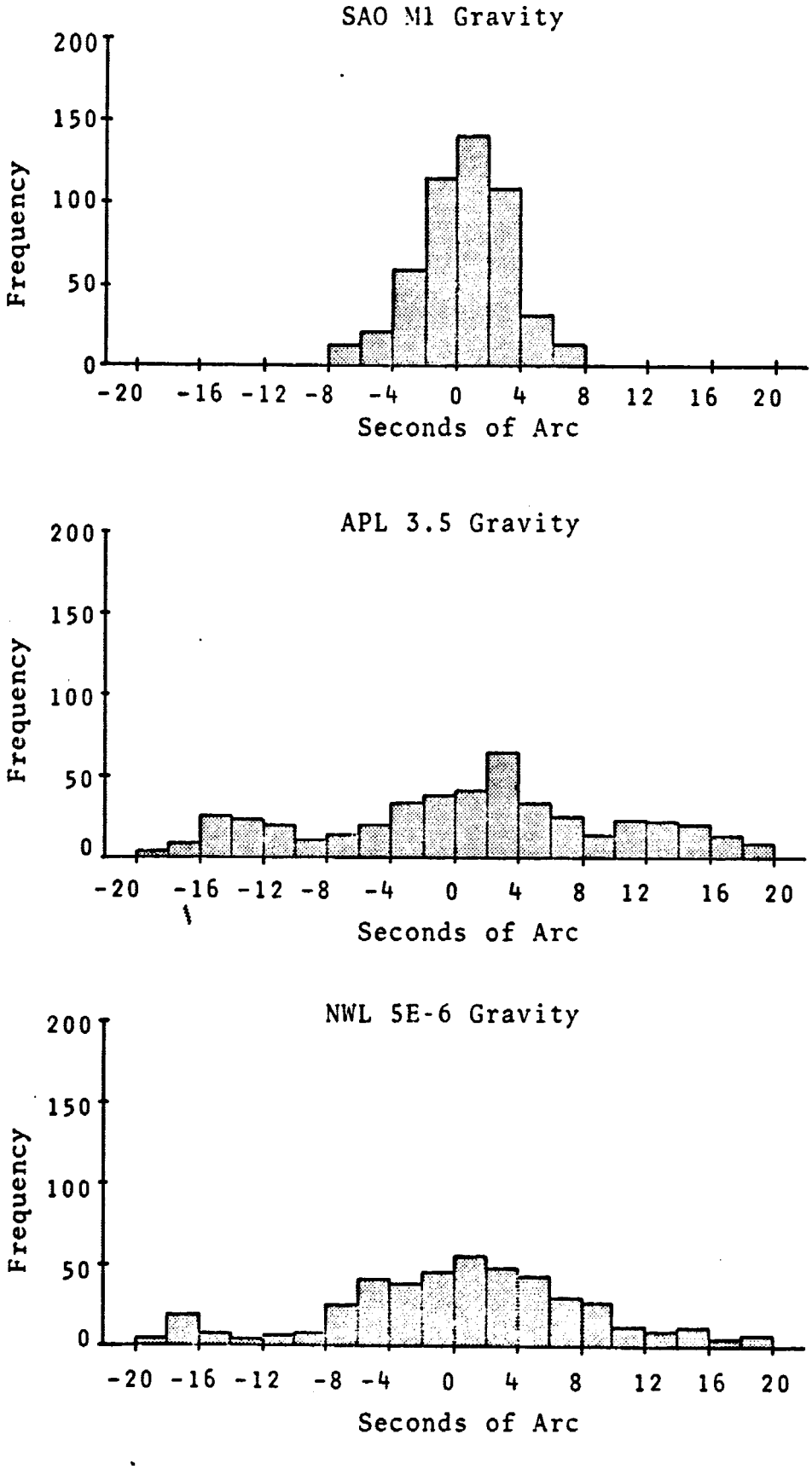

FIG. 3

Declination Residuals from $5\frac{1}{2}$ Day Arc

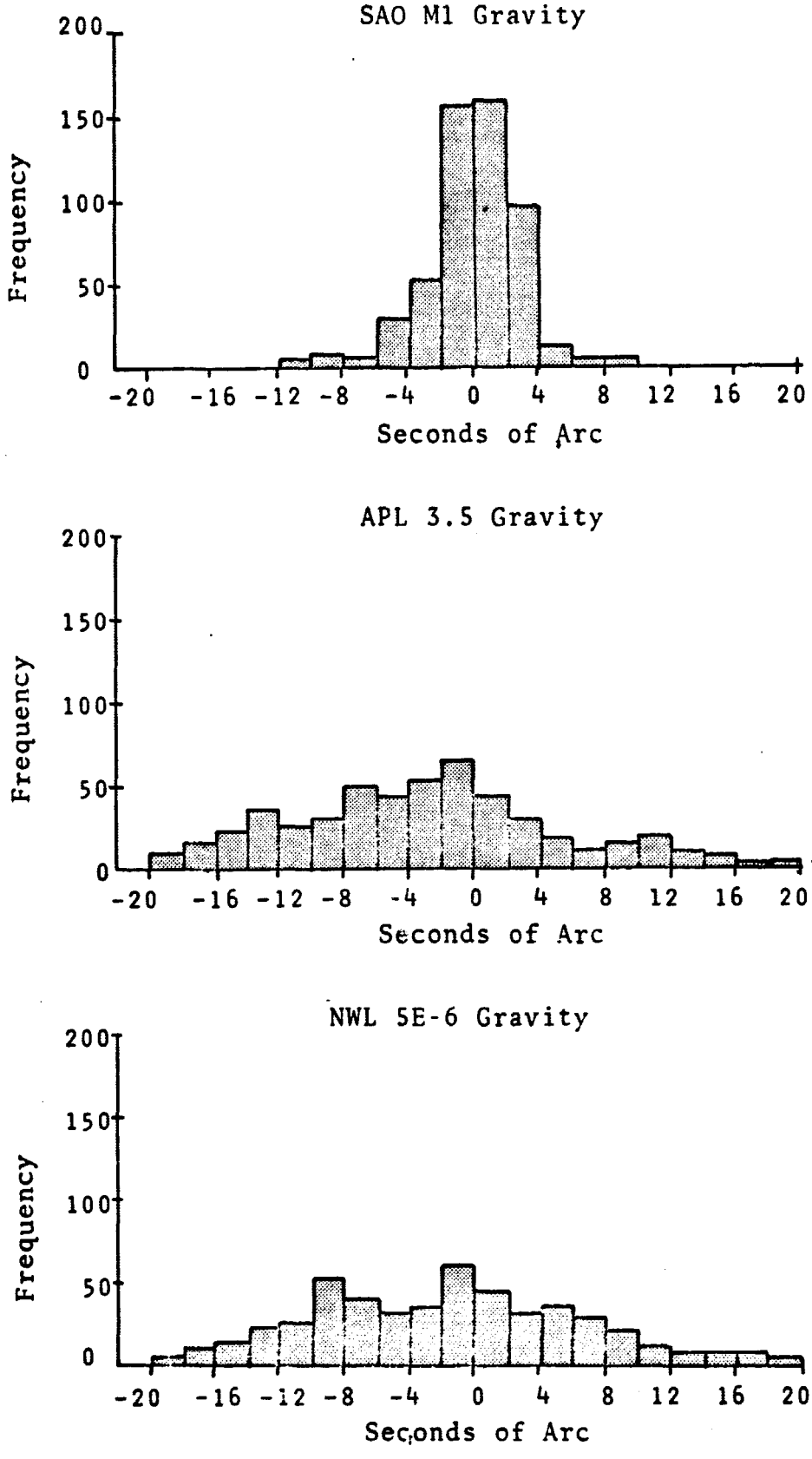

FIG. 4

4.0 TRAJECTORY DIFFERENCES

The along track, cross track, and radial differences between the orbital solutions discussed in Section 3.0 were computed. The differences between the orbital solutions obtained using the SAO M-1 set and the other two sets are shown in Figures 5-8.

The along track differences were the largest. They were as large as 400 meters for the 5 1/2 day arc and 200 meters for the 1 day arc. The differences have a period approximately equal to the period of the satellite (2 hrs), and, in addition, the along track differences have some other long period associated with them. The periods of the along track, cross track, and radial differences are not in phase, and in general, the minima occur where there is good data coverage; this is shown by the solid blocks in the figures.

DIFFERENCES BETWEEN TRAJECTORIES OBTAINED FROM SAO M1 AND APL 3.5 GRAVITY MODELS
1 DAY ARC

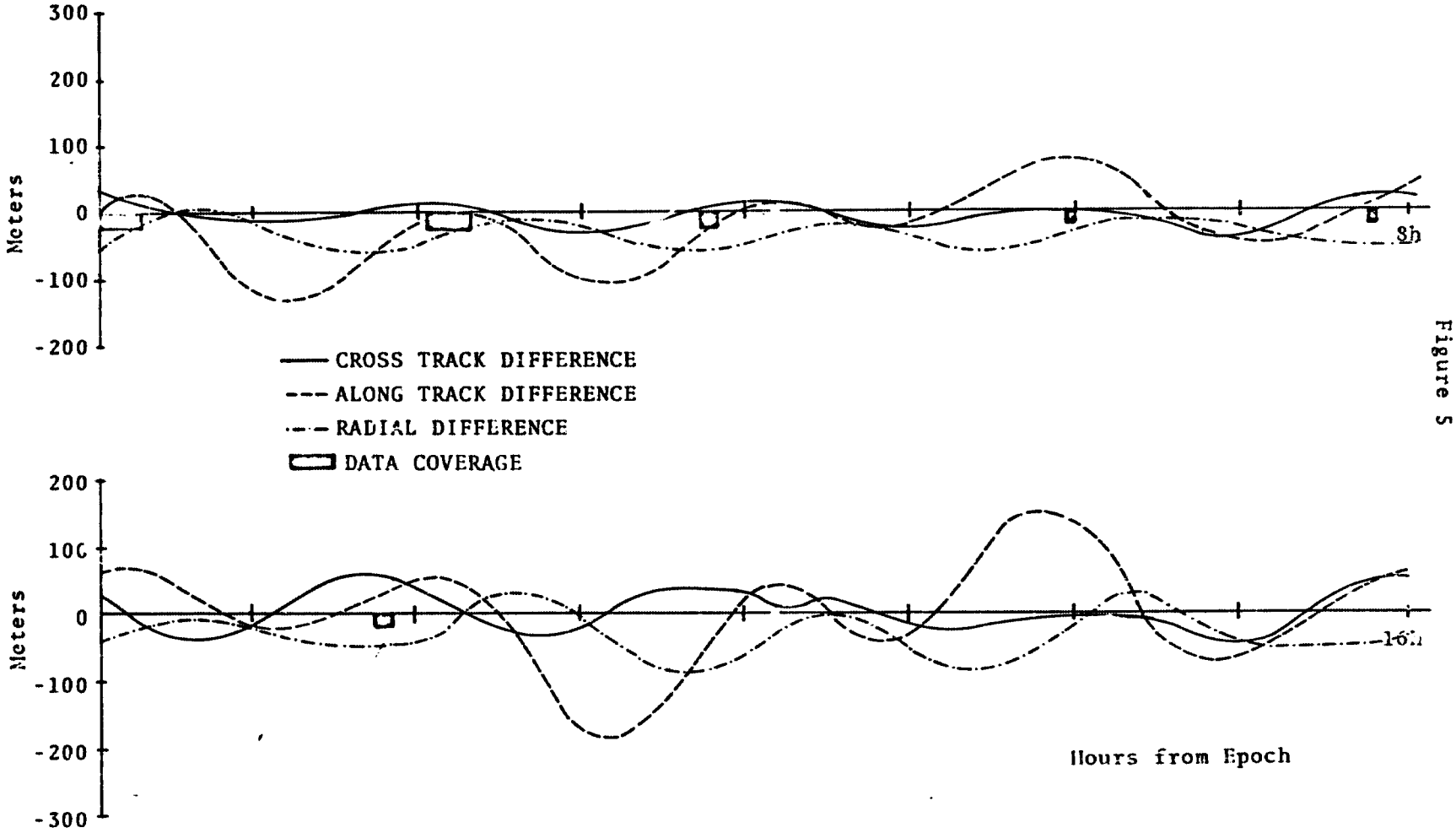

Figure 5

DIFFERENCES BETWEEN TRAJECTORIES OBTAINED FROM SAO M1 AND APL 3.5 GRAVITY MODELS
1 DAY ARC

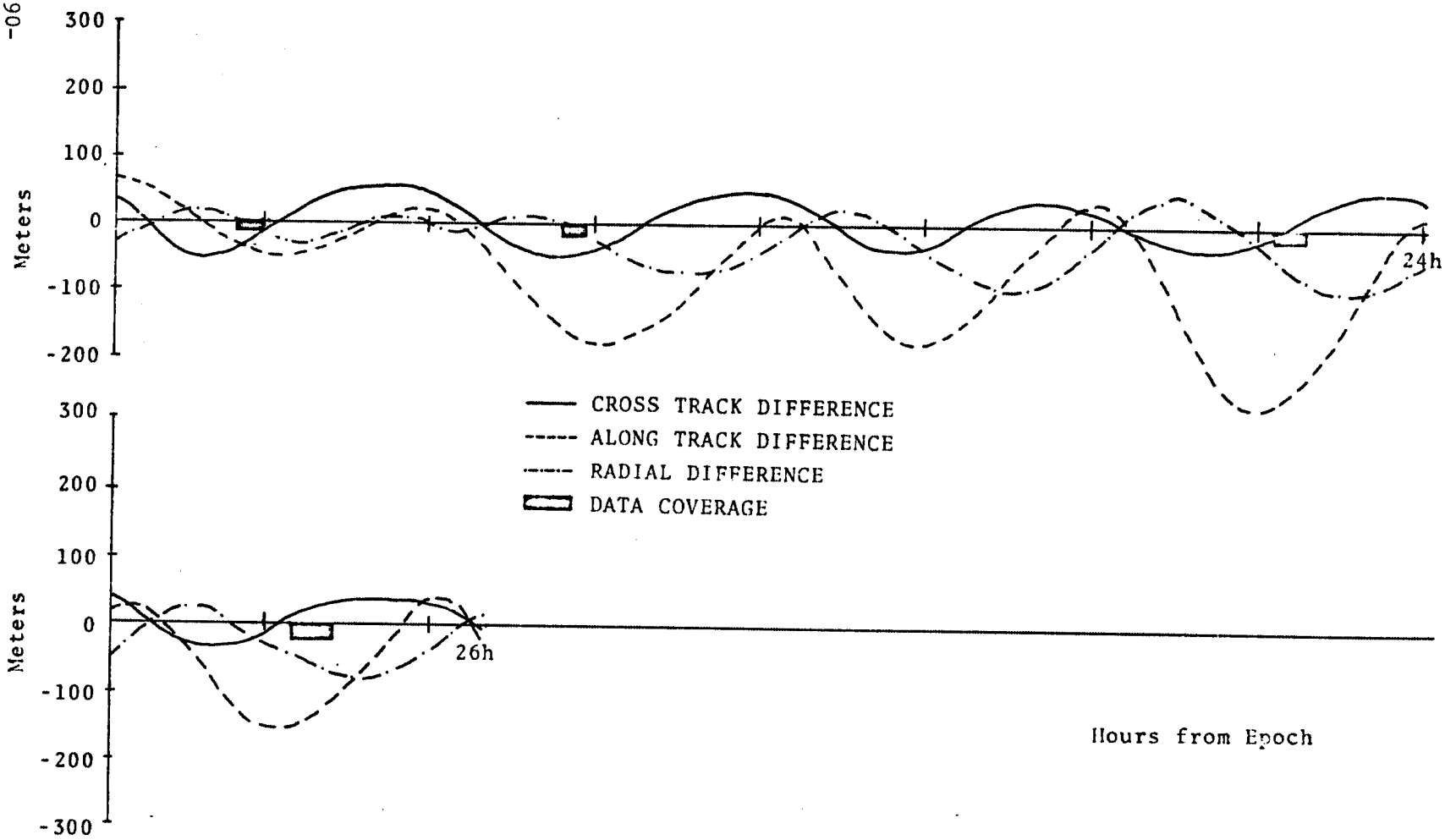

Figure 5 (cont)

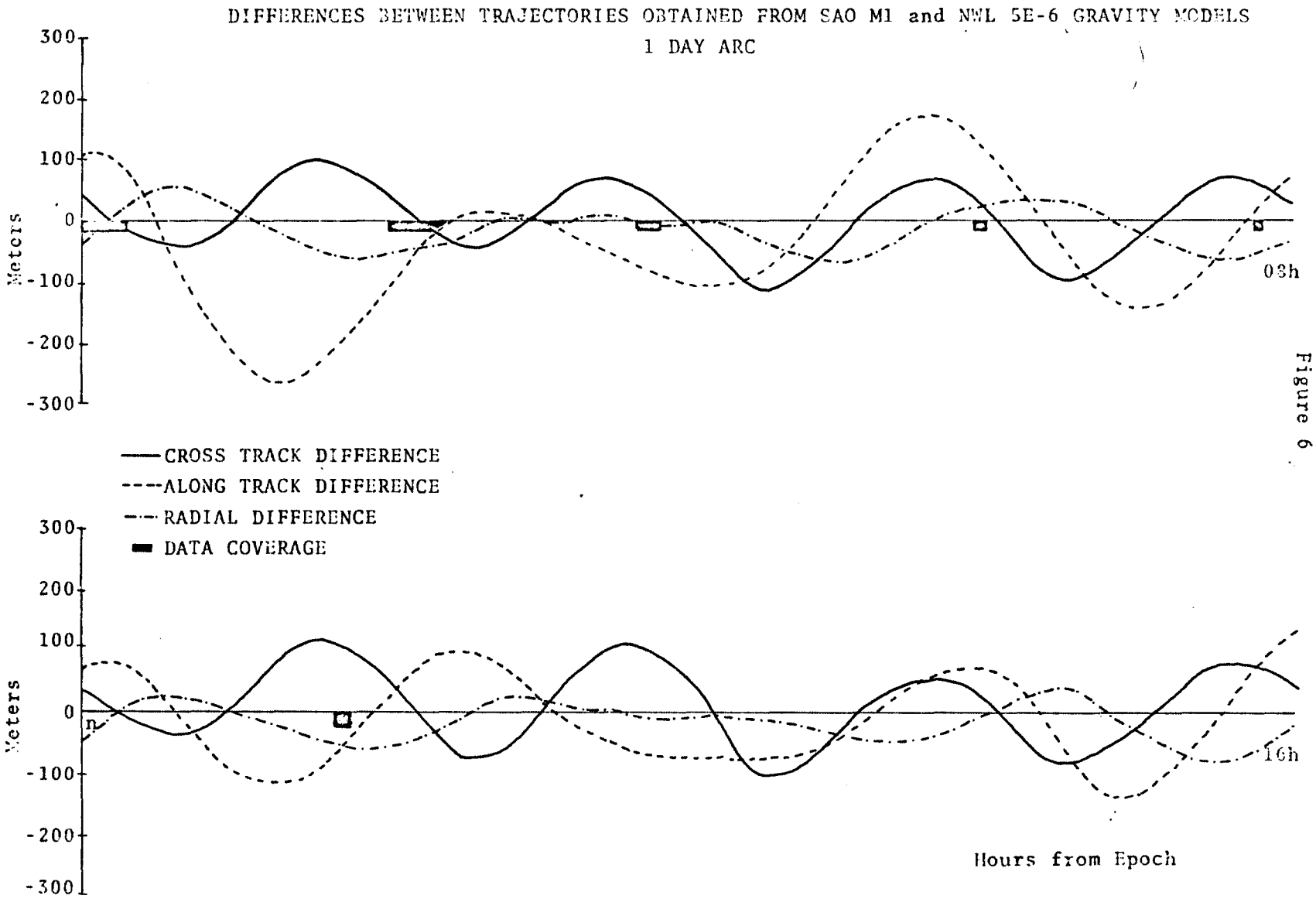
DIFFERENCES BETWEEN TRAJECTORIES OBTAINED FROM SAO M1 and NWL 5E-6 GRAVITY MODELS
1 DAY ARC
300
200
100
0
-100
-200
-300
Meters
03h
CROSS TRACK DIFFERENCE
ALONG TRACK DIFFERENCE
RADIAL DIFFERENCE
DATA COVERAGE
300
200
100
0
-100
-200
-300
Meters
16h
Hours from Epoch

Figure 6

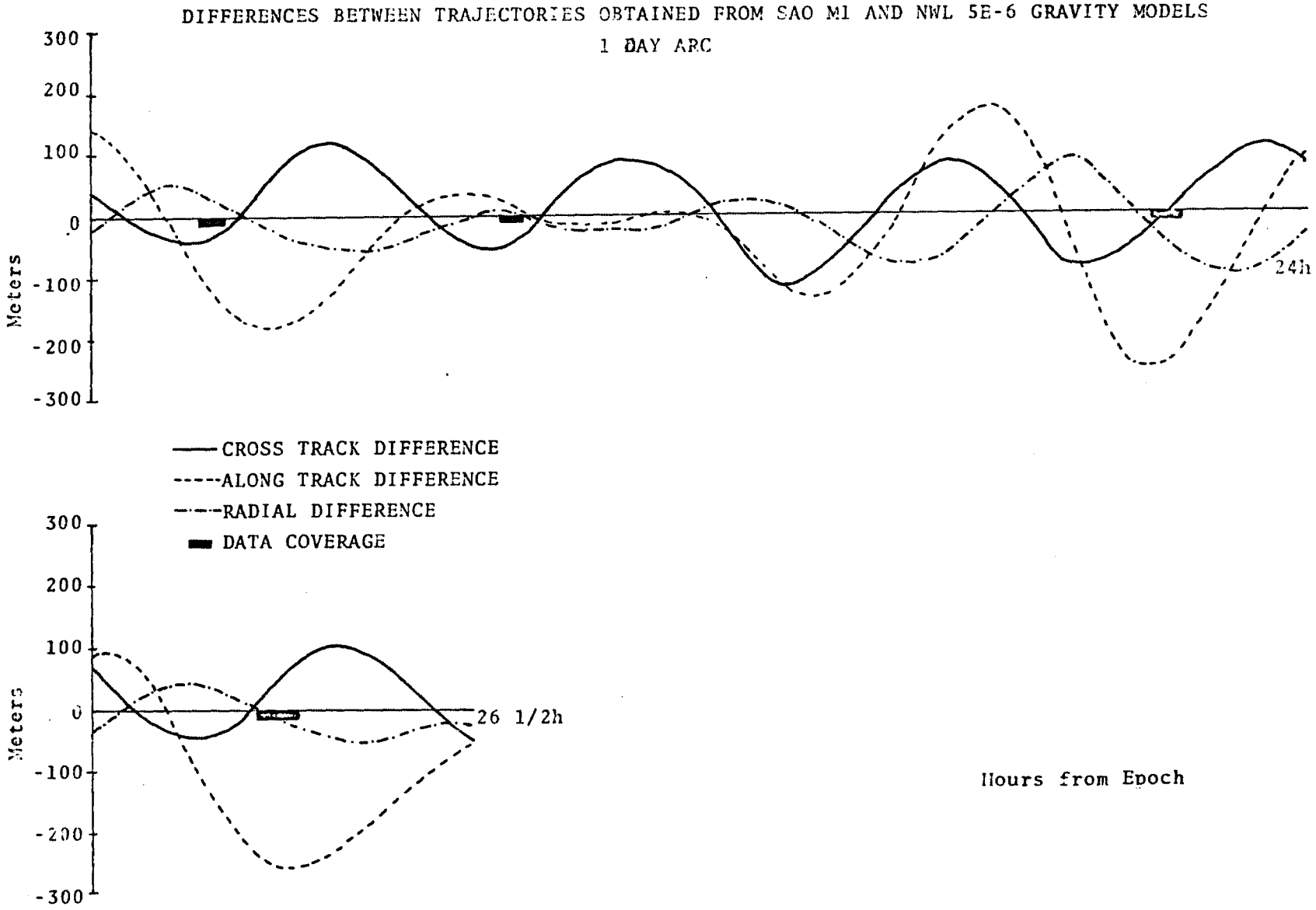

Figure 6 (cont)

DIFFERENCES BETWEEN TRAJECTORIES OBTAINED FROM SAO M1 AND APL 3.5 GRAVITY MODELS
5 1/2 DAY ARC

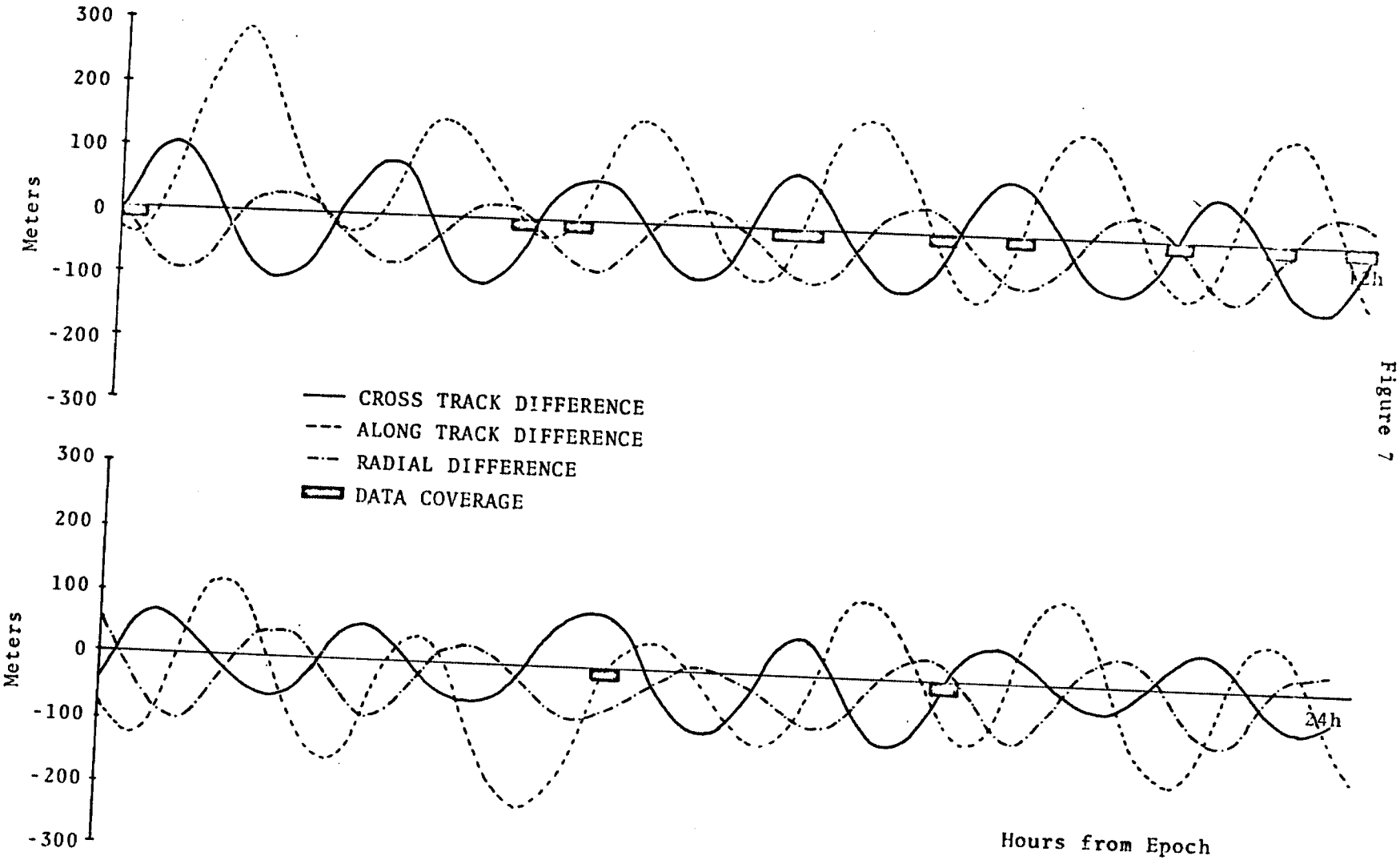

Figure 7

DIFFERENCES BETWEEN TRAJECTORIES OBTAINED FROM SAO M1 AND APL 3.5 GRAVITY MODELS
5 1/2 DAY ARC

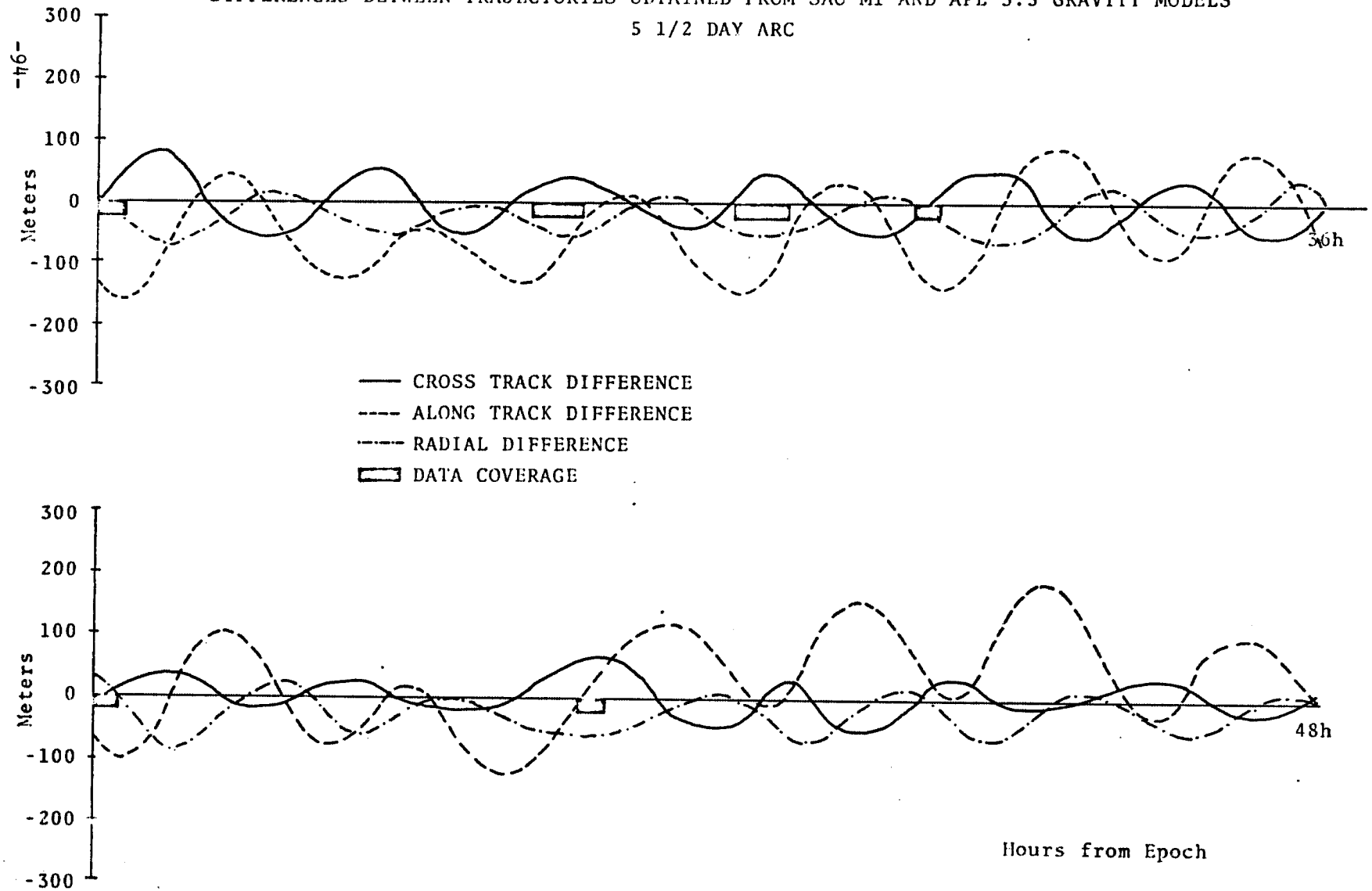

Figure 7 (cont)

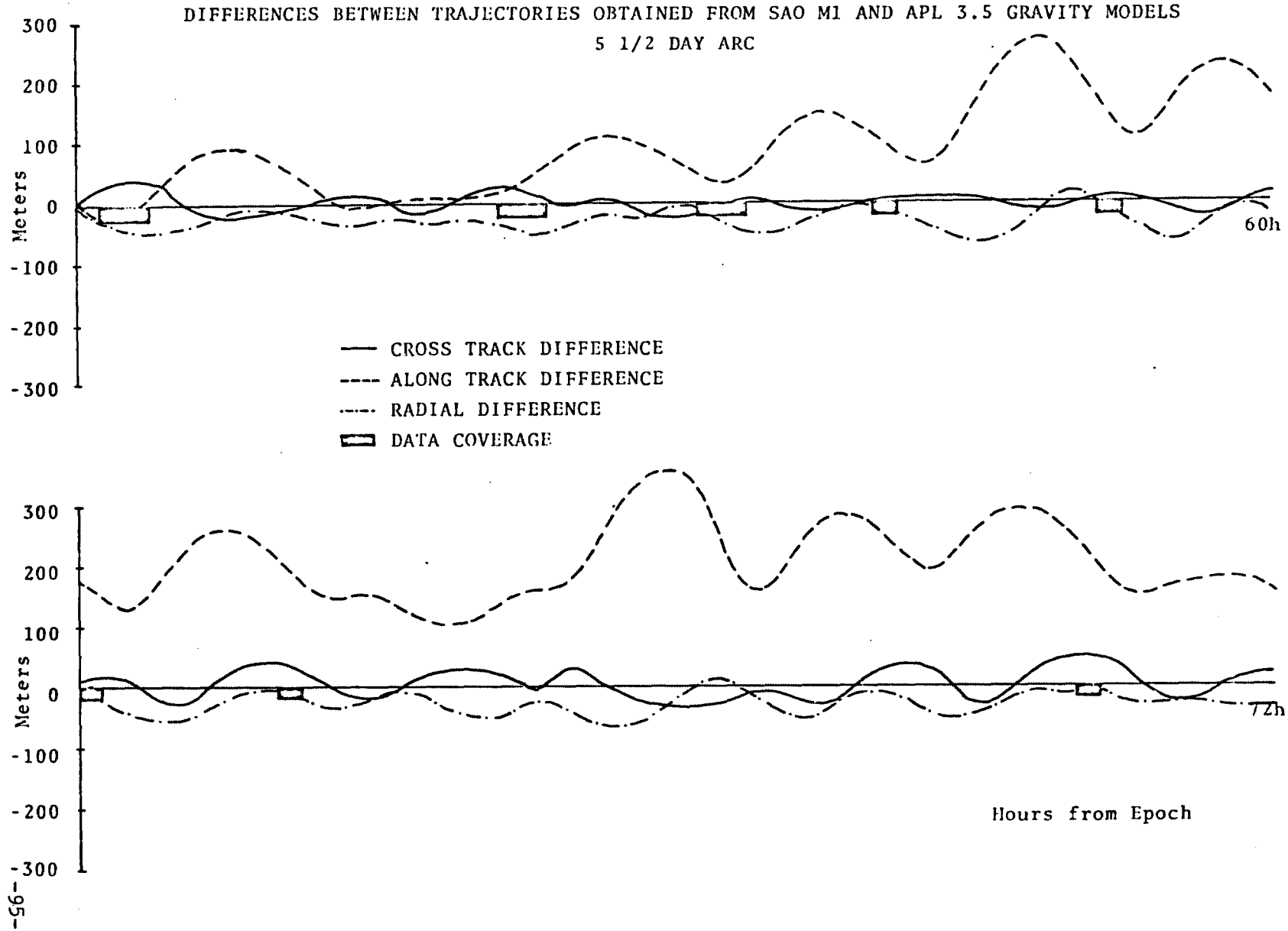

Figure 7 (cont)

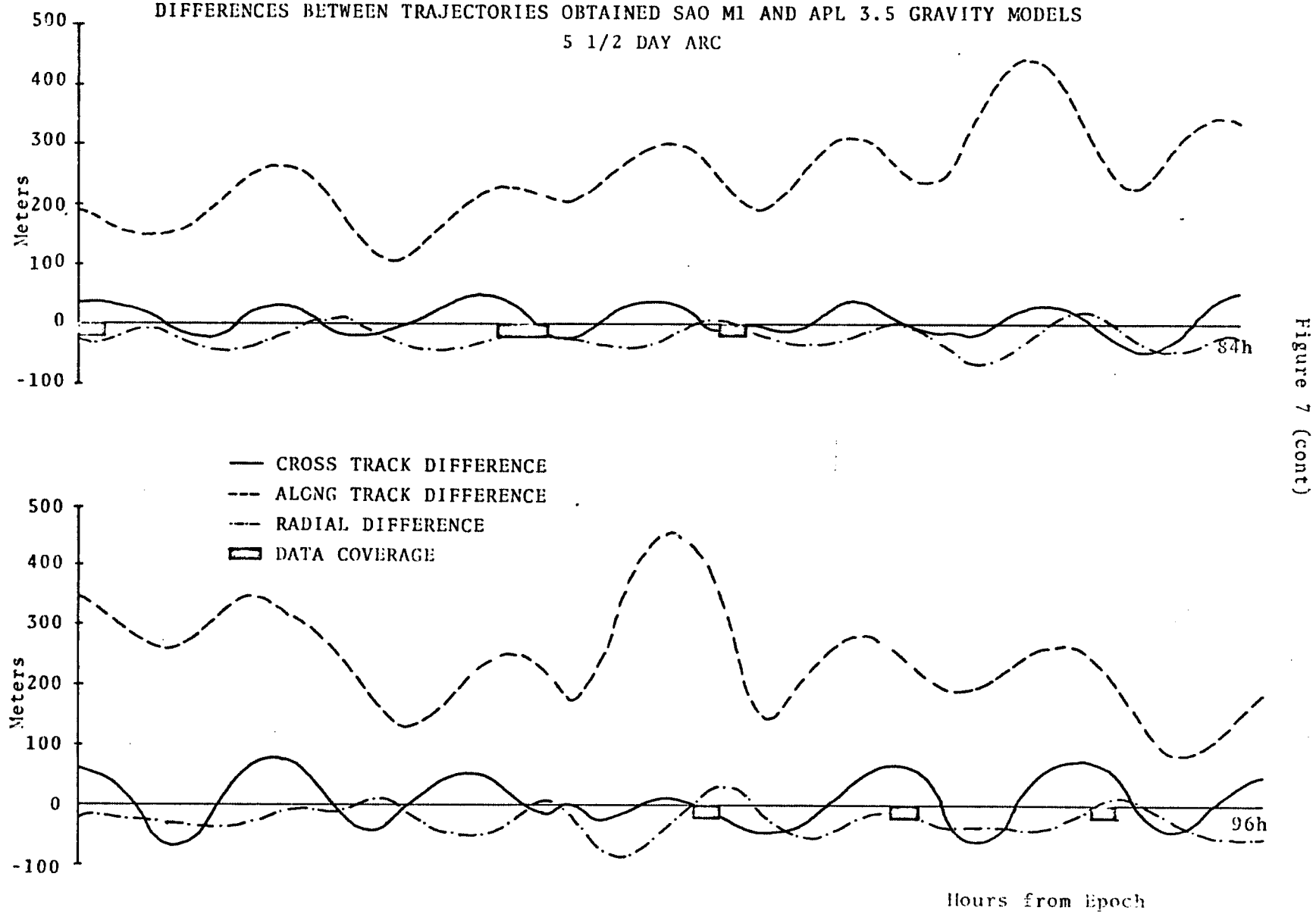

Figure 7 (cont)

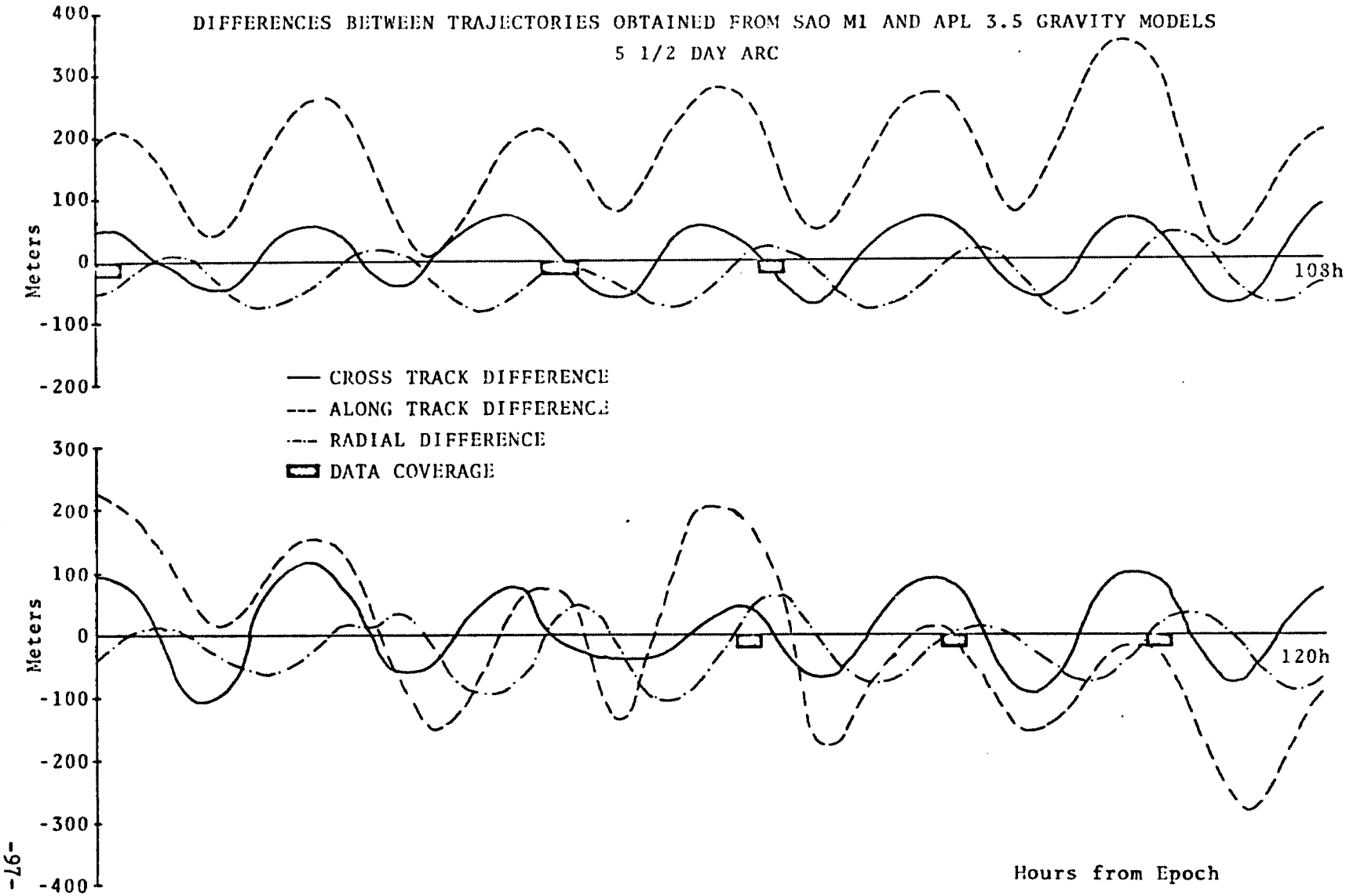

Figure 7 (cont)

DIFFERENCES BETWEEN TRAJECTORIES OBTAINED FROM SAO M1 AND APL 3.5 GRAVITY MODELS
5 1/2 DAY ARC

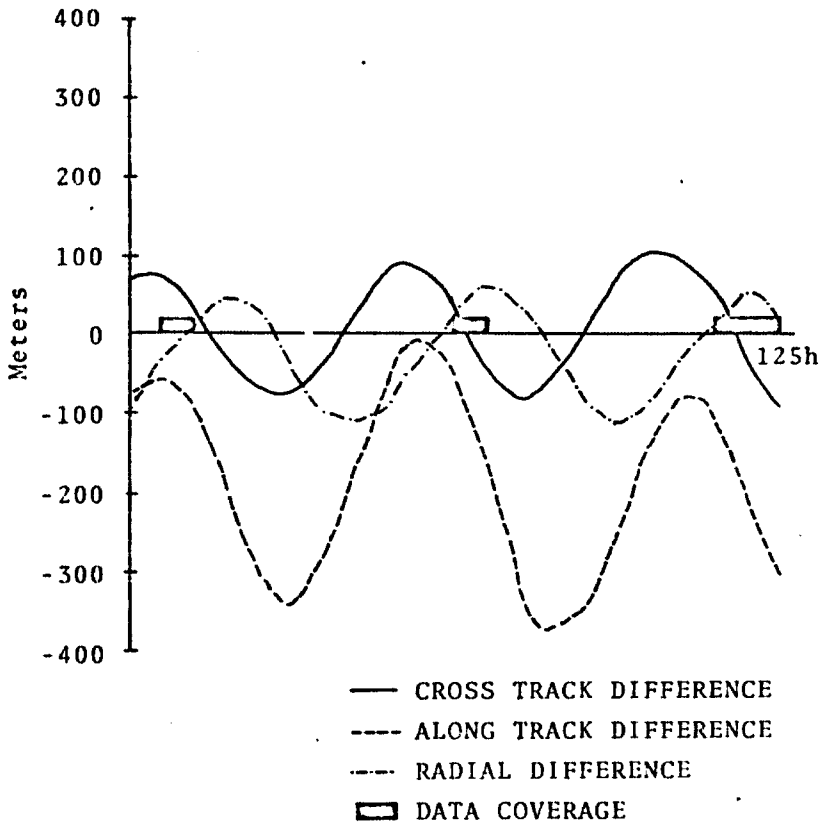

Hours from Epoch

Figure 7 (cont)

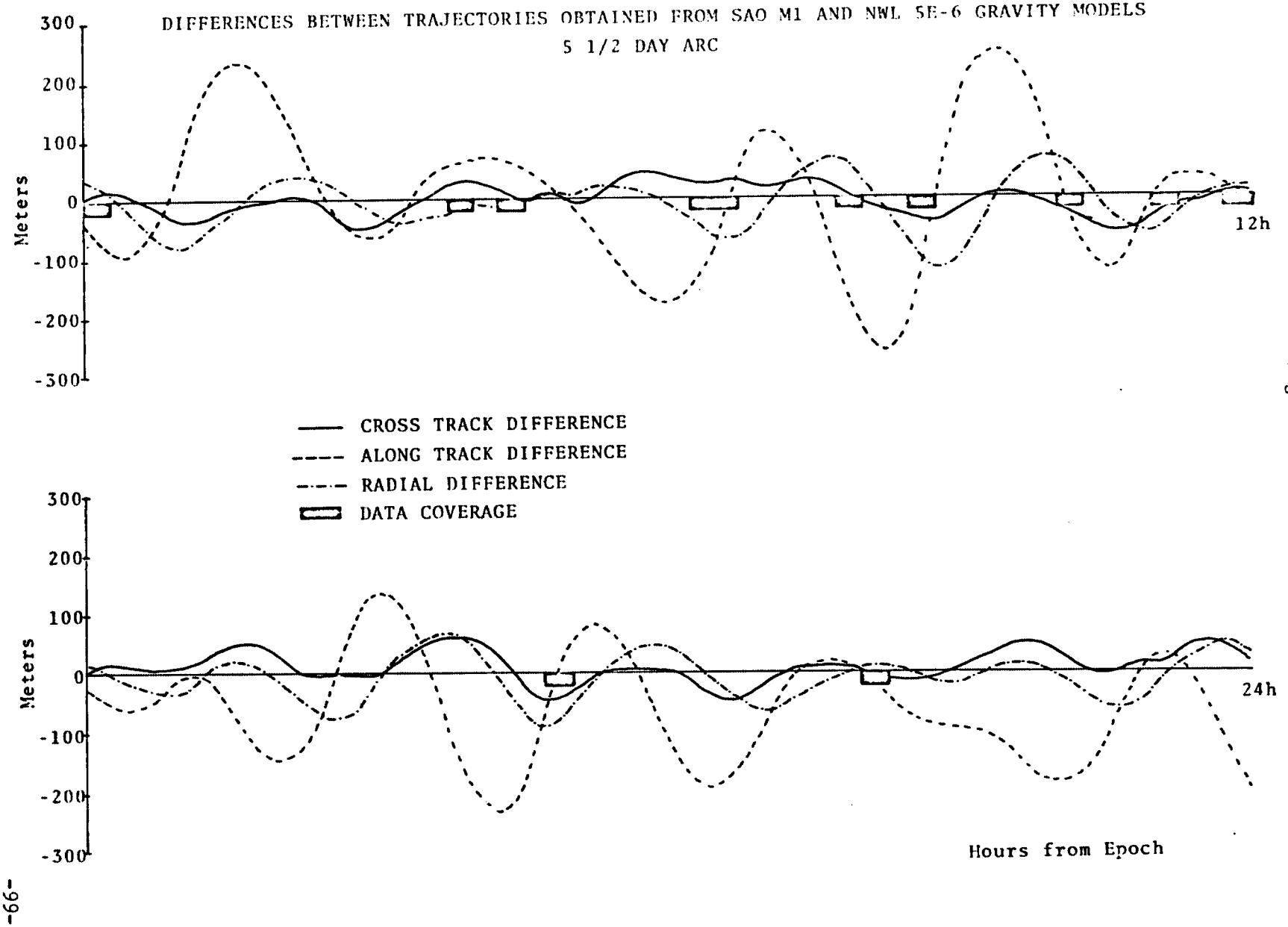
DIFFERENCES BETWEEN TRAJECTORIES OBTAINED FROM SAO M1 AND NWL 5E-6 GRAVITY MODELS
5 1/2 DAY ARC
300
200
100
0
-100
-200
-300
Meters
12h
CROSS TRACK DIFFERENCE
ALONG TRACK DIFFERENCE
RADIAL DIFFERENCE
DATA COVERAGE
300
200
100
0
-100
-200
-300
Meters
24h
Hours from Epoch

Figure 8

DIFFERENCES BETWEEN TRAJECTORIES OBTAINED FROM SAO M1 AND NWL 5E-6 GRAVITY MODELS
5 1/2 DAY ARC

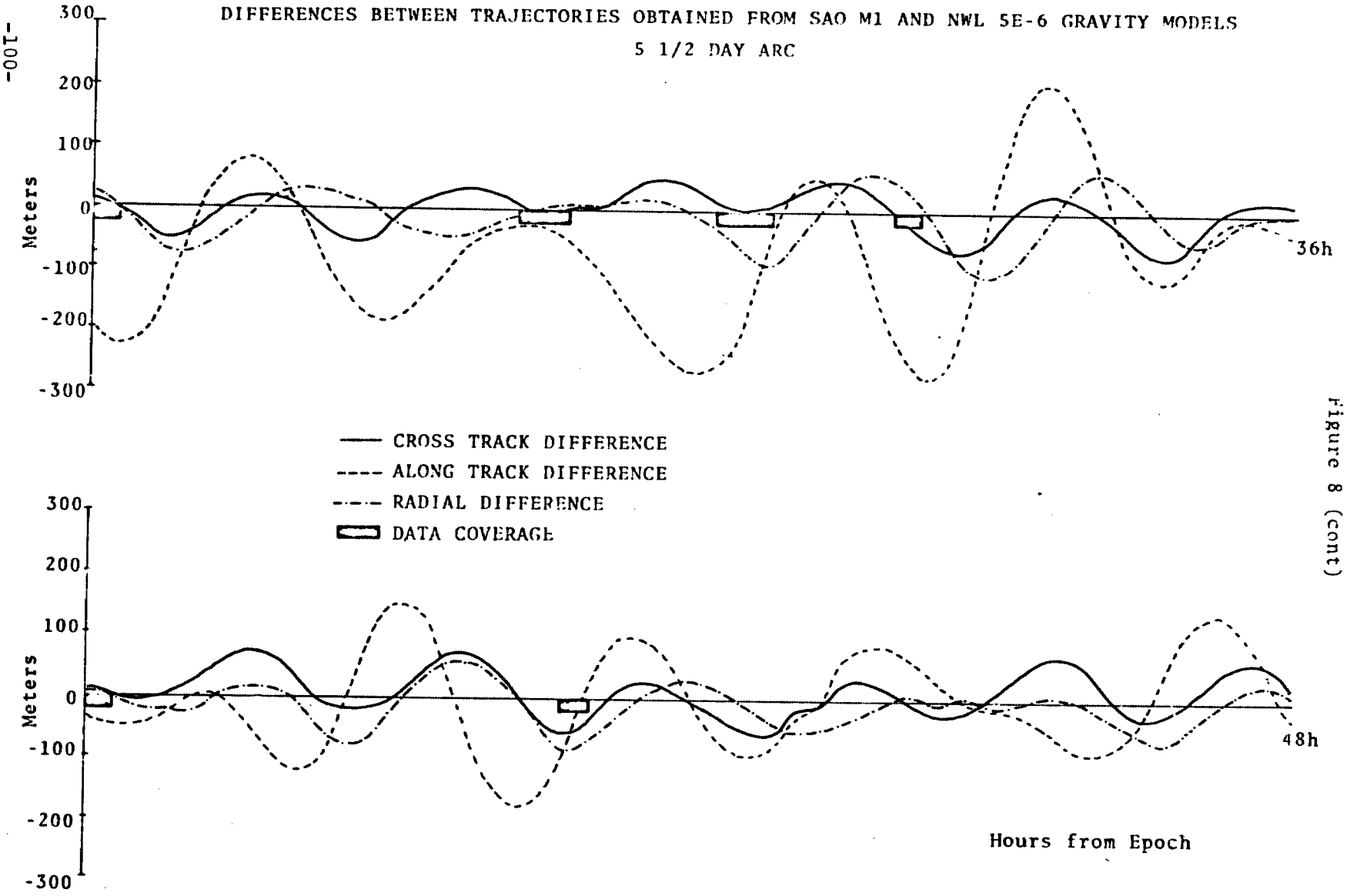

Figure 8 (cont)

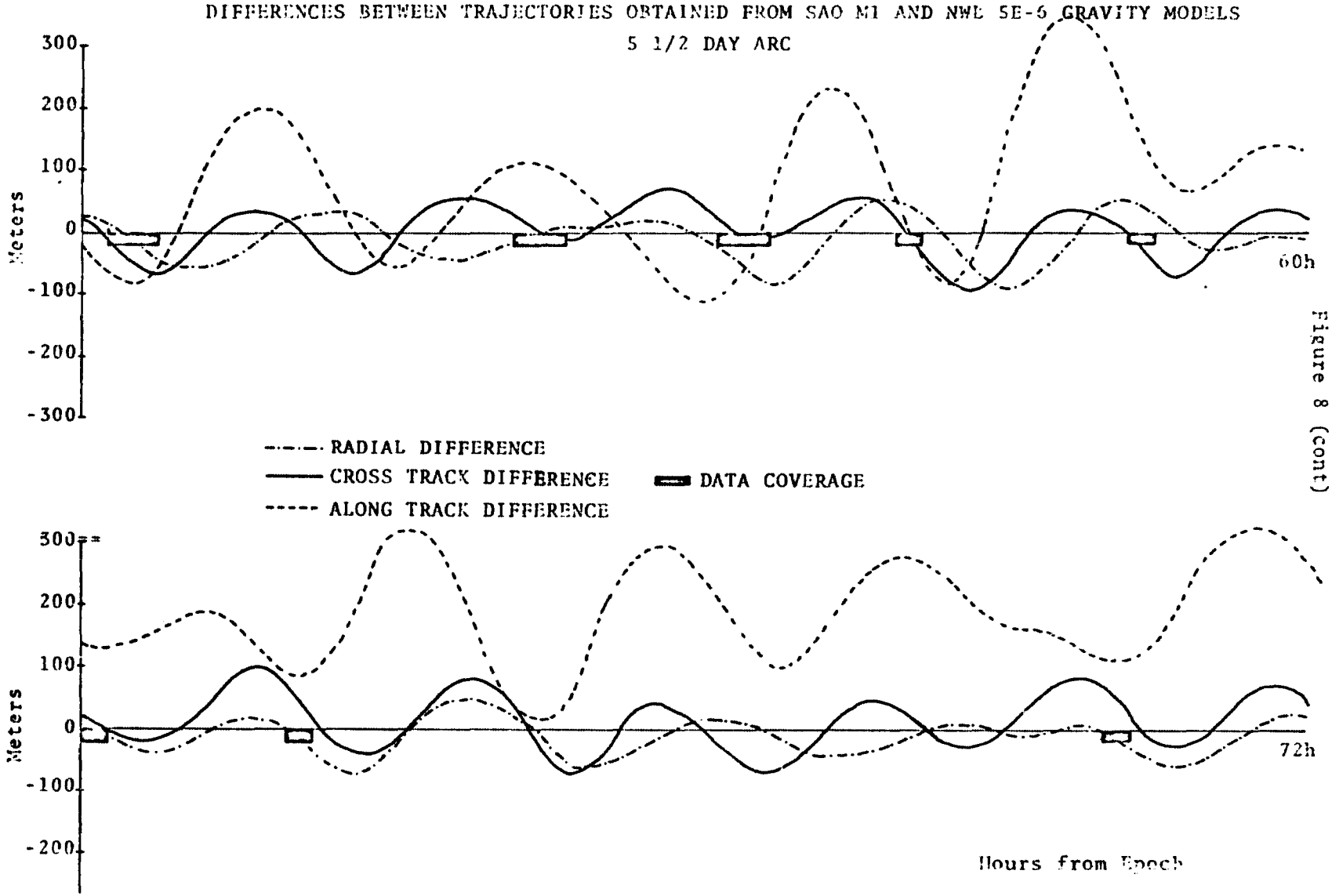

Figure 8 (cont)

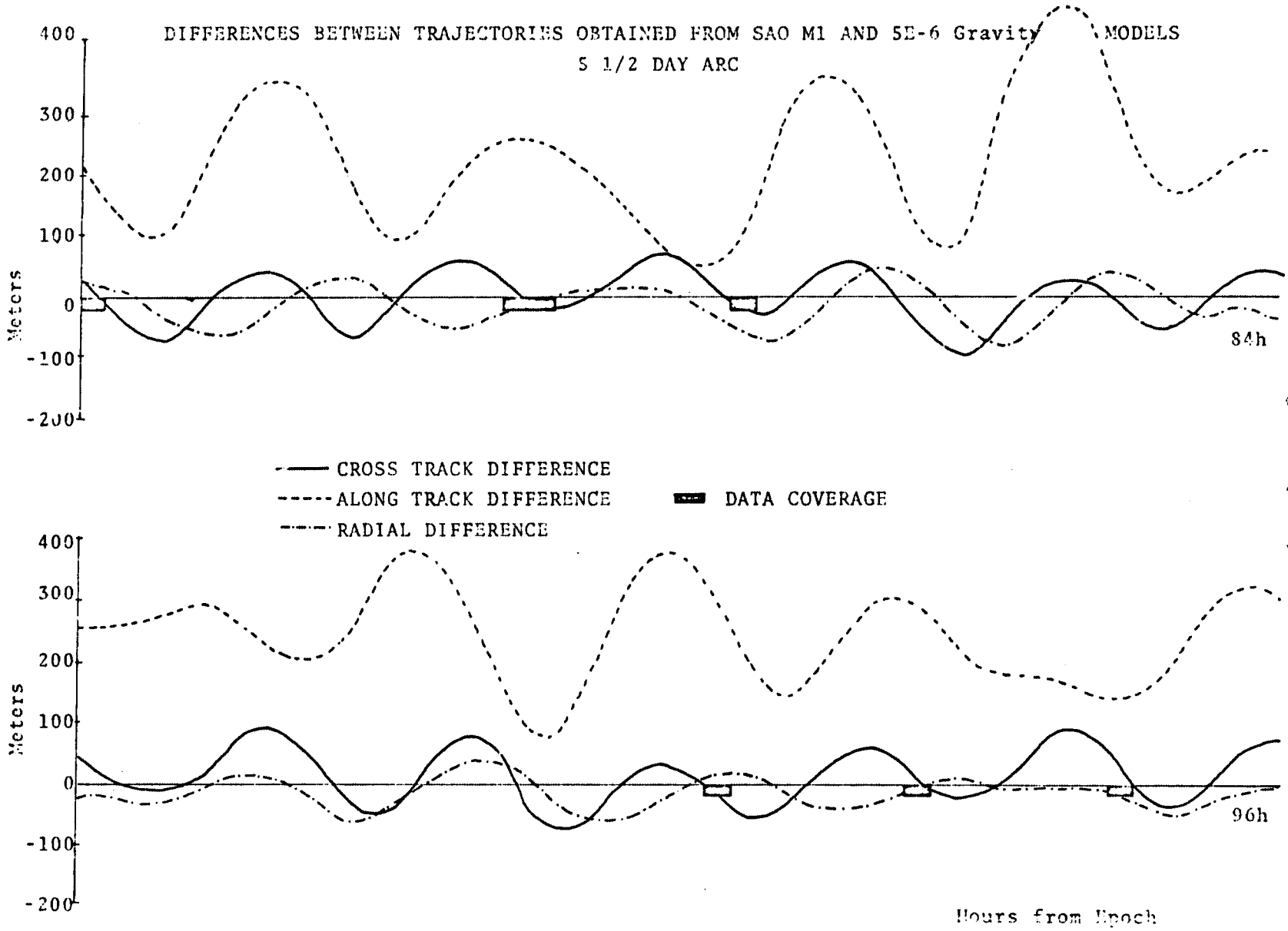

Figure 8 (cont)

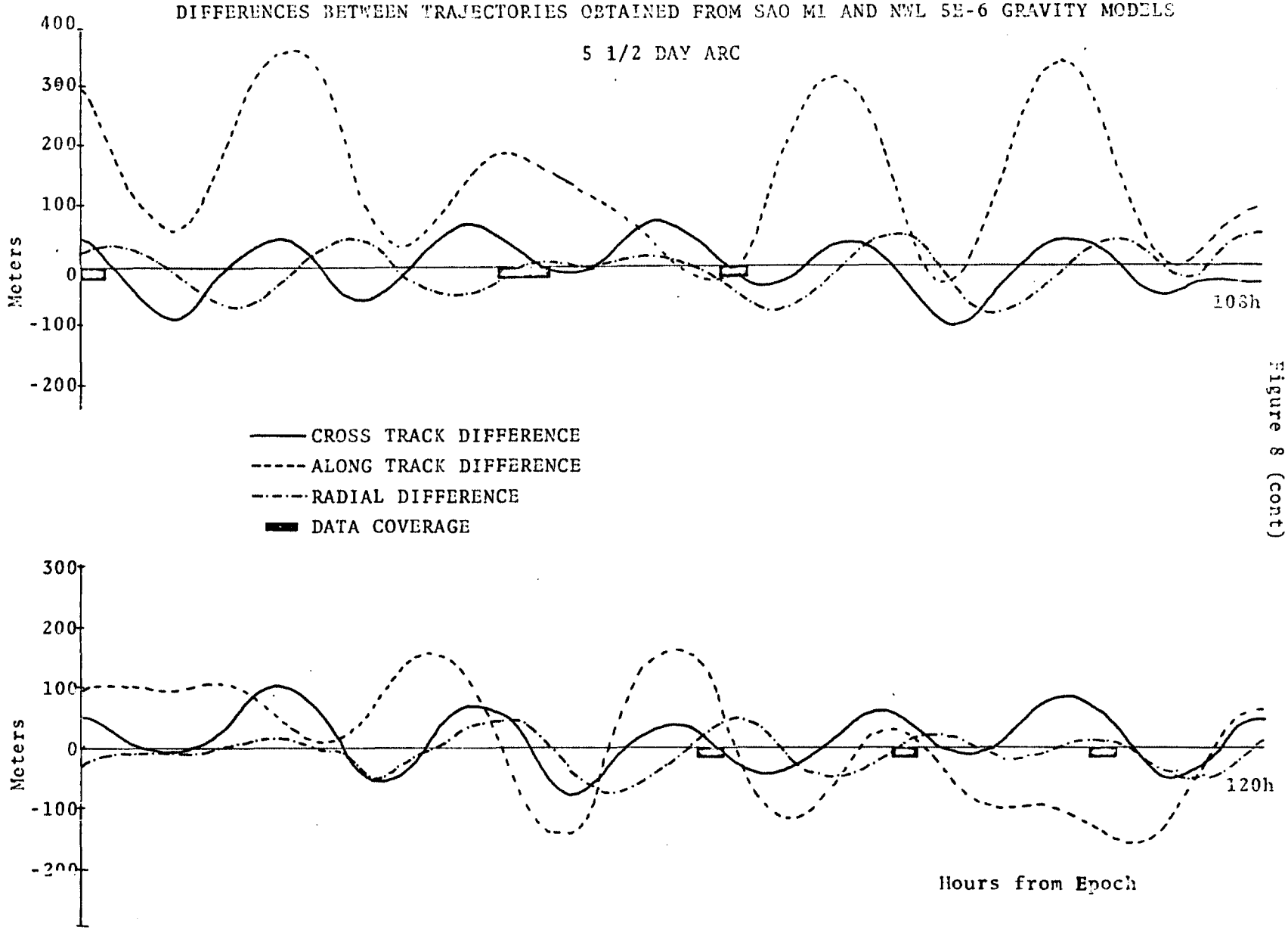

Figure 8 (cont)

DIFFERENCE BETWEEN TRAJECTORIES OBTAINED FROM SAO M1 AND NWL 5E-6 GRAVITY MODELS

5 1/2 DAY ARC

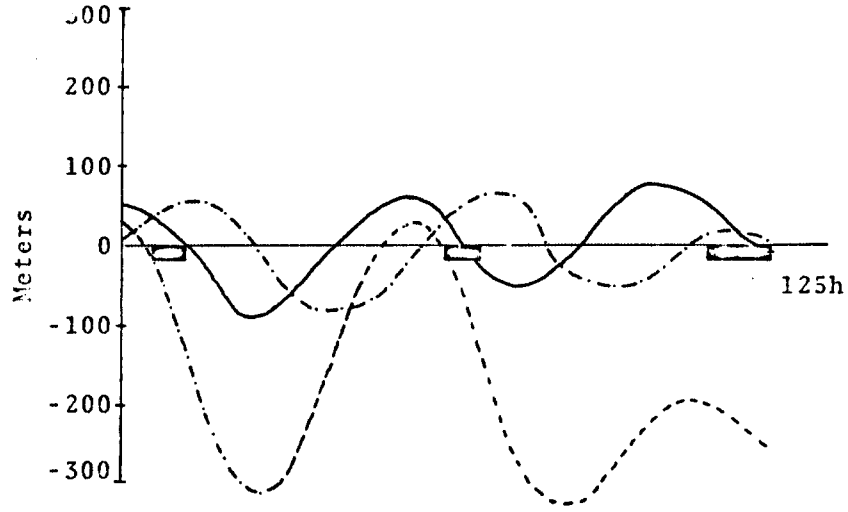

CROSS TRACK DIFFERENCE
ALONG TRACK DIFFERENCE
RADIAL DIFFERENCE
DATA COVERAGE

Hours from Epoch

Figure 8 (cont)

5.0 EVALUATION OF THE ROSMAN GRARR RANGE ACCURACY

The range measurements of the Goddard Range and Range Rate (GRARR) Tracking System at Rosman, North Carolina, were evaluated by comparing the actual measurements with values computed from optical reference orbits [5]. The 5 1/2 day arc and the 1 day arc discussed in Section 3.0 were used as the reference orbits.

For each GRARR pass over Rosman, zero-set errors, timing errors, and random errors were estimated from the residual differences between the observed and calculated ranges; these are summarized in Tables V - VII. The estimates obtained from the orbital solutions fitted using the SAO M-1 set of coefficients were less variable than those obtained using the other two sets. In addition, the estimates obtained from the shorter overlapping 1 day arc are only consistent with the 5 1/2 day arc estimates when the orbital solutions were obtained with the SAO M-1 set of coefficients.

TABLE V

SUMMARY OF ZERO-SET ERROR ESTIMATES
(meters)

PASS NO.	TRANSPONDER CHANNEL	SAO	M1	NWL	5E-6	APL	3.5
		1	2	1	2	1	2
652	A	-16.5		-26.5		-98.8	
653	A	- 6.1		-45.9		-35.9	
664	A	- 5.0		-18.0		-74.1	
665	A	- 2.0		-39.4		-16.3	
673	A	-19.1		-44.7		-15.8	
676	A	2.3	4.2	8.1	6.6	-25.8	-24.6
677	A	0.2	7.4	-51.8	-23.6	-20.2	3.8
685	A	-29.5	-20.7	-60.0	112.5	-46.7	-79.0
688	A	- 3.3	- 1.0	8.4	- 7.9	- 2.2	- 1.7
689	A	-14.9	- 7.7	-71.2	-35.8	-38.7	- 7.7
697	A	-16.0		-49.4		-52.8	
700	C	20.6		25.4		36.5	
708	C	16.8		10.5		7.9	
709	C	17.0		-17.7		-33.7	
712	A	- 9.5		-14.5		11.8	
Mean	A	-10.0		-33.7		-34.6	
S.d.	A	8.8		21.0		30.7	
Mean	C	18.1		6.1		3.6	

TABLE VI

SUMMARY OF TIMING ERROR ESTIMATES

(milliseconds)

PASS NO.	TRANSPONDER CHANNEL	SAO	M1	NWL	SE-6	APL	3.5
		1	2	1	2	1	2
652	A	-2.0		6.1		- 7.7	
653	A	1.5		-11.1		- 4.3	
664	A	-3.9		- 9.9		-22.7	
665	A	1.0		-23.7		-16.9	
673	A	-3.4		-17.4		- 6.5	
676	A	-6.3	-6.9	10.0	12.9	- 0.9	-1.2
677	A	-0.2	-0.3	- 5.0	- 7.3	3.4	0.1
685	A	-3.5	-0.6	14.2	-12.2	31.3	1.5
688	A	-5.0	-5.3	31.4	10.7	25.1	0.7
689	A	0.1	1.2	13.2	-12.5	25.6	-1.5
697	A	-3.0		19.6		38.9	
700	C	-5.4		18.1		18.9	
708	C	-2.3		3.3		2.7	
709	C	3.4		-18.9		5.5	
712	A	-2.8		-36.4		-28.2	
Mean	A	-2.4		- .8		3.1	
S.d.	A	2.4		9.8		22.1	
Mean	C	-1.4		.8		9.0	

TABLE VII

SUMMARY OF RANDOM ERROR ESTIMATES
(meters)

PASS NO.	TRANSPONDER CHANNEL	SAO	M1	NWL	5E-6	APL	3.5
		1	2	1	2	1	2
652	A	3.3		3.5		6.0	
653	A	3.6	24.6	10.5		7.3	
664	A	3.2		3.6		6.1	
665	A	4.5		12.0		3.6	
673	A	2.6		4.7		3.1	
676	A	2.9	3.0	3.9	5.3	5.0	3.8
677	A	3.2	4.0	10.4	4.7	2.8	5.3
685	A	2.5	2.3	3.5	10.5	2.6	5.2
688	A	4.5	5.0	8.3	10.3	7.0	8.2
689	A	4.1	3.8	7.4	5.0	3.9	3.9
697	A	3.4		3.5		3.8	
700	C	5.8		10.8		16.8	
708	C	4.5		3.9		5.3	
709	C	3.1		4.4		3.6	
712	A	6.0		8.0		22.7	
Mean	A	3.7		6.6		6.2	
S.d.							
Mean	C	4.5		6.4		8.6	

6.0 ESTIMATION OF COORDINATES FOR THE GRARR MADGAR SITE

Two independent estimates of the coordinates of the GRARR MADGAR site in Tananarive, Madagascar were obtained using each set of coefficients [6]. One estimate was obtained from optical flash sequence data taken at ITANAN during July 1966 and the other from range measurements taken at MADGAR during November 1965. The data sets used for these estimations are shown in Tables VIII and IX .

The two sets of coordinates estimated using the SAO M-1 coefficients were very consistent, within 5 meters of each other; whereas the estimates obtained using the other two sets of coefficients were not at all consistent. These estimates are shown in Table X and Figure 9.

TABLE VIII

SUMMARY OF DATA BY STATION
FOR JULY 9, 10, and 11

Station	No. of Measurements	
	Right Ascension	Declination
1TANAN	14	14
1ROSMA	7	7
1COLBA	14	14
1BPOIN	14	14
1DENVR	20	20
1JOBUR	14	14
1ORGAN	91	91
1OLFAN	28	28
1SPAIN	21	21
1QUIPA	28	28
1CURAC	28	28
1JUPTR	35	35
1VILDO	7	7
AUSBAK	14	14
1MAUIO	28	28
EDWAFB	2	2
TOTAL	365	365

TABLE IX

SUMMARY OF DATA BY STATION
FOR NOVEMBER 28 and 29

Station	No. of Measurements	
	Right Ascension	Declination
1ORGAN	59	59
1OLFAN	1	1
1SPAIN	1	1
1QUIPA	2	2
1CURAC	96	96
1JUPTR	127	127
1VILDO	1	1
TOTAL	287	287
	Range	
MADGAR	24	

TABLE X

ESTIMATED COORDINATES FOR MADGAR

SAO M1 Gravity Model

	Latitude	E. Longitude	Spheroid Height
Optical Estimate	-19° 1' 19.5"	47° 18' 7.9"	1380.0 meters
GRARR Estimate	-19° 1' 19.4"	47° 18' 8.0"	1382.6 meters
Difference	0.1"	-0.1"	-2.6 meters

APL 3.5 Gravity Model

	Latitude	E. Longitude	Spheroid Height
Optical Estimate	-19° 1' 22.6"	47° 18' 5.1"	1454.5 meters
GRARR Estimate	-19° 1' 23.7"	47° 18' 5.7"	1443.1 meters
Difference	-1.1"	-0.6"	11.4 meters

NWL 5E-6 Gravity Model

	Latitude	E. Longitude	Spheroid Height
Optical Estimate	-19° 1' 22.9"	47° 18' 4.8"	1458.0 meters
GRARR Estimate	-19° 1' 24.9"	47° 18' 7.5"	1467.4 meters
Difference	-2.0"	-2.7"	10.6 meters

ESTIMATED COORDINATES FOR MADGAR

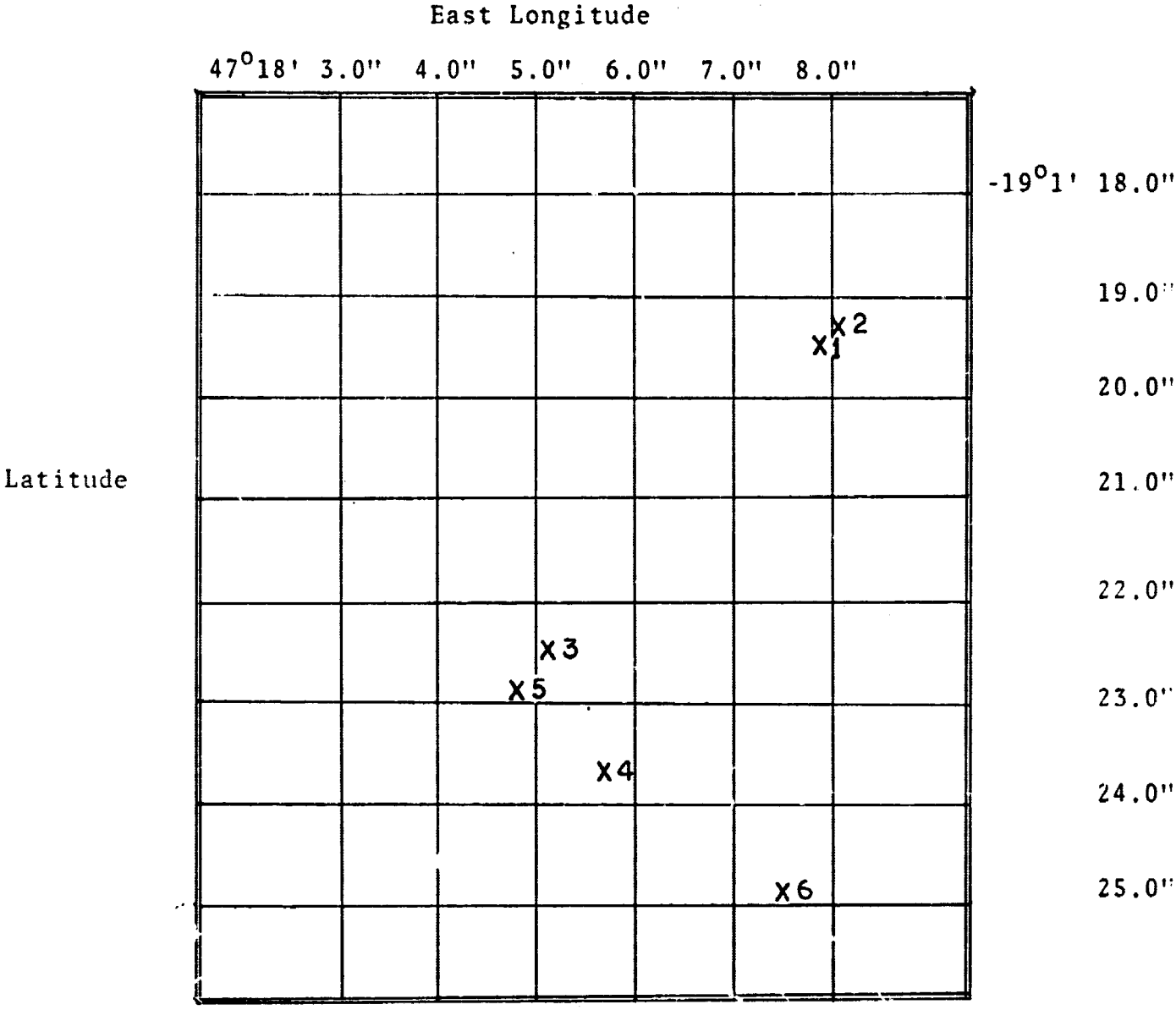

1 Optical Estimate - SAO M1 gravity
2 GRARR Estimate - SAO M1 gravity
3 Optical Estimate - APL 3.5 gravity
4 GRARR Estimate - APL 3.5 gravity
5 Optical Estimate - NWL 5E-6 gravity
6 GRARR Estimate - NWL 5E-6 gravity

7.0 REFERENCES

1. NASA Contract Document:
   Wolf Research and Development Corporation:
   Interim Status Report on Program Development
   and GEOS-A Data Analysis (NAS 5-9756-44A, 55, 71)
   August 1967

2. SAO Special Report No. 200 Vol. 1
   Geodetic Parameters for a 1966 Smithsonian Institution Standard Earth
   C. A. Lundquist and G. Veis, 1966

3. Journal of Geophysical Research Vol. 70, #18
   The Earth's Gravitational Field as deduced from the Doppler Tracking of Five Satellites
   W. H. Guier and R. R. Newton September 1965

4. NWL Report No. 1977
   Computational Methods employed in deriving Geodetic Results from Doppler Observations of Artificial Earth Satellites
   R. J. Anderle April 1965

5. NASA Document, X-552-67-
   Evaluation of the Goddard Range and Range Rate System at Rosman by Intercomparison with GEOS-I Long Arc Orbital Solutions
   F.J. Lerch, J.G. Marsh, B. O'Neill November 1967

6. NASA Document, X-552-67-540
   The Determination and Comparison of the GRARR MADGAR site location
   F.J. Lerch, C.E. Doll, S.J. Moss, B.O'Neill October 1967

APPENDIX A-1

FORCE MODELS USED IN NONAME

1.1 Force Models

The data reduction program in its present form incorporates four force models. These are:

1. The earth gravitational field
2. The solar and lunar gravitational perturbations
3. Solar radiation pressure
4. Atmospheric drag

The program is designed such that the gravitational coefficients and pertinent physical characteristics of satellites, such as reflectivity, cross-sectional area mass, and drag coefficient can be simply changed through card input or block data statement.

1.2 The Earth's Gravitational Field

The formulation of the geopotential used is:

$$u = \frac{GM}{r}\left\{1 + \sum_{n=2}^{k}\sum_{m=0}^{n}\left(\frac{a}{r}\right)^{n} P_n^m(\sin\phi)\left[C_{nm}\cos m\lambda + S_{nm}\sin m\lambda\right]\right\} \quad (1)$$

where

G	is the universal gravitational constant
M	is the mass of the earth
r	is the geocentric satellite distance
a	is the earth's mean equatorial radius
ϕ	is the sub-satellite latitude
λ	is the sub-satellite east longitude
$P_m^n(\sin\phi)$	is the associated spherical harmonic of degree n and order m.

The design of the potential function requires that denormalized gravitational coefficiences $C_{n,m}$ and $S_{n,m}$ be used. The program is presently capable of accepting coefficients up to (20,20) or any sub-set of these.

The transformation of the geopotential in earth-fixed coordinates (r,ϕ,λ) to gravitational accelerations in inertial coordinates (x,y,z) is accomplished as follows:

$$\ddot{x}_\oplus = \frac{\partial u}{\partial r}\frac{\partial r}{\partial x} + \frac{\partial u}{\partial \phi}\frac{\partial \phi}{\partial x} + \frac{\partial u}{\partial \lambda}\frac{\partial \lambda}{\partial x} \; ; \; \ddot{y}_\oplus \; , \; \ddot{z}_\oplus \qquad (2)$$

DENORMALIZED COEFFICIENTS

COEFFICIENT	MODEL		
	SAO M-1	APL 3.5	NWL 5E-6
C(2,0)	-1082.645×10^{-6}	-1082.7×10^{-6}	-1082.691×10^{-6}
S(2,0)			
C(2,1)			$+0.021\times10^{-6}$
S(2,1)			$+0.080\times10^{-6}$
C(2,2)	$+1.536\times10^{-6}$	$+1.53693\times10^{-6}$	$+1.579\times10^{-6}$
S(2,2)	-0.872×10^{-6}	-7.73306×10^{-7}	-0.981×10^{-6}
C(3,0)	$+2.546\times10^{-6}$	$+2.676\times10^{-6}$	$+2.603\times10^{-6}$
S(3,0)			
C(3,1)	$+2.091\times10^{-6}$	$+1.98743\times10^{-6}$	$+0.320\times10^{-6}$
S(3,1)	$+0.287\times10^{-6}$	$+2.32227\times10^{-9}$	$+0.296\times10^{-6}$
C(3,2)	$+0.251\times10^{-6}$	$+4.16368\times10^{-7}$	$+0.334\times10^{-6}$
S(3,2)	-0.184×10^{-6}	-2.31957×10^{-7}	-0.309×10^{-6}
C(3,3)	$+0.782\times10^{-7}$	$+9.21581\times10^{-8}$	$+0.082\times10^{-6}$
S(3,3)	$+0.226\times10^{-6}$	$+1.36535\times10^{-7}$	$+0.227\times10^{-6}$
C(4,0)	$+1.649\times10^{-6}$	$+1.4\times10^{-6}$	$+1.521\times10^{-6}$
S(4,0)			
C(4,1)	-0.543×10^{-6}	-5.33539×10^{-7}	-0.470×10^{-6}
S(4,1)	-0.445×10^{-6}	-4.17705×10^{-7}	-0.545×10^{-6}
C(4,2)	$+0.738\times10^{-7}$	$+9.56813\times10^{-8}$	$+0.061\times10^{-6}$
S(4,2)	$+0.148\times10^{-6}$	$+9.92367\times10^{-8}$	$+0.150\times10^{-6}$
C(4,3)	$+0.509\times10^{-7}$	$+5.05821\times10^{-8}$	$+0.062\times10^{-6}$
S(4,3)	-0.113×10^{-7}	$+4.22035\times10^{-10}$	-0.148×10^{-7}

COEFFICIENT	MODEL		
	SAO M-1	APL 3.5	NWL 5E-6
C(4,4)	-0.112×10^{-8}	-4.44974×10^{-9}	-0.087×10^{-7}
S(4,4)	$+0.486\times10^{-8}$	$+4.01026\times10^{-9}$	$+0.071\times10^{-7}$
C(5,0)	$+0.210\times10^{-6}$	$+0.028\times10^{-6}$	$+0.149\times10^{-6}$
S(5,0)			
C(5,1)	-0.677×10^{-7}	$+1.1732\times10^{-7}$	0.027×10^{-6}
S(5,1)	-0.882×10^{-7}	-1.42925×10^{-7}	-0.102×10^{-6}
C(5.2)	$+0.102\times10^{-6}$	$+4.34364\times10^{-8}$	$+0.103\times10^{-6}$
S(5,2)	-0.375×10^{-7}	-5.54684×10^{-8}	-0.053×10^{-6}
C(5,3)	-0.172×10^{-7}	$+3.01637\times10^{-9}$	-0.128×10^{-7}
S(5,3)	$+0.231\times10^{-9}$	$+3.41906\times10^{-9}$	-0.041×10^{-7}
C(5,4)	-0.206×10^{-8}	-3.80289×10^{-9}	-0.043×10^{-7}
S(5,4)	$+0.498\times10^{-9}$	-2.02443×10^{-9}	$+0.012\times10^{-7}$
C(5,5)	$+0.384\times10^{-9}$	-8.26819×10^{-11}	$+0.053\times10^{-8}$
S(5,5)	-0.146×10^{-8}	-1.64625×10^{-9}	-0.146×10^{-8}
C(6,0)	-0.646×10^{-6}	-0.37×10^{-6}	-0.790×10^{-6}
S(6,0)			
C(6,1)	-0.370×10^{-7}	-1.64676×10^{-10}	-0.669×10^{-7}
S(6,1)	-0.212×10^{-7}	$+7.93877\times10^{-8}$	$+0.151\times10^{-6}$
C(6,2)	$+0.858\times10^{-8}$	-2.00289×10^{-8}	$+0.160\times10^{-7}$
S(6,2)	-0.455×10^{-7}	-1.93447×10^{-8}	-0.568×10^{-7}
C(6,3)	-0.112×10^{-8}	$+1.09952\times10^{-8}$	-0.004×10^{-7}
S(6,3)	$+0.643\times10^{-9}$	$+1.05971\times10^{-9}$	-0.028×10^{-7}
C(6,4)	-0.167×10^{-9}	-1.16176×10^{-9}	-0.073×10^{-8}
S(6,4)	-0.196×10^{-8}	-1.92567×10^{-9}	-0.120×10^{-8}

	MODEL		
COEFFICIENT	SAO M-1	APL 3.5	NWL 5E-6
C(6,5)	-0.253×10^{-9}	-1.45272×10^{-9}	-0.075×10^{-9}
S(6,5)	-0.370×10^{-9}	$-4.10877\times1-^{-10}$	-0.643×10^{-9}
C(6,6)	-0.932×10^{-11}	$+3.34093\times10^{-12}$	-0.075×10^{-9}
S(6,6)	-0.361×10^{-10}	-5.39581×10^{-11}	-0.084×10^{-9}
C(7,0)	$+0.333\times10^{-6}$	$+0.593\times10^{-6}$	$+0.407\times10^{-6}$
S(7,0)			
C(7,1)	$+0.144\times10^{-6}$	$+9.22957\times10^{-8}$	$+0.242\times10^{-6}$
S(7,1)	$+0.114\times10^{-6}$	$+6.84716\times10^{-8}$	$+0.607\times10^{-7}$
C(7,2)	$+0.362\times10^{-7}$	$+4.56777\times10^{-8}$	$+0.349\times10^{-7}$
S(7,2)	$+0.162\times10^{-7}$	$+5.97415\times10^{-9}$	-0.194×10^{-7}
C(7,3)	$+0.352\times10^{-8}$	$+5.54703\times10^{-9}$	$+0.045\times10^{-7}$
S(7,3)	$+0.254\times10^{-9}$	-2.91156×10^{-9}	$+0.634\times10^{-7}$
C(7,4)	-0.323×10^{-9}	-2.90499×10^{-10}	-0.010×10^{-7}
S(7,4)	-0.217×10^{-9}	$+1.01887\times10^{-12}$	-0.005×10^{-7}
C(7,5)	$+0.269\times10^{-10}$	-2.01098×10^{-11}	$+0.195\times10^{-10}$
S(7,5)	$+0.191\times10^{-10}$	-6.62187×10^{-11}	$+0.074\times10^{-10}$
C(7,6)	-0.145×10^{-10}	-3.15953×10^{-11}	-0.331×10^{-10}
S(7,6)	$+0.437\times10^{-11}$	$+5.26126\times10^{-11}$	-0.169×10^{-10}
C(7,7)	$+0.102\times10^{-11}$	$+1.63987\times10^{-12}$	
S(7,7)	$+0.178\times10^{-11}$	-2.67684×10^{-12}	
C(8,0)	$+0.270\times10^{-6}$	-0.07×10^{-6}	
S(8,0)			

	MODEL		
COEFFICIENT	SAO M-1	APL 3.5	NWL 5E-6
C(8,1)	-0.515×10^{-7}	-1.01772×10^{-7}	
S(8,1)	$+0.447\times10^{-7}$	-3.32803×10^{-8}	
C(8,2)	$+0.214\times10^{-8}$	$+7.77975\times10^{-9}$	
S(8,2)	$+0.320\times10^{-8}$	-3.09153×10^{-9}	
C(8,3)	-0.374×10^{-9}	-5.55748×10^{-10}	
S(8,3)	$+0.404\times10^{-10}$	$+2.19185\times10^{-9}$	
C(8,4)	-0.277×10^{-9}	-9.00718×10^{-11}	
S(8,4)	-0.157×10^{-10}	$+4.90885\times10^{-11}$	
C(8,5)	-0.959×10^{-11}	$+1.45523\times10^{-11}$	
S(8,5)	$+0.214\times10^{-10}$	-4.51591×10^{-13}	
C(8,6)	-0.475×10^{-12}	-6.12476×10^{-13}	
S(8,6)	$+0.888\times10^{-11}$	$+1.85949\times10^{-11}$	
C(8,7)	-0.444×10^{-13}	$+8.6531\times10^{-13}$	
S(8,7)	$+0.158\times10^{-12}$	-3.57393×10^{-13}	
C(8,8)	-0.316×10^{-12}	-1.85733×10^{-13}	
S(8,8)	$+0.130\times10^{-12}$	$+1.20134\times10^{-13}$	
C(9,0)	$+0.532\times10^{-7}$	-0.177×10^{-6}	
S(9,0)			
C(9,1)	$+0.760\times10^{-7}$		
S(9,1)	$+0.780\times10^{-8}$		
C(9,2)	-0.277×10^{-9}		
S(9,2)	$+0.242\times10^{-8}$		

	MODEL		
COEFFICIENT	SAO M-1	APL 3.5	NWL 5E-6
C(10,10)	$+0.541\times10^{-7}$		
S(10,10)			
C(10,1)	$+0.649\times10^{-7}$		
S(10,1)	-0.779×10^{-7}		
C(10,2)	-0.624×10^{-8}		
S(10,2)	-0.250×10^{-8}		
C(10,3)	-0.379×10^{-9}		
S(10,3)	$+0.175\times10^{-9}$		
C(10,4)	-0.436×10^{-10}		
S(10,4)	-0.654×10^{-10}		
C(11,0)	-0.302×10^{-6}	$+0.5\times10^{-6}$	
S(11,0)			
C(11,1)	-0.313×10^{-7}		
S(11,1)	$+0.885\times10^{-8}$		
C(12,0)	$+0.357\times10^{-6}$	-0.31×10^{-6}	
S(12,0)			
C(12,1)	-0.923×10^{-7}		
S(12,1)	-0.402×10^{-7}		
C(12,2)	-0.470×10^{-8}		
S(12,2)	-0.233×10^{-9}		
C(12,12)	-0.278×10^{-18}		
S(12,12)	$+0.718\times10^{-20}$		
C(13,0)	$+0.114\times10^{-6}$		
S(13,0)			

	MODEL		
COEFFICIENT	SAO M-1	APL 3.5	NWL 5E-6
C(13,12)	-0.126×10^{-18}		
S(13,12)	$+0.117\times10^{-18}$		
C(13,13)	-0.216×10^{-19}	-1.71580×10^{-19}	-0.102×10^{-19}
S(13,13)	$+0.282\times10^{-19}$	$+1.73739\times10^{-20}$	$+0.039\times10^{-18}$
C(14,0)	-0.179×10^{-6}		
S(14,0)			
C(14,1)	-0.788×10^{-8}		
S(14,1)	$+0.280\times10^{-8}$		
C(14,11)	$+0.947\times10^{-21}$		
S(14,11)	-0.473×10^{-21}		
C(14,12)	$+0.140\times10^{-20}$		
S(14,12)	-0.132×10^{-19}		
C(14,14)	-0.193×10^{-21}	-8.78308×10^{-22}	
S(14,14)	-0.414×10^{-22}	-5.10323×10^{-22}	
C(15,9)	-0.241×10^{-18}		
S(15,9)	-0.483×10^{-18}		
C(15,12)	-0.138×10^{-19}		
S(15,12)	-0.190×10^{-20}		
C(15,13)	-0.117×10^{-21}		-0.109×10^{-20}
S(15,13)	-0.927×10^{-21}		-0.103×10^{-20}
C(15,14)	$+0.114\times10^{-22}$	$+2.24976\times10^{-24}$	$+0.002\times10^{-20}$
S(15,14)	-0.558×10^{-22}	-2.07453×10^{-23}	-0.007×10^{-20}

where the subscript "⊙" denotes accelerations due to the earth's field.

1.3 Solar and Lunar Gravitational Perturbations

The perturbations caused by a third body, e.g., the sun or moon, on a satellite orbit are treated by defining a disturbing function R[I] which can be treated as the potential function U. For the solar perturbation $R_\odot$ takes the form

$$R_\odot = \frac{GMm_\odot}{r_\odot}\left[\left(1 - \frac{2r}{r_\odot}S + \frac{r^2}{r_\odot^2}\right)^{-1/2} - \frac{r}{r_\odot}\right] \qquad (3)$$

where $S = \cos(r, r_\odot)$

$m_\odot$ is the mass of the sun in earth masses

$r_\odot$ is the geocentric distance to the sun

r is the geocentric distance to the satellite

G is the universal gravitational constant

M is the mass of the earth

The acceleration of the satellite due to the sun is then

$$\ddot{x}_\odot = \frac{\partial R_\odot}{\partial r}\frac{\partial r}{\partial x}\ ;\ \ddot{y}_\odot,\ \ddot{z}_\odot \qquad (4)$$

---

[1] Kozai, Y, Smithsonian Astrophysical Observatory Special Report 22, pp. 7-10.

The lunar perturbations are found from equation (3) by substituting the lunar mass and distance for those of the sun.

The lunar and solar ephermerides are computed internal to the program. These positions are computed at ten equal intervals over each five day period and least squares fit to a fourth order polynomial in time about the midpoint of the five day period. The positions of these bodies are then determined at each data point by evaluating the polynomial at the observation time.

1.4 Solar Radiation Pressure

The acceleration acting on a satellite due to solar radiation pressure is formulated as follows [2].

$$\ddot{x}_{RAD} = -\frac{AP_{\odot}}{m} \gamma\nu \, L_x; \; \ddot{y}_{RAD}, \; \ddot{z}_{RAD} \qquad (5)$$

where

- L is the inertial unit vector from the geocenter to the sun and whose components are L_x, L_y, L_z.
- A is the cross sectional area of the satellite
- m is the satellite mass
- γ is a factor depending on the reflective characteristics of the satellite

---

[2] H. Koelle, Handbook of Astronautical Engineering, pp. 8-33, McGraw-Hill, 1961.

ν is the eclipse factor such that:

$$\nu = \begin{cases} 0 \text{ when satellite is in earth's shadow} \\ 1 \text{ when satellite is illuminated by the sun} \end{cases}$$

$P_\odot$ is the solar radiation pressure in the vicinity of the earth,

$$4.5 \times 10^{-6} \ \frac{\text{Newton}}{m^2}$$

At present, it is assumed that the satellite is specularly reflecting with reflectivity, ρ, and thus

$$\gamma = (1 + \rho). \tag{6}$$

The vector $\hat{L}$ and the eclipse factor are determined from the solar ephemeris subroutine previously described, the satellite ephemeris, and involve the approximation of a cylindrical earth shadow.

1.5 Atmospheric Drag

The atmospheric decelerations are computed as follows:

$$\ddot{x}_{DRAG} = -\frac{\rho C_D A v v_x}{2m} \ ; \ \ddot{y}_{DRAG}, \ \ddot{z}_{DRAG} \tag{7}$$

where

ρ is the ambient atmospheric density

C_D is the satellite drag coefficient

A is the projected area of the satellite on a plane perpendicular to direction of motion

m is the satellite mass.

The velocity vector $\vec{v}$ given in inertial coordinates by

$$\vec{v} = v_x\hat{i} + v_y\hat{j} + v_z\hat{k} \tag{8}$$

can be chosen to be either the velocity relative to the atmosphere which implies that the atmosphere rotates with the earth or the inertial velocity which assumes that the atmosphere is static. Presently, the former assumption is made.

The density, ρ, is computed from the 1962 U.S. Standard Atmosphere.

APPENDIX A-2

PREPROCESSING OF OPTICAL OBSERVATIONS

2.1 Preprocessing of Optical Data

The first step in the processing of optical observations is usually performed by the observing source. This consists of developing a plate or film, identifying the image or images of the satellite and the images of several reference stars whose right ascensions and declinations are well known. The initial measurements of both satellite images and reference stars consist of linear rectangular coordinates. From the knowledge of the spherical coordinates of the reference stars, the right ascensions and declinations of the satellite images may be calculated. These coordinates as received by the preprocessor may be referred to the mean equator and equinox of date, true equator and equinox of date, or mean equator and equinox of some standard epoch.

The preprocessor then transforms these observations to a common coordinate system. Currently, the preprocessor transforms all right ascensions and declinations to the true equator and equinox of the epoch of the elements being processed. If the observations were originally referred to the mean equator and equinox of a particular epoch, it

is only necessary to precess from that epoch to the epoch of the elements. However, if they were referred to the true equator and equinox of a particular epoch, it is necessary first to transform them to the mean equator and equinox of that same epoch and then precess to the epoch of the elements.

Finally, a transformation must be made from the mean equator and equinox of the epoch of the elements to the true equator and equinox of the epoch of the elements.

2.2 Nutation

The transformations from the true equator and equinox of date to the mean equator and equinox of date is

$$Y = NX$$

where

$$Y = \begin{bmatrix} \cos \delta_m & \cos \alpha_m \\ \cos \delta_m & \sin \alpha_m \\ \sin \delta_m & \end{bmatrix}$$

$$X = \begin{bmatrix} \cos \delta_T & \cos \alpha_T \\ \cos \delta_T & \sin \sigma_T \\ \sin \delta_T & \end{bmatrix}$$

$$N = \begin{bmatrix} 1 & +\Delta\psi\cos\varepsilon_m & +\Delta\psi\sin\varepsilon_m \\ -\Delta\psi\cos\varepsilon_m & 1 & +\Delta\varepsilon \\ -\Delta\psi\sin\varepsilon_m & -\Delta\varepsilon & 1 \end{bmatrix}$$

where

α_m, δ_m = right ascension and declination referred to mean equator and equinox of date

α_T, δ_T = right ascension and declination referred to true equator and equinox of date

ε_m = mean obliquity of date

$\Delta\psi$ = nutation in longitude

$\Delta\varepsilon$ = nutation in obliquity

The inverse transformation is simply:

$$X = N^{-1}X = N^{T}X$$

2.3 Precession

The transformation from the mean equator and equinox of 1950.0 to the mean equator and equinox of an arbitrary epoch t1 is

$$Y = PX$$

where

$$Y = \begin{bmatrix} \cos\delta_{t1} & \cos\alpha_{t1} \\ \cos\delta_{t1} & \sin\alpha_{t1} \\ \sin\delta_{t1} & \end{bmatrix}$$

$$X = \begin{bmatrix} \cos\delta_{1950.0} & \cos\alpha_{1950.0} \\ \cos\delta_{1950.0} & \sin\alpha_{1950.0} \\ \sin\delta_{1950.0} & \end{bmatrix}$$

$$P = \begin{bmatrix} (\cos z\cos\theta\cos\zeta - \sin z\sin\zeta) & (-\cos z\cos\theta\sin\zeta - \sin z\cos\zeta) & (-\cos z\sin\theta) \\ (\sin z\cos\theta\cos\zeta + \cos z\sin\zeta) & (-\sin z\cos\theta\sin\zeta + \cos z\cos\zeta) & (-\sin z\sin\theta) \\ (\sin\theta\cos\zeta) & (-\sin\theta\sin\zeta) & (\cos\theta) \end{bmatrix}$$

The inverse transformation is

$$X = P^{-1}Y = P^{T}Y$$

Since the expression for z, θ, ζ are tied to 1950.0 as an epoch, the precession between 2 different epochs, neither of which is 1950.0, must be performed in two steps, using 1950.0 as an intermediary epoch.

APPENDIX A-3

STATION POSITION TRANSFORMATIONS

3.1 Station Position Transformations

The analysis of "long arc" passes of the GEOS-A satellite requires that the various tracking station *a priori* positions be available on a uniform world geodetic system in order that the results not be biased by interdatum uncertainties. The world geodetic system selected for these analyses is the SAO Standard Earth (C-5 datum).

A priori estimates of the tracking station positions and their uncertainties relative to the geo-center (earth's center of mass) are derived from the knowledge of the following:

a. Baker-Nunn camera station positions on the original datums.

b. Baker-Nunn camera station positions on the SAO C-5 datum.

c. The positions of the various tracking sites in their original datums.

d. Intra-datum survey connections between the Baker-Nunn sites and the various tracking sites.

e. Empirical formulae for the estimation of surface survey uncertainties between the Baker-Nunn sites and the tracking sites.

The method used to effect this transformation is simple and straight forward and has been checked to ascertain its compatibility with the more rigorous and arduous transformation formulae commonly used to compute datum shifts. It should be noted that this method can be used only when the type of information that has been calculated for the Baker-Nunn sites is available. That is to say, one must have available the positions of the control stations (Baker-Nunn sites) in the original datum and in the new reference system, and a direct survey tie between the control stations and the tracking stations which are to be transformed.

3.2 SAO Standard Earth Reference System

The reference system used in the derivation of the a priori positional information is the SAO Standard Earth as described in [1]. The ellipsoidal parameters are a_e = 6,378,165 meters and f = 1/298.25. This system is the best available geocentric (earth's center of mass) terrestrial system. The Z axis is oriented in the direction of the mean pole of 1900-1905 and the X axis in the direction of the mean observatory. Since the definition of UT-1 was based on the U. S. Naval Observatory's time determination the X axis is directed toward the meridian 75°-03'-55".94 East of the U. S. Naval Observatory.

The uncertainty related to this system is defined

(by [1] to be about ±10 meters for the origin (geocentricity), 0".2 for the direction of the axes, and a few parts per million in scale. The scale actually depends on the adopted value for GM which in this instance is $3.986032 \times 10^{20} cm^3 sec^{-2}$. The absolute coordinates of the Baker-Nunn stations are given to an accuracy of ±15 to 20 meters. The fact that this system is oriented to the mean pole of 1900-1905 must be taken into consideration when station positions as derived from the tracking data are obtained. Unless corrections for polar motion are applied, the positions derived from the tracking data will be based on the instantaneous pole at the time of observation.

3.3 Coordinate Transformations

All of the Baker-Nunn camera stations are connected to individual major geodetic datums and their coordinates in these datums are known. The coordinates of the Baker-Nunn camera stations on the SAO Standard Earth are also known, having been derived by SAO through the reduction of approximately 35,000 satellite observations with wide orbital variety. The coordinates of the Baker-Nunn camera stations are given in both the ellipsoidal and three-dimensional cartesian coordinate systems. For ease and simplicity of calculation, we have elected to use the cartesian coordinates to obtain our transformations. By comparing the original datum coordinates with the derived mass-centered coordinates, one derives the "datum shift" for the particular datum. The "datum shift" is simply the total transformation to be applied to the original datum coordinates to obtain the new mass-centered coordinates. Once the

"datum shift" has been derived for the Baker-Nunn station this shift is then applied in a weighting scheme to derive the SAO Standard Earth coordinates for tracking stations that have positions given in the same original datum as the Baker-Nunn and are connected to the Baker-Nunn station through conventional surface surveys. A weighting scheme (which is described below) is used since the Baker-Nunn stations were allowed to adjust independently and subsequently where more than one Baker-Nunn station was located on a single datum, the individual stations show slightly different "datum shifts".

As an example of the single station case, consider Baker-Nunn camera station 9005, TOKYO. Its coordinates on the Tokyo (JAP) datum are:

X: -3,946,554 (meters)

Y: +3,365,774 (meters)

Z: +3,698,151 (meters)

Its geocentric (mass centered) coordinates on the SAO Standard Earth are:

X_g: -3,946,703 (meters)

Y_g: +3,366,291 (meters)

Z_g: +3,698,849 (meters)

The transformation to be applied to tracking stations on the Tokyo datum is therefore:

$$X_g - X = \Delta X = -149 \text{ meters}$$

$$Y_g - Y = \Delta Y = +517 \text{ meters}$$

$$Z_g - Z = \Delta Z = +698 \text{ meters}$$

The ΔX, ΔY, ΔZ is applied to the tracking station coordinates on Tokyo datum. This in effect then furnishes an a priori estimate of the coordinates of the tracking station in the SAO Standard Earth reference system.

As mentioned above, the coordinates of the Baker-Nunn camera stations are furnished in both the ellipsoidal and three-dimensional cartesian coordinate systems. However, the coordinates of the various tracking stations may be given in ellipsoidal coordinates only, thereby requiring the calculation of the three-dimensional cartesian coordinates. This is done using the following standard formulation:

$$X = (\nu + h + N) \cos \phi \cos \lambda$$

$$Y = (\nu + h + N) \cos \phi \sin \lambda$$

$$Z = [(1 - e^2)\nu + h + N] \sin \phi$$

where:

ϕ = geodetic latitude

λ = geodetic longitude

$\nu = a_e/(1 - e^2 \sin^2\phi)^{1/2}$

a_e = semi major axis of reference ellipsoid

e^2 = eccentricity squared of reference ellipsoid

h = height of station above the geoid (mean sea level elevation)

N = height of the geoid above or below the spheroid.

In the case where the tracking station information only contains mean sea level elevations, the geoid height is derived from geoid contour charts for the particular reference spheroid. These charts are based on gravitational coefficients derived from satellite observations.

Having derived the a priori estimates of the tracking station positions on the SAO Standard Earth we now derive estimates of the uncertainties of these positions relative to the earth's center of mass.

3.4 A Priori Uncertainty Derivation

In order to derive a priori estimates of the uncertainty in the tracking station positions, use is made of an empirical formula derived by Lansing Simmons, USC & GS, to describe the accuracy of first order triangulation. The formula states that the relative accuracy between two points connected by conventional first-order triangulation (1 part in 25,000) is approximately:

$$1/20{,}000\sqrt[3]{M},$$

where M is distance between the two stations in statute miles. As an example consider two stations 1000 miles apart, and connected by standard triangulation. The proportional accuracy would therefore be 1 part in 200,000 or approximately 26.4 ft. This means that the relative uncertainty between the two stations caused by the surface survey errors is approximately 26 ft. or 8 meters. Accepting the stated accuracy of the Baker-Nunn stations relative to the center mass as $\pm$ 20 meters, one can then take the root sum square of the uncertainty in the Baker-Nunn station relative to the center of mass and the surface survey uncertainty between the Baker-Nunn and the tracking station as derived by the Simmons formula as a conservative estimate of the uncertainty of the tracking station relative to the center of mass. The formula then becomes:

$$\sigma_g = \sqrt{\sigma_s^2 + 20^2}$$

where

σ_g = uncertainty of the tracking station relative to the center of mass.

σ_s = survey uncertainty as computed by Simmons formula.

3.5 Weighting Scheme for Multi-Station Connections

In the case where a tracking station is located on a datum which contains more than one Baker-Nunn station, we use a weighted average of the geocentric coordinates of the tracking station derived from the general formula

$$P = \left(\frac{W_1}{W_1+W_2 \ldots W_n}\right) P_1 + \left(\frac{W_2}{W_1+W_2 \ldots W_n}\right) P_2$$

$$+ \ldots \left(\frac{W_n}{W_1+W_2 \ldots W_n}\right) P_n$$

where:

P	is the weighted position
$W_1 \ldots W_n$	are the weights
P_1	is the station position derived from Baker-Nunn Station 1
P_2	is the station position derived from Baker-Nunn Station 2
P_n	is the station position derived from Baker-Nunn Station n

The weights used are inversely proportional to the distances between the Baker-Nunn stations and the tracking station to be transformed. This weighting scheme allows us to take into consideration the varying shifts of the Baker-Nunn stations while placing proper emphasis on the contribution of individual stations upon the transformation. As an example, consider the case where the tracking station is located close to one of the Baker-Nunn stations in the datum. One can rightfully expect that the tracking station would shift approximately the same amount and in the same direction as the co-located Baker-Nunn and that the effect of the other Baker-Nunn stations would be minimal. In the case where the tracking station were located equidistant from several Baker-Nunn stations one would assume equal contribution to the transformation from each of the Baker-Nunn shifts.

While the above weighting scheme is apparently quite adequate, investigations are continuing into other weighting schemes. Foremost of these is the computation of the weights (W_n) as being inversely proportional to the square of the distances between the Baker-Nunn stations and tracking station to be transformed. Another procedure being investigated is the distance cut-off, whereby a very distant Baker-Nunn coordinate shift will have essentially no effect on the station to be transformed. This cut-off distance is being presently considered in the range of 5000 km.

The transformed station coordinates derived using these weighting schemes are being compared in separate NO-NAME data reduction runs. Identical observational data are being reduced in each run, and the observational residuals are being compared.

3.6 Isolated Datums

An ellipsoidal transformation is performed for a tracking station on an isolated datum such as the Tananarive datum. For these station positions, the ΔU, ΔV, and ΔW shifts are unknown and considered to be zero. The shifts are computed as follows:

$$\Delta N = (a\,\Delta f + f\,\Delta a)\sin^2\phi - \Delta a$$

$$\Delta\phi = 206265[(a\,\Delta f + f\,\Delta a)\sin 2\phi]/R_m$$

$$R_m = \frac{a(1-e^2)}{[(1-e^2\sin^2\phi)^{1/2}]^{3/2}}$$

where

a	=	6378165. meters
f	=	1/298.25
Δa	=	6378165. minus original survey ellipsoid value of a.
Δf	=	1/298.25 minus original survey ellipsoid value of F.
ϕ	=	Latitude of tracker in original system
e^2	=	$2f - f^2$

X-552-67-540

THE DETERMINATION AND COMPARISON OF THE GRARR MADGAR SITE LOCATION

Francis J. Lerch
Clarence E. Doll
Mission Trajectory Determination Branch
Mission and Trajectory Analysis Division
Tracking and Data Systems Directorate

Samuel J. Moss
Brian O'Neill
Wolf Research and Development Corporation
Applied Sciences Department
College Park, Maryland

October 1967

GODDARD SPACE FLIGHT CENTER
Greenbelt, Maryland

THE DETERMINATION AND COMPARISON OF THE GRARR MADGAR SITE LOCATION

Francis J. Lerch
Clarence E. Doll
Samuel J. Moss
Brian O'Neill

ABSTRACT

Improved coordinates for the MADGAR range and range rate site have been estimated from GEOS-I data sets using the NONAME orbit determination program. These coordinates have been compared with a preliminary estimate obtained under contract with Goddard Space Flight Center by the Applied Physics Laboratory using thirty-nine passes of SRN-9 Doppler data from three satellites.

Two independent estimates were obtained using the NONAME orbit determination program; one estimate was obtained from optical flash sequence data taken at 1TANAN (MOTS 40" camera) during July 1966 and the other from range measurements taken at MADGAR during November 1965. These two estimates of the site location are within five meters of each other; whereas the Applied Physics Laboratory estimate is separated by fifty meters, mainly in longitude.

The comparison of the Applied Physics Laboratory MADGAR location estimate with the optically determined NONAME estimate is shown by plots of the residual differences of the range and range rate measurements from five reference orbits. The five reference orbits were determined solely from optical flash sequence data, and they had a maximum root mean square of fit of less than two seconds of arc. The residual difference for both range and range rate measurements clearly indicate that a significantly better set of MADGAR coordinates was obtained from the NONAME orbit determination program.

Table I

Estimated MADGAR C-5 Station Coordinates
(GRARR S-band Antenna)

	Latitude	East Longitude	Spheroid Height
Optical estimate	-19° 1' 19.5"	47° 18' 7.9"	1380.0 meters
GRARR estimate	-19° 1' 19.4"	47° 18' 8.0"	1382.6
APL estimate	-19° 1' 19.5"	47° 18' 6.2"	1381.0

(The C-5 ellipsoid semi-major axis is 6,378,165 meters and the flattening is 1/298.25)

PRECEDING PAGE BLANK NOT FILMED.

CONTENTS

ILLUSTRATIONS

TABLES

THE DETERMINATION AND COMPARISON OF THE GRARR MADGAR SITE LOCATION

1.0 INTRODUCTION

The coordinates of the two STADAN tracking stations in Tananarive, Madagascar were estimated separately using two independent data sets. The stations are the MOTS 40" camera station 1TANAN, and the GRARR station MADGAR.

The new locations were estimated using the NONAME Orbit Determination Program[1]; the data used in the estimation process was tracking data from SAO Baker-Nunn cameras, STADAN MOTS 40" cameras, and a STADAN Range and Range Rate instrument. The location of each station was estimated separately using independent data sets; a data set from July, 1966, was used to estimate 1TANAN, and another from November, 1965, was used to estimate MADGAR.

The estimated locations are shown in Table II; the shifts between the original and estimated coordinates were 6.9 seconds in latitude for 1TANAN and 6.8

Table II

Coordinates of 1TANAN and MADGAR

	1TANAN			MADGAR		
Latitude	Deg.	Min.	Secs.	Deg.	Min.	Secs.
Original location	-19	0	26.4	-19	1	12.6
Estimated location	-19	0	33.6	-19	1	19.4
Shift			+ 6.9			+ 6.8
East Longitude						
Original location	47	17	59.2	47	18	8.2
Estimated location	47	17	58.9	47	18	8.0
Shift			- 0.3			- 0.2
Spheroid Height (Meters)						
Original location		1305.5			1329.5	
Estimated location		1355.9			1382.6	
Shift		50.4			53.1	

[1]The NONAME orbit determination program was developed under NASA contract by Wolf Research and Development Corporation for the Mission and Trajectory Analysis Division (Reference 1).

seconds for MADGAR, in East longitude -0.3 seconds and -0.2 seconds, respectively, and in spheroid height 50.4 meters and 53.1 meters, respectively. Thus, the relative location of the two stations has only changed slightly. The shifts between the original coordinates and the estimated coordinates of 1TANAN were applied to the original MADGAR coordinates to obtain the optical estimate of the MADGAR location.

2.0 DETERMINATION OF STATION LOCATIONS

Orbits were estimated from two data sets using the NONAME Orbit Determination Program, operating in the data reduction mode. The program used a Bayesian least squares technique to estimate six orbital parameters and the three coordinates of the station being estimated.

The following data sets were used:

(1) July 9, 10 and 11, using 730 measurements.
(2) November 28 and 29, using 598 measurements.

The majority of the measurements were from SAO Baker-Nunn camera stations; the remainder were from STADAN MOTS 40" camera stations and MADGAR GRARR.

The coordinates of 1TANAN were estimated using data set (1), and the coordinates of MADGAR were estimated using data set (2). A representation of the geometry of the passes over 1TANAN and MADGAR is given in Figure 1. Summaries of the data sets are given in Tables III and IV.

3.0 COMPARISON OF STATION LOCATIONS

To compare the new locations, the original, NONAME, and APL coordinates[2] of MADGAR were used in turn to obtain the residual differences for ten passes of GRARR observations from five reference orbits.

The reference orbits were estimated using optical data only, and they all had an rms of fit of 2 seconds of arc or less. The following periods and data sets were used:

(1) November 23 and 24, 1965 using 519 measurements.
(2) November 27, 28 and 29, 1965 using 826 measurements.

[2]This is a preliminary result obtained by APL under a NASA contract from the Mission and Trajectory Analysis Division.

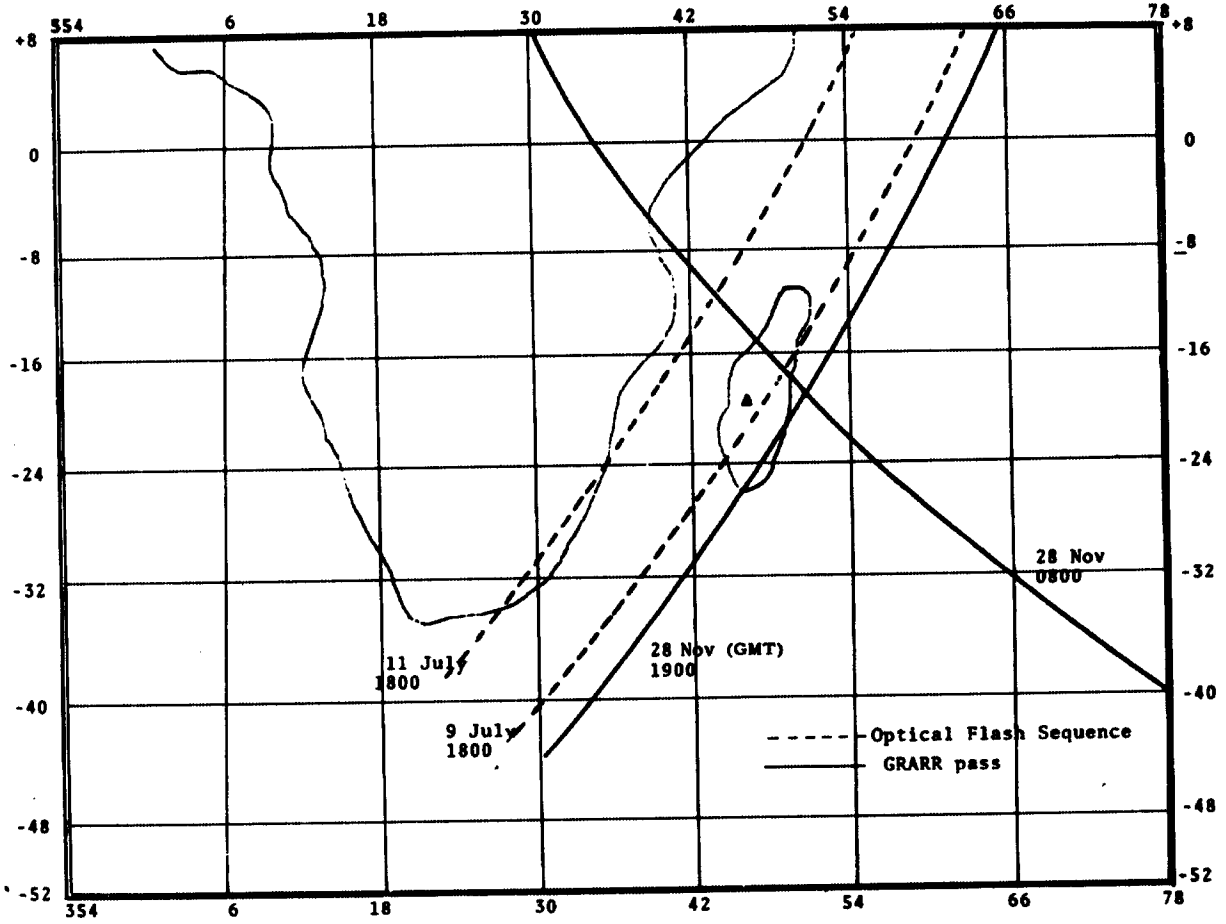

Figure 1. Optical and GRARR Passes over Tananarive

Table III

Summary of Data by Station for July 9, 10, and 11

Station	No. of Measurements	
	Right Ascension	Declination
1TANAN	14	14
1ROSMA	7	7
1COLBA	14	14
1BPOIN	14	14
1DENVR	20	20
1JOBUR	14	14
1ORGAN	91	91
1OLFAN	28	28
1SPAIN	21	21
1QUIPA	28	28
1CURAC	28	28
1JUPTR	35	35
1VILDO	7	7
AUSBAK	14	14
1MAUIO	28	28
EDWAFB	2	2
TOTAL	365	365

Table IV

Summary of Data by Station for November 28 and 29

Station	No. of Measurements	
	Right Ascension	Declination
1ORGAN	59	59
1OLFAN	1	1
1SPAIN	1	1
1QUIPA	2	2
1CURAC	96	96
1JUPTR	127	127
1VILDO	1	1
TOTAL	287	287
	Range	
MADGAR	24	

(3) November 28 and 29, 1965 using 574 measurements.
(4) July 17 and 18, using 780 measurements.
(5) July 22, 23 and 24, using 641 measurements.

Summaries of these data sets are given in Tables V - IX.

Table V

Summary of Data by Station for November 23 and 24

Station	No. of Measurements	
	Right Ascension	Declination
1EDINB	17	10
1FTMYR	41	44
1PURIO	19	19
1BPOIN	11	13
BEDFRE	13	13
1ORGAN	62	55
1CURAC	59	51
1JUPTR	34	34
1COLBA	4	2
1OLFAN	3	2
1SPAIN	2	2
1QUIPA	1	1
1VILDO	3	3
AUSBAK	0	1
TOTAL	269	250

The geometry of the ten GRARR passes during these periods is shown in Figures 2 and 3. The residual differences obtained using the three locations are summarized in Figures 4-23. The range residuals in these figures have been corrected for refraction, transponder delay, and known cable bias; no corrections were applied to the range rate residuals. Figures 4-23, clearly indicated that the NONAME estimated coordinates are a significant improvement on the other two sets.

The residuals obtained using the NONAME location are smaller in sixteen out of the twenty plots, by as much as 45 meters in range and 50 cm/sec in range rate in some cases. In three of the plots the size of the residuals is approximately equal, and in one plot the residuals obtained using the APL location are slightly smaller. The sizes of the differences between the two sets of residuals correspond to the 50 meter separation in the longitude coordinate in combination with the pass geometry.

Table VI

Summary of Data by Station for November 27, 28 and 29

Station	No. of Measurements	
	Right Ascension	Declination
1EDINB	12	14
1FTMYR	21	21
1COLBA	10	11
1JUM40	6	6
1ORGAN	66	73
1SPAIN	1	1
1QUIPA	133	128
1JUPTR	169	148
1VILDO	2	2
AUSBAK	1	1
TOTAL	422	406

Table VII

Summary of Data by Station for November 28 and 29

Station	No. of Measurements	
	Right Ascension	Declination
1ORGAN	60	60
1OLFAN	1	1
1SPAIN	1	1
1QUIPA	2	2
1CURAC	96	96
1JUPTR	127	127
1VILDO	1	1
TOTAL	288	288

Table VIII

Summary of Data by Station for July 17 and 18

Station	No. of Measurements	
	Right Ascension	Declination
1JOBUR	13	13
1ORGAN	73	73
1OLFAN	31	31
1SPAIN	48	48
1QUIPA	21	21
1JUPTR	112	112
1VILDO	14	14
1MAUIO	29	29
AUSBAK	49	49
TOTAL	390	390

Table IX

Summary of Data by Station for July 22, 23 and 24

Station	No. of Measurements	
	Right Ascension	Declination
1ORGAN	145	163
1OLFAN	31	35
1SPAIN	31	35
1QUIPA	27	27
1VILDO	21	21
1MAUIO	15	13
AUSBAK	49	
TOTAL	319	322

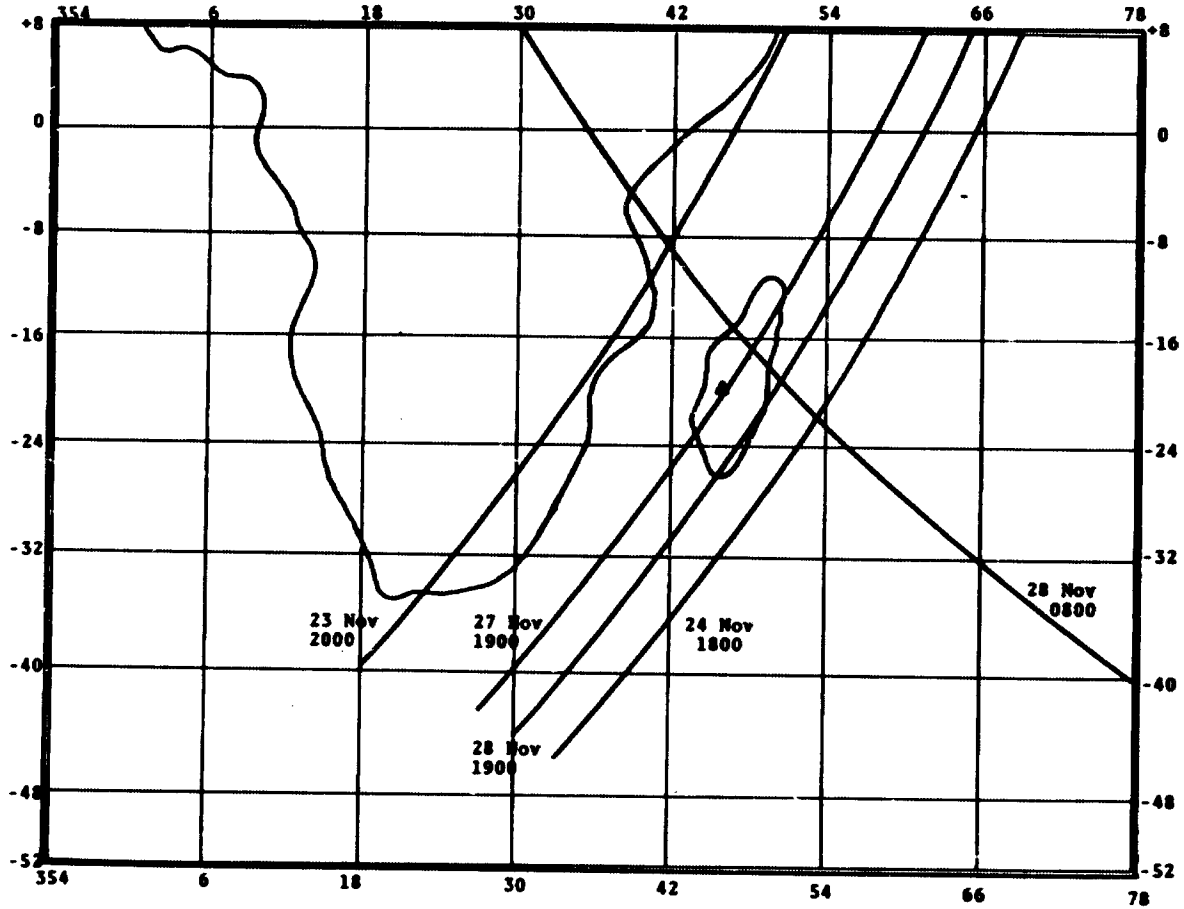

Figure 2. GRARR Passes over MADGAR

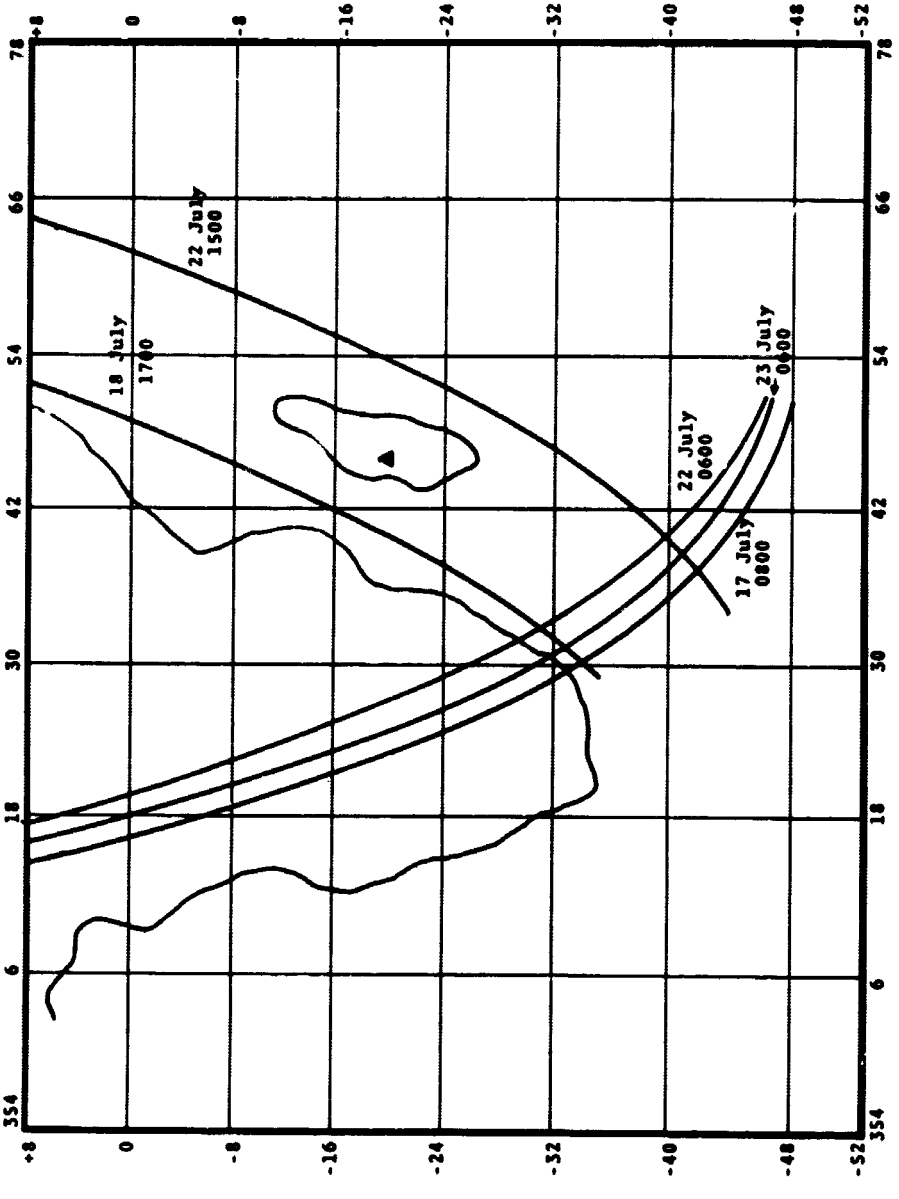

Figure 3. GRARR Passes over MADGAR

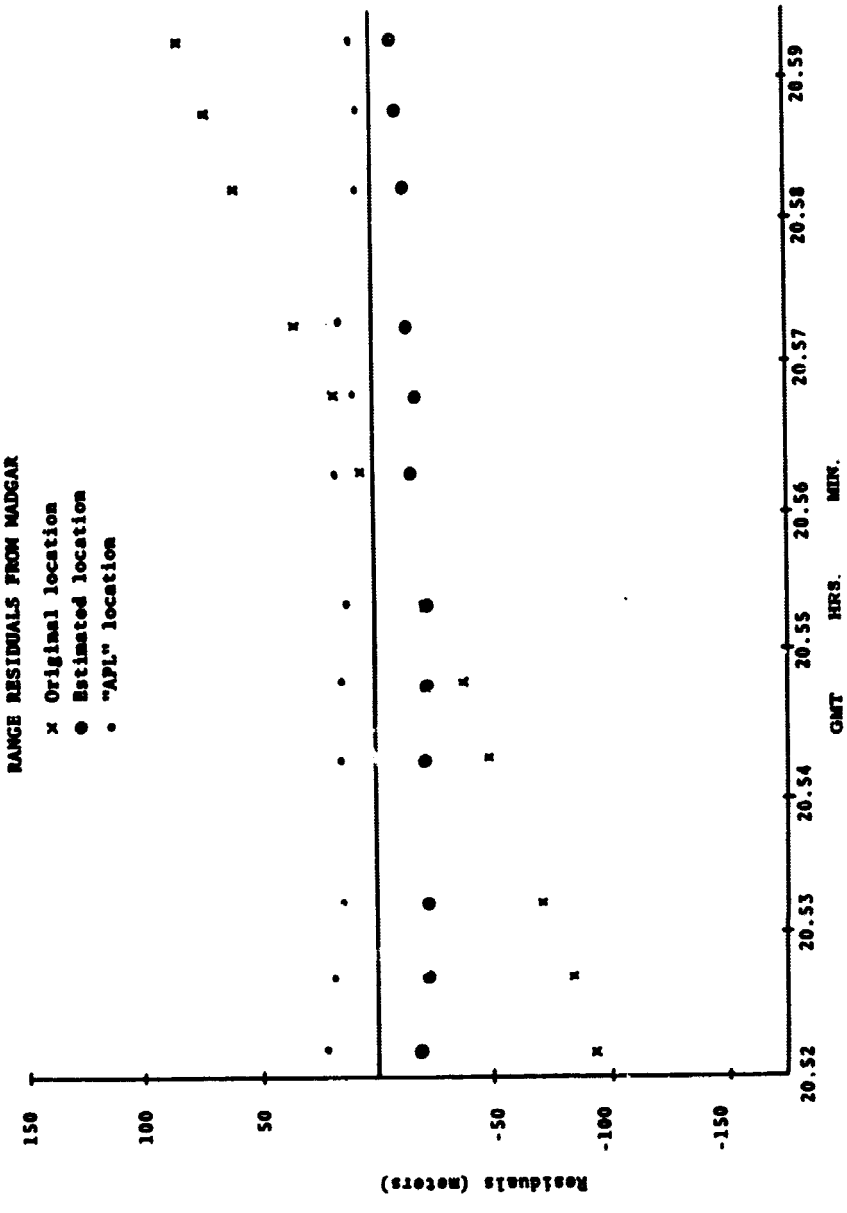

Figure 4. November 23, 1965

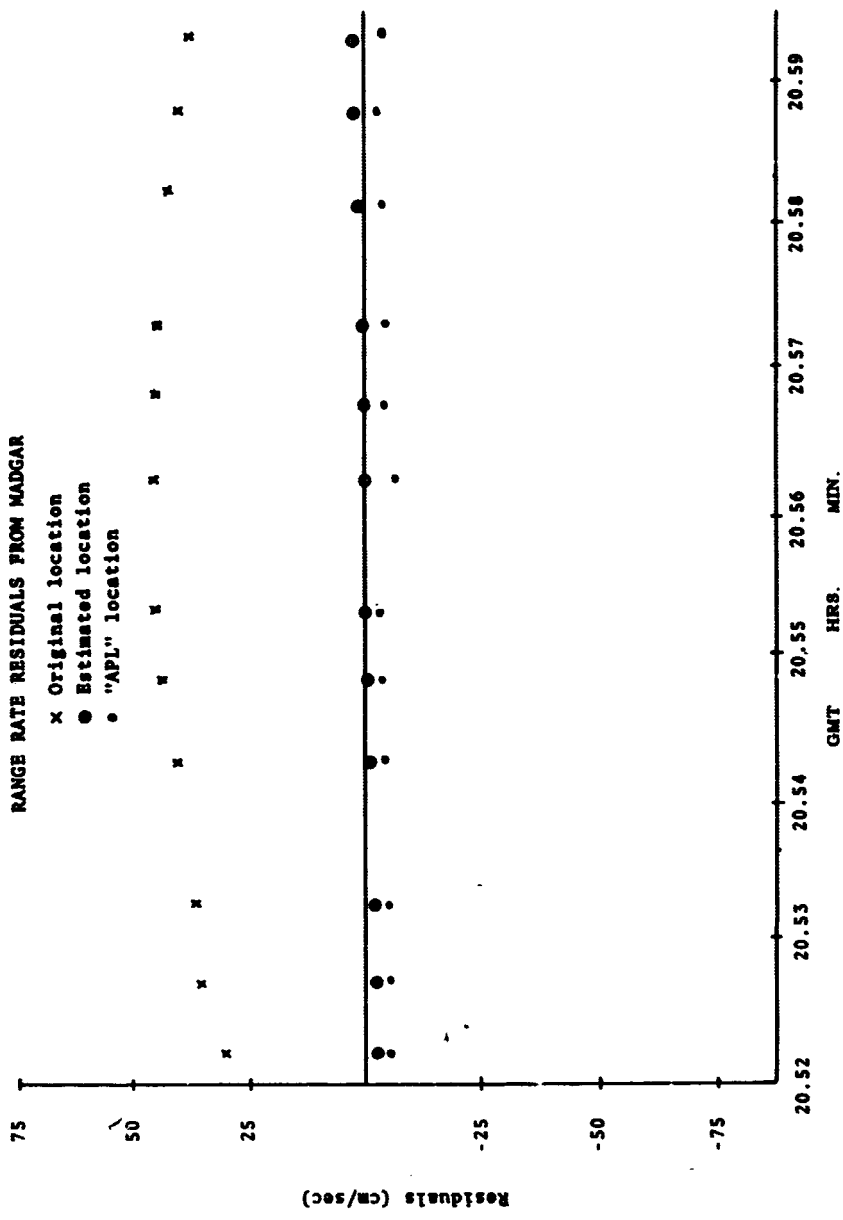

Figure 5. November 23, 1965

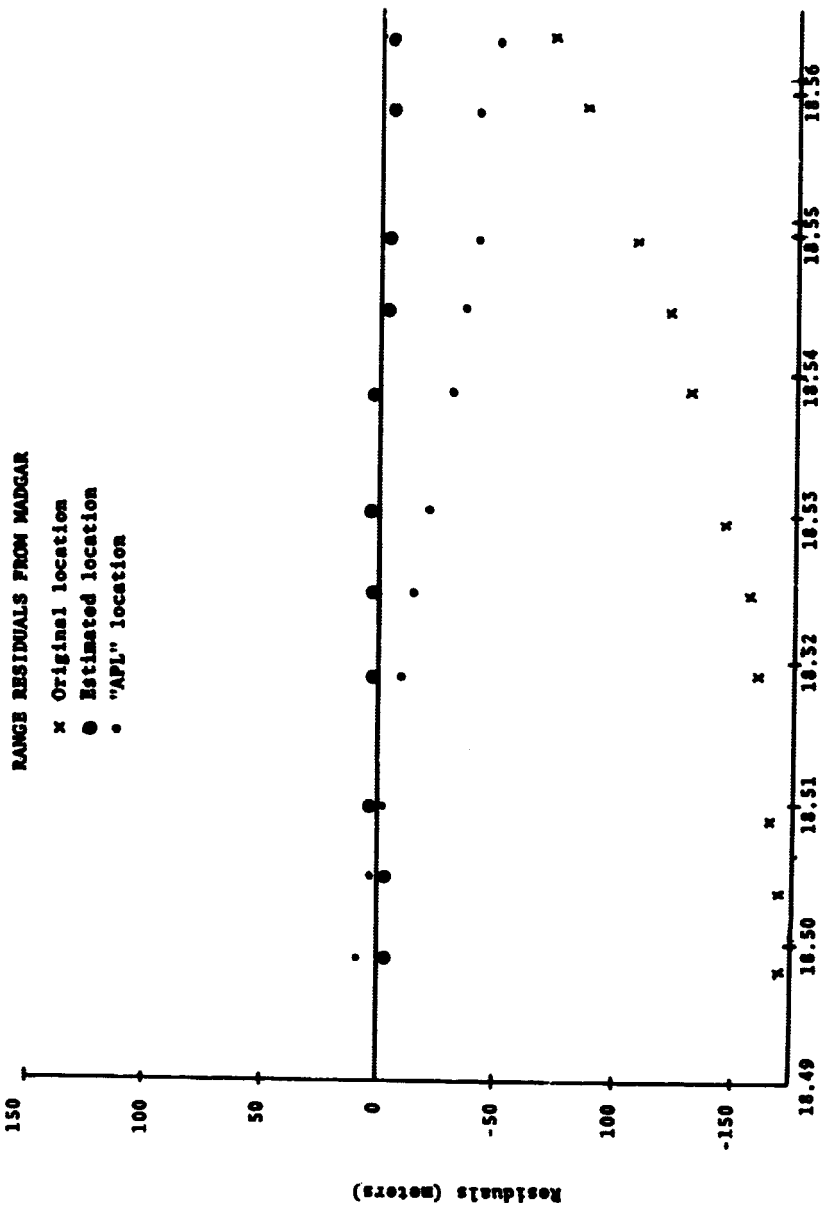

Figure 6. November 24, 1965

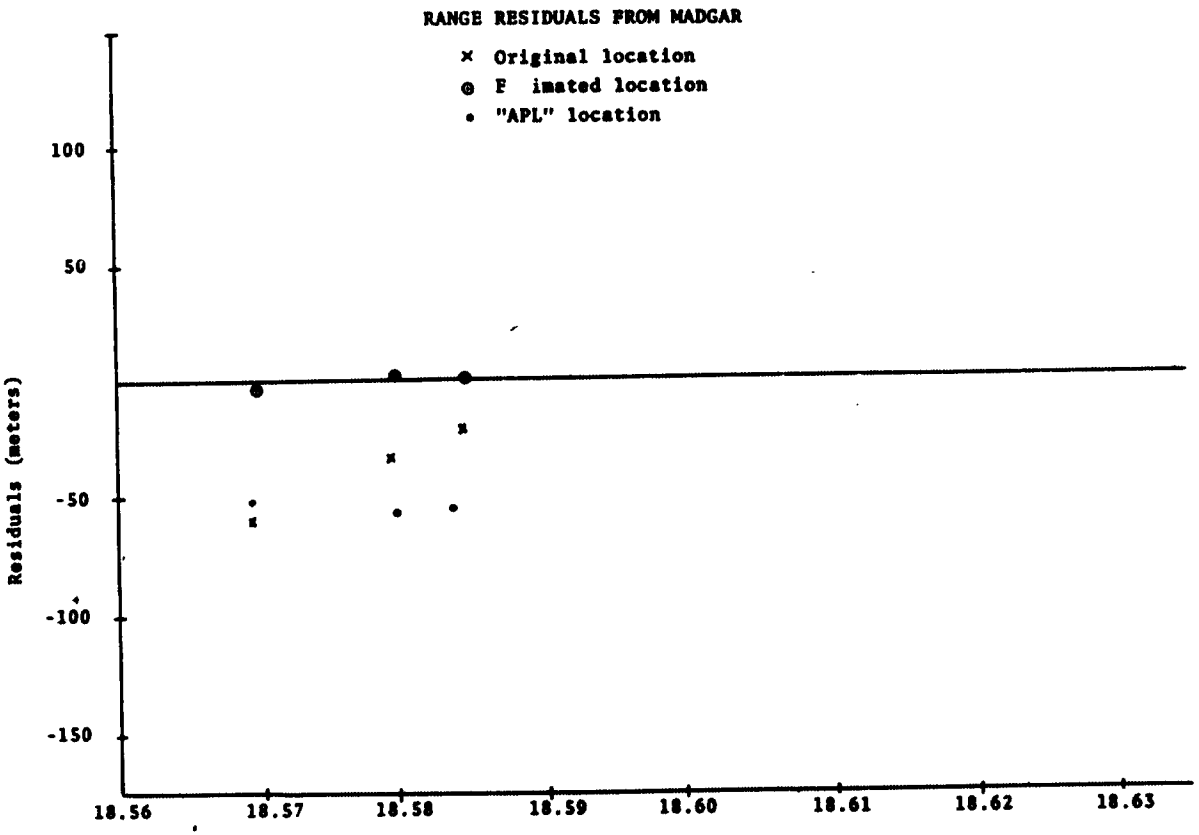

Figure 6 (Cont.). November 24, 1965

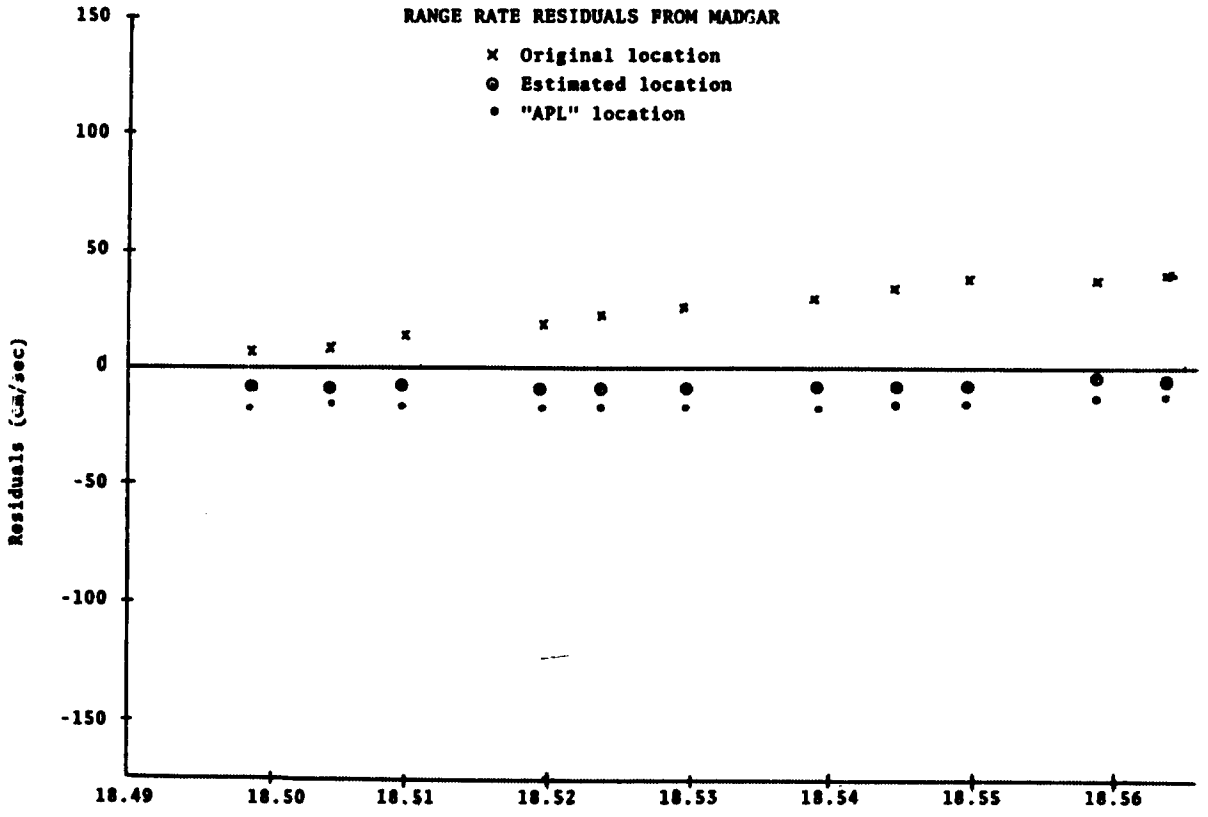

Figure 7. November 24, 1965

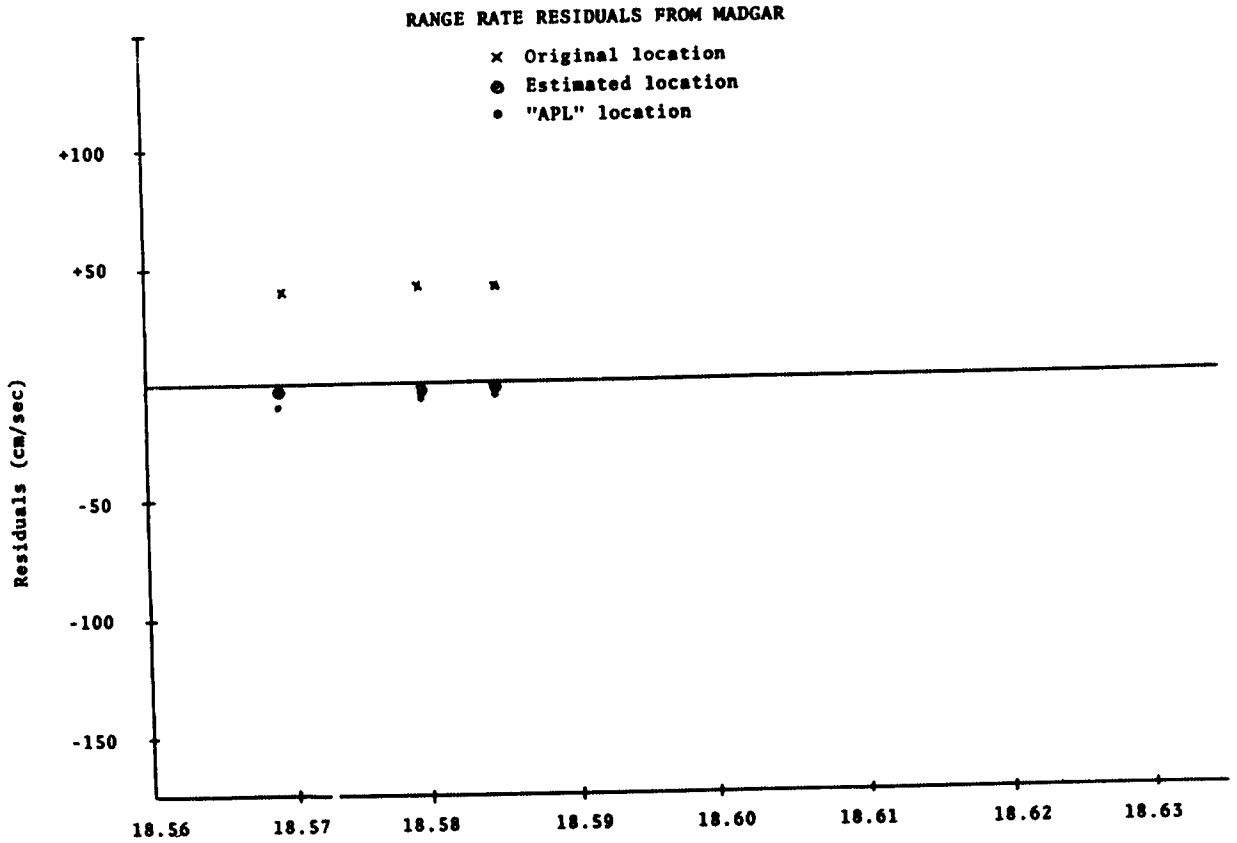

Figure 7 (Cont.). November 24, 1965

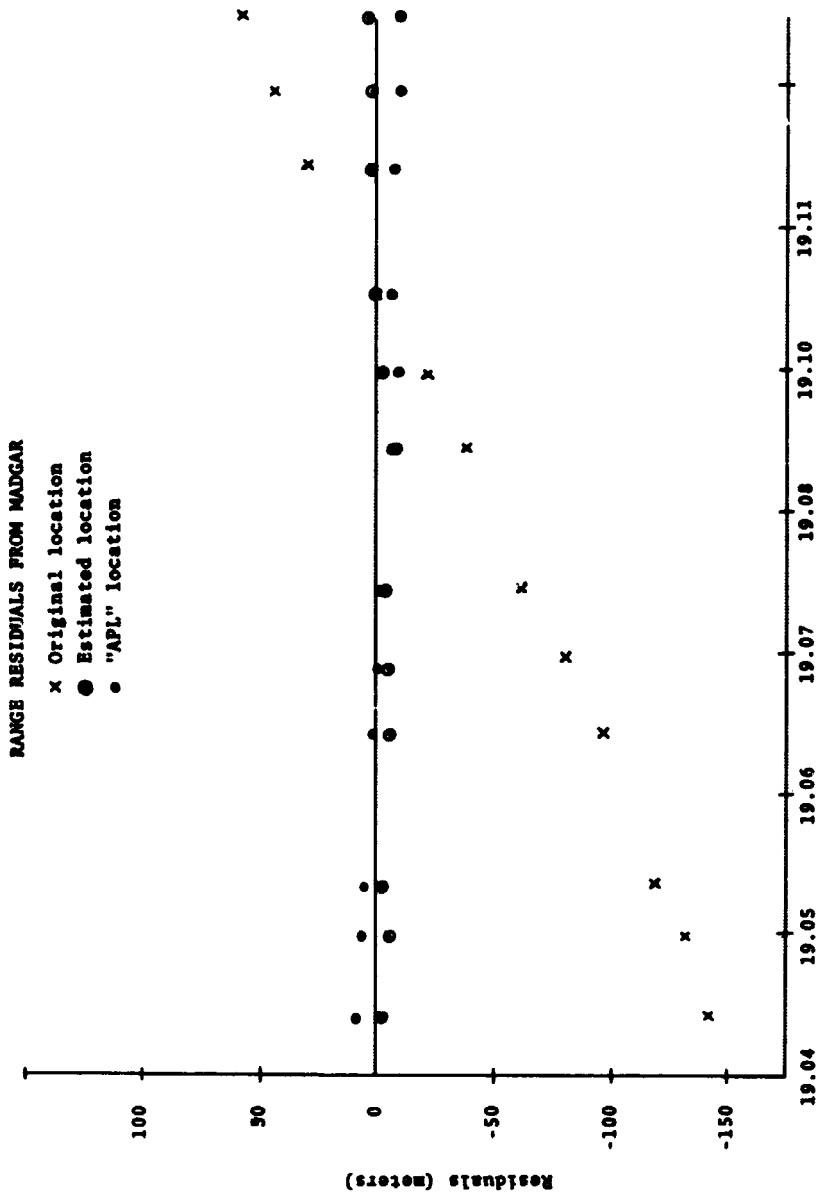

Figure 8. November 27, 1965

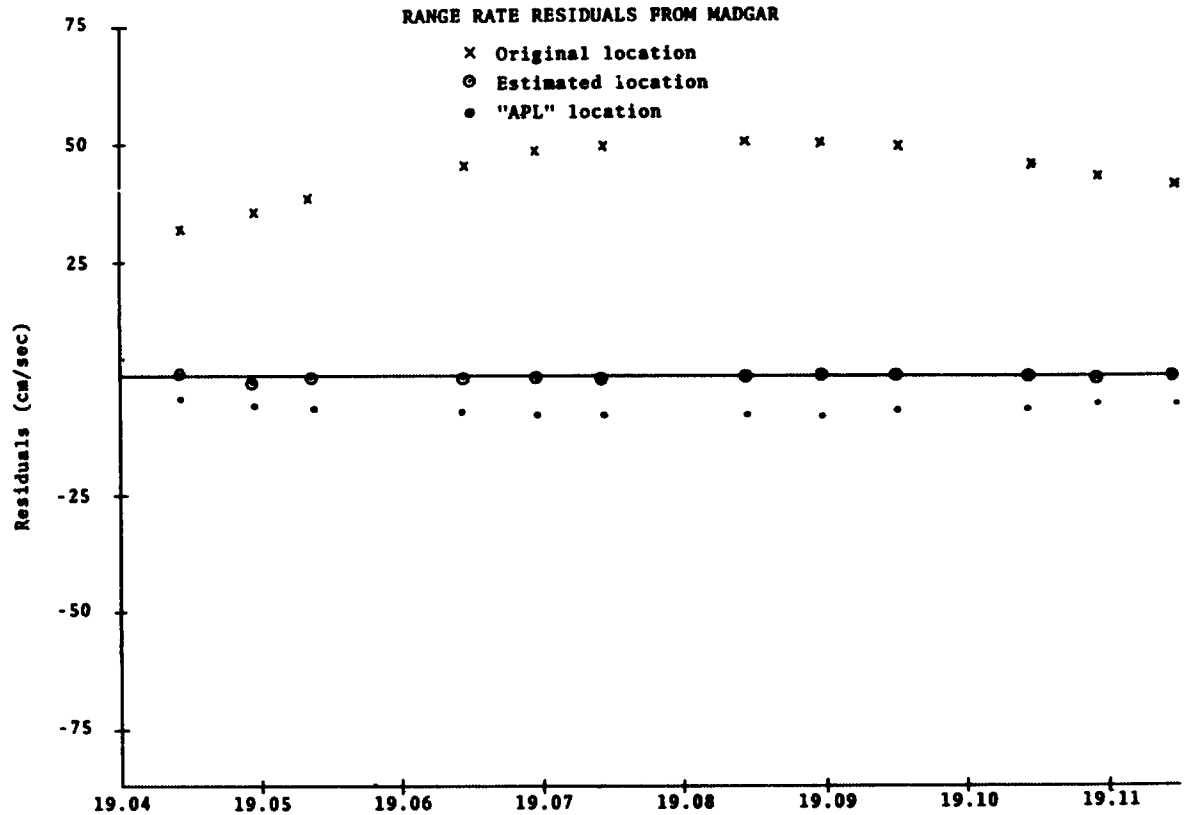

Figure 9. November 27, 1965

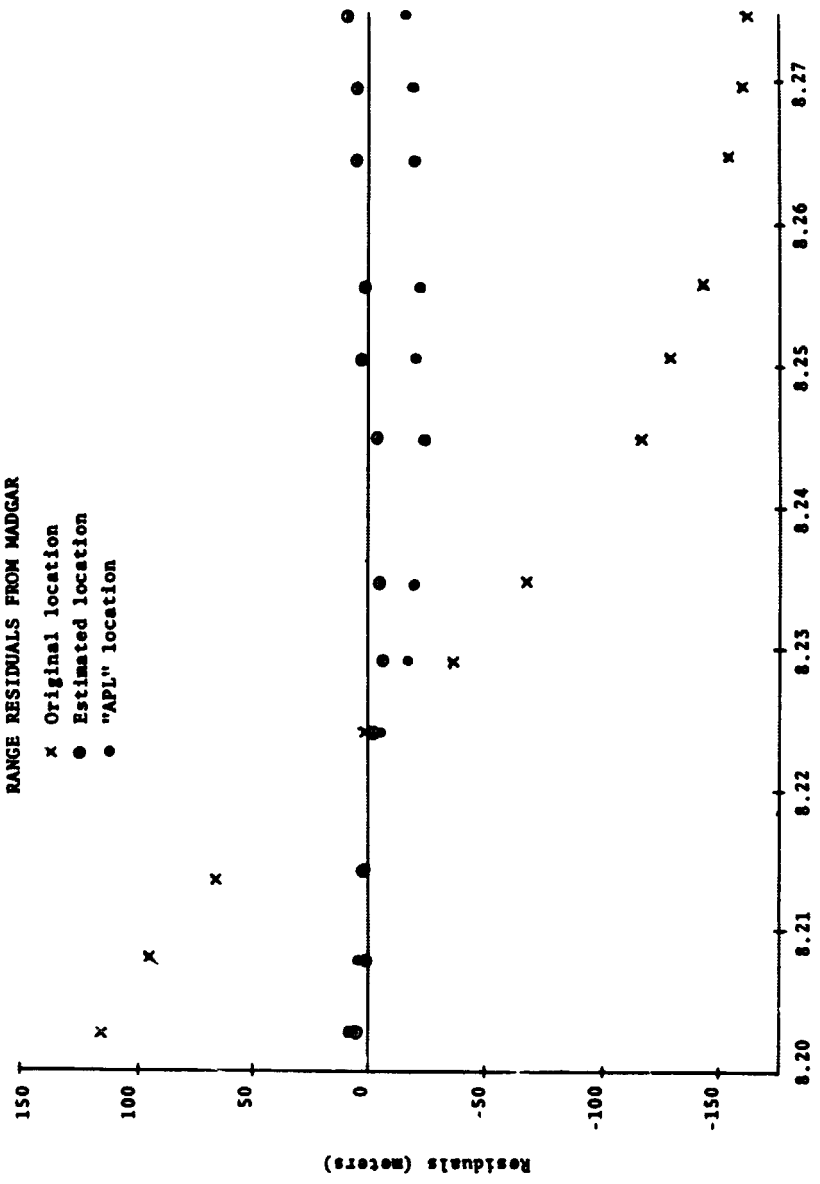

Figure 10. November 28, 1965

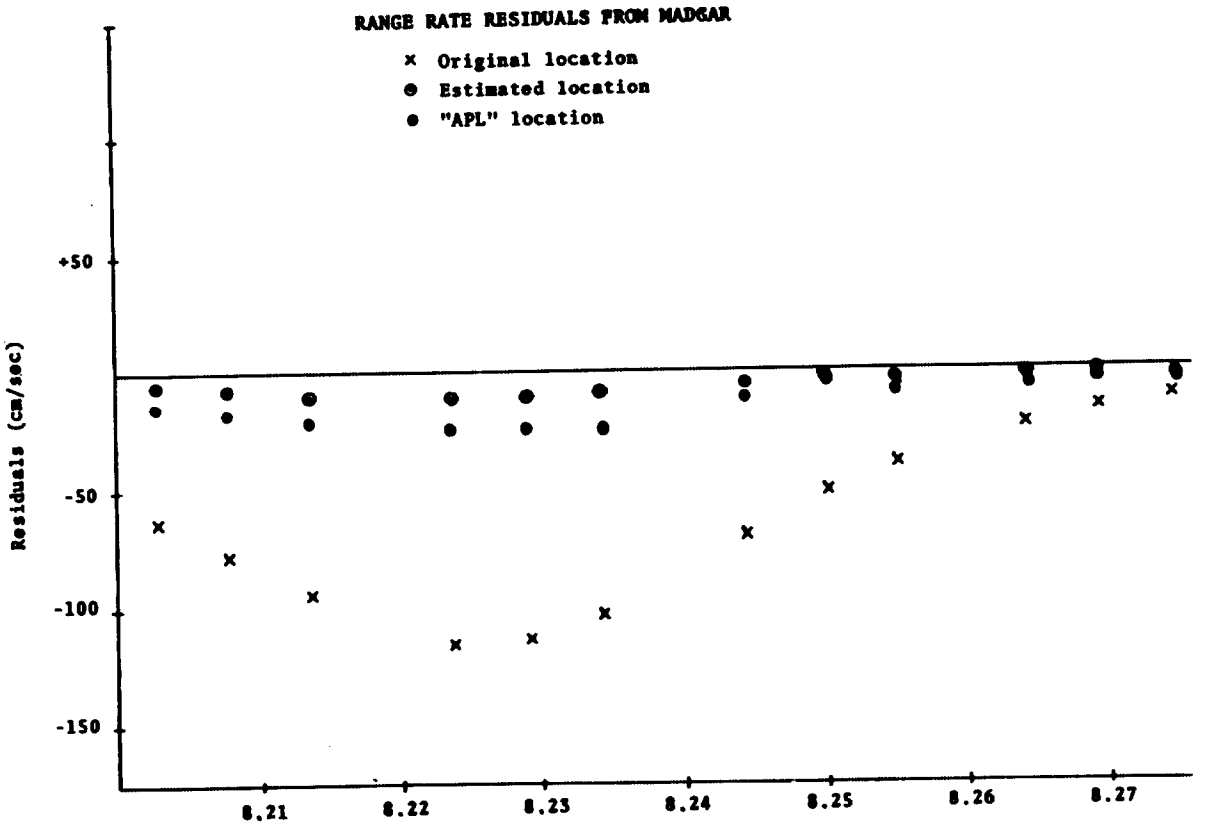

Figure 11. November 28, 1965

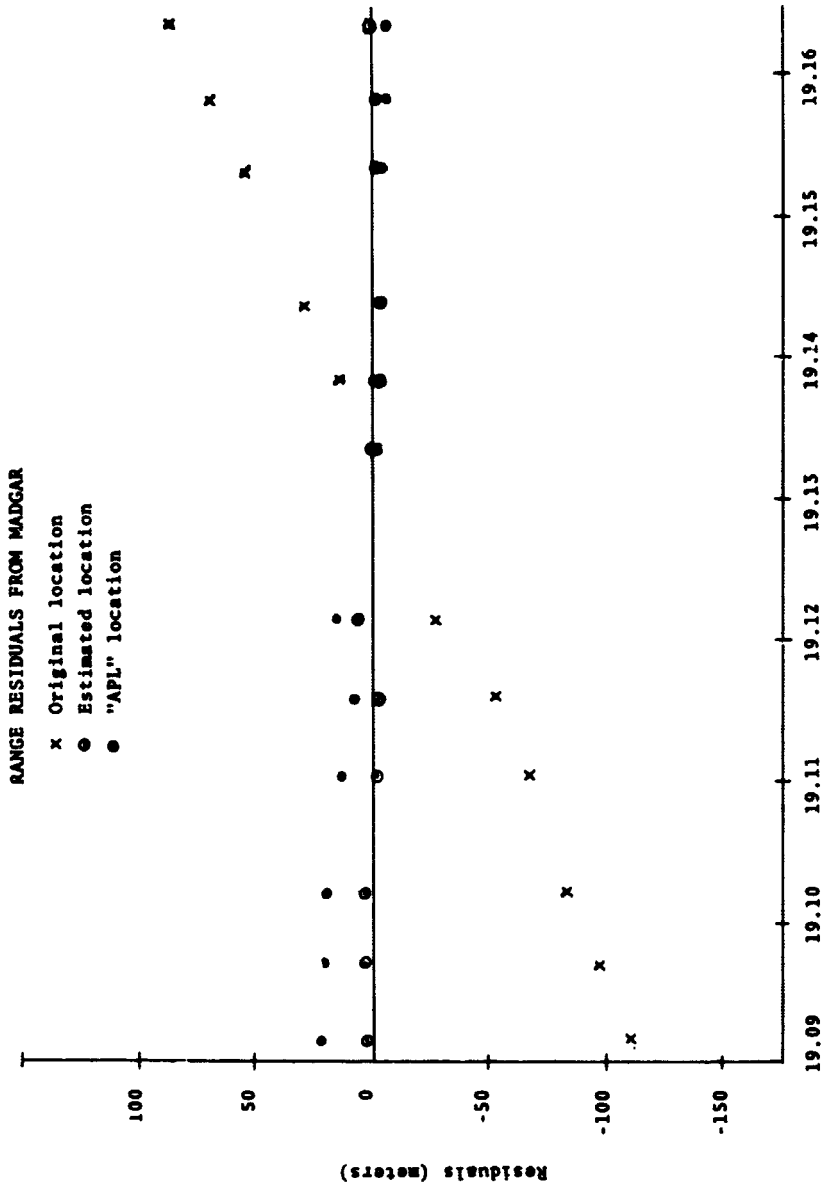

Figure 12. November 28, 1965

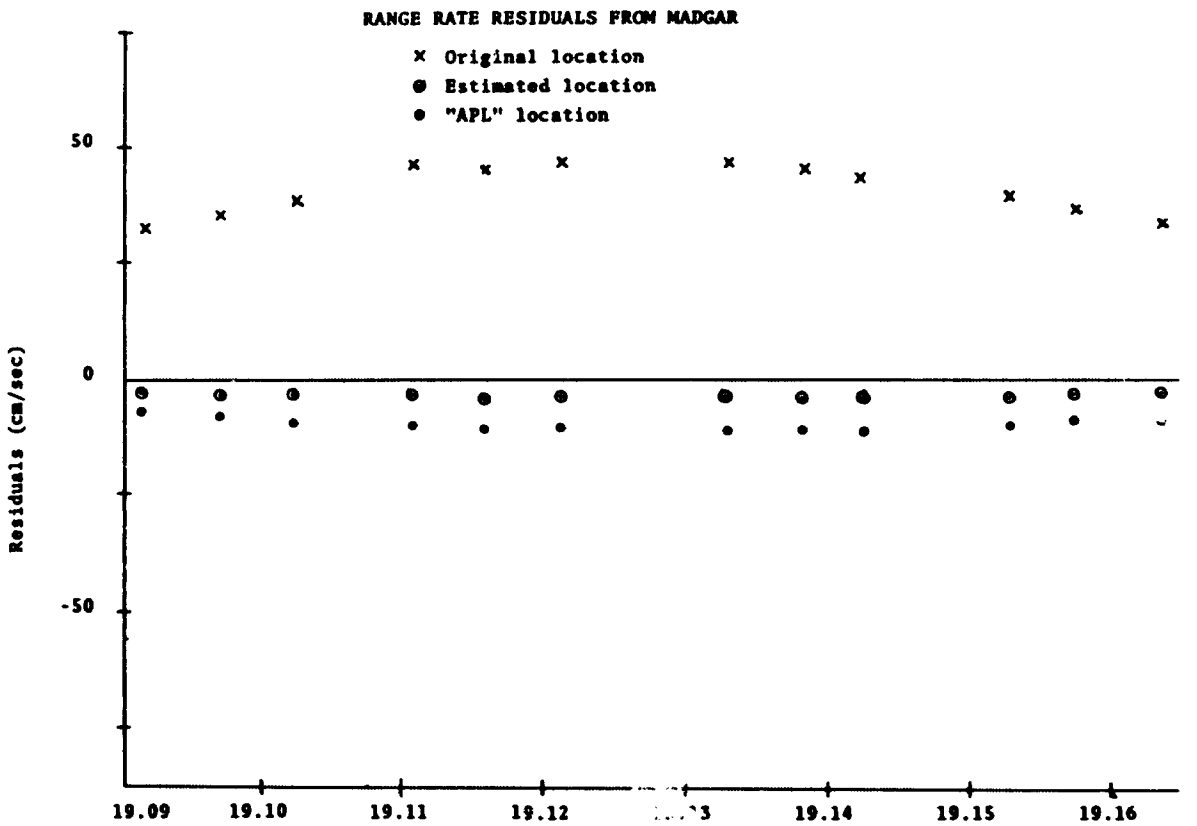

Figure 13. November 28, 1965

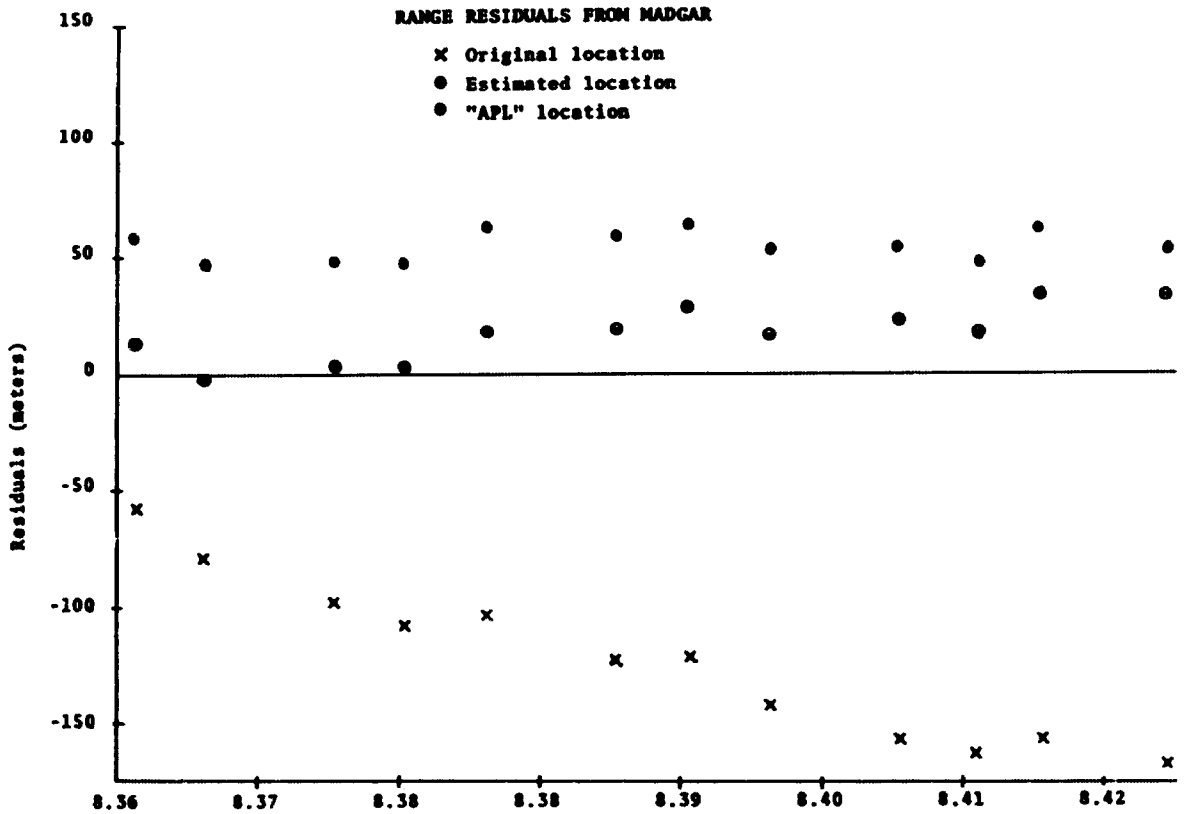

Figure 14. July 17, 1966

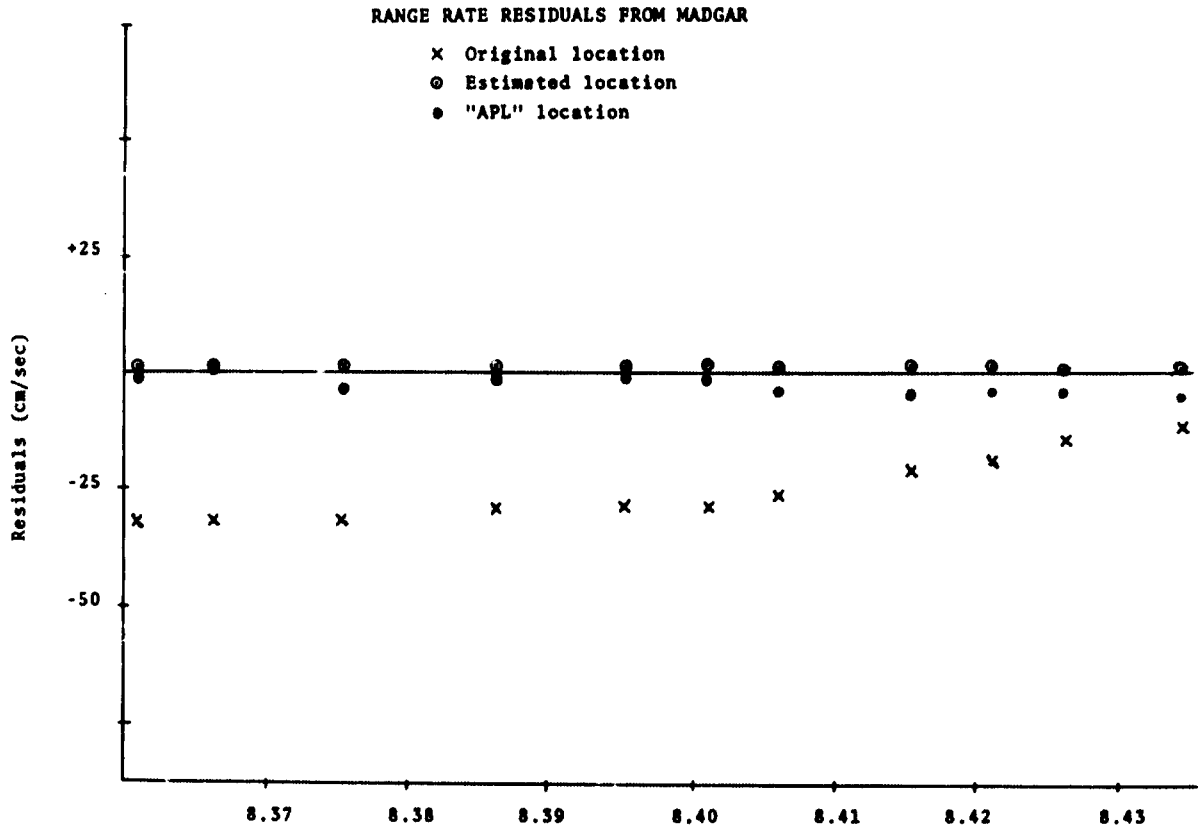

Figure 15. July 17, 1966

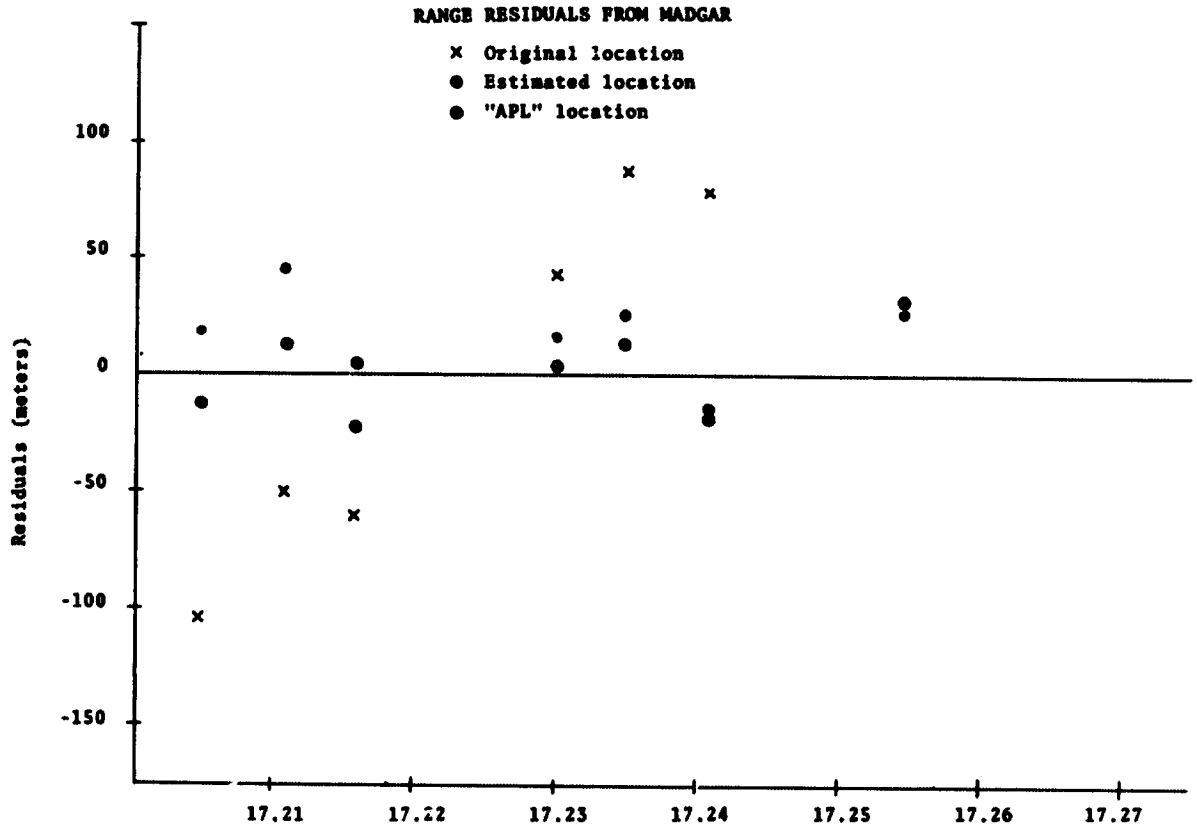

Figure 16. July 18, 1966

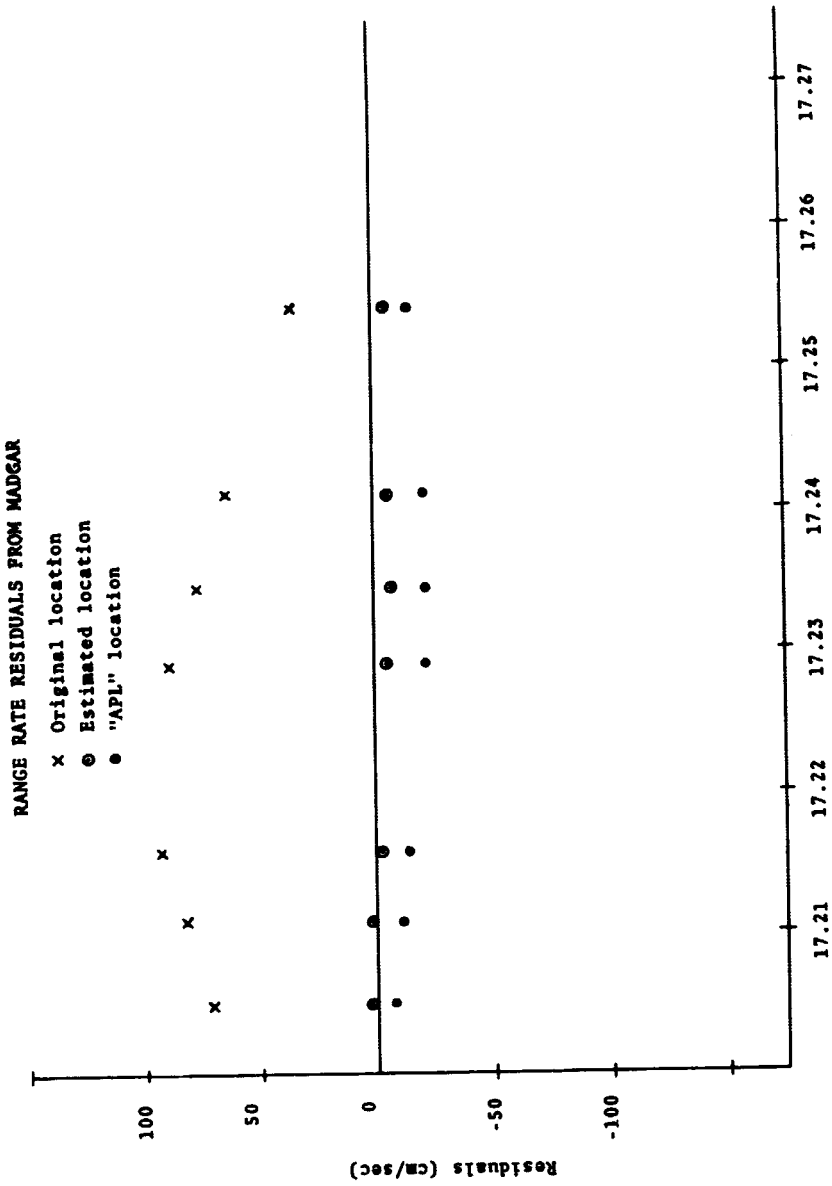

Figure 17. July 18, 1966

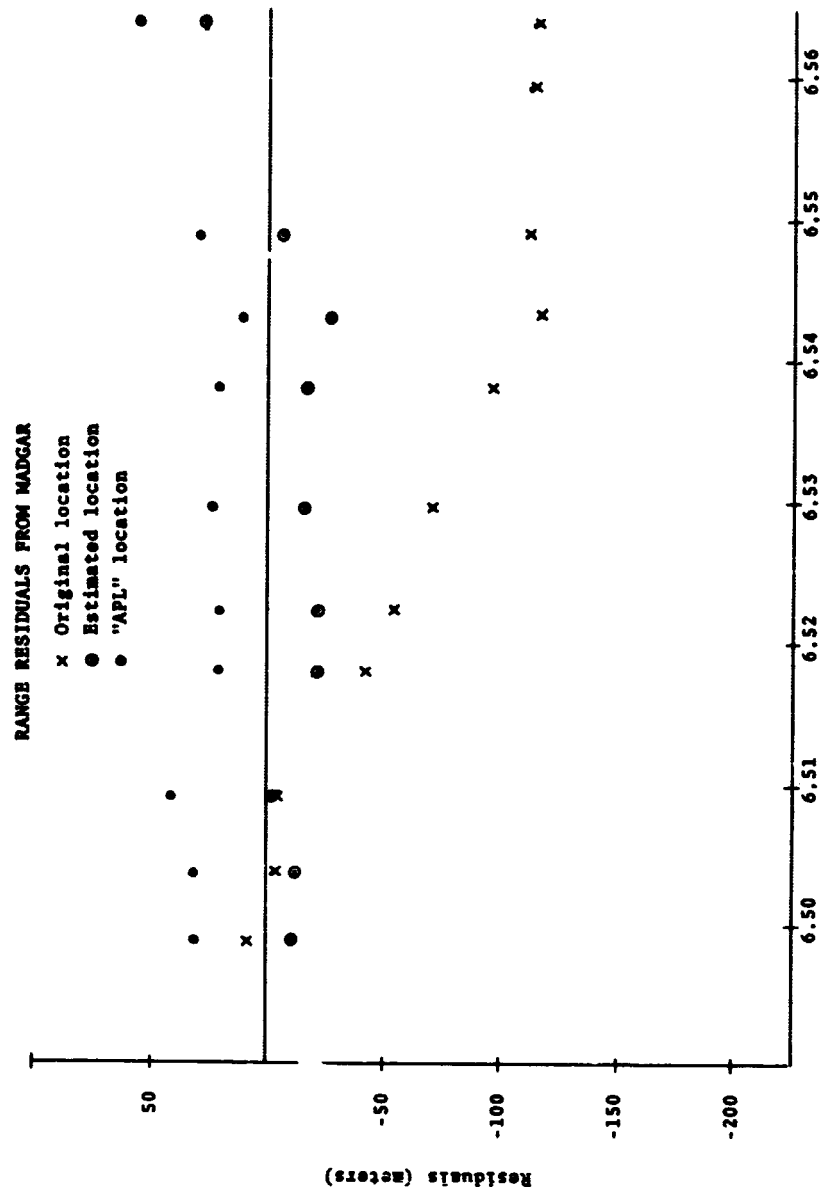

Figure 18. July 22, 1966

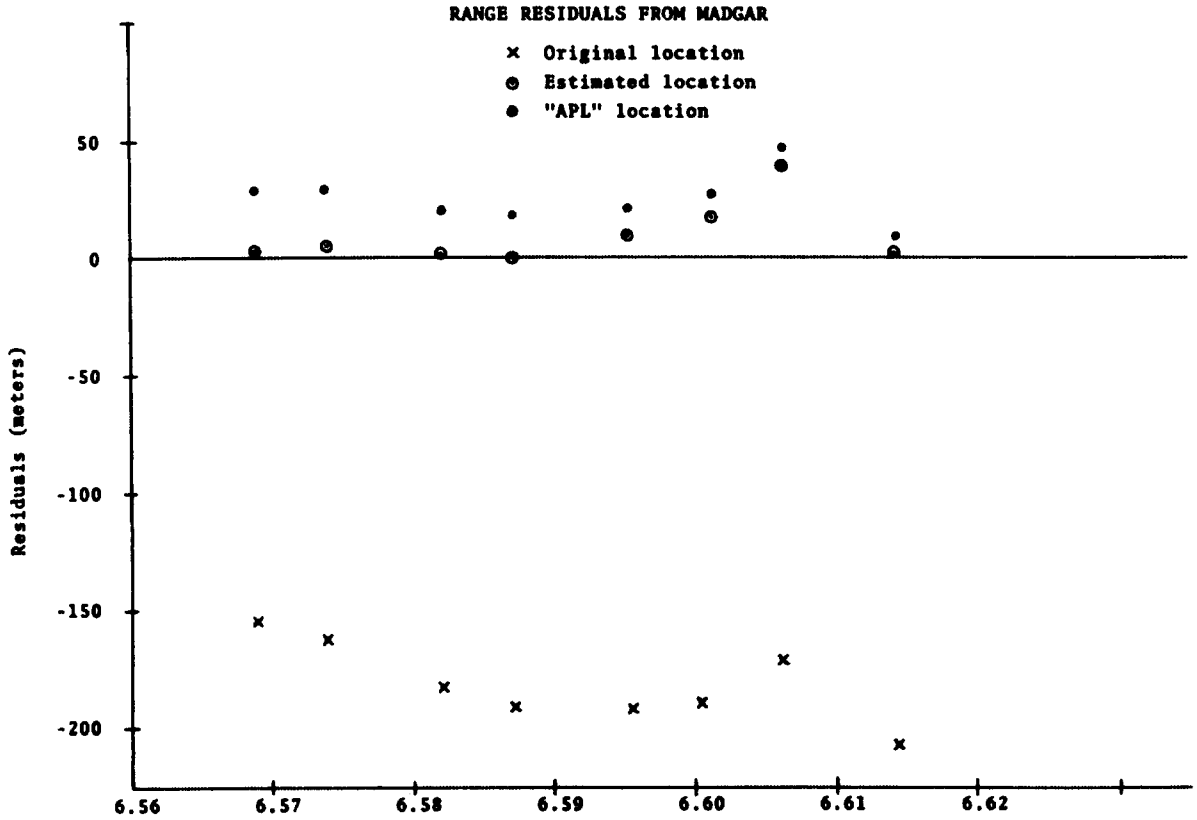

Figure 18 (Cont.). July 22, 1966

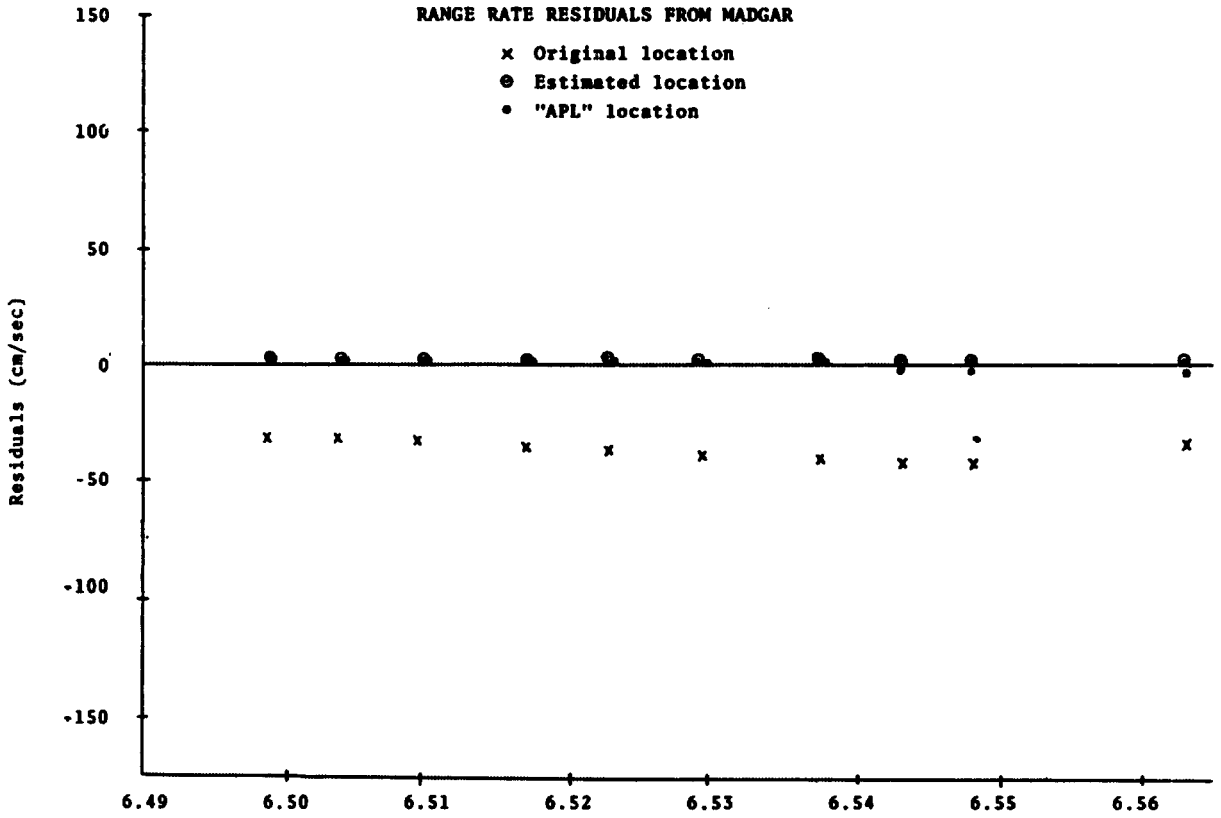

Figure 19. July 22, 1966

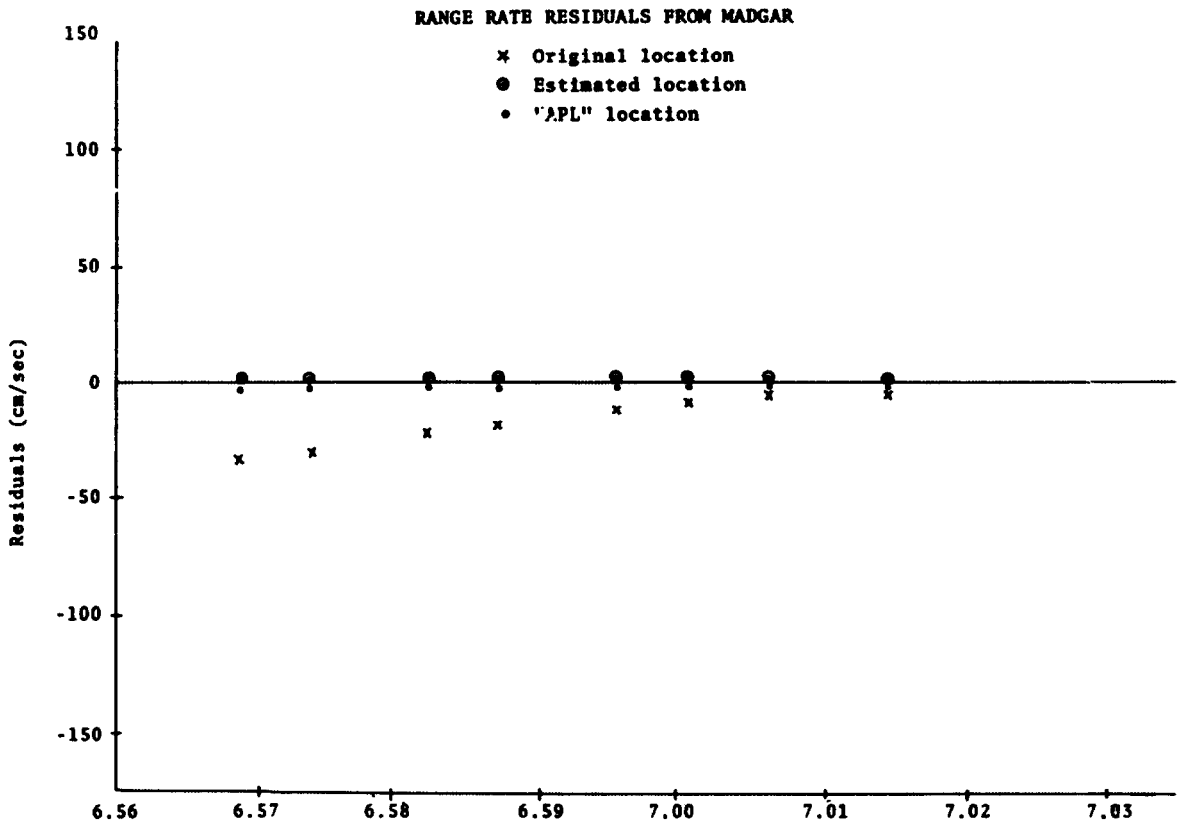

Figure 19 (Cont.). July 22, 1966

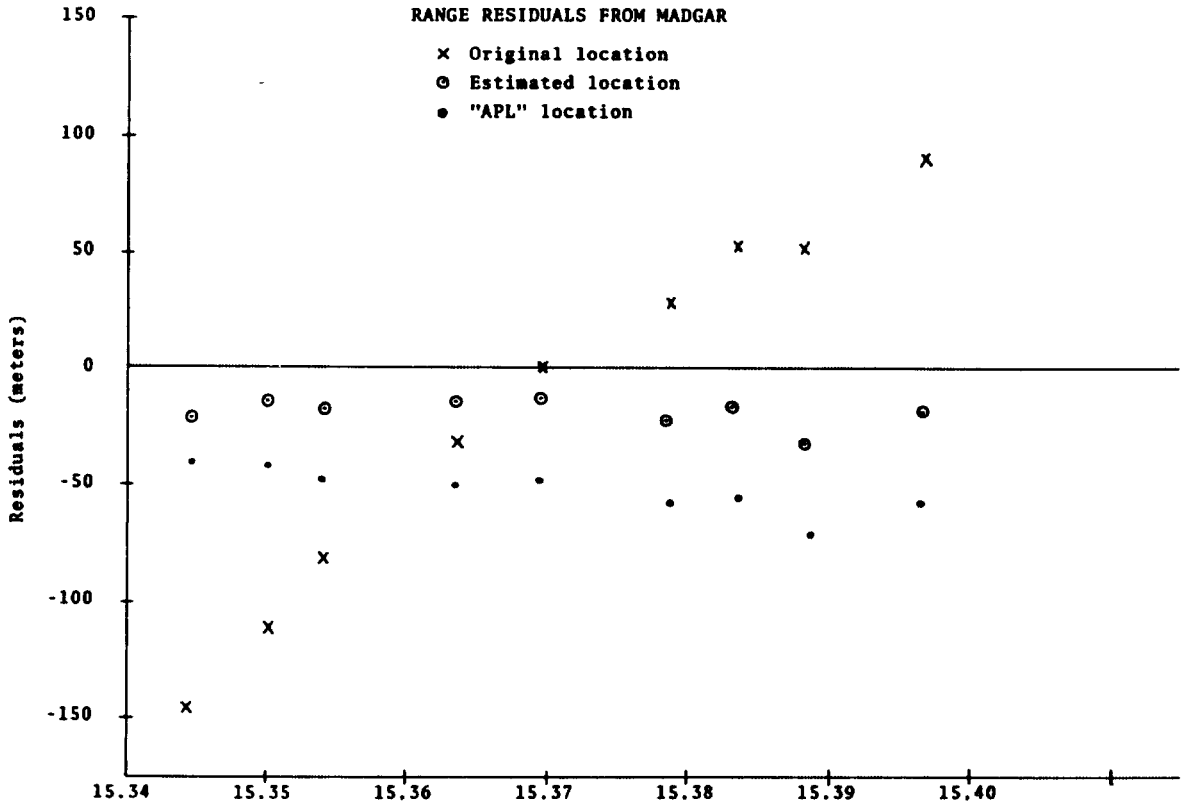

Figure 20. July 22, 1966

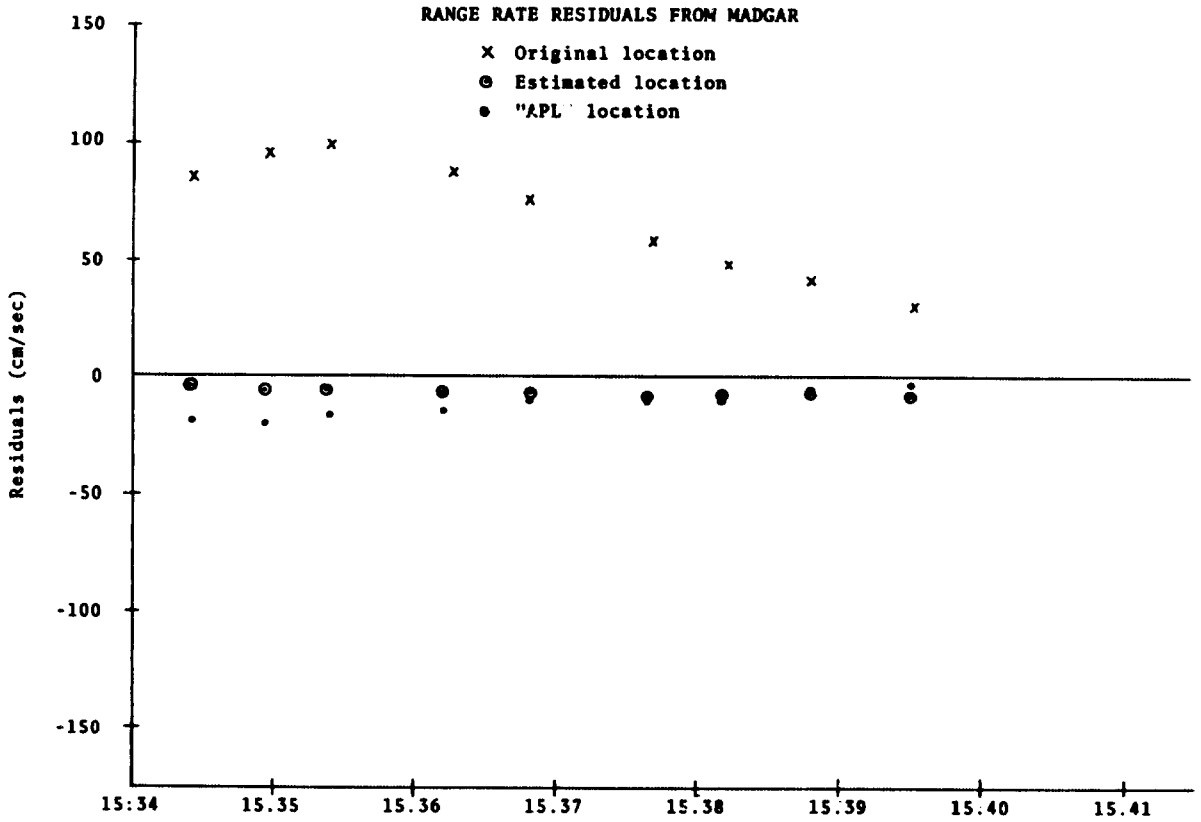

Figure 21. July 22, 1966

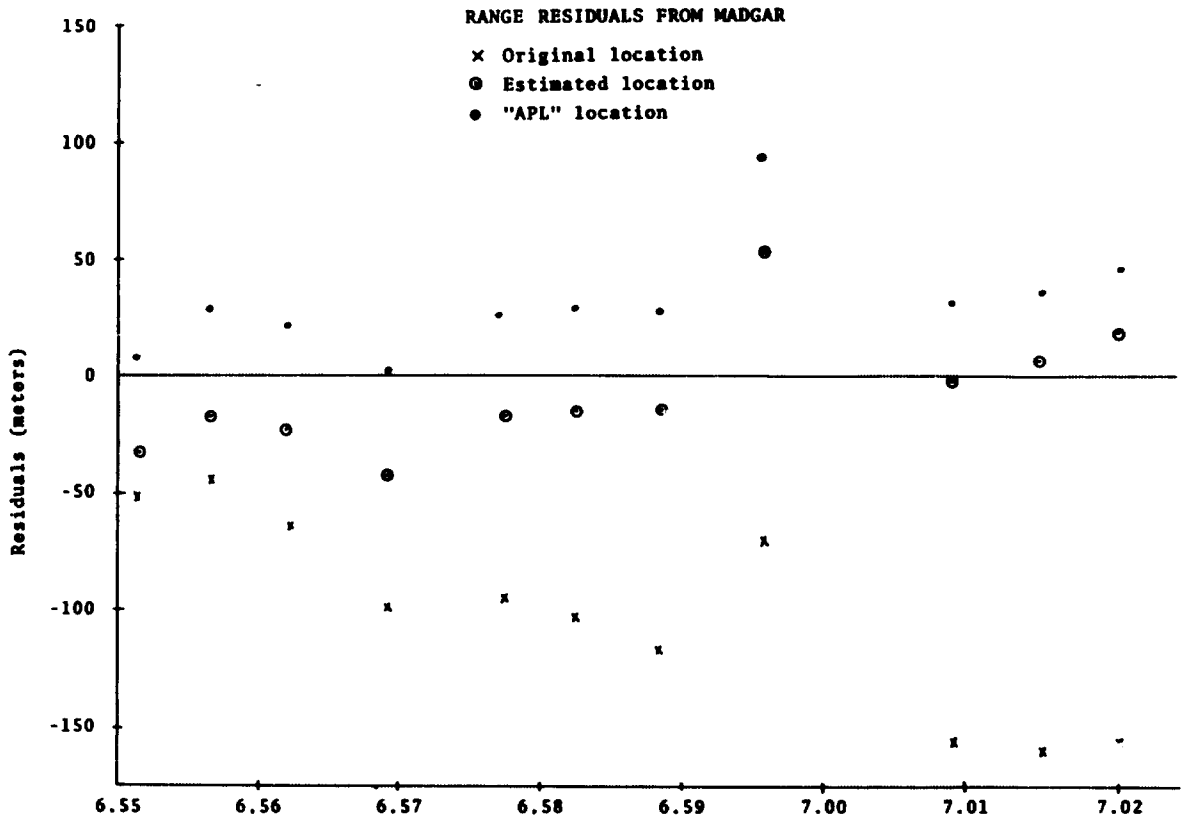

Figure 22. July 23, 1966

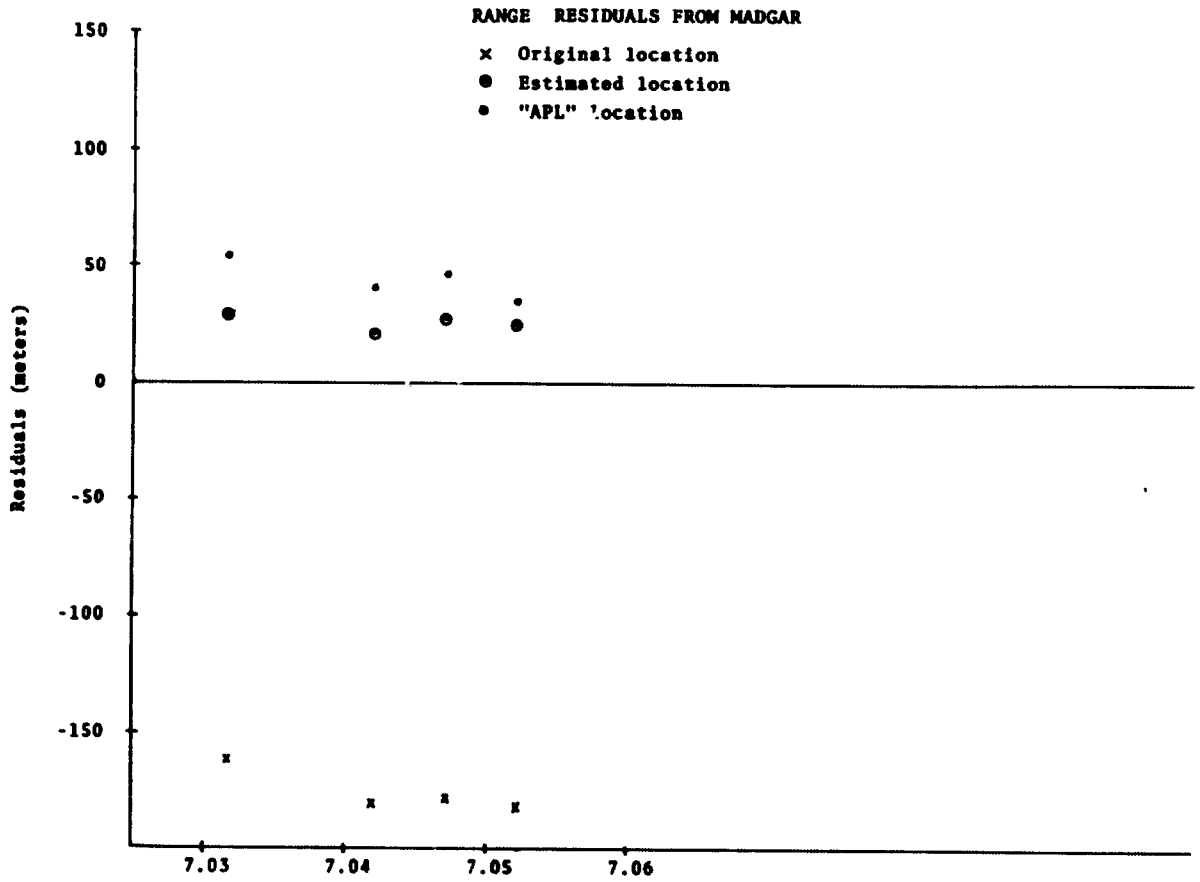

Figure 22 (Cont.). July 23, 1966

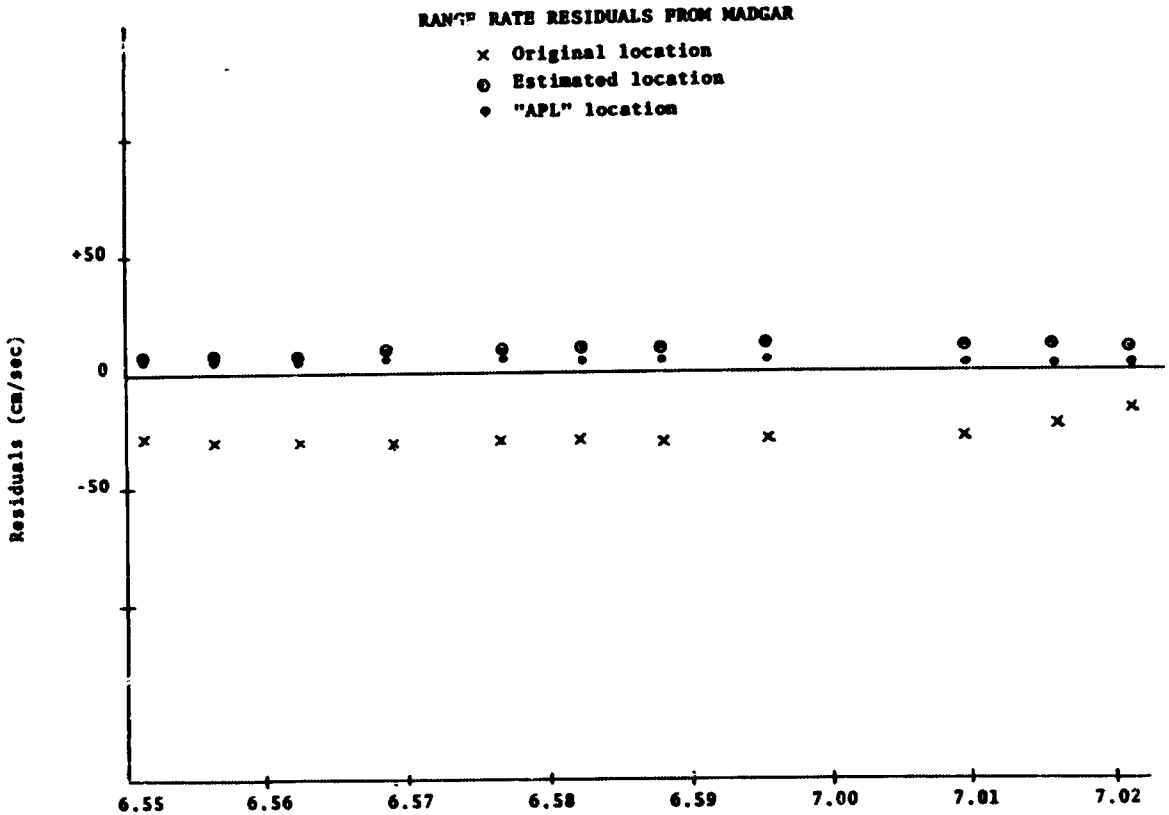

Figure 23. July 23, 1966

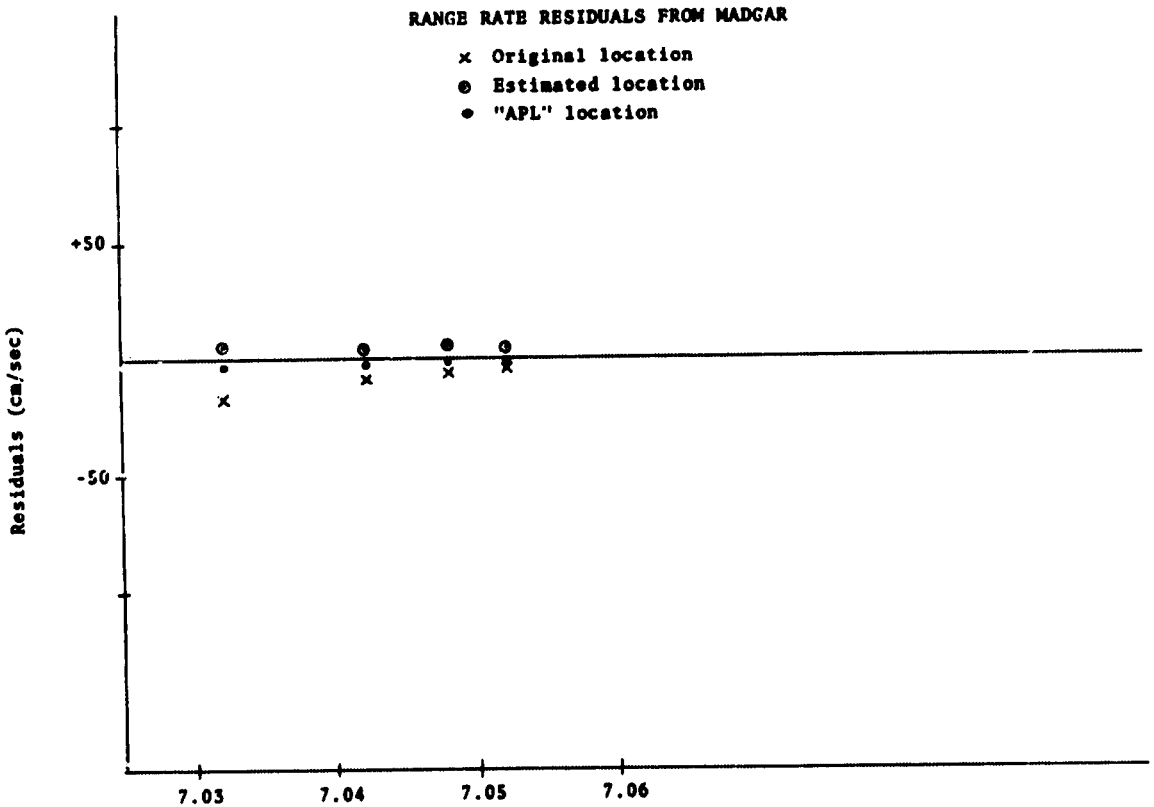

Figure 23 (Cont.). July 23, 1966

REFERENCES

1. NASA Contract Document:

Wolf Research and Development Corporation: Interim Status Report on Program Development and GEOS-A Data Analysis (NAS 5-9756-44A, 55, 71), August 1967.

EVALUATION OF THE GODDARD RANGE AND RANGE RATE SYSTEM AT ROSMAN BY INTERCOMPARISON WITH GEOS-I LONG ARC ORBITAL SOLUTIONS

Francis J. Lerch
James G. Marsh
Mission Trajectory Determination Branch
Mission and Trajectory Analysis Division
Tracking and Data Systems Directorate
GODDARD SPACE FLIGHT CENTER

Brian O'Neill
Wolf Research and Development Corporation
Applied Sciences Department
College Park, Maryland

under

NASA CONTRACT NO. NAS5-9756

November 1967

GODDARD SPACE FLIGHT CENTER
GREENBELT, MARYLAND

SUMMARY

This report presents some of the results of an evaluation of the range measurements of the Goddard Range and Range Rate (GRARR) Tracking System at Rosman, North Carolina. Optical reference orbits were taken as a standard for the comparison of the accuracy of the range measurements. The optical reference orbits utilized GEOS-I flash sequence data sets and some optical passive data from five major geodetic optical tracking networks. The networks and camera types consisted of the SAO-Baker-Nunn, GSFC STADAN and SPEOPT MOTS 40" and 24", USAF PC-1000, and the US C&GS BC-4.

Thirty passes of range and range rate measurements consisting of all GRARR passes from the GEOS-I satellite, during two periods in January 1966, were evaluated. The observed range measurements were compared with values calculated from the optically determined reference orbits. For each pass, zero-set errors, timing errors, and random errors were estimated from the residual differences between the observed and calculated ranges.

The GEOS-I satellite carried two range and range rate transponder channels, denoted A and C. Twenty-six of the passes evaluated were from the A channel, and four were from the C channel. A summary of the zero-set and timing error estimates is presented in the following table for the two periods considered both separately and combined.

Summary of Rosman GRARR Zero-Set and Timing Error Estimates

Period	Transponder Channel	Zero-Set Error (meters)		Timing error (m.s.)	
		Mean	S.d.	Mean	S.d.
1	A	-10.1	8.8	-2.4	2.4
	C	18.1		-1.4	
2	A	-5.6	11.6	-1.9	5.1
1 and 2	A	-7.8	10.3	-2.1	4.0
	C	25.0		-0.6	

These estimates are based on long arc orbital solutions of approximately three to six days in arc length. The results are supported by several overlapping shorter arc solutions which vary in arc length from two hours to two days.

CONTENTS

APPENDICES

TABLES

Table I

Summary of Orbital Solutions

Period 1

Solution No.	Approximate Arc Length	Time of 1st Measurement	Time of final Measurement
1	5-1/2 days	12/31/65 01 hr	01/05/66 06 hr
2	2-1/2 days	01/01/66 01 hr	01/03/66 08 hr
3	2-1/2 days	01/03/66 01 hr	01/05/66 06 hr
4	2 days	01/02/66 01 hr	01/04/66 06 hr
5	1 day	01/02/66 06 hr	01/03/66 08 hr
6	2 hrs	01/02/66 06 hr	01/02/66 08 hr

Period 2

1	4 days	01/11/66 01 hr	01/15/66 05 hr
2	3 days	01/12/66 03 hr	01/15/66 05 hr
3	2 days	01/13/66 05 hr	01/15/66 05 hr
4	2 days	01/15/66 04 hr	01/17/66 05 hr

METHOD OF EVALUATION

The data used in the analysis was taken from the GEOS-I satellite, the first in a series of flashing light geodetic satellites launched by the National Aeronautics and Space Administration (NASA) as part of the National Geodetic Satellite program. The satellite was equipped with a flashing light beacon synchronized with an on-board clock, laser reflectors and a variety of electronic tracking instrumentation.

The range accuracy of the Goddard Range and Range Rate (GRARR) system was evaluated by comparing the actual measurements with values calculated from reference orbits that best fitted sets of optical tracking data. Right ascension and declination measurements from camera tracking stations were used to determine the reference orbits because they are known to be unbiased and relatively free of systematic errors.

The orbits used for this evaluation were estimated from the orbit determination program NONAME [1]. The following earth and force models were used in this evaluation:

- SAO C5 Standard Earth [Appendix A4]
- SAO M1 Gravity Model [Appendix A3]
- Perturbations due to solar and lunar gravity [Appendix A3]

•Perturbations due to solar radiation pressure [Appendix 3]

Ten reference orbits were fitted to data sets from two periods in January 1966; the first period was December 31, 1965 to January 5, 1966, and the second was January 11 to January 17, 1966. Nine of the orbits were fitted to long arcs (greater than 6 revolutions) and the other orbit was fitted to a medium arc (1/4 to 6 revolutions). Several of the orbits were fitted to overlapping data sets. This was done to assess the effects any errors in the orbits were having on the evaluation of the GRARR system. The majority of the observations used to determine the orbits were taken in North America, and the only observations around the world were passive, i.e., were camera observations of the satellite when the beacon was not flashing. Summaries of the orbital solutions and root mean squares of fit are given in Tables I and II. A complete description of the orbital solutions and data sets is given in Appendix A1.

Table II

Root Mean Squares about the Orbital Solutions

Period 1

Orbital Sol^{n}	No. of Obs.	Rms of fit (secs. of arc)
1	1057	3.08
2	631	2.58
3	532	2.74
4	644	2.45
5	444	2.33
6	236	2.17

Period 2

1	1133	3.16
2	956	2.94
3	704	2.80
4	853	2.80

EVALUATION OF THE GRARR MEASUREMENTS

The GRARR measurements used in this evaluation have been smoothed over two minute intervals using a sixth order polynomial; smoothed values were computed every thirty-two seconds within an interval. The residual differences between the actual smoothed GRARR range measurements and the values computed from the reference orbits were used to obtain estimates of known systematic errors in the system. For the purposes of this evaluation, no observations taken when the elevation of the satellite from the station was less than 20^{o} have been used; however, there did not appear to be any significant deterioration in the quality of the observations at these low elevations. The GRARR passes are summarized in Tables III and IV.

The following error model was fitted to the range residuals:

$$\Delta R = \Delta B + \Delta t\dot{R} + F(\dot{R}) + \frac{3}{\text{Sin } E} - 9.7$$

where

ΔR = observed range minus calculated range,

ΔB = error in the zero-set value of the range,

Δt = error in the timing,

$F(\dot{R})$ = error due to the transponder delay [2],

E = elevation angle of the satellite,

and

9.7 = known bias in the system at Rosman [2].

This model was fitted independently to the range residuals from each pass using the method of least squares to solve for the unknown parameters, ΔB and Δt. The estimates of these parameters are summarized in Tables V-VIII. The random errors or the standard deviations of the residual differences about the error model fit are summarized in Tables IX and X.

The zero-set error estimates for the A channel passes from period 1 had a mean value of -10.0 meters and a standard deviation of 8.8 meters, and the three C channel passes had a mean value of 18.1 meters. The A channel passes from period 2 had a mean zero-set error estimate of -5.6 meters and a standard deviation of 11.6 meters, and the one C channel pass had a zero-set error estimate of 45.3 meters. The overall mean zero-set error estimates were -7.8 meters with a standard deviation of 10.3 meters for the A channel passes, and 25.0 meters for the C channel passes.

The timing-error estimates for many passes were larger than would be expected, and it is probable that other systematic error sources are contributing to these estimates. The A channel passes for period 1 had a mean

value of -2.4 milliseconds and the C channel passes had a mean value of -1.4 milliseconds. The A channel passes for period 2 had a mean value of -1.9 milliseconds and the one C channel pass had a timing-error estimate of 2.0 milliseconds. The overall mean timing error estimate for the A channel passes was -2.1 milliseconds with a standard deviation of 4.0 milliseconds.

A timing error of up to 2 milliseconds can possibly be attributed to the orbital solution, however, the consistent results obtained from the shorter overlapping solutions indicate that these errors are due to other sources, either the GRARR system itself, or station survey errors, etc. Further analysis and a possible expansion of the error model is necessary before a complete explanation of these errors is possible.

Table III

SUMMARY OF GRARR PASSES AT ROSRAN FROM PERIOD 1

Pass No.	Transponder Channel	Date	Time	No. of Obs. in Pass		Max. Elevation Angle
				R/R	Optical	
652	A	12/31/65	06^H	18	18	31.3^o
653	A	12/31/65	08^H	28	30	65.4^o
664	A	1/1/66	06^H	28	78	36.6^o
665	A	1/1/66	08^H	32	95	51.8^o
673	A	1/1/66	23^H	34	0	53.5^o
676	A	1/2/66	06^H	32	106	43.3^o
677	A	1/2/66	08^H	28	138	40.2^o
685	A	1/2/66	23^H	34	10	46.5^o
688	A	1/3/66	06^H	30	101	52.2^o
689	A	1/3/66	08^H	14	79	30.1^o
697	A	1/3/66	23^H	44	0	40.8
700	C	1/4/66	06^H	36	100	62.7^o
708	C	1/4/66	21^H	48	0	84.2^o
709	C	1/4/66	23^H	42	14	35.8^o
712	A	1/5/66	06^H	36	66	76.6^o

Table IV

SUMMARY OF GRARR PASSES AT ROSRAN FROM PERIOD 2

Pass No.	Transponder Channel	Date	Time	No. of Obs. in Pass		Max. Elevation Angle
				R/R	Optical	
803	A	1/12/66	20^H	68	0	87.7°
804	A	1/12/66	22^H	22	0	33.1°
806	A	1/13/66	02^H	44	4	26.4°
807	A	1/13/66	04^H	46	91	83.7°
815	A	1/13/66	20^H	46	0	77.2°
818	A	1/14/66	02^H	42	0	30.2°
819	A	1/14/66	04^H	32	60	74.3°
827	C	1/14/66	20^H	38	0	67.6°
831	A	1/15/66	04^H	48	115	60.6°
839	A	1/15/66	20^H	44	0	58.8°
842	A	1/16/66	02^H	52	81	40.8°
843	A	1/16/66	04^H	50	68	47.9°
850	A	1/16/66	18^H	48	0	57.5°
854	A	1/17/66	02^H	50	59	48.3°
855	A	1/17/66	05^H	26	81	37.4°

Table V

Summary of Zero-Set Error Estimates from Period I

(meters)

Pass No.	Transponder Channel	Orbital Solution					
		1	2	3	4	5	6
652	A	-16.5					
653	A	- 6.1					
664	A	- 5.0	-8.0				
665	A	- 2.0	2.8				
673	A	-19.1	-13.9				
676	A	2.3	6.6		2.7	4.2	5.2
677	A	0.2	1.4		6.0	7.4	4.4
685	A	-29.5	-24.2		-25.4	-20.7	
688	A	- 3.3	1.0	- 9.4	- 2.7	- 1.0	
689	A	-14.9	-14.3	-12.6	- 8.6	- 7.7	
697	A	-16.0		-18.4	-11.5		
700	C	20.6		15.8	21.5		
708	C	16.8		19.0			
709	C	17.0		14.1			
712	A	- 9.5		-13.0			
Mean	A	-10.0					
S.d.	A	8.8					
Mean	C	18.1					

Table VI

Summary of Timing Error Estimates
from Period 1
(milliseconds)

Pass No.	Transponder Channel	Orbital Solution					
		1	2	3	4	5	6
652	A	-2.0					
653	A	1.5					
664	A	-3.9	-5.0				
665	A	1.0	0.9				
673	A	-3.4	-0.6				
676	A	-6.3	-6.1		-6.4	-6.9	-3.5
677	A	-0.2	-0.4		-0.1	-0.3	-2.3
685	A	-3.5	0.4		-3.1	-0.6	
688	A	-5.9	-5.1	-4.8	-6.6	-5.3	
689	A	0.1	0.6	1.4	-0.3	1.2	
697	A	-3.0		-3.4	-3.1		
700	C	-5.4		-4.8	-6.5		
708	C	-2.3		-2.4			
709	C	3.4		2.2			
712	A	-2.8		-2.9			
Mean	A	-2.4					
S.d.	A	2.4					
Mean	C	-1.4					

Table VII

Summary of Zero-Set Error Estimates from Period 2

(meters)

Pass No.	Transponder Channel	Orbital Solution			
		1	2	3	4
803	A	8.7	10.7		
804*	A	21.4	27.3		
806	A	-14.4	- 8.6		
807	A	-14.8	-15.1	-16.9	
815	A	- 3.1	- 0.4	- 1.7	
818	A	-12.8	- 7.4	- 7.1	
819	A	10.8	9.1	6.1	
827	C	45.3	48.6	44.8	
831	A	13.5	10.5	8.1	8.8
839	A				10.5
842	A				-19.3
843	A				-13.8
850*	A				2.1
854	A				- 9.1
855	A				-18.4
Mean	A	- 5.6			
S.d.	A	11.6			

* Passes 804 and 850 were omitted from the mean value calculations since pass 804 had a maximum elevation angle of 33°, and no optical data was available within approximately 8 hours of these passes.

Table VIII

Summary of Timing Error Estimates from Period 2

(milliseconds)

Pass No.	Transponder Channel	Orbital Solution			
		1	2	3	4
803	A	5.4	6.1		
804*	A	13.5	14.1		
806	A	- 8.8	- 9.2		
807	A	- 2.7	- 3.1	- 4.6	
815	A	6.4	7.4	5.9	
818	A	- 7.8	- 8.0	- 8.1	
819	A	- 1.9	- 2.0	- 2.6	
827	C	2.0	3.1	2.0	
831	A				- 3.3
839	A				5.8
842	A				- 6.3
843	A				0.7
850*	A				12.4
854	A				- 7.7
855	A				- 2.0
Mean	A	- 1.9			
S.d.	A	5.1			

* Passes 804 and 850 were omitted from the mean value calculation since pass 804 had a maximum elevation angle of only 33°, and no optical data was available within approximately 8 hours of these passes.

Table IX

Summary of Random Error Estimates from Period I

(meters)

Pass No.	Transponder Channel	Orbital Solutions					
		1	2	3	4	5	6
652	A	3.3					
653	A	3.6					
664	A	3.2	3.1				
665	A	4.5	5.2				
673	A	2.6	2.2				
676	A	2.9	3.0		2.9	3.0	2.9
677	A	3.2	3.5		3.8	4.0	3.5
685	A	2.5	2.3		2.5	2.3	
688	A	4.5	5.2	4.1	4.7	5.3	
689	A	4.1	4.0	4.1	3.9	3.8	
697	A	3.4		3.4	3.4		
700	C	5.8		4.7	6.4		
708	C	4.5		4.9			
709	C	3.1		3.2			
712	A	6.0		4.8			
Mean	A	3.7					
Mean	C	4.5					

Table X

Summary of Random Error Estimates from Period 2

(meters)

Pass No.	Transponder Channel	Orbital Solution			
		1	2	3	4
803	A	10.7	11.7		
804	A	7.6	7.8		
806	A	3.1	3.3		
807	A	8.6	8.4	7.8	
815	A	6.3	7.1	7.0	
818	A	2.8	2.9	2.9	
819	A	6.7	6.2	5.1	
827	C	7.0	7.6	7.9	
831	A	10.5	9.8	7.9	11.6
839	A				7.3
842	A				5.3
843	A				5.5
850	A				9.2
854	A				6.5
855	A				2.2
Mean	A	6.6			

References

1. NASA Contract Document:
   Wolf Research and Development Corporation: Interim Status Report on Program Development and GEOS-A Data Analysis (NAS 5-9756-44A,55,71), August 1967.

2. NASA-GSFC Final Report on GRARR/GEOS-A Data Validation, (GSFC I-Document in Preparation).

APPENDIX A-1

Summary of Data Sets and Orbital Solutions

1.1 OPTICAL DATA

The optically determined reference orbits that are used as standards in this report were determined from right ascension and declination measurements taken with STADAN and SPEOPT MOTS 40" and 24" cameras, SAO Baker-Nunn and Geodetic 36" cameras, USAF PC-1000 cameras and United States Coast and Geodetic Survey BC-4 cameras. The locations of some of these cameras are shown in Figures 1 and 2. These figures serve to illustrate that the majority of the observations were taken in North America.

Observations from two periods in January 1966 were used. The two periods were:

1. December 31, 1965 to January 5, 1966
2. January 11 to January 17, 1966

The complete data sets that were used from each period are summarized in Tables I and II, and Figures 3 and 4. Tables I and II summarize the observations by tracking station, and Figures 3 and 4 indicate the data coverage by time.

Six overlapping orbits were estimated using subsets of data from Period 1, and four overlapping orbits were estimated using the data from Period 2. These orbital solutions are summarized in Tables III - V and Figures 5 and 6. The lengths of the arcs in these solutions range from two hours to approximately 5-1/2 days in length, and root mean squares about the orbital solutions are given in Table VI.

Figure 1

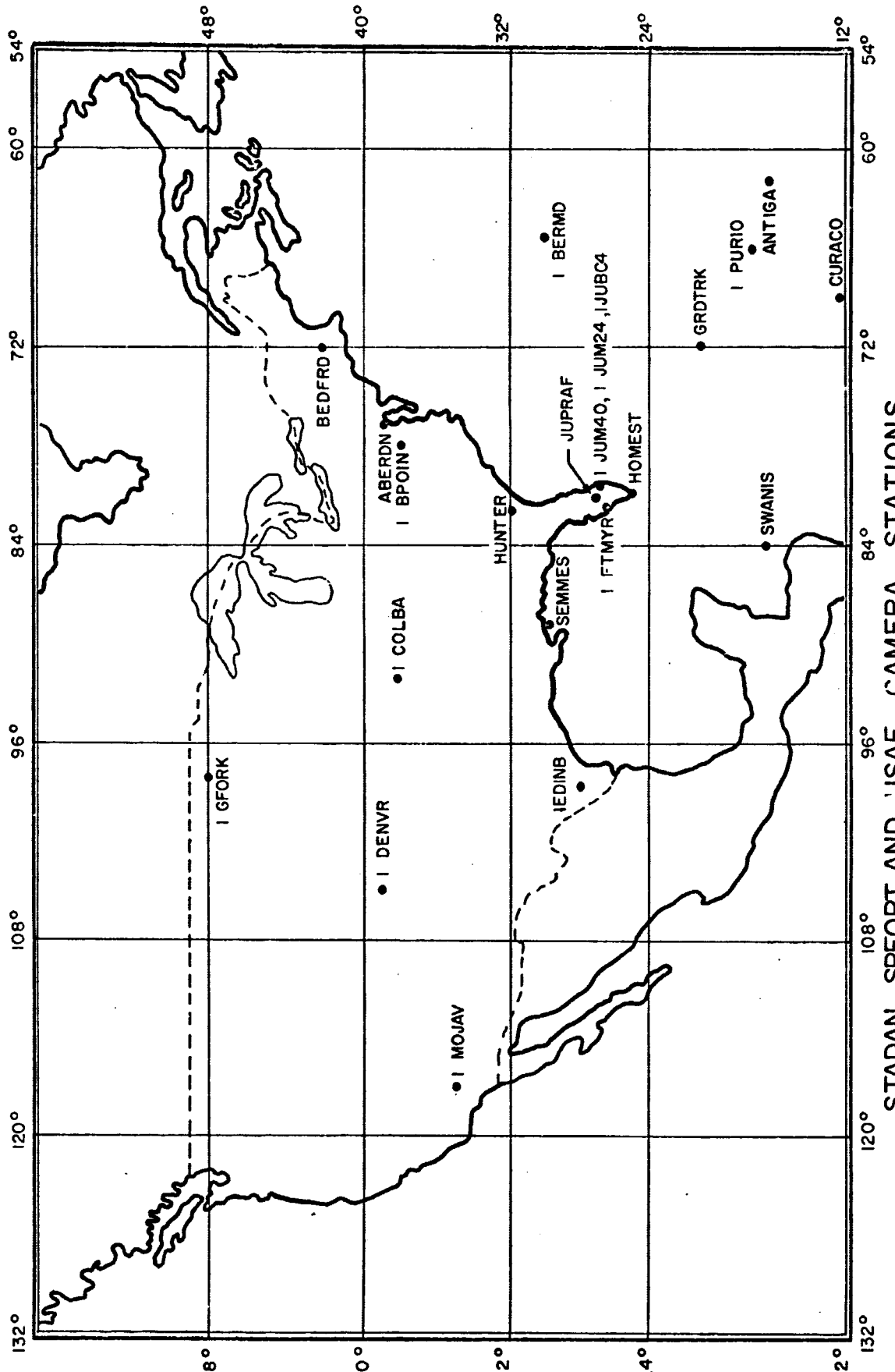
STADAN, SPEOPT AND USAF CAMERA STATIONS
BEDFRD
ABERDN
BPOIN
COLBA
GFORK
DENVR
MOJAV
HUNTER
JUPRAF
JUM40, JUM24, JUBC4
HOMEST
FTMYR
SEMMES
IEDINB
BERMD
GRDTRK
PURIO
ANTIGA
CURACO
SWANIS
132°
120°
108°
96°
84°
72°
60°
54°
48°
40°
32°
24°
12°

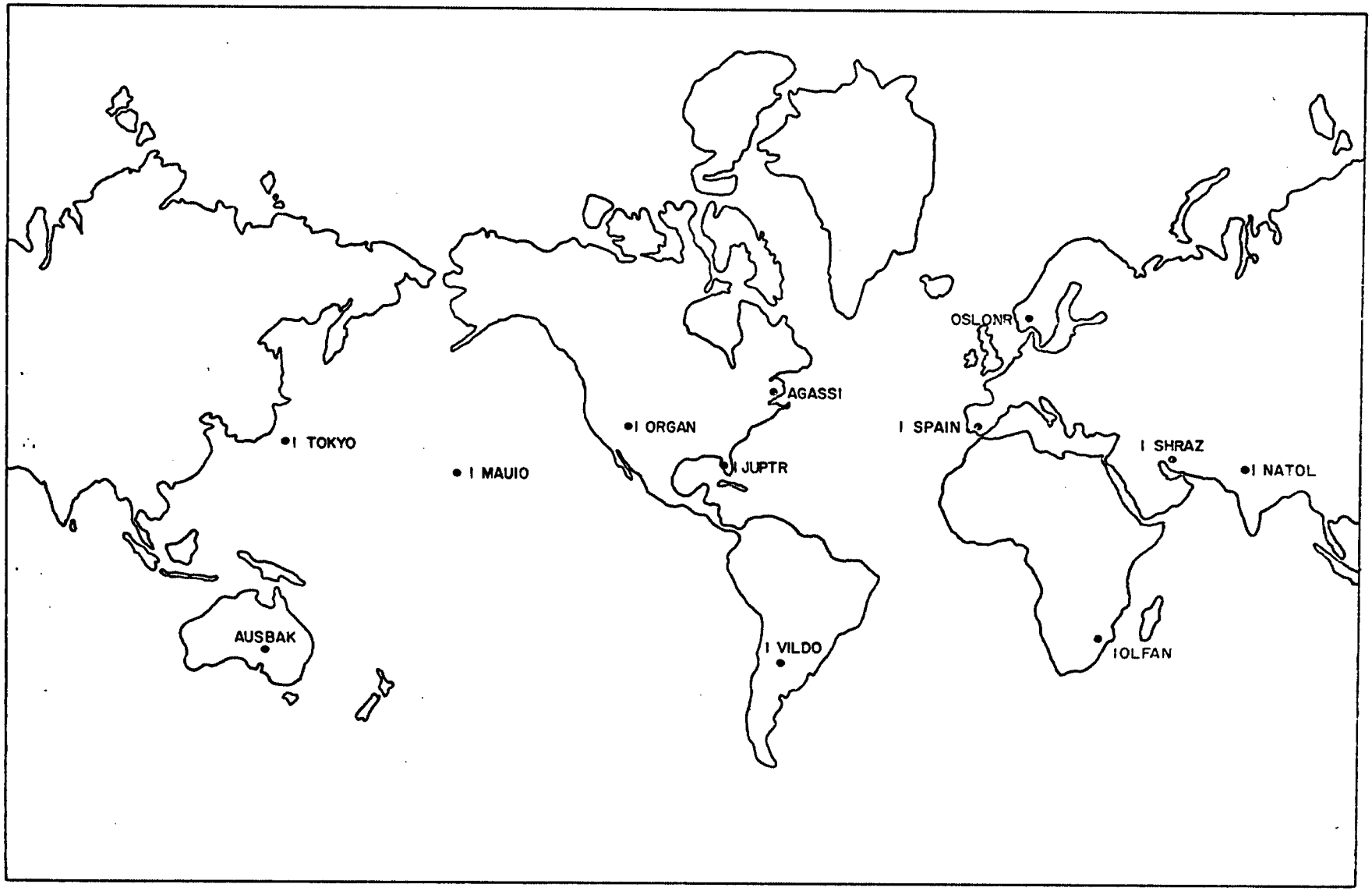

SAO BAKER - NUNN STATIONS

Figure 2

TABLE I

SUMMARY OF OPTICAL MEASUREMENTS BY STATION

FOR PERIOD 1

NETWORK	STATION	CAMERA TYPE	NO. OF OBSERVATIONS
SAO	1ORGAN	BAKER-NUNN	2
	1JUPTR	BAKER-NUNN	26
	1NATOL	BAKER-NUNN	8
	OSLONR	BAKER-NUNN	4
	AUSBAK	BAKER-NUNN	4
	1SHRAZ	BAKER-NUNN	2
	1SPA1N	BAKER-NUNN	6
	1TOKYO	BAKER-NUNN	12
	1VILDO	BAKER-NUNN	2
	1MAUIO	BAKER-NUNN	2
	AGASSI	Geodetic 36"	10
	TOTAL:		78
SPEOPT	1COLBA	MOTS 40"	164
	1JUM40	MOTS 40"	22
	1BERMD	MOTS 40"	84
	1PURIO	MOTS 40"	14
	1DENVR	MOTS 40"	70
	1JUM24	MOTS 24"	26
	TOTAL:		380
STADAN	1FTMYR	MOTS 40"	82
	1BPOIN	MOTS 40"	53
	1GFORK	MOTS 40"	26
	1MOJAV	MOTS 40"	25
	TOTAL:		186
USAF	HUNTER	PC-1000	59
	SWANIS	PC-1000	14
	GRDTRK	PC-1000	7
	ANTIGA	PC-1000	26
	SEMMES	PC-1000	60
	CURACO	PC-1000	40
	HOMEST	PC-1000	94
	JUPRAF	PC-1000	17
	BEDFRD	PC-1000	22
	ABERDN	PC-1000	74
	TOTAL:		413

TOTAL OF ALL OBSERVATIONS = 1057

TABLE II

SUMMARY OF OPTICAL MEASUREMENTS BY STATION FOR PERIOD 2

NETWORK	STATION	CAMERA TYPE	NO. OF OBSERVATIONS
SAO	1OLFAN	BAKER-NUNN	6
	1TOKYO	BAKER-NUNN	4
	1JUPTR	BAKER-NUNN	84
	1VILDO	BAKER-NUNN	8
	AUSBAK	BAKER-NUNN	8
	AGASSI	Geodetic 36"	63
	OSLONR	BAKER-NUNN	1
	TOTAL		174
SPEOPT	1EDINB	MOTS 40	109
	1COLBA	MOTS 40	92
	1BERMD	MOTS 40	10
	1PURIO	MOTS 40	34
	1GSFCP	MOTS 40	40
	1DENVR	MOTS 40	82
	1JUM24	MOTS F24	62
	1JUM40	MOTS F40	70
	1JUBC4	BC4	65
	TOTAL		654
STADAN	1BPOIN	MOTS 40	41
	1FTMYR	MOTS 40	168
	1MOJAV	MOTS 40	87
	1COLEG	MOTS 40	30
	1GFORK	MOTS 40	74
	1ROSMA	MOTS 40	34
	TOTAL		434
USAF	ANTIGA	PC-1000	52
	BEDFRD	PC-1000	85
	SEMMES	PC-1000	60
	GRDTRK	PC-1000	74
	CURACO	PC-1000	21
	TRNDAD	PC-1000	21
	HUNTER	PC-1000	12
	JUPRAF	PC-1000	73
	ABERDN	PC-1000	74
	HOMEST	PC-1000	108
	TOTAL		580
US C&GS	TIMINS	BC4	14

TOTAL OF ALL OBSERVATIONS = 1856

TABLE III

Summary of Orbital Solutions

Period 1

Solution No.	Approximate Arc Length	Time of 1st Measurement	Time of final Measurement
1	5-1/2 days	12/31/65 01 hr	01/05/66 06 hr
2	2-1/2 days	01/01/66 01 hr	01/03/66 08 hr
3	2-1/2 days	01/03/66 01 hr	01/05/66 06 hr
4	2 days	01/02/66 01 hr	01/04/66 06 hr
5	1 day	01/02/66 06 hr	01/03/66 08 hr
6	2 hrs	01/02/66 06 hr	01/02/66 08 hr

Period 2

1	4 days	01/11/66 01 hr	01/15/66 05 hr
2	3 days	01/12/66 03 hr	01/15/66 05 hr
3	2 days	01/13/66 05 hr	01/15/66 05 hr
4	2 days	01/15/66 04 hr	01/17/66 05 hr

TABLE IV

Subsets of Optical Measurements used in Orbital Solutions from Period 1

		No. of Observations				
Network	Station	Arc 2	Arc 3	Arc 4	Arc 5	Arc 6
SAO	1ORGAN		2			
	1JUPTR	26		26	26	26
	1NATOL	4	2	2	2	
	OSLONR		4			
	AUSBAK	2				
	1SHRAZ	2		2	2	
	1SPAIN		4	4		
	1TOKYO	6	2	4	4	
	1VILDO		2			
	AGASSI		10			
	TOTAL	40	26	38	34	26
SPEOPT	1COLBA	71	164	136	71	
	1JUM40	16		16	16	16
	1BERMD	64	40	50	36	10
	1PURIO		14			
	1DENVR	42	14	28	14	14
	1JUM24	21		21	21	21
	TOTAL	212	232	251	158	61
STADAN	1FTMYR	82	42	54	54	12
	1BPOIN		46	26		
	1GFORK	26	9	9	9	
	1MOJAV	25		25	25	25
	TOTAL	133	97	113	91	37
USAF	HUNTER	59	14	47	47	23
	SWANIS	14	14	14	14	
	GRDTRK		7	7		
	ANTIGA	12	14	14		
	SEMMES	50		36	36	36
	CURACO	26	28	40	26	12
	HOMEST	66	28	38	24	24
	JUPRAF	17		17	17	17
	BEDFRD		22	14		
	ABERDN		50	14		
	TOTAL	244	177	241	164	112
GRAND TOTAL		631	532	644	444	236

TABLE V

Subsets of Optical Measurements Used in Orbital Solution from Period 2

Network	Station	No. of Observations			
		Arc 1	Arc 2	Arc 3	Arc 4
SAO	1OLFAN	6	4		
	1TOKYO	4	2	2	
	1JUPTR				84
	1VILDO	8	6	6	2
	AUSBAK	6	4	4	2
	AGASSI	63	46	12	12
	OSLONR				1
	TOTAL	87	62	24	101
SPEOPT	1EDINB	72	48	20	65
	1COLBA	92	92	92	38
	1BERMD				10
	1PURIO	20	14	14	14
	1GSFCP	40	40	26	
	1DENVR	56	56	56	26
	1JUM24	22	22	22	54
	1JUM40	28	28	28	56
	1JUBC4	38	38	38	41
	TOTAL	368	338	296	304
STADAN	1BPOIN	37	37	18	8
	1FTMYR	103	103	75	78
	1MOJAV	52	52	52	42
	1COLEG	17	17	17	13
	1GFORK	40	14	14	34
	1ROSMA	22			12
	TOTAL	271	223	176	187
USAF	ANTIGA	38	83	24	24
	BEDFRD	58	58	26	27
	SEMMES	50	26		10
	GRDTRK	46	34	34	38
	CURACO	21	21	21	10
	TRNDAD	11	11		10
	HUNTER	12			
	JUPRAF	38	38	38	53
	ABERDN	68	42	14	20
	HOMEST	51	51	51	69
	TOTAL	393	319	208	261
USC&GS	TIMINS	14	14		
GRAND TOTAL		1133	956	704	853

TABLE VI

Root Mean Squares about the Orbital Solutions

Period 1

Orbital Sol^{n}	No. of Obs.	Rms of fit (secs. of arc)
1	1057	3.08
2	631	2.58
3	532	2.74
4	644	2.45
5	444	2.33
6	236	2.17

Period 2

1	1133	3.16
2	956	2.94
3	704	2.80
4	853	2.80

Figure 3

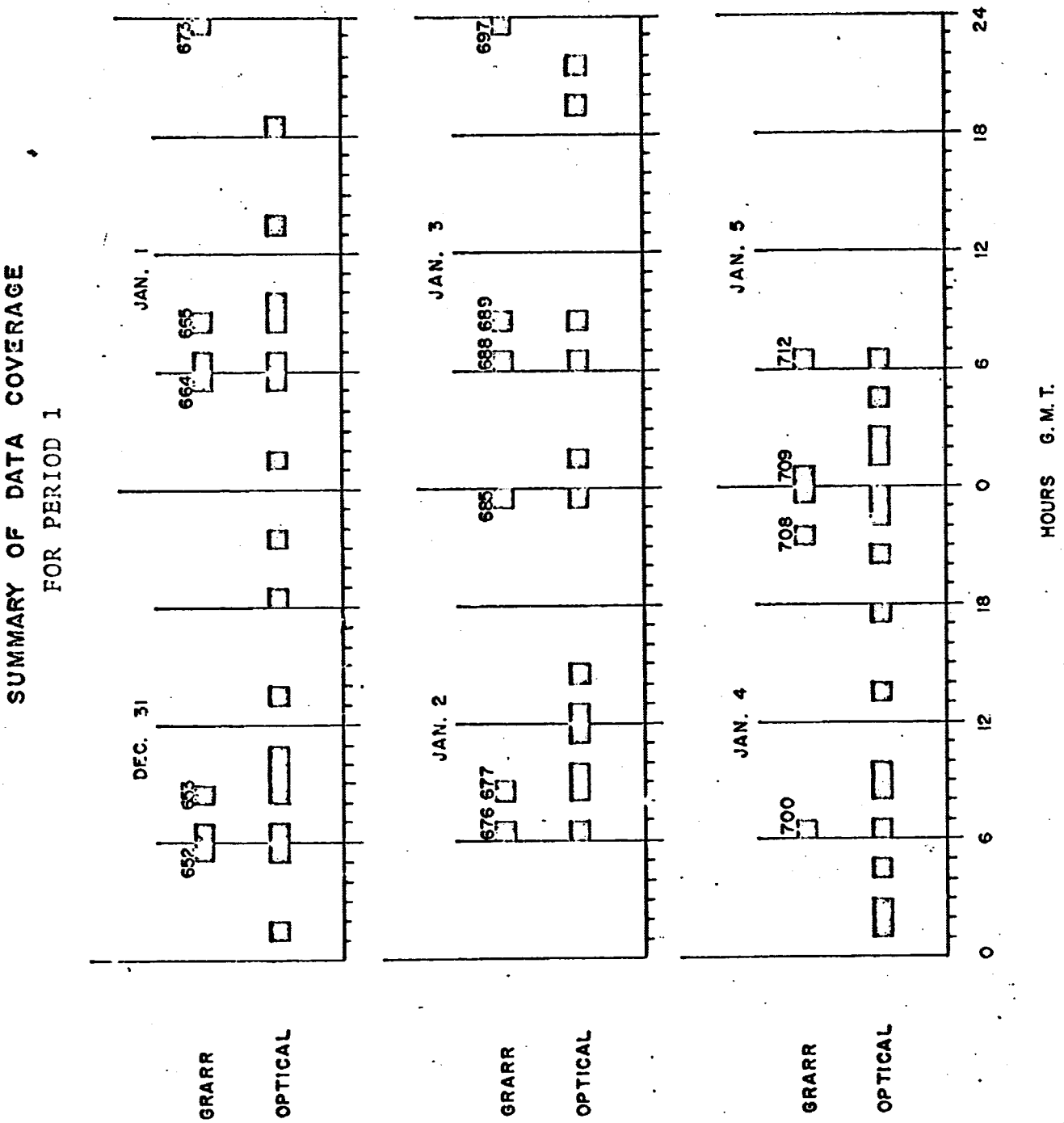
SUMMARY OF DATA COVERAGE
FOR PERIOD 1
DEC. 31
JAN. 1
JAN. 2
JAN. 3
JAN. 4
JAN. 5
652
653
664
665
673
676
677
685
688
689
697
700
708
709
712
GRARR
OPTICAL
0
6
12
18
24
HOURS G.M.T.

Figure 4

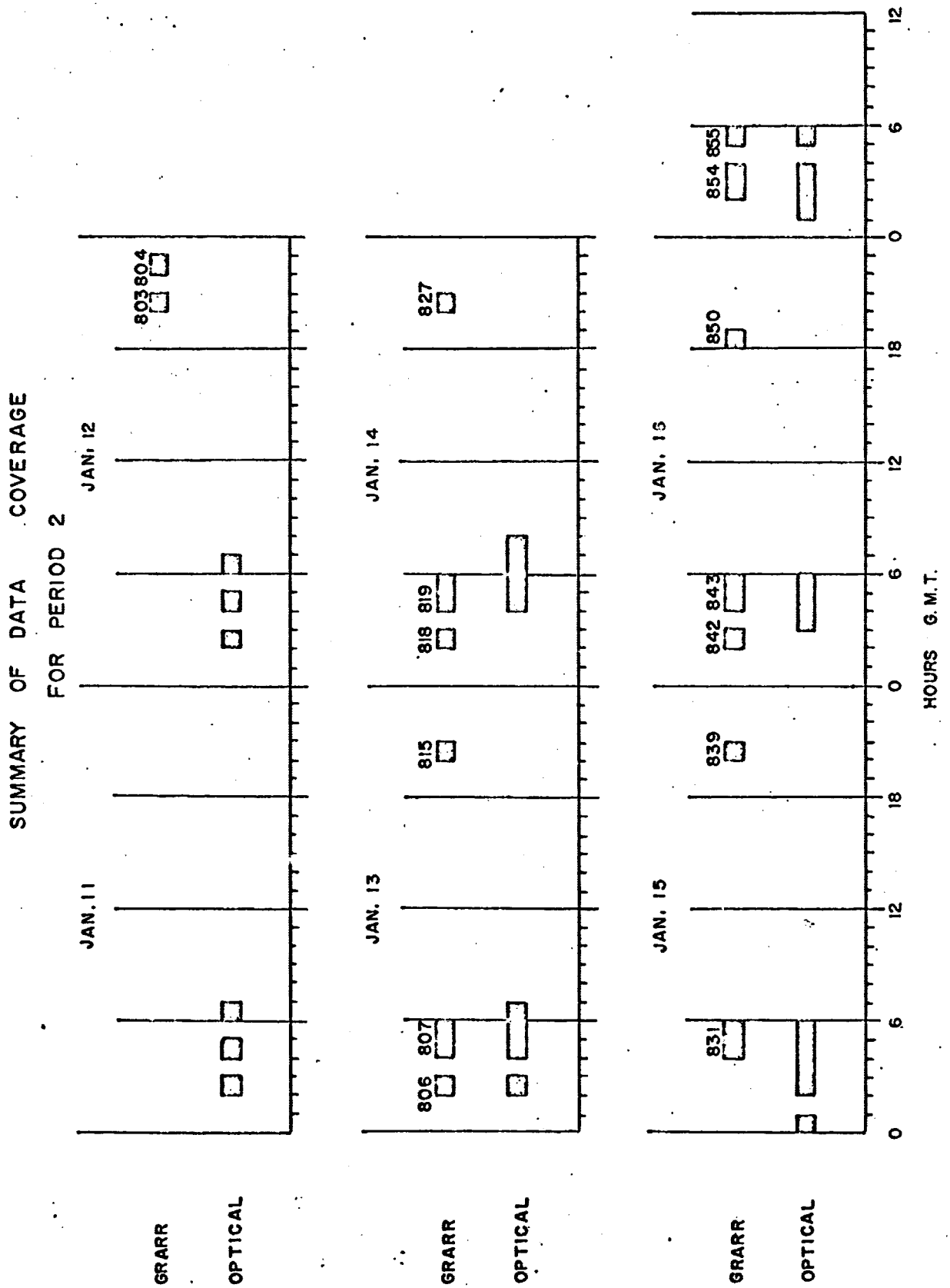
SUMMARY OF DATA COVERAGE
FOR PERIOD 2
JAN. 11
JAN. 12
JAN. 13
JAN. 14
JAN. 15
JAN. 15
GRARR
OPTICAL
GRARR
OPTICAL
GRARR
OPTICAL
803 804
827
850
806 807
815
818 819
839
842 843
831
854 855
0
6
12
18
0
6
12
18
0
6
12
HOURS G.M.T.

Figure 5

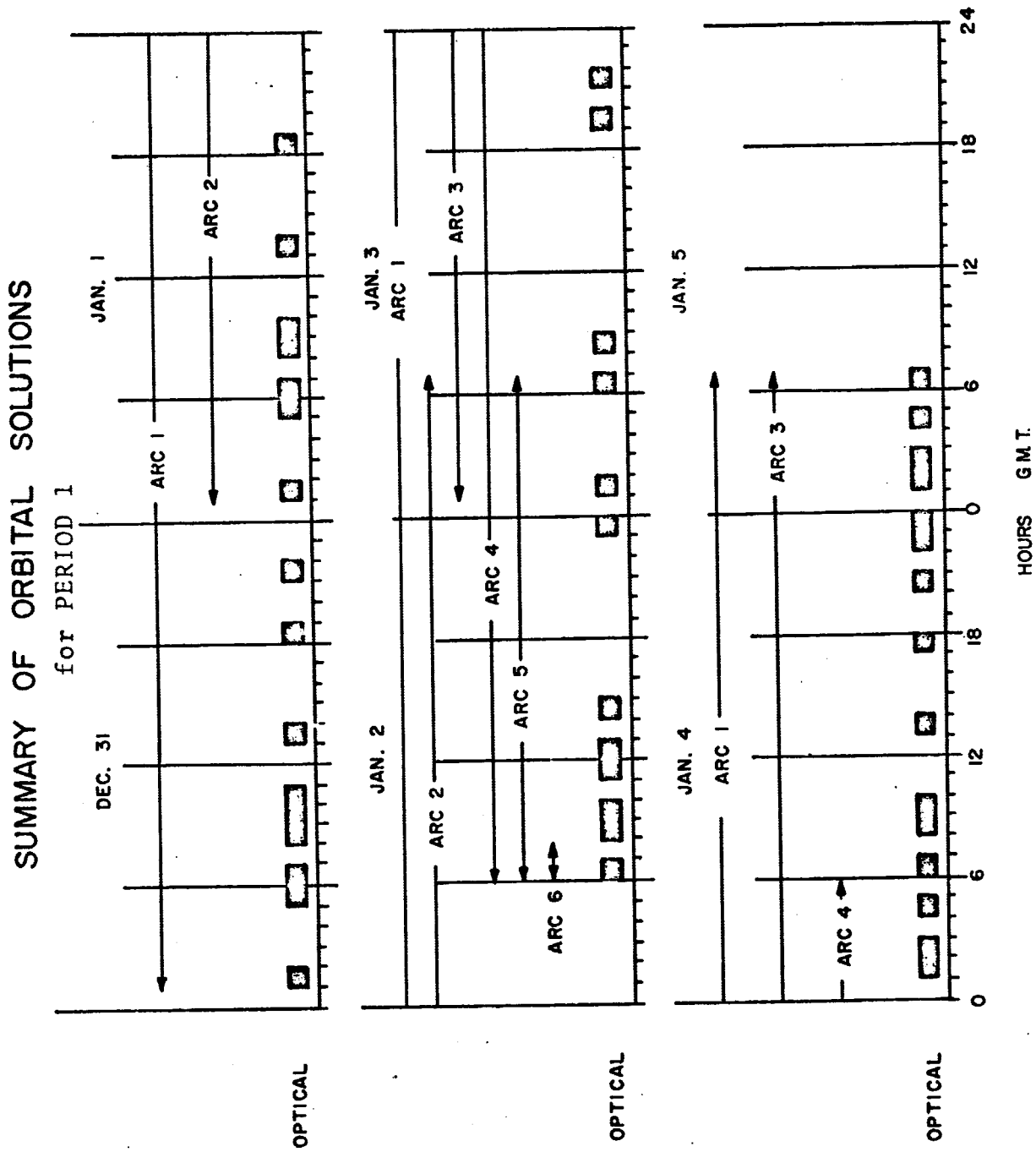
SUMMARY OF ORBITAL SOLUTIONS
for PERIOD 1
DEC. 31
JAN. 1
ARC 1
ARC 2
OPTICAL
JAN. 2
ARC 2
ARC 4
ARC 5
ARC 6
JAN. 3
ARC 1
ARC 3
OPTICAL
JAN. 4
ARC 1
ARC 4
JAN. 5
ARC 3
OPTICAL
0
6
12
18
24
HOURS G.M.T.

Figure 6

SUMMARY OF ORBITAL SOLUTIONS
for PERIOD 2

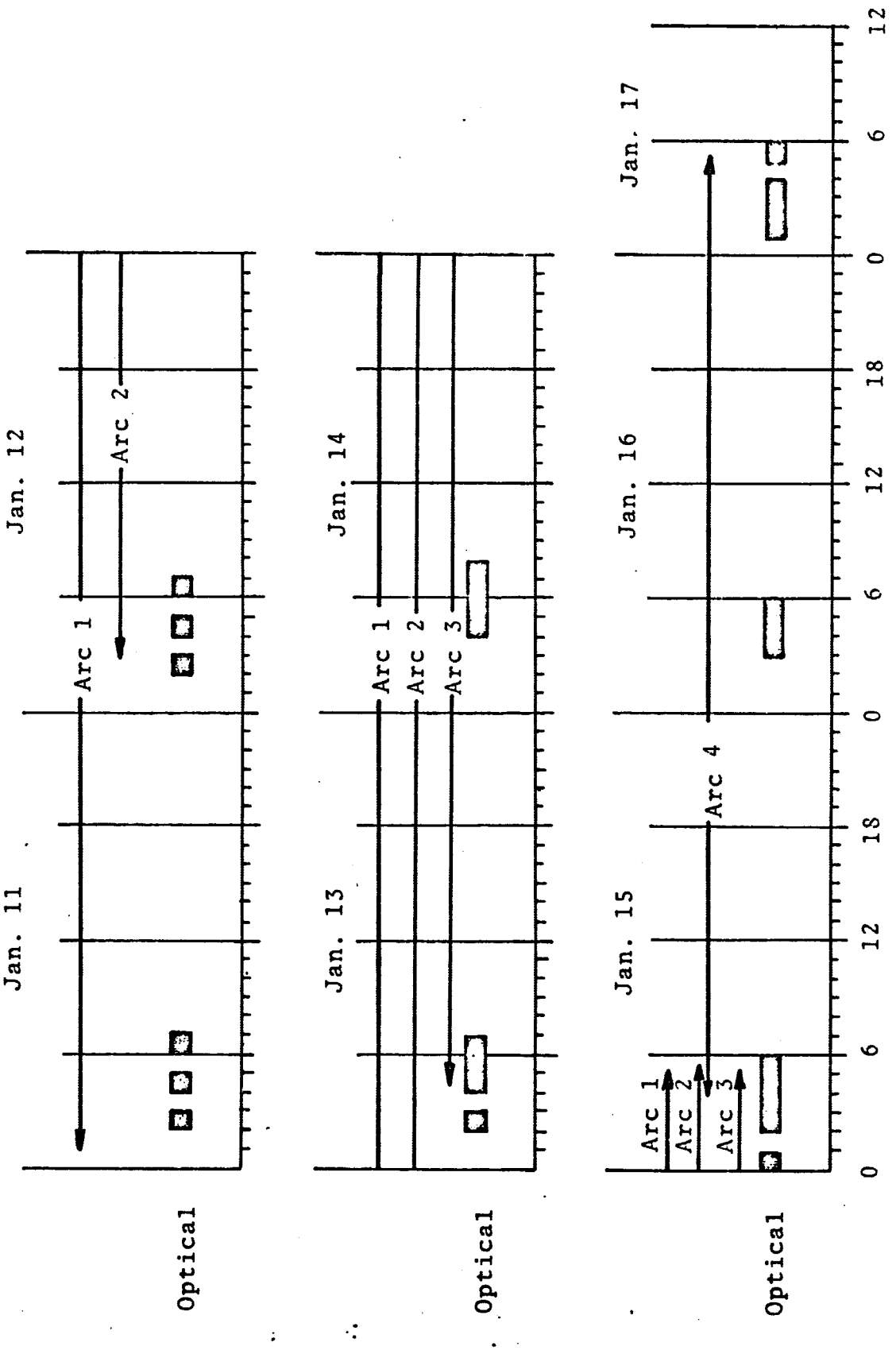

1.2 GRARR DATA

The Goddard Range and Range Rate (GRARR) system was designed as a high-precision tracking system able to accurately determine the range and radial velocity of a spacecraft by measuring phase shift and Doppler. Each station uses an S-band and a VHF system. Only the S-band system was used in this evaluation.

The GRARR observations used in this evaluation had been smoothed using a sixth order polynomial smoothing program. The data was smoothed over two minute periods and smoothed values were obtained at 32 second intervals within these periods.

The GRARR passes evaluated in this report are summarized in Tables VII and VIII. These tables indicate the data and time of each pass, number of GRARR observations, number of simultaneous optical observations maximum elevation of pass, and the satellite transponder channel. The geometry of these passes is represented in Figures 7 - 13.

TABLE VII

SUMMARY OF GRARR PASSES AT ROSRAN FROM PERIOD 1

Pass No.	Transponder Channel	Date	Time	No. of Obs. in Pass		Max. Elevation Angle
				R/R	Optical	
652	A	12/31/65	06^H	18	18	31.3^o
653	A	12/31/65	08^H	28	30	65.4^o
664	A	1/1/66	06^H	28	78	36.6^o
665	A	1/1/66	08^H	32	95	51.8^o
673	A	1/1/66	23^H	34	0	53.5^o
676	A	1/2/66	06^H	32	106	43.3^o
677	A	1/2/66	08^H	28	138	40.2^o
685	A	1/2/66	23^H	34	10	46.5^o
688	A	1/3/66	06^H	30	101	52.2^o
689	A	1/3/66	08^H	14	79	30.1^o
697	A	1/3/66	23^H	44	0	40.8
700	C	1/4/66	06^H	36	100	62.7^o
708	C	1/4/66	21^H	48	0	84.2^o
709	C	1/4/66	23^H	42	14	35.8^o
712	A	1/5/66	06^H	36	66	76.6^o

TABLE VIII

SUMMARY OF GRARR PASSES AT ROSRAN FROM PERIOD 2

Pass No.	Transponder Channel	Date	Time	No. of Obs. in Pass		Max. Elevation Angle
				R/R	Optical	
803	A	1/12/66	20^H	68	0	87.7°
804	A	1/12/66	22^H	22	0	33.1°
806	A	1/13/66	02^H	44	4	26.4°
807	A	1/13/66	04^H	46	91	83.7°
815	A	1/13/66	20^H	46	0	77.2°
818	A	1/14/66	02^H	42	0	30.2°
819	A	1/14/66	04^H	32	60	74.3°
827	C	1/14/66	20^H	38	0	67.6°
831	A	1/15/66	04^H	48	115	60.6°
839	A	1/15/66	20^H	44	0	58.8°
842	A	1/16/66	02^H	52	81	40.8°
843	A	1/16/66	04^H	50	68	47.9°
850	A	1/16/66	18^H	48	0	57.5°
854	A	1/17/66	02^H	50	59	48.3°
855	A	1/17/66	05^H	26	81	37.4°

Figure 7

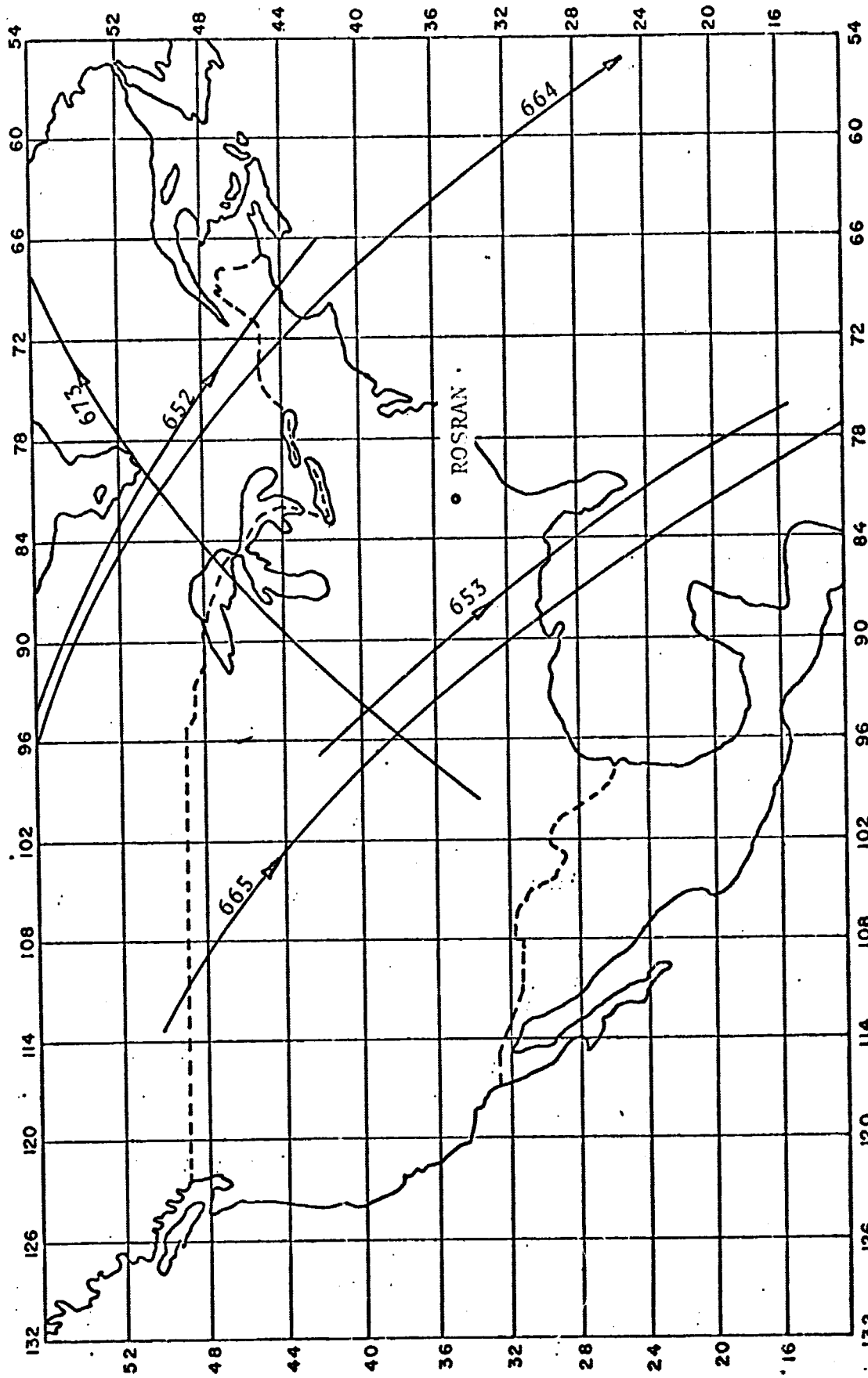

GRARR PASSES
January 1 & December 31

Figure 8

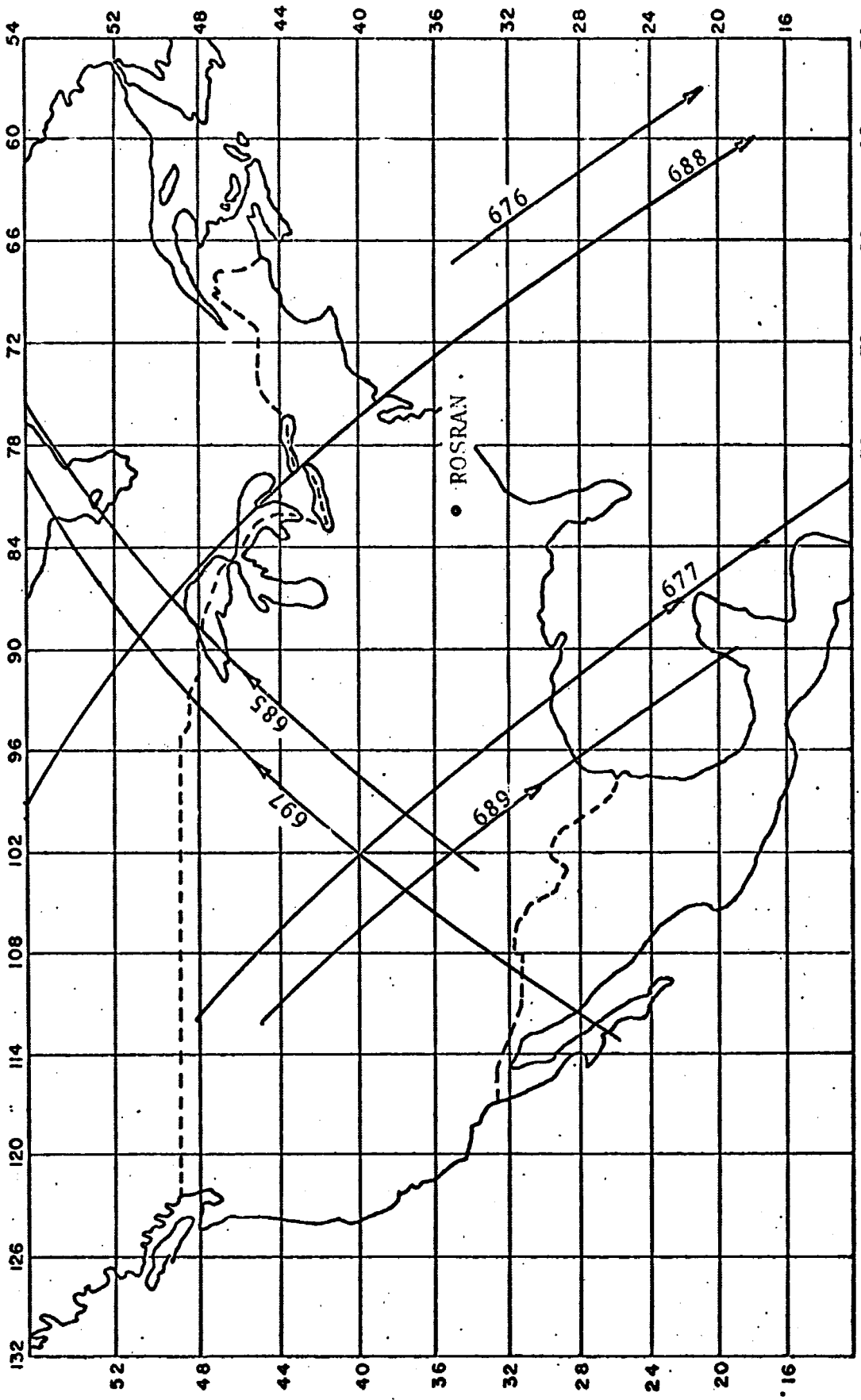

GRARR PASSES
January 2 & 3, 1966

Figure 9

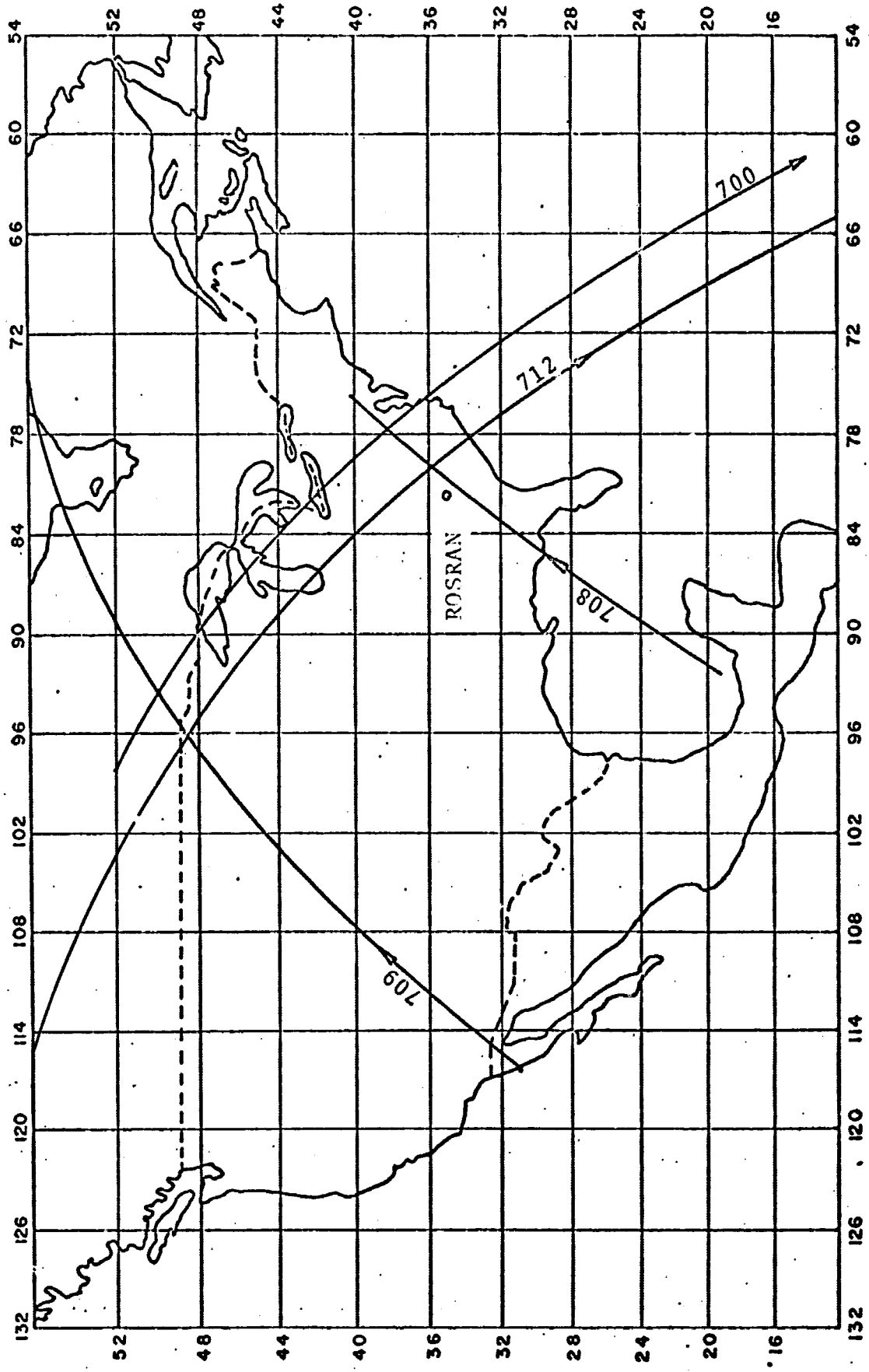

GRARR PASSES

January 4 & 5, 1966

Figure 10

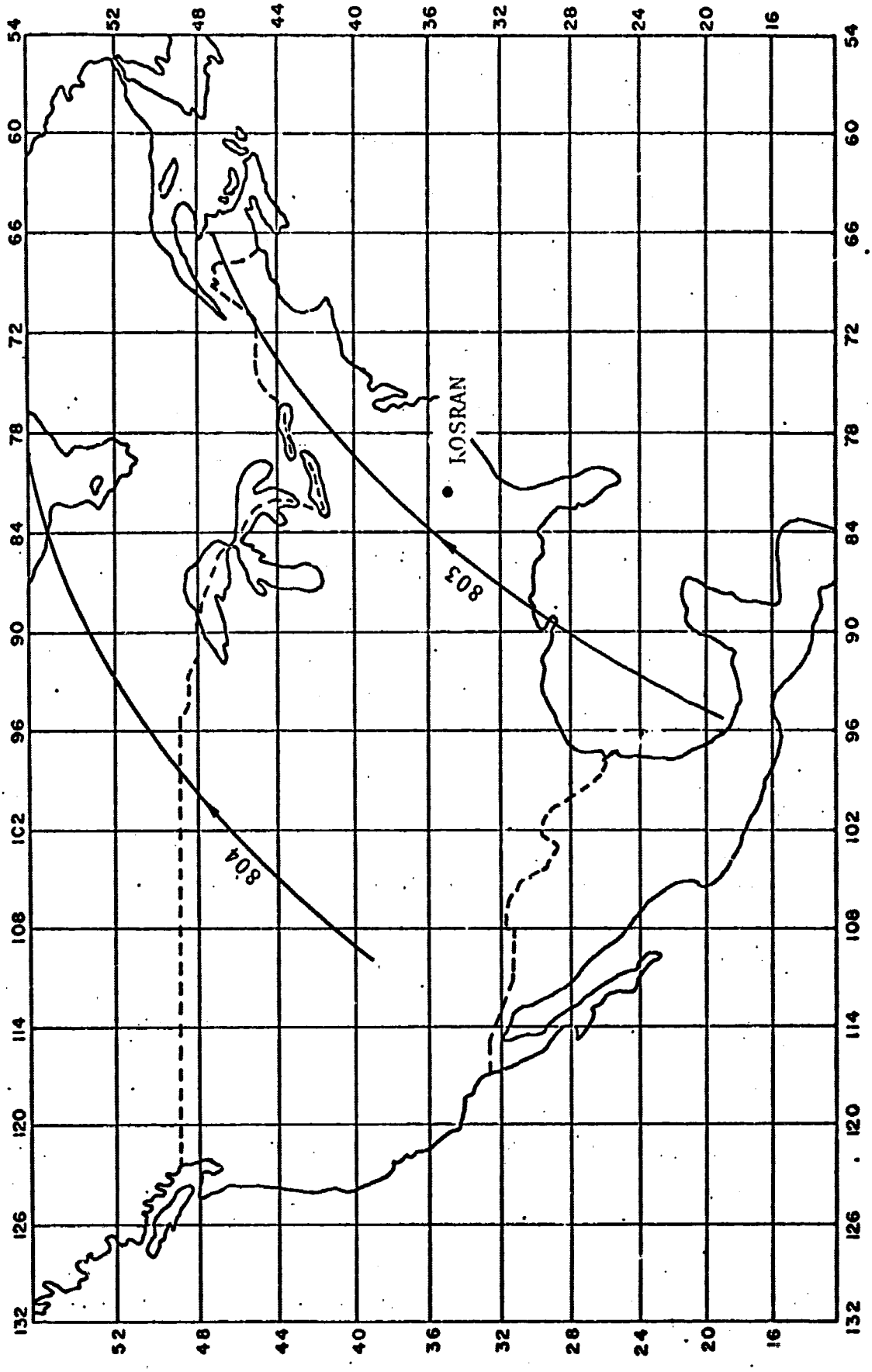

Figure 11

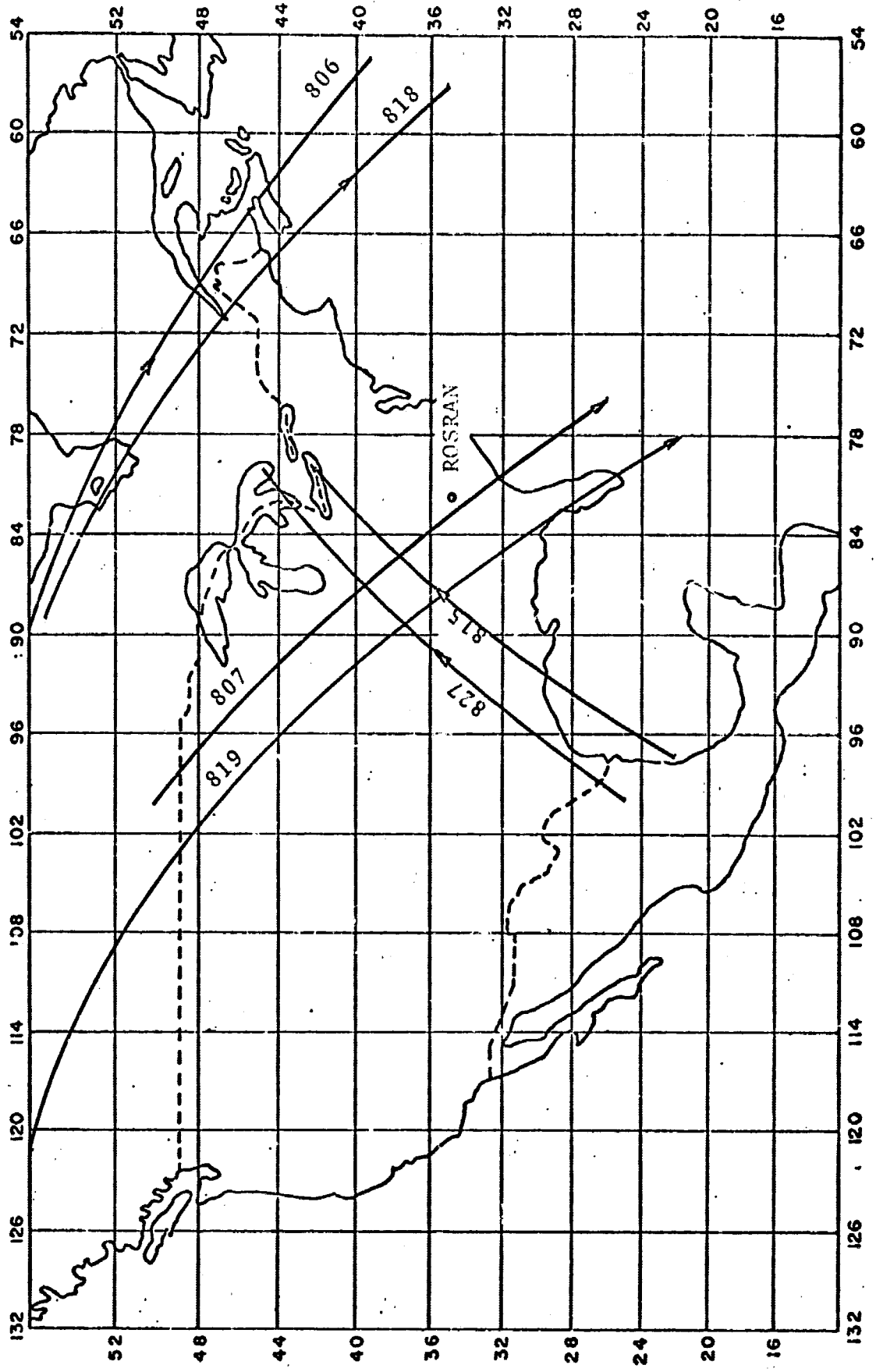

GRARR PASSES
January 13, & 14, 1966

Figure 12

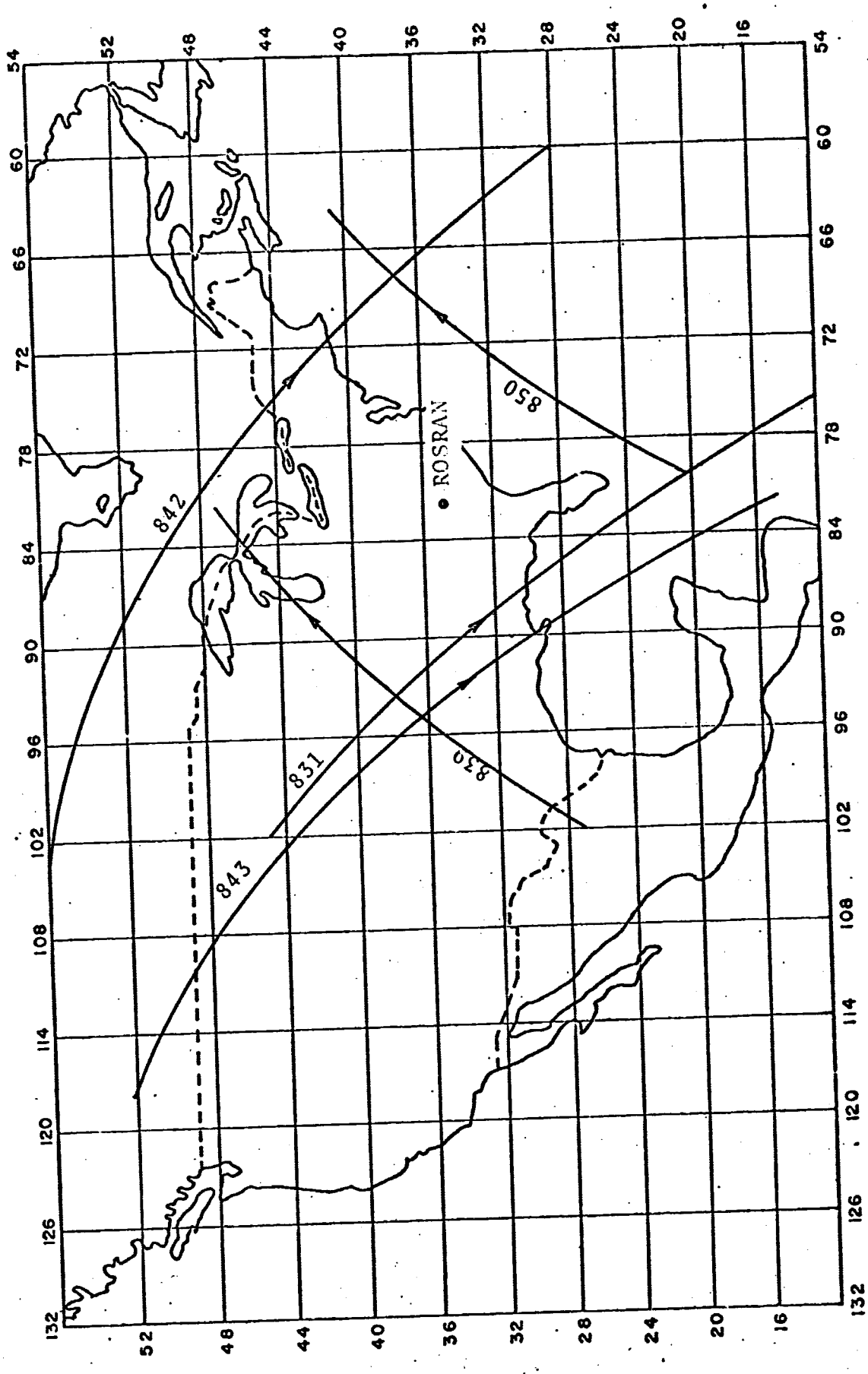

GRARR PASSES
January 15 & 16, 1966

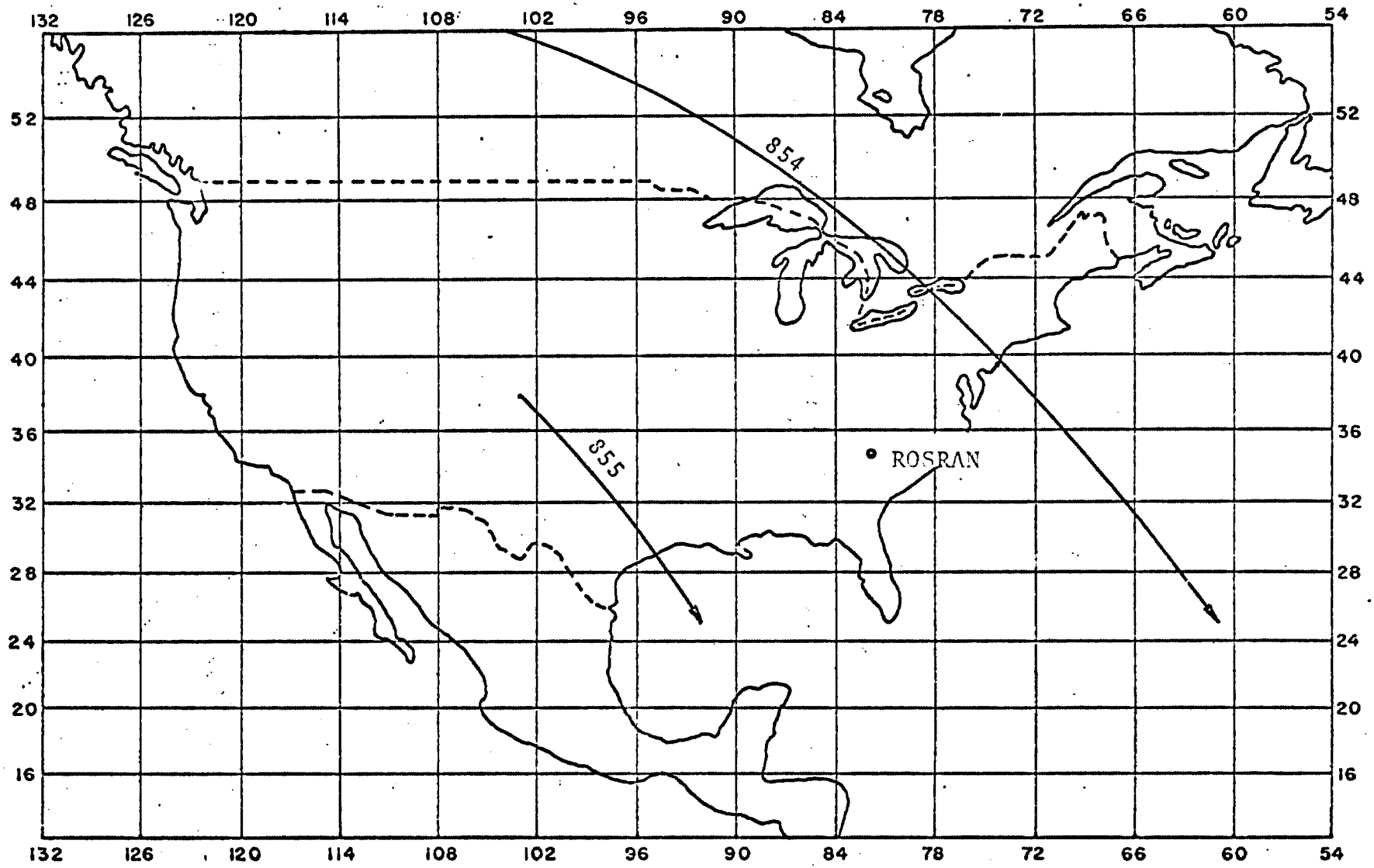

GRARR PASSES

January 17, 1966

APPENDIX A-2

Preprocessing of Optical Observations

2.1 Preprocessing of Optical Data

The first step in the processing of optical observations is usually performed by the observing source. This consists of developing a plate or film, identifying the image or images of the satellite and the images of several reference stars whose right ascensions and declinations are well known. The initial measurements of both satellite images and reference stars consist of linear rectangular coordinates. From the knowledge of the spherical coordinates of the reference stars, the right ascensions and declinations of the satellite images may be calculated. These coordinates as received by the preprocessor may be referred to the mean equator and equinox of date, true equator and equinox of date, or mean equator and equinox of some standard epoch.

The preprocessor then transforms these observations to a common coordinate system. Currently, the preprocessor transforms all right ascensions and declinations to the true equator and equinox of the epoch of the elements being processed. If the observations were originally referred to the mean equator and equinox of a particular epoch, it

is only necessary to precess from that epoch to the epoch of the elements. However, if they were referred to the true equator and equinox of a particular epoch, it is necessary first to transform them to the mean equator and equinox of that same epoch and then precess to the epoch of the elements.

Finally, a transformation must be made from the mean equator and equinox of the epoch of the elements to the true equator and equinox of the epoch of the elements.

2.2 Nutation

The transformations from the true equator and equinox of date to the mean equator and equinox of date is

$$Y = NX$$

where

$$Y = \begin{bmatrix} \cos \delta_m & \cos \alpha_m \\ \cos \delta_m & \sin \alpha_m \\ \sin \delta_m & \end{bmatrix}$$

$$X = \begin{bmatrix} \cos \delta_T & \cos \alpha_T \\ \cos \delta_T & \sin \sigma_T \\ \sin \delta_T & \end{bmatrix}$$

$$N = \begin{bmatrix} 1 & +\Delta\psi\cos\varepsilon_m & +\Delta\psi\sin\varepsilon_m \\ -\Delta\psi\cos\varepsilon_m & 1 & +\Delta\varepsilon \\ -\Delta\psi\sin\varepsilon_m & -\Delta\varepsilon & 1 \end{bmatrix}$$

where

α_m, δ_m = right ascension and declination referred to mean equator and equinox of date

α_T, δ_T = right ascension and declination referred to true equator and equinox of date

ε_m = mean obliquity of date

$\Delta\psi$ = nutation in longitude

$\Delta\varepsilon$ = nutation in obliquity

The inverse transformation is simply:

$$X = N^{-1}X = N^{T}X$$

2.3 Precession

The transformation from the mean equator and equinox of 1950.0 to the mean equator and equinox of an arbitrary epoch t1 is

$$Y = PX$$

where

$$Y = \begin{bmatrix} \cos\delta_{t1} & \cos\alpha_{t1} \\ \cos\delta_{t1} & \sin\alpha_{t1} \\ \sin\delta_{t1} & \end{bmatrix}$$

$$X = \begin{bmatrix} \cos\delta_{1950.0} & \cos\alpha_{1950.0} \\ \cos\delta_{1950.0} & \sin\alpha_{1950.0} \\ \sin\delta_{1950.0} & \end{bmatrix}$$

$$P = \begin{bmatrix} (\cos z\cos\theta\cos\zeta - \sin z\sin\zeta) & (-\cos z\cos\theta\sin\zeta - \sin z\cos\zeta) & (-\cos z\sin\theta) \\ (\sin z\cos\theta\cos\zeta + \cos z\sin\zeta) & (-\sin z\cos\theta\sin\zeta + \cos z\cos\zeta) & (-\sin z\sin\theta) \\ (\sin\theta\cos\zeta) & (-\sin\theta\sin\zeta) & (\cos\theta) \end{bmatrix}$$

The inverse transformation is

$$X = P^{-1}Y = P^{T}Y$$

Since the expression for z, θ, ζ are tied to 1950.0 as an epoch, the precession between 2 different epochs, neither of which is 1950.0, must be performed in two steps, using 1950.0 as an intermediary epoch.

APPENDIX A-3

Force Models used in NONAME

3.1 Force Models

The data reduction program in its present form incorporates four force models. These are:

1. The earth gravitational field
2. The solar and lunar gravitational perturbations
3. Solar radiation pressure
4. Atmospheric drag

The program is designed such that the gravitational coefficients and pertinent physical characteristics of satellites, such as reflectivity, cross-sectional area mass, and drag coefficient can be simply changed through card input or block data statement.

3.2 The Earth's Gravitational Field

The formulation of the geopotential used is:

$$u = \frac{GM}{r}\left\{1 + \sum_{n=2}^{k}\sum_{m=0}^{n}\left(\frac{a}{r}\right)^{n} P_n^m(\sin\phi)\left[C_{nm}\cos m\lambda + S_{nm}\sin m\lambda\right]\right\} \quad (1)$$

where

G	is the universal gravitational constant
M	is the mass of the earth
r	is the geocentric satellite distance
a	is the earth's mean equatorial radius
ϕ	is the sub-satellite latitude
λ	is the sub-satellite east longitude
$P_m^n(\sin\phi)$	is the associated spherical harmonic of degree n and order m.

The design of the potential function requires that denormalized gravitational coefficiences $C_{n,m}$ and $S_{n,m}$ be used. The program is presently capable of accepting coefficients up to (20,20) or any sub-set of these.

The denormalized gravitational coefficiences determined by SAO are listed in table 2. These coefficients have been used extensively in NONAME for the reduction of optical data. The same data have been reduced by NONAME using various other gravity models. An intercomparison of the results is being prepared for publication in the near future.

The transformation of the geopotential in earth-fixed coordinates (r,ϕ,λ) to gravitational accelerations in inertial coordinates (x,y,z) is accomplished as follows:

$$\ddot{x}_\bullet = \frac{\partial u}{\partial r}\frac{\partial r}{\partial x} + \frac{\partial u}{\partial \phi}\frac{\partial \phi}{\partial x} + \frac{\partial u}{\partial \lambda}\frac{\partial \lambda}{\partial x} \; ; \; \ddot{y}_\bullet \; , \; \ddot{z}_\bullet \qquad (2)$$

TABLE 2

SAO DENORMALIZED COEFFICIENTS M-1

$C(2,0) = -1082.645 \cdot 10^{-6}$		$C(5,4) = -0.206 \cdot 10^{-8}$	
$S(2,0) = 0$		$S(5,4) = +0.498 \cdot 10^{-9}$	
$C(2,2) = +1.536 \cdot 10^{-6}$		$C(5,5) = +0.384 \cdot 10^{-9}$	
$S(2,2) = -0.872 \cdot 10^{-6}$		$S(5,5) = -0.146 \cdot 10^{-8}$	
$C(3,0) = +2.546 \cdot 10^{-6}$		$C(6,0) = -0.646 \cdot 10^{-6}$	
$S(3,0) = 0$		$S(6,0) = 0$	
$C(3,1) = +2.091 \cdot 10^{-6}$		$C(6,1) = -0.370 \cdot 10^{-7}$	
$S(3,1) = +0.287 \cdot 10^{-6}$		$S(6,1) = -0.212 \cdot 10^{-7}$	
$C(3,2) = +0.251 \cdot 10^{-6}$		$C(6,2) = +0.858 \cdot 10^{-8}$	
$S(3,2) = -0.184 \cdot 10^{-6}$		$S(6,2) = -0.455 \cdot 10^{-7}$	
$C(3,3) = +0.782 \cdot 10^{-7}$		$C(6,3) = -0.112 \cdot 10^{-8}$	
$S(3,3) = +0.226 \cdot 10^{-6}$		$S(6,3) = +0.643 \cdot 10^{-9}$	
$C(4,0) = +1.649 \cdot 10^{-6}$		$C(6,4) = -0.167 \cdot 10^{-9}$	
$S(4,0) = 0$		$S(6,4) = -0.196 \cdot 10^{-8}$	
$C(4,1) = -0.543 \cdot 10^{-6}$		$C(6,5) = -0.253 \cdot 10^{-9}$	
$S(4,1) = -0.445 \cdot 10^{-6}$		$S(6,5) = -0.370 \cdot 10^{-9}$	
$C(4,2) = +0.738 \cdot 10^{-7}$		$C(6,6) = -0.932 \cdot 10^{-11}$	
$S(4,2) = +0.148 \cdot 10^{-6}$		$S(6,6) = -0.361 \cdot 10^{-10}$	
$C(4,3) = +0.509 \cdot 10^{-7}$		$C(7,0) = +0.333 \cdot 10^{-6}$	
$S(4,3) = -0.113 \cdot 10^{-7}$		$S(7,0) = 0$	
$C(4,4) = -0.112 \cdot 10^{-8}$		$C(7,1) = +0.144 \cdot 10^{-6}$	
$S(4,4) = +0.486 \cdot 10^{-8}$		$S(7,1) = +0.114 \cdot 10^{-6}$	
$C(5,0) = +0.210 \cdot 10^{-6}$		$C(7,2) = +0.362 \cdot 10^{-7}$	
$S(5,0) = 0$		$S(7,2) = +0.162 \cdot 10^{-7}$	
$C(5,1) = -0.677 \cdot 10^{-7}$		$C(7,3) = +0.352 \cdot 10^{-8}$	
$S(5,1) = -0.882 \cdot 10^{-7}$		$S(7,3) = +0.254 \cdot 10^{-9}$	
$C(5,2) = +0.102 \cdot 10^{-6}$		$C(7,4) = -0.323 \cdot 10^{-9}$	
$S(5,2) = -0.375 \cdot 10^{-7}$		$S(7,4) = -0.217 \cdot 10^{-9}$	
$C(5,3) = -0.172 \cdot 10^{-7}$		$C(7,5) = +0.269 \cdot 10^{-10}$	
$S(5,3) = +0.231 \cdot 10^{-9}$		$S(7,5) = +0.191 \cdot 10^{-10}$	

TABLE 2 (Cont'd)

$C(7,6)$	$-0.145 \cdot 10^{-10}$	$C(10,01)$	$+0.649 \cdot 10^{-7}$
$S(7,6)$	$+0.437 \cdot 10^{-11}$	$S(10,01)$	$-0.779 \cdot 10^{-7}$
$C(7,7)$	$+0.102 \cdot 10^{-11}$	$C(10,02)$	$-0.624 \cdot 10^{-8}$
$S(7,7)$	$+0.178 \cdot 10^{-11}$	$S(10,02)$	$-0.250 \cdot 10^{-8}$
$C(8,0)$	$+0.270 \cdot 10^{-6}$	$C(10,03)$	$-0.379 \cdot 10^{-9}$
$S(8,0)$	0	$S(10,03)$	$+0.175 \cdot 10^{-9}$
$C(8,1)$	$-0.515 \cdot 10^{-7}$	$C(10,04)$	$-0.436 \cdot 10^{-10}$
$S(8,1)$	$+0.447 \cdot 10^{-7}$	$S(10,04)$	$-0.654 \cdot 10^{-10}$
$C(8,2)$	$+0.214 \cdot 10^{-8}$	$C(11,0)$	$-0.302 \cdot 10^{-6}$
$S(8,2)$	$+0.320 \cdot 10^{-8}$	$S(11,0)$	0
$C(8,3)$	$-0.374 \cdot 10^{-9}$	$C(11,01)$	$-0.313 \cdot 10^{-7}$
$S(8,3)$	$+0.404 \cdot 10^{-10}$	$S(11,01)$	$+0.885 \cdot 10^{-8}$
$C(8,4)$	$-0.277 \cdot 10^{-9}$	$C(12,0)$	$+0.357 \cdot 10^{-6}$
$S(8,4)$	$-0.157 \cdot 10^{-10}$	$S(12,0)$	0
$C(8,5)$	$-0.959 \cdot 10^{-11}$	$C(12,01)$	$-0.923 \cdot 10^{-7}$
$S(8,5)$	$+0.214 \cdot 10^{-10}$	$S(12,01)$	$-0.402 \cdot 10^{-7}$
$C(8,6)$	$-0.475 \cdot 10^{-12}$	$C(12,02)$	$-0.470 \cdot 10^{-8}$
$S(8,6)$	$+0.888 \cdot 10^{-11}$	$S(12,02)$	$-0.233 \cdot 10^{-9}$
$C(8,7)$	$-0.444 \cdot 10^{-13}$	$C(12,12)$	$-0.278 \cdot 10^{-18}$
$S(8,7)$	$+0.158 \cdot 10^{-12}$	$S(12,12)$	$+0.718 \cdot 10^{-20}$
$C(8,8)$	$-0.316 \cdot 10^{-12}$	$C(13,0)$	$+0.114 \cdot 10^{-6}$
$S(8,8)$	$+0.130 \cdot 10^{-12}$	$S(13,0)$	0
$C(9,0)$	$+0.532 \cdot 10^{-7}$	$C(13,12)$	$-0.126 \cdot 10^{-18}$
$S(9,0)$	0	$S(13,12)$	$+0.117 \cdot 10^{-18}$
$C(9,1)$	$+0.760 \cdot 10^{-7}$	$C(13,13)$	$-0.216 \cdot 10^{-19}$
$S(9,1)$	$+0.780 \cdot 10^{-8}$	$S(13,13)$	$+0.282 \cdot 10^{-19}$
$C(9,2)$	$-0.277 \cdot 10^{-9}$	$C(14,0)$	$-0.179 \cdot 10^{-6}$
$S(9,2)$	$+0.242 \cdot 10^{-8}$	$S(14,0)$	0
$C(10,0)$	$+0.541 \cdot 10^{-7}$	$C(14,01)$	$-0.788 \cdot 10^{-8}$
$S(10,0)$	0	$S(14,01)$	$+0.280 \cdot 10^{-8}$

TABLE 2 (Cont'd)

C(14,11)	=	$+0.947 \cdot 10^{-21}$
S(14,11)	=	$-0.473 \cdot 10^{-21}$
C(14,12)	=	$+0.140 \cdot 10^{-20}$
S(14,12)	=	$-0.132 \cdot 10^{-19}$
C(14,14)	=	$-0.193 \cdot 10^{-21}$
S(14,14)	=	$-0.414 \cdot 10^{-22}$
C(15,09)	=	$-0.241 \cdot 10^{-18}$
S(15,09)	=	$-0.483 \cdot 10^{-18}$
C(15,12)	=	$-0.138 \cdot 10^{-19}$
S(15,12)	=	$-0.190 \cdot 10^{-20}$
C(15,13)	=	$-0.117 \cdot 10^{-20}$
S(15,13)	=	$-0.927 \cdot 10^{-21}$
C(15,14)	=	$+0.114 \cdot 10^{-22}$
S(15,14)	=	$-0.558 \cdot 10^{-22}$

where the subscript "⊕" denotes accelerations due to the earth's field.

3.3 Solar and Lunar Gravitational Perturbations

The perturbations caused by a third body, e.g., the sun or moon, on a satellite orbit are treated by defining a disturbing function R[1] which can be treated as the potential function U. For the solar perturbation $R_\odot$ takes the form

$$R_\odot = \frac{GMm_\odot}{r_\odot}\left[\left(1 - \frac{2r}{r_\odot}S + \frac{r^2}{r_\odot^2}\right)^{-1/2} - \frac{r}{r_\odot}\right] \qquad (3)$$

where $S = \cos(r, r_\odot)$

$m_\odot$ is the mass of the sun in earth masses

$r_\odot$ is the geocentric distance to the sun

r is the geocentric distance to the satellite

G is the universal gravitational constant

M is the mass of the earth

The acceleration of the satellite due to the sun is then

$$\ddot{x}_\odot = \frac{\partial R_\odot}{\partial r}\frac{\partial r}{\partial x}\ ;\ \ddot{y}_\odot,\ \ddot{z}_\odot \qquad (4)$$

---

[1] Kozai, Y, Smithsonian Astrophysical Observatory Special Report 22, pp. 7-10.

The lunar perturbations are found from equation (3) by substituting the lunar mass and distance for those of the sun.

The lunar and solar ephermerides are computed internal to the program. These positions are computed at ten equal intervals over each five day period and least squares fit to a fourth order polynomial in time about the midpoint of the five day period. The positions of these bodies are then determined at each data point by evaluating the polynomial at the observation time.

3.4 Solar Radiation Pressure

The acceleration acting on a satellite due to solar radiation pressure is formulated as follows [2].

$$\ddot{x}_{RAD} = -\frac{AP_{\odot}}{m}\gamma, L_x;\ \ddot{y}_{RAD},\ \ddot{z}_{RAD} \qquad (5)$$

where

- L is the inertial unit vector from the geocenter to the sun and whose components are L_x, L_y, L_z.
- A is the cross sectional area of the satellite
- m is the satellite mass
- γ is a factor depending on the reflective characteristics of the satellite

[2] H. Koelle, Handbook of Astronautical Engineering, pp. 8-33, McGraw-Hill, 1961.

ν is the eclipse factor such that:

$$\nu = \begin{cases} 0 \text{ when satellite is in earth's shadow} \\ 1 \text{ when satellite is illuminated by the sun} \end{cases}$$

$P_\odot$ is the solar radiation pressure in the vicinity of the earth,

$$4.5 \times 10^{-6} \ \frac{\text{Newton}}{m^2}$$

At present, it is assumed that the satellite is specularly reflecting with reflectivity, ρ, and thus

$$\gamma = (1 + \rho). \tag{6}$$

The vector $\hat{L}$ and the eclipse factor are determined from the solar ephemeris subroutine previously described, the satellite ephemeris, and involve the approximation of a cylindrical earth shadow.

3.5 Atmospheric Drag

The atmospheric decelerations are computed as follows:

$$\ddot{x}_{DRAG} = -\frac{\rho C_D A v v_x}{2m} \ ; \ \ddot{y}_{DRAG}, \ \ddot{z}_{DRAG} \tag{7}$$

where

ρ is the ambient atmospheric density

C_D is the satellite drag coefficient

A is the projected area of the satellite on a plane perpendicular to direction of motion

m is the satellite mass.

The velocity vector $\vec{v}$ given in inertial coordinates by

$$\vec{v} = v_x\hat{i} + v_y\hat{j} + v_z\hat{k} \tag{8}$$

can be chosen to be either the velocity relative to the atmosphere which implies that the atmosphere rotates with the earth or the inertial velocity which assumes that the atmosphere is static. Presently, the former assumption is made.

The density, ρ, is computed from the 1962 U.S. Standard Atmosphere.

APPENDIX A-4

Station Position Transformations

4.1 Station Position Transformations

The analysis of "long arc" passes of the GEOS-A satellite requires that the various tracking station a priori positions be available on a uniform world geodetic system in order that the results not be biased by interdatum uncertainties. The world geodetic system selected for these analyses is the SAO Standard Earth (C-5 datum).

A priori estimates of the tracking station positions and their uncertainties relative to the geo-center (earth's center of mass) are derived from the knowledge of the following:

a. Baker-Nunn camera station positions on the original datums.

b. Baker-Nunn camera station positions on the SAO C-5 datum.

c. The positions of the various tracking sites in their original datums.

d. Intra-datum survey connections between the Baker-Nunn sites and the various tracking sites.

e. Empirical formulae for the estimation of surface survey uncertainties between the Baker-Nunn sites and the tracking sites.

The method used to effect this transformation is simple and straight forward and has been checked to ascertain its compatibility with the more rigorous and arduous transformation formulae commonly used to compute datum shifts. It should be noted that this method can be used only when the type of information that has been calculated for the Baker-Nunn sites is available. That is to say, one must have available the positions of the control stations (Baker-Nunn sites) in the original datum and in the new reference system, and a direct survey tie between the control stations and the tracking stations which are to be transformed.

4.2 SAO Standard Earth Reference System

The reference system used in the derivation of the a priori positional information is the SAO Standard Earth as described in [1]. The ellipsoidal parameters are a_e = 6,378,165 meters and f = 1/298.25. This system is the best available geocentric (earth's center of mass) terrestrial system. The Z axis is oriented in the direction of the mean pole of 1900-1905 and the X axis in the direction of the mean observatory. Since the definition of UT-1 was based on the U. S. Naval Observatory's time determination the X axis is directed toward the meridian 75°-03'-55".94 East of the U. S. Naval Observatory.

The uncertainty related to this system is defined

(by [1] to be about ±10 meters for the origin (geocentricity), 0".2 for the direction of the axes, and a few parts per million in scale. The scale actually depends on the adopted value for GM which in this instance is $3.986032 \times 10^{20} cm^3 sec^{-2}$. The absolute coordinates of the Baker-Nunn stations are given to an accuracy of ±15 to 20 meters. The fact that this system is oriented to the mean pole of 1900-1905 must be taken into consideration when station positions as derived from the tracking data are obtained. Unless corrections for polar motion are applied, the positions derived from the tracking data will be based on the instantaneous pole at the time of observation.

4.3 Coordinate Transformations

All of the Baker-Nunn camera stations are connected to individual major geodetic datums and their coordinates in these datums are known. The coordinates of the Baker-Nunn camera stations on the SAO Standard Earth are also known, having been derived by SAO through the reduction of approximately 35,000 satellite observations with wide orbital variety. The coordinates of the Baker-Nunn camera stations are given in both the ellipsoidal and three-dimensional cartesian coordinate systems. For ease and simplicity of calculation, we have elected to use the cartesian coordinates to obtain our transformations. By comparing the original datum coordinates with the derived mass-centered coordinates, one derives the "datum shift" for the particular datum. The "datum shift" is simply the total transformation to be applied to the original datum coordinates to obtain the new mass-centered coordinates. Once the

"datum shift" has been derived for the Baker-Nunn station this shift is then applied in a weighting scheme to derive the SAO Standard Earth coordinates for tracking stations that have positions given in the same original datum as the Baker-Nunn and are connected to the Baker-Nunn station through conventional surface surveys. A weighting scheme (which is described below) is used since the Baker-Nunn stations were allowed to adjust independently and subsequently where more than one Baker-Nunn station was located on a single datum, the individual stations show slightly different "datum shifts".

As an example of the single station case, consider Baker-Nunn camera station 9005, TOKYO. Its coordinates on the Tokyo (JAP) datum are:

X: -3,946,554 (meters)

Y: +3,365,774 (meters)

Z: +3,698,151 (meters)

Its geocentric (mass centered) coordinates on the SAO Standard Earth are:

X_g: -3,946,703 (meters)

Y_g: +3,366,291 (meters)

Z_g: +3,698,849 (meters)

The transformation to be applied to tracking stations on the Tokyo datum is therefore:

$$X_g - X = \Delta X = -149 \text{ meters}$$

$$Y_g - Y = \Delta Y = +517 \text{ meters}$$

$$Z_g - Z = \Delta Z = +698 \text{ meters}$$

The ΔX, ΔY, ΔZ is applied to the tracking station coordinates on Tokyo datum. This in effect then furnishes an a priori estimate of the coordinates of the tracking station in the SAO Standard Earth reference system.

As mentioned above, the coordinates of the Baker-Nunn camera stations are furnished in both the ellipsoidal and three-dimensional cartesian coordinate systems. However, the coordinates of the various tracking stations may be given in ellipsoidal coordinates only, thereby requiring the calculation of the three-dimensional cartesian coordinates. This is done using the following standard formulation:

$$X = (\nu + h + N) \cos \phi \cos \lambda$$

$$Y = (\nu + h + N) \cos \phi \sin \lambda$$

$$Z = [(1 - e^2)\nu + h + N] \sin \phi$$

where:

ϕ = geodetic latitude

λ = geodetic longitude

$\nu = a_e/(1 - e^2 \sin^2\phi)^{1/2}$

a_e = semi major axis of reference ellipsoid

e^2 = eccentricity squared of reference ellipsoid

h = height of station above the geoid (mean sea level elevation)

N = height of the geoid above or below the spheroid.

In the case where the tracking station information only contains mean sea level elevations, the geoid height is derived from geoid contour charts for the particular reference spheroid. These charts are based on gravitational coefficients derived from satellite observations.

Having derived the a priori estimates of the tracking station positions on the SAO Standard Earth we now derive estimates of the uncertainties of these positions relative to the earth's center of mass.

4.4 A Priori Uncertainty Derivation

In order to derive a priori estimates of the uncertainty in the tracking station positions, use is made of an empirical formula derived by Lansing Simmons, USC & GS, to describe the accuracy of first order triangulation. The formula states that the relative accuracy between two points connected by conventional first-order triangulation (1 part in 25,000) is approximately:

$$1/20{,}000\sqrt[3]{M},$$

where M is distance between the two stations in statute miles. As an example consider two stations 1000 miles apart, and connected by standard triangulation. The proportional accuracy would therefore be 1 part in 200,000 or approximately 26.4 ft. This means that the relative uncertainty between the two stations caused by the surface survey errors is approximately 26 ft. or 8 meters. Accepting the stated accuracy of the Baker-Nunn stations relative to the center mass as $\pm$ 20 meters, one can then take the root sum square of the uncertainty in the Baker-Nunn station relative to the center of mass and the surface survey uncertainty between the Baker-Nunn and the tracking station as derived by the Simmons formula as a conservative estimate of the uncertainty of the tracking station relative to the center of mass. The formula then becomes:

$$\sigma_g = \sqrt{\sigma_s^2 + 20^2}$$

where

σ_g = uncertainty of the tracking station relative to the center of mass.

σ_s = survey uncertainty as computed by Simmons formula.

4.5 Weighting Scheme for Multi-Station Connections

In the case where a tracking station is located on a datum which contains more than one Baker-Nunn station, we use a weighted average of the geocentric coordinates of the tracking station derived from the general formula

$$P = \left(\frac{W_1}{W_1+W_2\ldots W_n}\right) P_1 + \left(\frac{W_2}{W_1+W_2\ldots W_n}\right) P_2$$

$$+ \ldots \left(\frac{W_n}{W_1+W_2\ldots W_n}\right) P_n$$

where:

P is the weighted position

$W_1 \ldots W_n$ are the weights

P_1 is the station position derived from Baker-Nunn Station 1

P_2 is the station position derived from Baker-Nunn Station 2

P_n is the station position derived from Baker-Nunn Station n

The weights used are inversely proportional to the distances between the Baker-Nunn stations and the tracking station to be transformed. This weighting scheme allows us to take into consideration the varying shifts of the Baker-Nunn stations while placing proper emphasis on the contribution of individual stations upon the transformation. As an example, consider the case where the tracking station is located close to one of the Baker-Nunn stations in the datum. One can rightfully expect that the tracking station would shift approximately the same amount and in the same direction as the co-located Baker-Nunn and that the effect of the other Baker-Nunn stations would be minimal. In the case where the tracking station were located equidistant from several Baker-Nunn stations one would assume equal contribution to the transformation from each of the Baker-Nunn shifts.

While the above weighting scheme is apparently quite adequate, investigations are continuing into other weighting schemes. Foremost of these is the computation of the weights (W_n) as being inversely proportional to the square of the distances between the Baker-Nunn stations and tracking station to be transformed. Another procedure being investigated is the distance cut-off, whereby a very distant Baker-Nunn coordinate shift will have essentially no effect on the station to be transformed. This cut-off distance is being presently considered in the range of 5000 km.

The transformed station coordinates derived using these weighting schemes are being compared in separate NO-NAME data reduction runs. Identical observational data are being reduced in each run, and the observational residuals are being compared.

4.6 Isolated Datums

An ellipsoidal transformation is performed for a tracking station on an isolated datum such as the Tananarive datum. For these station positions, the ΔU, ΔV, and ΔW shifts are unknown and considered to be zero. The shifts are computed as follows:

$$\Delta N = (a\,\Delta f + f\,\Delta a)\sin^2\phi - \Delta a$$

$$\Delta\phi = 206265[(a\,\Delta f + f\,\Delta a)\sin 2\phi]/R_m$$

$$R_m = \frac{a(1-e^2)}{[(1-e^2\sin^2\phi)^{1/2}]^{3/2}}$$

where

a	=	6378165. meters
f	=	1/298.25
Δa	=	6378165. minus original survey ellipsoid value of a.
Δf	=	1/298.25 minus original survey ellipsoid value of F.
ϕ	=	Latitude of tracker in original system
e^2	=	$2f - f^2$

X-552-67-

INTERCOMPARISON OF THE MINITRACK AND OPTICAL TRACKING NETWORKS USING GEOS-I LONG ARC ORBITAL SOLUTIONS

PART I

F. J. Lerch
J. G. Marsh
R. J. Sandifer
W. A. Taylor

December 1967

GODDARD SPACE FLIGHT CENTER
GREENBELT, MARYLAND

This paper presents one particular phase of our current investigation of the capability of the Minitrack tracking system by utilizing a GEOS-I long arc trajectory determined by optical observations only. We felt that there would be some merit in analyzing the Minitrack data before they had been corrected for refraction and other effects. The geometry of the Minitrack antenna reception pattern and the method of tracking suggests that it may be possible to separate out the relative effect on the residuals of those phenomena which are not refraction dependent.

The data as obtained from the NASA Space Science Data Center consist of 1 to 3 observation pairs of direction cosines per station pass. These data obtained from the Data Center have been reduced by Goddard from approximately 30 observation pairs of phase difference measurements per station-pass as transmitted to Goddard by the tracking station. Goddard transforms these data to direction cosines and reduces them to approximately 1 to 3 data pairs by means of a polynomial smoothing process. This is the only pre-processing performed on the data before it is transmitted to the Data Center or used by Goddard's own differential correction program. [The R.M.S. fit of the polynomial smoothing process averages].

During normal operations the Minitrack stations do not track below 70° elevation except during early launch phases before an orbit is well determined. In the case of GEOS-I, an exception was made and tracking was performed almost down to the horizon. For the current analysis we have observations available down to about 15° elevation.

The optical orbit used as a reference trajectory is almost identical to the one labeled "period 1" used by Mr. Marsh

in his analysis of the GRARR system at Rosman. We have included one additional SAO flash sequence from Jupiter, Florida. This reference orbit extends 5 1/4 days from December 31, 1965 to January 5, 1966. The 1059 optical observations available for that period are more descriptive of the available station coverage if they are described in terms of "Station-Passes". With this method of description, the 1059 optical observations can be summarized as a total of 91 station-passes.

Of the 91 station-passes, 21 were passive -- all from the SAO Network. Seventy station-passes consisted of active flash sequence observations, only two of which came from the SAO Network. The remaining 68 active station-passes were distributed as follows:

30 passes	USAF Network	PC-1000 cameras
24 passes	SPEOPT Network	MOTS 40" cameras
14 passes	STADAN Network	MOTS 40" cameras

As can be seen from the first slide, the 68 passes from the Air Force, STADAN, and SPEOPT networks were all located on North American continent or its near vicinity. In addition, the only two active passes from SAO, at Agassi and Jupiter, are also on the North American continent. The only world wide optical coverage came from passive SAO observations from the stations shown in the next slide. At least one observation was obtained from every station shown except Olifantsfontein in South Africa. The orbital fit for the 5 1/4 days of optical observations was 3".0 using the SAO M-1 gravity model modified by the GEOS-I resonant harmonics

as redetermined by SAO. All tracking station locations were transformed to the SAO C-5 system.

A summary of Minitrack observations used in the analysis is shown in the next slide. This data summary consists of 158 station-passes compared to 91 station-passes of optical data. For the Minitrack data also, the orientation is strongly towards the North American continent with 29 passes at Blossom Point, Maryland, 26 passes at St. Johns, Newfoundland and 25 passes at Mojave, California. The next slide shows the locations of these stations. At least one observation was obtained from every station shown except Tananarive.

An arbitrary cut-off point of $.5 \times 10^{-3}$ in direction cosine residuals was used in the rejection of data to be used in the analysis. Approximately 5% of all Minitrack data available from the NASA Data Center during the period of analysis exceeded this figure. For this purpose, the Minitrack residuals were calculated on the basis of the orbit determined by optical data only. A subsequent orbit described at the end of this paper, determined from unpre-processed Minitrack data only, gave an orbital fit of $.19 \times 10^{-3}$. On the basis of this figure then, 5% of the Minitrack data available from the NASA Data Center exceeded approximately 2.5 times the Minitrack orbital fit, where the data was actually rejected on the basis of their residuals calculated from an orbit determined on the basis of optical data only.

Also, for the purpose of analyzing the Minitrack data, the residuals were calculated on the basis of the orbit deter-

mined by optical observations only. The following analysis depends upon the geometrical configuration of the Minitrack antenna pattern shown in the next slide. There are two possible modes of tracking. In the Equatorial Mode, the so-called "fine-beam" is oriented in a North-South direction, with the long portion of the beam stretching 50° on each side of the zenith and only 5° on each side of the zenith in the East-West direction. When tracking in the Polar Tracking Mode, the long portion of the beam is oriented East-West and the narrow portion oriented North-South. The particular mode of tracking is usually determined by the direction in which the satellite is approaching the station. It is possible to switch electronically from one mode to the other fairly quickly and we had several passes of GEOS-I tracked in both modes during the same pass.

The observations available as data are the direction cosines ℓ and m. The direction cosine ℓ is equal to the cosine of the angle α measured from the East axis. The direction cosine m is equal to cosine of the angle β measured from the North axis. A vector directed towards the satellite is indicated in both the Equatorial and Polar tracking modes. The 100° by 10° wedge shaped pattern is defined by the locus of points where the signal from the satellite's Minitrack beacon drops 3 decibels from the zenith signal. Under normal conditions, the satellite is only tracked when it is located within this wedge shaped beam which is called the "fine-beam".

By considering the geometry of the antenna pattern more carefully, we see that when in the Equatorial tracking

mode, the angle α will never be less than 85^{o} and the angle β will be approximately equal to the elevation angle. In the polar tracking mode, the situation is reversed and we have a configuration where β is always greater than 85^{o} and α is approximately equal to the elevation angle. For analysis purposes, we are going to make the assumption that any systematic errors due to refraction are not present in the residuals of the direction cosine ℓ when tracking in the Equatorial mode. Whatever systematic effect may be present in $\Delta\ell_{eq}$, we will call a "beam only" effect, i.e., systematic errors due to position in the long part of the beam only. We will assume that the residuals Δm_{eq} contains both systematic "beam only" effects and systematic "refraction" effects. In the Polar tracking mode, again, the situation is reversed and we assume that any residual $\Delta\ell$ polar contains both "beam only" and "refraction" systematic effects while Δm polar contains only systematic "beam only" effects. We are neglecting any systematic effects which may be due to position across the narrow part of the beam.

The next slide shows on the left side the direction cosine ℓ residuals plotted versus elevation angle for Blossom Point, Maryland. On the right is a similar plot for the direction cosine m residuals versus elevation angle for Blossom Point, Maryland. The residuals have been scaled by a factor of 10^{3}. If the residual resulted from an observation obtained while tracking in an Equatorial mode, the residual is plotted as a dot. If the residual resulted from an observation obtained while tracking in a Polar mode, the residual point has a circle around it. One observation was obtained from tracking in a side lobe, i.e., outside the

"fine-beam". This residual is marked with a triangle.

In the Δm plot, the "beam only" and "beam only + refraction" effects are pronounced. As we would expect, the dots flair out towards larger values at low elevation angles, whereas the circles remain relatively closer spaced about the abscissa regardless of elevation. In the $\Delta \ell$ plots on the left, we expect the dots to be more closely spaced as a function of elevation while the circles flair out at the lower elevation angles. The expected trend is present although not to the degree that we see in the m residual plot.

In order to obtain an overall picture of the "beam only" effect versus the "beam only + refraction" effects, we have summarized in the next slide the total effect of the residuals from all stations by means of a 3 dimensional histogram showing relative frequency as a function of both magnitude of the residual in steps of $.1 \times 10^{-3}$ and by elevation angle in steps of 20^{o}. The histogram labeled "beam only" effect is obtained from the frequency of $\Delta \ell_{eq}$ and Δm_{polar}. The "beam only + refraction" effect is obtained from the frequency of $\Delta \ell_{polar}$ and Δm_{eq} residuals. The mean value and standard deviations of the residuals in the elevation dimension are printed at the top. For the "beam only" effect, the mean values in the different elevation dimensions remain fairly close to 0. In the "beam only + refraction" histogram at low elevations, there is a definite shift of the mean value of the residuals to the negative. In the 10^{o} to 30^{o} elevation dimension, the shift amounts to $-.2 \times 10^{-3}$ which is of the order of magnitude to be expected due to refraction effects only, and is in the correct direction.

In order to illustrate other statistical properties of the data, we have summarized the residuals in the next slide into histograms by station neglecting the particular mode of tracking. The station name and number of observations appears at the bottom of the page. The ℓ residuals for each station appears at the top graph and the m residual as the bottom graph. We see that in the case of Mojave, there is a programmed positive bias of the ℓ direction cosine residuals, and a negative bias of the m direction cosine residuals. A strong bias in the opposite direction occurs for College, Alaska with a negative bias on the ℓ residuals and a positive bias on the m residuals.

In order to obtain an estimate of the "position in space" differences between orbits as obtained by Minitrack data only and optical data only, trajectories obtained from the two solutions were calculated, differenced, and resolved into along track, cross track, and radial differences. The orbital fit from Minitrack data only, not corrected for refraction or other effects, was $.19 \times 10^{-3}$ for the 5 1/4 day arc. The orbital fit from optical data only was 3".0. In both this calculation and the previous analysis, the start and end points of the Minitrack data were chosen to correspond to the equivalent times of the optical data so that there would be no systematic orbital shift due to overlap effects. In the next slide, we see that the trajectory differences were most pronounced in the along track direction. The along track difference takes the approximate form of a sine curve of a 2 hour period (the period of GEOS-I) with an amplitude of approximately 110 meters superimposed upon a small secular term. In the upper plot, representing differences during

the first 5 hours of the arc, the sine curve minimum occurs at approximately -50 meters. During the final 5 hours of the 5 1/4 day arc shown in the bottom plot, the minimum occurs at approximately +30 meters. This represents a secular term in the differences of approximately 80 meters/ 5 days or 16 meters day.

Among other plans for our future analysis of the Minitrack observations, we intend to do the following:

1. Apply accurate tropospheric & ionospheric refraction corrections based upon best available data.

2. Adjust the STADAN station locations dynamically, particularly for those stations where there is a pronounced bias in the ℓ and m residuals.

3. Improve the timing of our observations by making use of the "Final Times of Emission" bulletins which are now becoming available from the Naval Observatory for our particular period of interest.

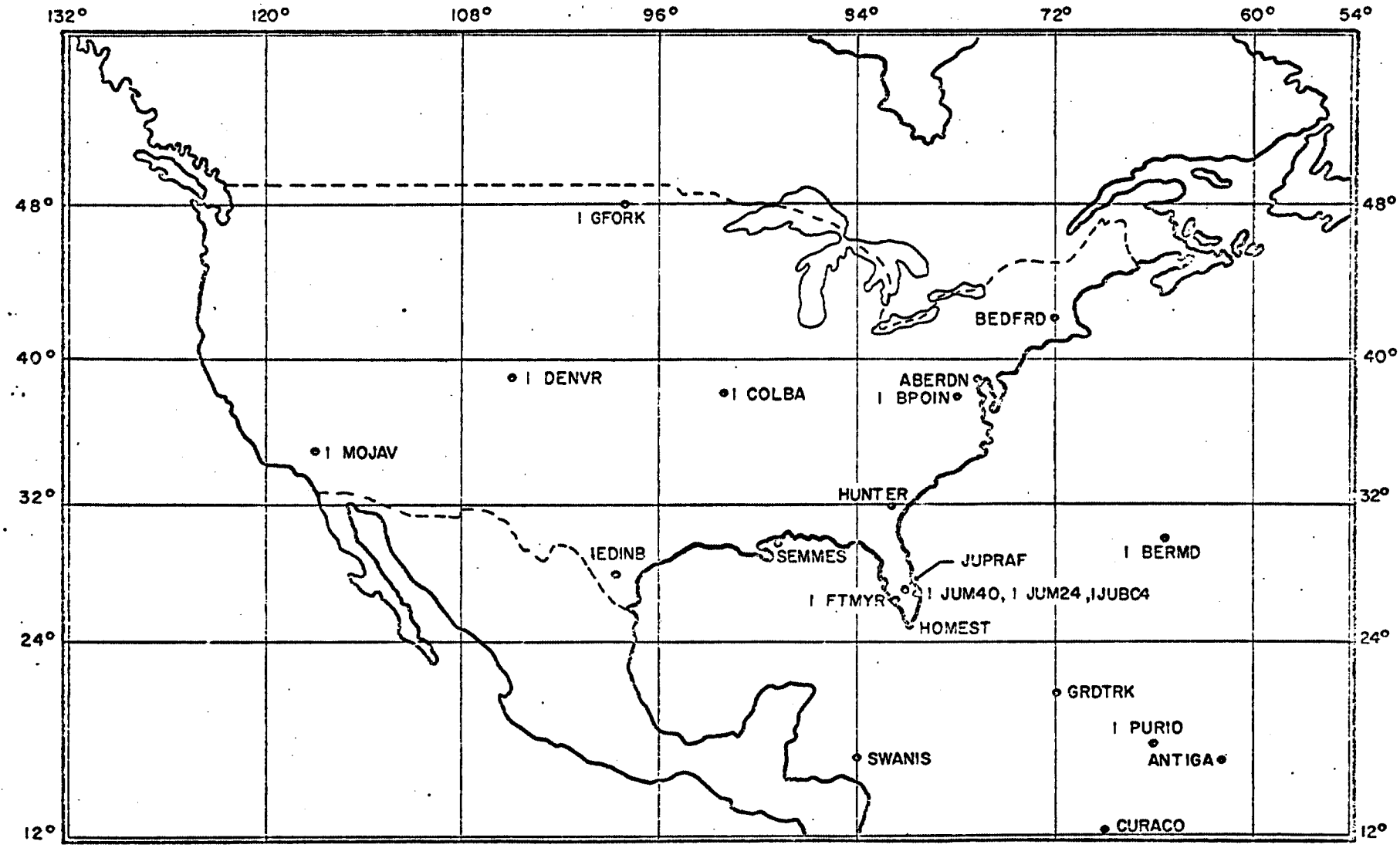

STADAN, SPEOPT AND USAF CAMERA STATIONS

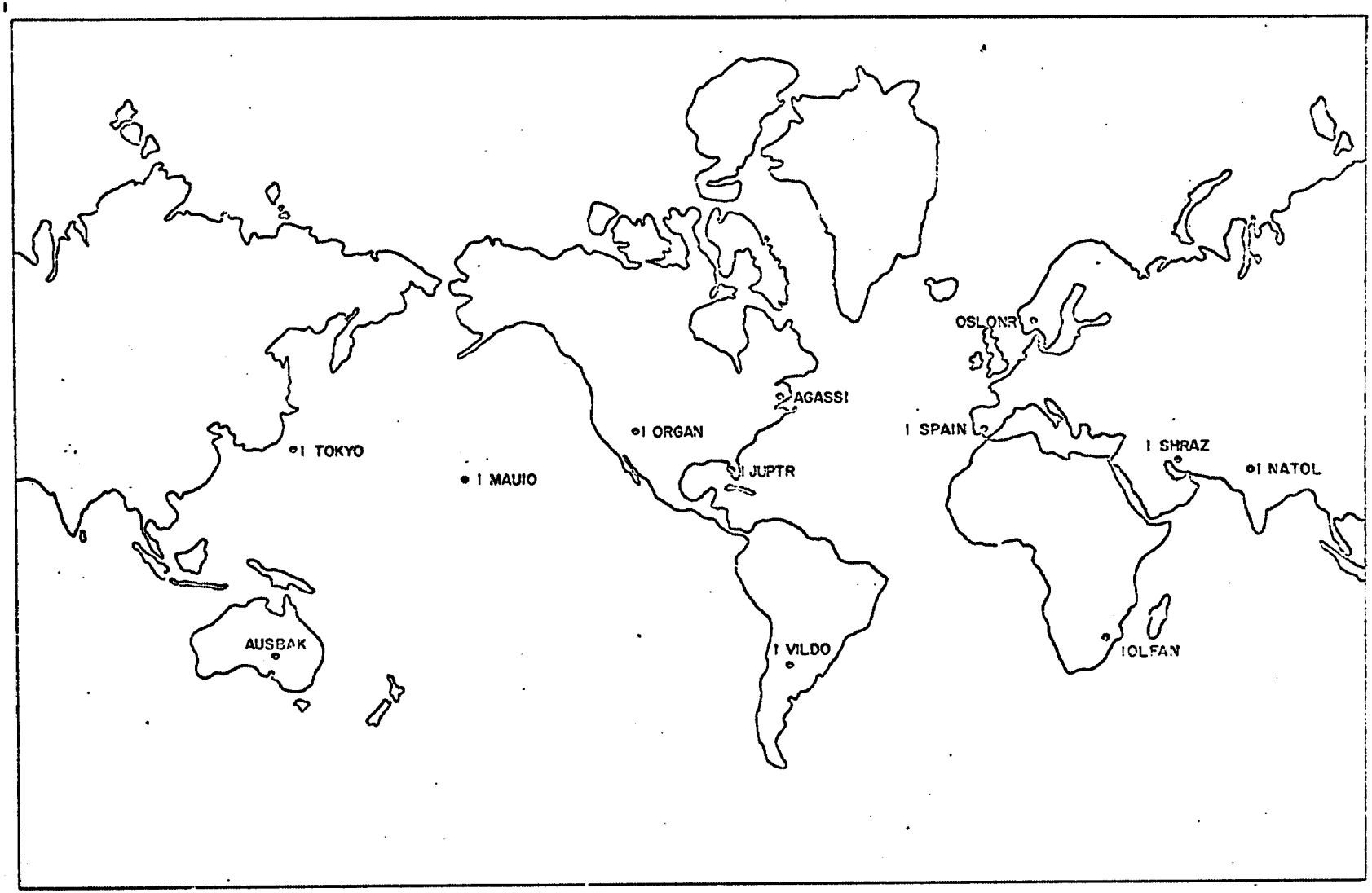

SAO BAKER - NUNN STATIONS

SUMMARY OF MINITRACK OBSERVATIONS

USED IN

INTERCOMPARISONS FOR THE PERIOD $1^h\ 38^m$ 12/31/65 to $6^h\ 45^m$ 1/5/66

(approximately 63 Orbital Revolutions)

	No. of Observations			
Station	ℓ	m	no. of passes	Location
1. BPOIN6	46	46	29	Blossom Point, Maryland
2. COLFG6	21	21	18	College, Alaska
3. FT. MR6	17	17	12	Fort Myers, Florida
4. GFORK6	27	27	19	East Grand Fork, Minnesota
5. JOBUR6	2	2	2	Johannesburg, South Africa
6. LIMAP6	6	6	4	Lima, Peru
7. MOJAV6	36	36	25	Mojave, California
8. NEWFL6	36	36	26	St. Johns, Newfoundland
9. OOMER6	4	4	4	Woomera, Australia
10. QUITO6	4	4	3	Quito, Ecuador
11. SNTAG6	4	4	4	Santiago, Chile
12. WNKFL6	15	15	12	Winkfield, England
			158	Total Station-Passes
TOTAL	218	+ 218	=	436

R.M.S. Orbital Fit Using Minitrack Data Only = $.19 \times 10^{-3}$

All Minitrack Data Rejected Whose Residuals From Optically Determined Orbit Exceeded $.5 \times 10^{-3}$ (5% of Smoothed Data Available from Data Center)

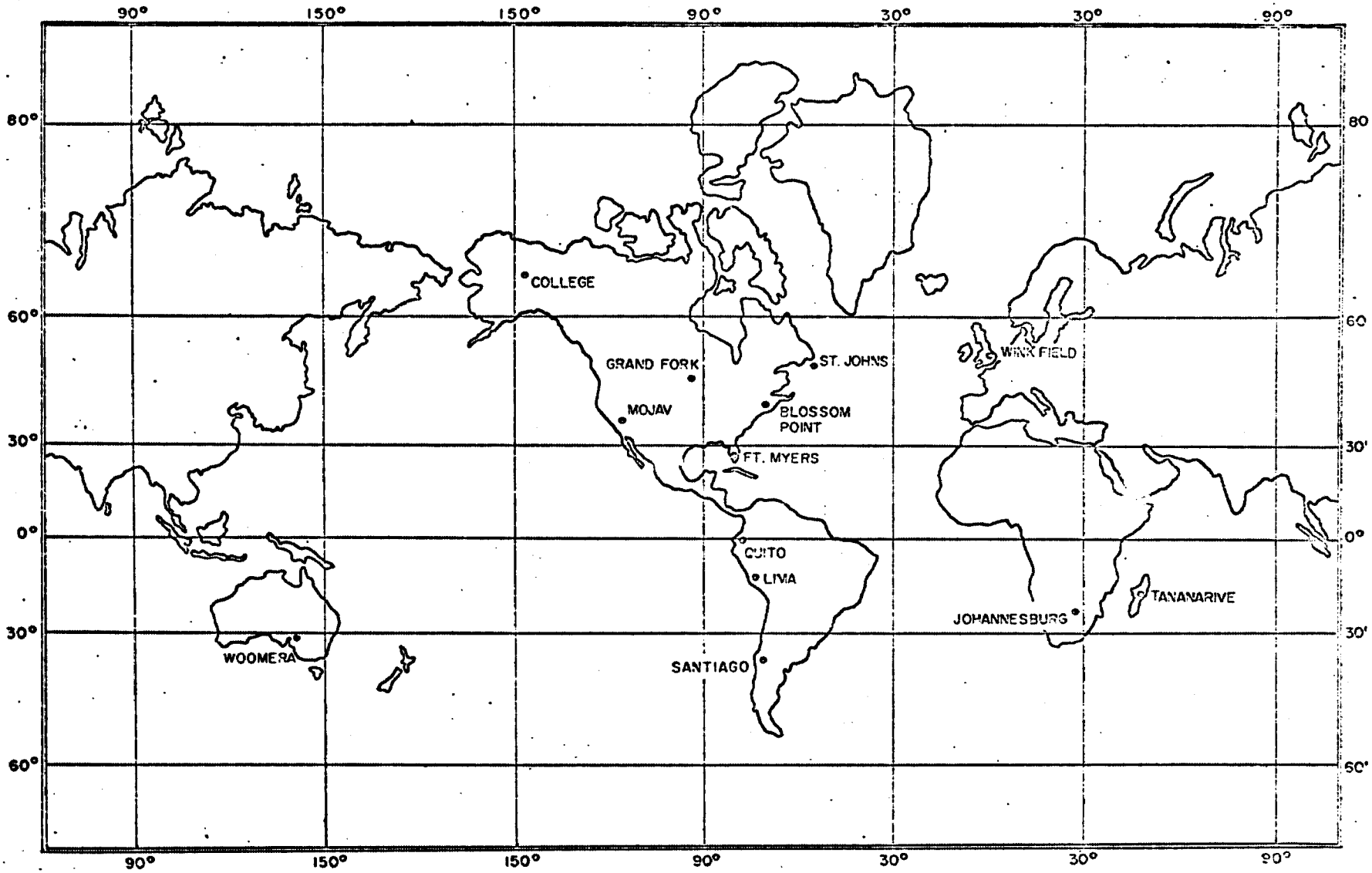
90°
150°
150°
90°
30°
30°
90°
80°
60°
30°
0°
30°
60°
COLLEGE
GRAND FORK
MOJAV
ST. JOHNS
BLOSSOM POINT
FT. MYERS
WINK FIELD
QUITO
LIMA
SANTIAGO
WOOMERA
JOHANNESBURG
TANANARIVE

Minitrack Measurements

$\ell = \cos \alpha$

$m = \cos \beta$

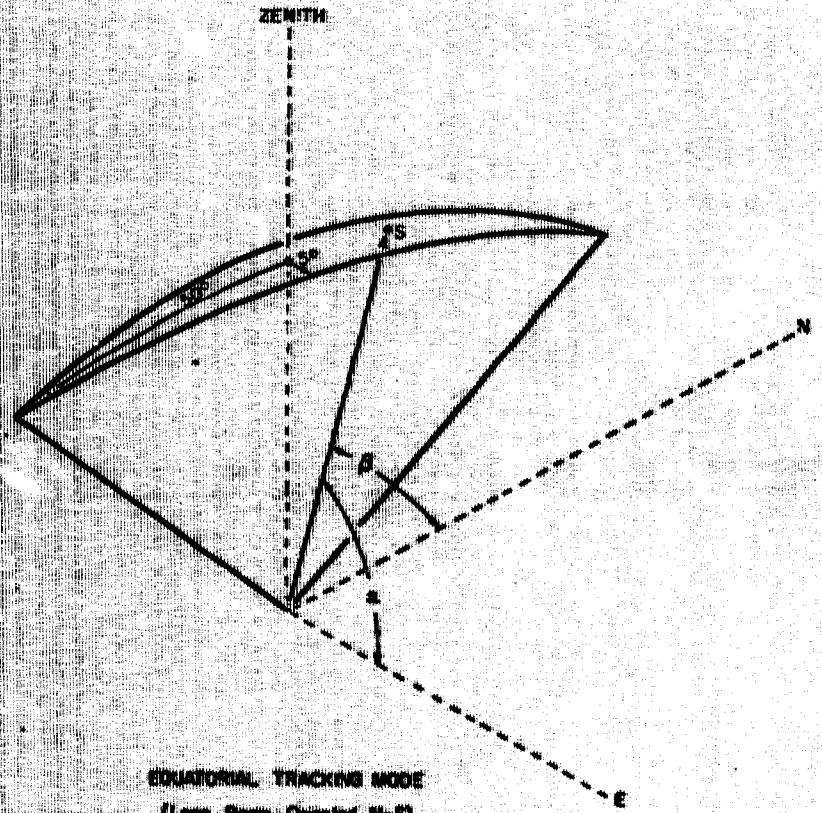

EQUATORIAL TRACKING MODE
(Long Beam Oriented N-S)

ℓ - Long Beam Dependent Only

m - Long Beam & Refraction Dependent

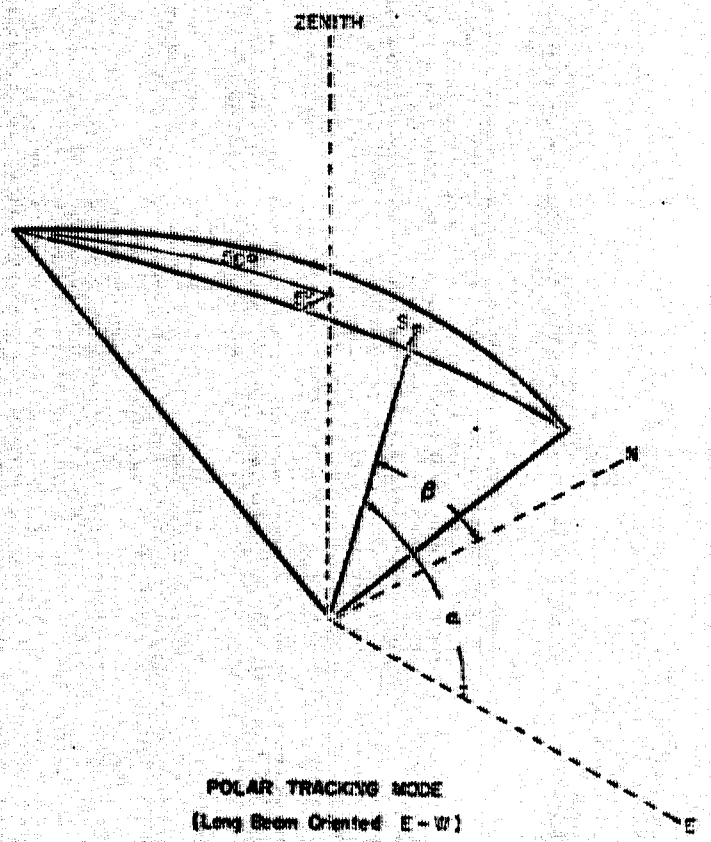

POLAR TRACKING MODE
(Long Beam Oriented E-W)

ℓ - Long Beam & Refraction Dependent

m - Long Beam Dependent only.

Approximate Reception Pattern of the
Five Beam of the GSFC Minitrack Antenna Array

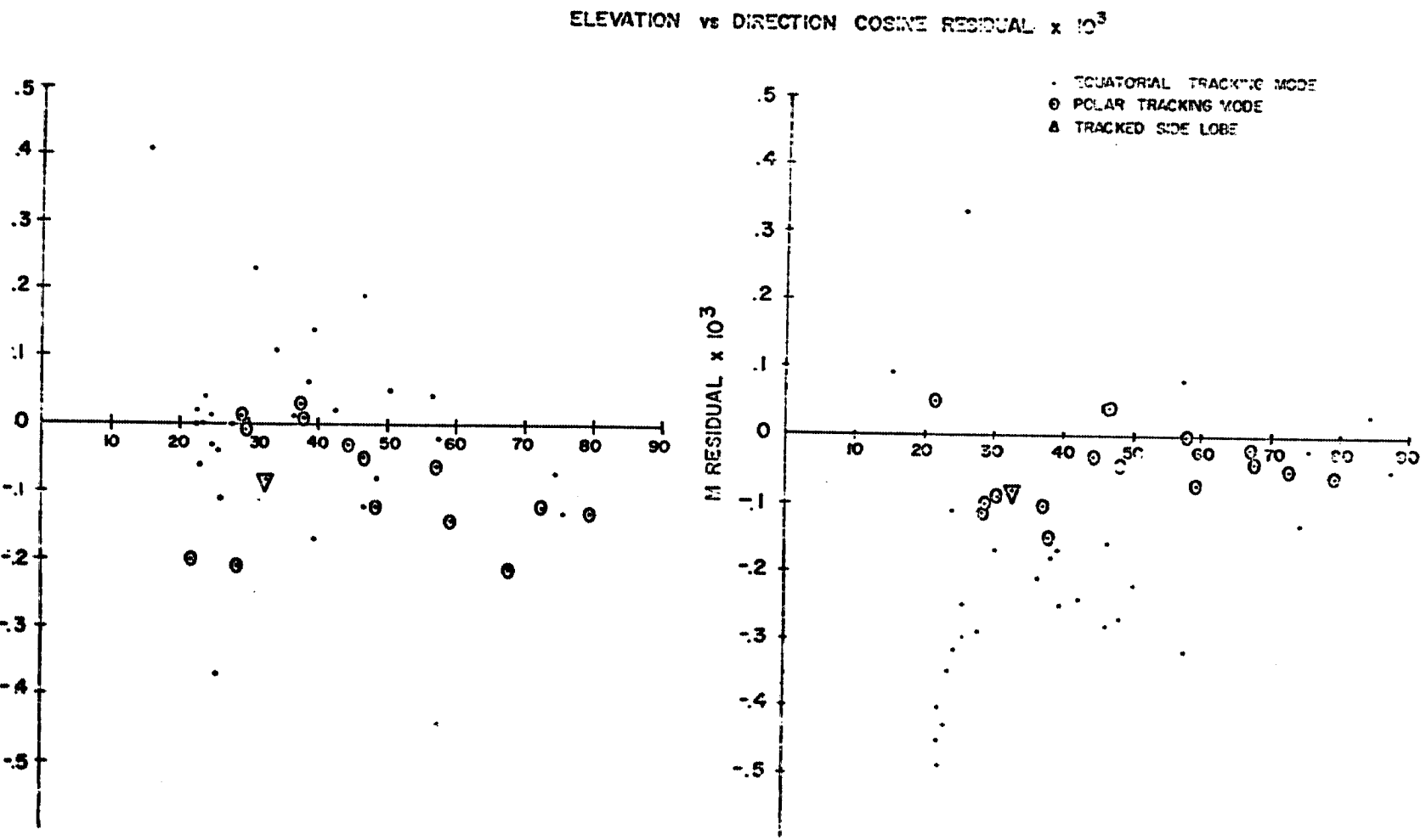

Minitrack Station BPOIN6 (Blossom Point, Md)

46 Observations

HISTOGRAMS of MINITRACK RESIDUALS

BEAM ONLY

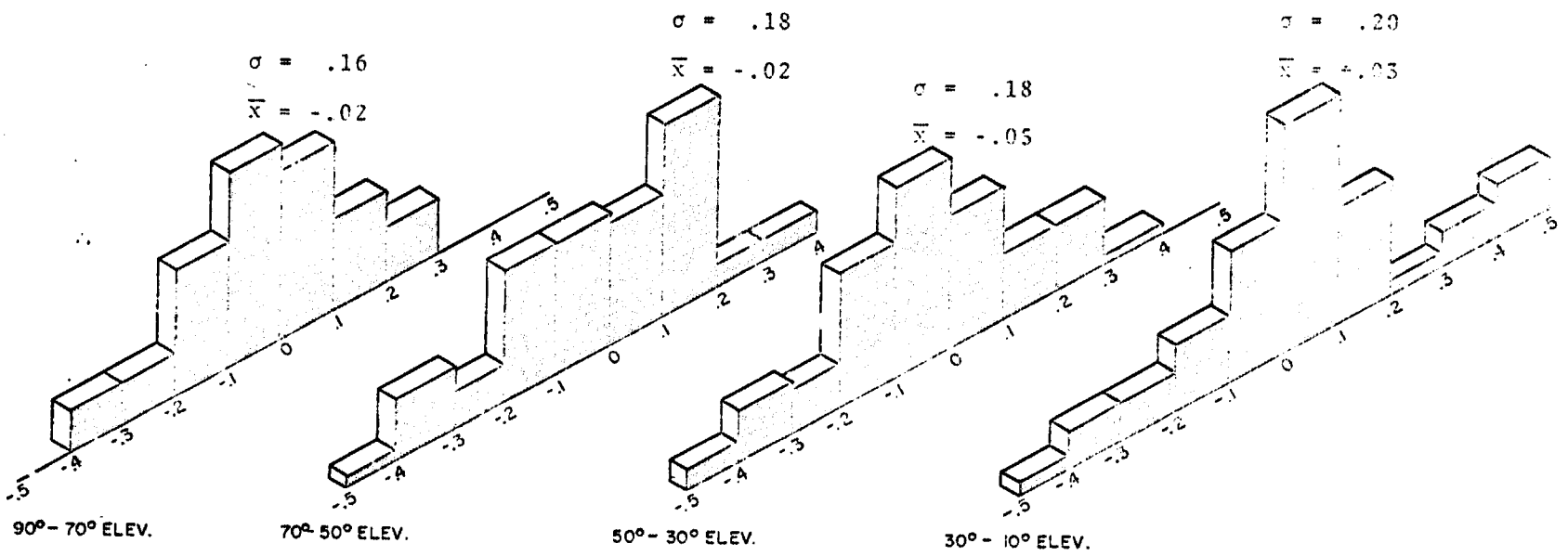

HISTOGRAMS of MINITRACK RESIDUALS

BEAM and REFRACTION

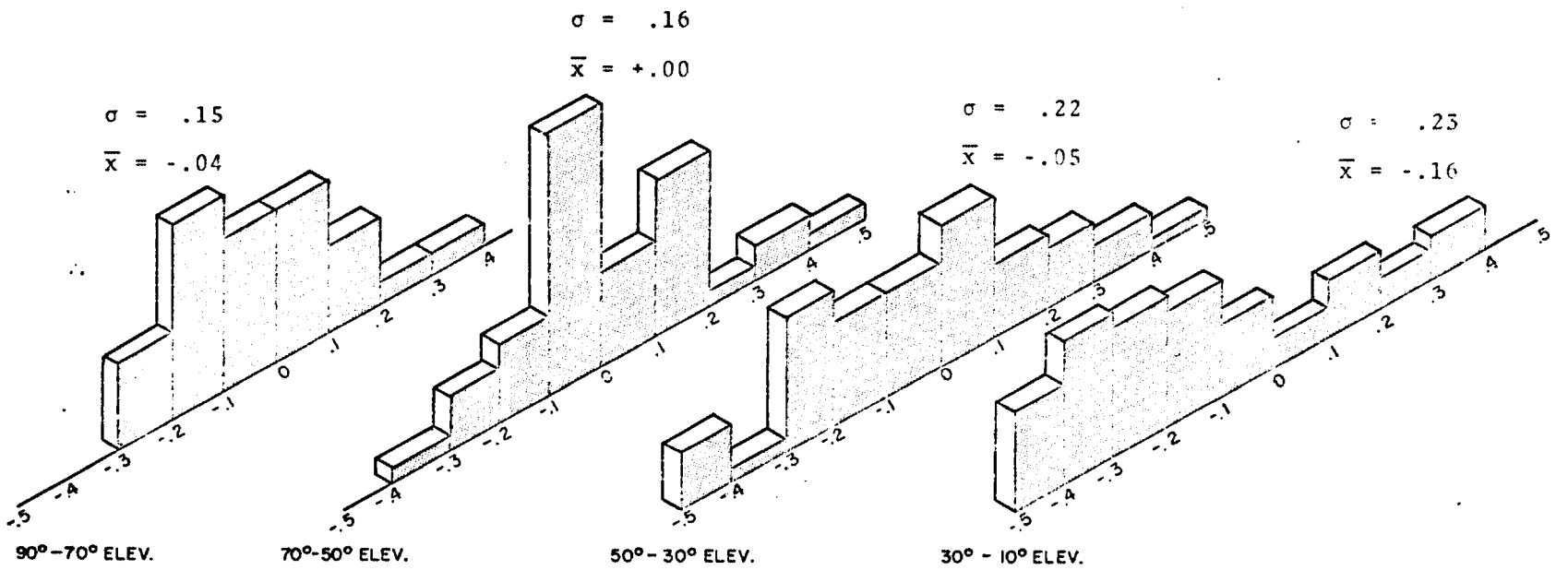

Histogram of Minitrack Residuals from Optically Determined Orbit

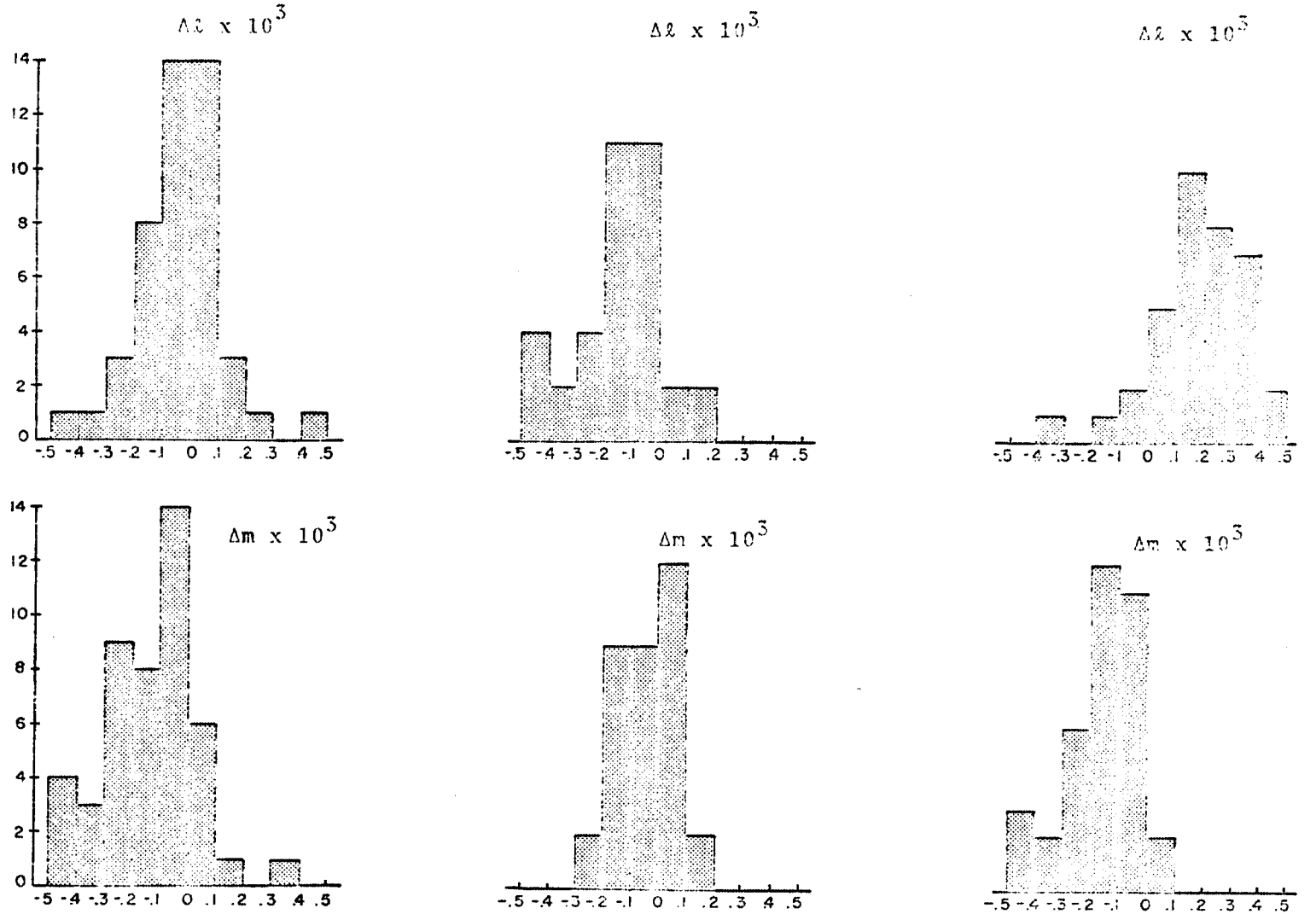

STATION:	BPOIN6	NEWFL6	MOJAV6
NUMBER OF OBSERVATIONS:	46	36	36

Histogram of Minitrack Residuals from
Optically Determined Orbit

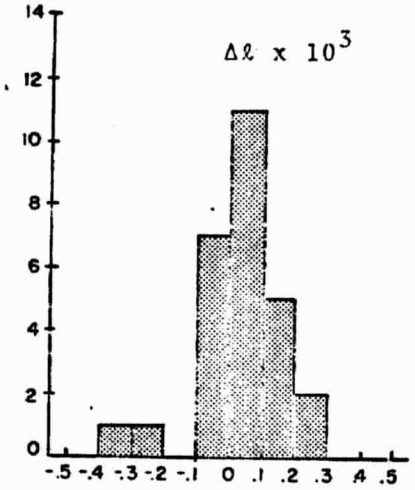

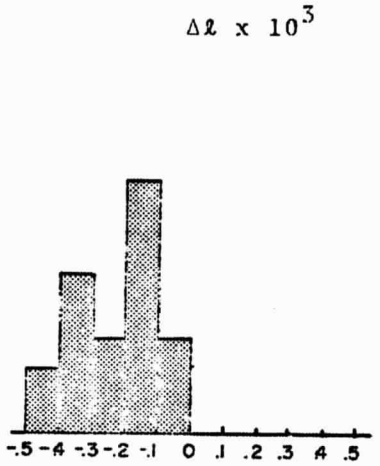

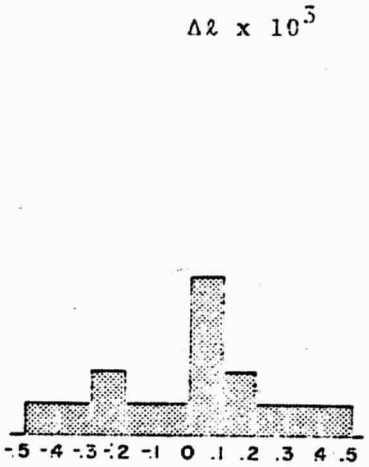

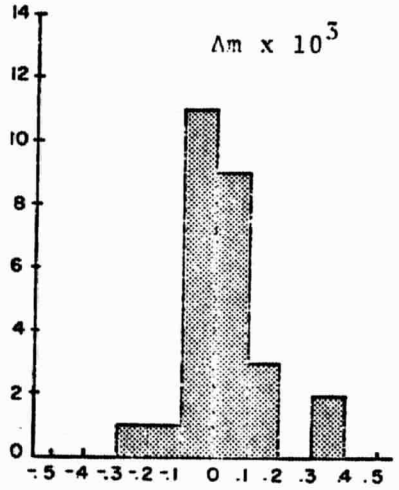

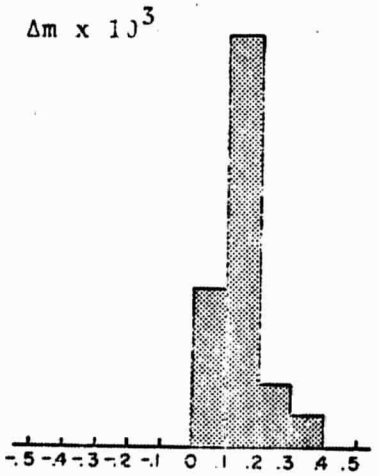

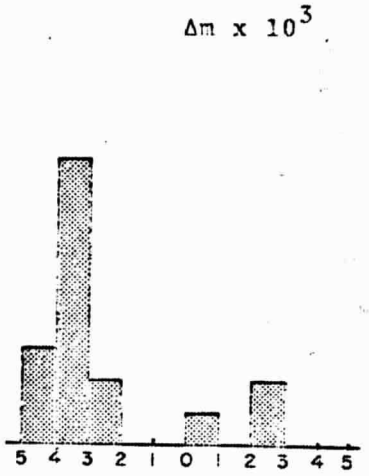

STATION:	GFORK6	COLEG6	FTMYR6
NUMBER OF OBSERVATIONS	27	21	17

Histogram of Minitrack Residuals from
Optically Determined Orbit

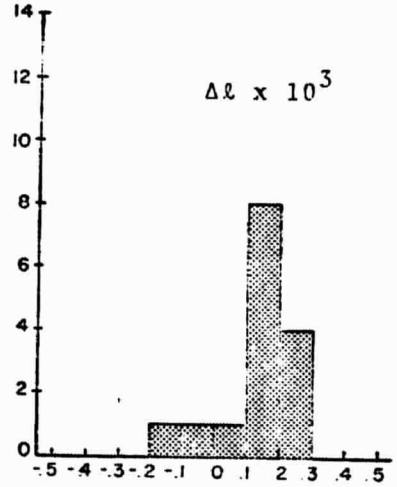

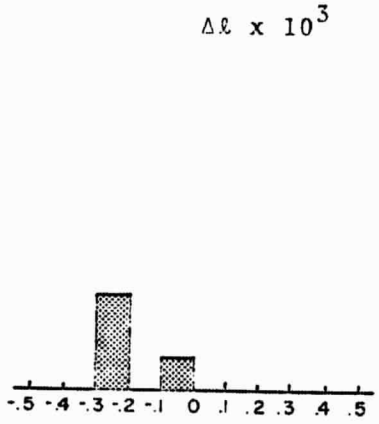

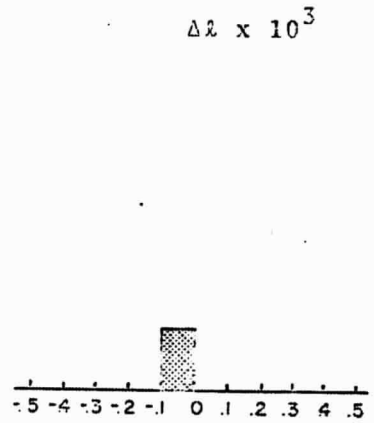

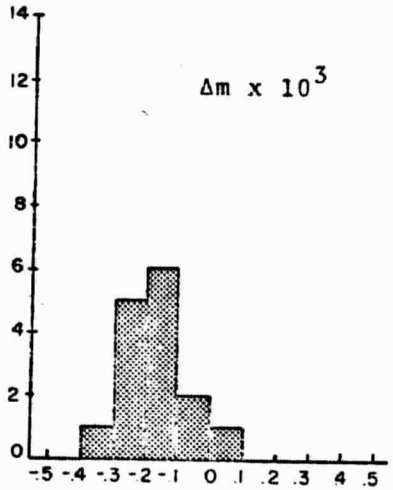

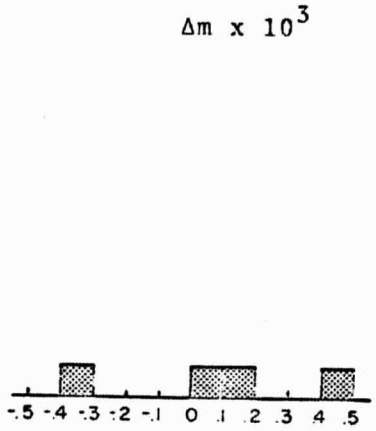

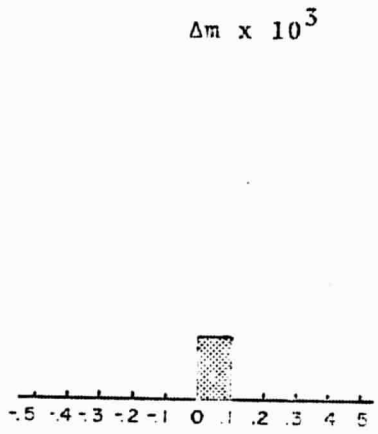

STATION:	WNKFL 6	COMER 6	JOBURG6
NUMBER OF OBSERVATIONS:	15	4	2

Optically Determined Orbit

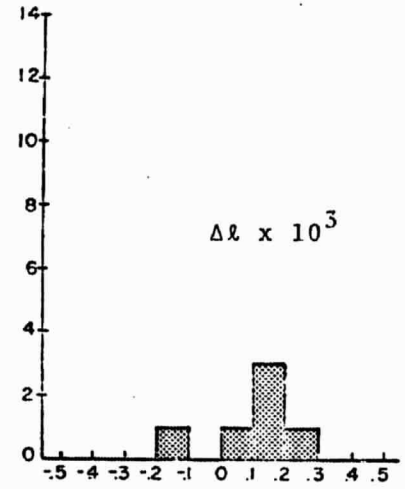

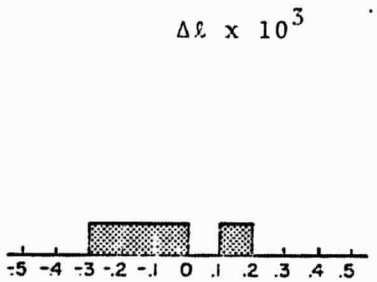

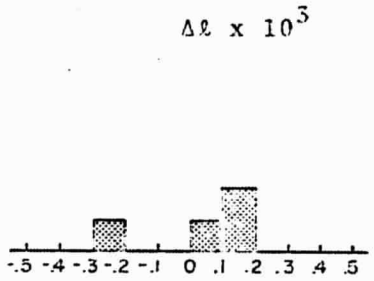

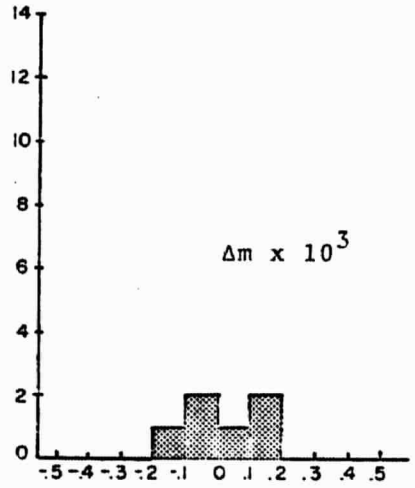

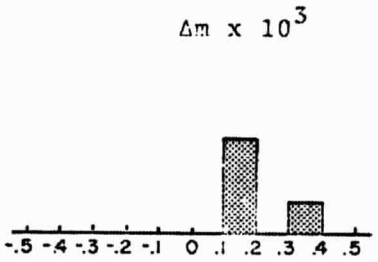

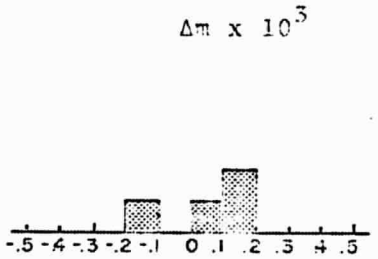

STATION :	LIMAP6	QUITO6	SNTAG6
NUMBER OF OBSERVATIONS :	6	4	4

Differences Between Trajectories Obtained by
Minitrack Data Only & Optical Data Only

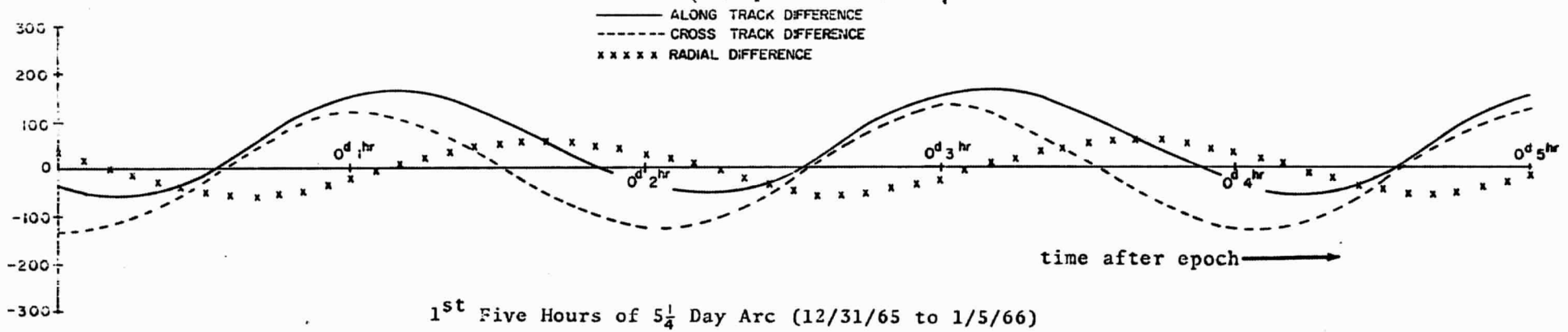

1st Five Hours of $5\frac{1}{4}$ Day Arc (12/31/65 to 1/5/66)

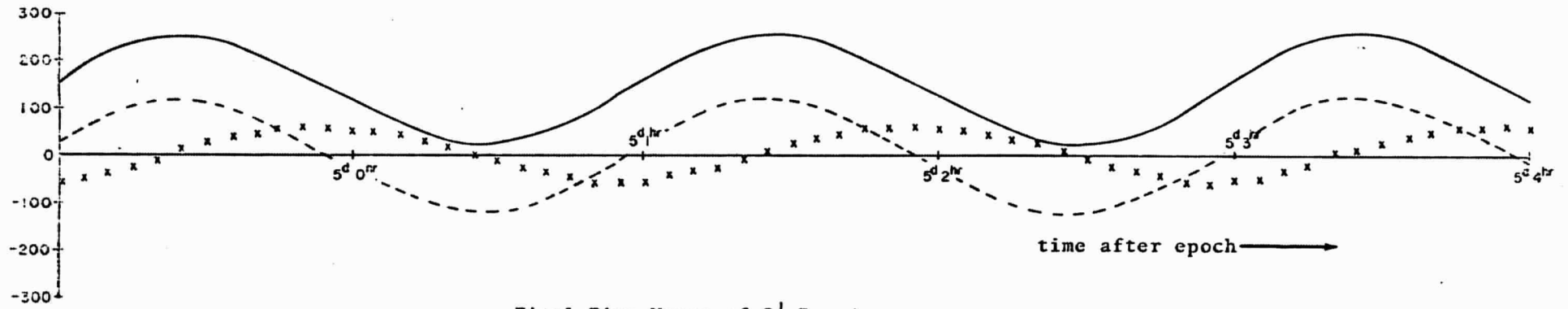

Final Five Hours of $5\frac{1}{4}$ Day Arc

Number of Minitrack Observations in Minitrack Only Solution = 436

Number of Optical Observations in Optical Only Solution = 1059

AN INTERCOMPARISON OF SOME RESULTS FROM GEOS-I DATA BASED UPON SECOR SHORT ARC vs OPTICAL LONG ARC REFERENCE ORBITS

Francis J. Lerch
James G. Marsh
Mission Trajectory Determination Branch
Mission and Trajectory Analysis Division
Tracking and Data Systems Directorate
GODDARD SPACE FLIGHT CENTER

Samuel J. Moss
Brian O'Neill
Wolf Research and Development Corporation
Applied Sciences Department
College Park, Maryland

under
NASA CONTRACT NO. NAS 5-9756

December 1967

GODDARD SPACE FLIGHT CENTER
GREENBELT, MARYLAND

Special Note

Since the results of this paper were first obtained and presented at the GEOS NASA Headquarters Meeting on December 12-14, 1967, the Army Map Service has reported to the authors that the SECOR data analyzed in this report is faulty and not truly representative of the SECOR tracking system. Also all the GEOS-I SECOR data in the Geodetic Satellite Data Service of the National Space Science Data Center is being replaced by data reprocessed by the Army Map Service. It is felt, however, that this paper has the following merit. It demonstrates the wide differences in results that may be obtained between certain short arc and long arc methods for evaluating and intercomparing tracking data when the data contains unexpectedly large systematic errors and biases.

The paper compares SECOR and GRARR data results based upon SECOR short arc vs. optical long arc reference orbits. The evaluation of the SECOR data based upon the optical long arc reference orbits, although valid for these faulty data sets, should not reflect on the capability of the SECOR tracking system. It should be emphasized, however, that certain short arc reference orbits based on optical data have produced results consistent with the optical long arc reference orbits.

In reviewing the paper the Army Map Service indicated that the relative timing errors (when associated with the clock) between the SECOR stations in a given quad pass cannot be as large as 10 milliseconds if the data is preprocessed correctly. The paper points out that these timing errors may arise from other sources.

Statements referring to the evaluation of the SECOR system within the paper should only apply to the evaluation of the specific preprocessed data sets defined in the paper.

SUMMARY

This report presents some of the results of the evaluation of the range measurements from the U. S. Army SECOR Tracking System. The data considered here were taken on the GEOS-I satellite by stations in the Eastern United States, at Herndon, Virginia, Greenville, Mississippi, Homestead, Florida and Ft. Stewart, Georgia, in the period December 31, 1965 to January 5, 1966.

Optical reference orbits were taken as a standard for this evaluation and compared with results obtained using SECOR short arcs as reference. The optical reference orbits utilized GOES-I flash sequence data and some passive observations from five major geodetic optical tracking networks. The networks and camera types consisted of the SAO Baker-Nunn, the GSFC STADAN and SPEOPT MOTS 40" and 24", USAF PC-1000, and the U.S.C. and G.S. BC-4. The SECOR data consisted of fourteen station passes during four "quad" passes over the United States. Simultaneous data from the Goddard range and range rate system (GRARR) was also available during these four passes affording the opportunity to intercompare the evaluation of this instrument based on an optical reference orbit with earlier results obtained using the SECOR data as a standard.[1]

The results presented here were obtained by comparing measured ranges from both the SECOR and GRARR systems with those computed from the optical reference orbit. For each station pass, estimates of the zero-set, timing, and

---

[1] Evaluation of Range Accuracy for the Goddard Range and Range Rate System at Rosman, X-514-66-513 by John Berbert, Robert Reich, and John Stephenson.

random errors were made based on the residual differences between the observed and calculated range. Whereas SECOR zero-set errors ranged from +17 meters to -13 meters as determined from a short arc SECOR reference orbit, these same errors had values ranging from +60 meters to -6 meters referenced to the long arc optical orbit. Significantly, the GRARR A-channel zero-set errors, which ranged from -8 meters to -17 meters using the SECOR orbit were between +2 and -2 meters using the optical orbit. The data used in this evaluation were obtained from Mr. John Berbert, GEOS Principal Investigator, and is identical with that used in reference (1).

SECOR data available in the second week of January were also investigated. Preliminary results indicate that some of these data contained ambiguities of 256 meters and 512 meters and associated timing errors of approximately fifty milliseconds. These data were obtained from the Geodetic Satellite Data Service (GSDS), National Space Science Data Center. This report does not address itself to the evaluation of this data set primarily because the large timing errors are believed to be due to an improper time indicator on the data submitted to GSDS. It is therefore recommended that this data be re-evaluated at the preprocessing level before any further detailed analysis be performed on it.

CONTENTS

1.0 METHOD OF EVALUATION

The range accuracy of the U. S. Army SECOR system was evaluated by comparing the observed measurements with values computed from reference orbits. This report compares the SECOR calibration results obtained using long arc optical reference orbits and those obtained from SECOR short arcs. The data evaluated were in the period December 31, 1965 through January 5, 1966 taken on the GEOS-I satellite.

The SECOR data consisted of fourteen station passes during four satellite passes over the United States. Four SECOR stations were involved in taking these data; they were located at: Herndon, Virginia, Greenville, Mississippi, Homestead, Florida and Ft. Stewart, Georgia. In addition to the simultaneous SECOR and optical data during these four passes, GRARR measurements from Rosman, North Carolina were available. These data previously analyzed by Berbert[1] were evaluated for this document in exactly the same manner as the SECOR measurements. The four passes are summarized in Table I and Figure 1.

SECOR data in the second week in January, 1966 were also investigated. Preliminary results on this data indicate that these data still contained ambiguities of 256 and 512 meters and associated timing errors of approximately fifty milliseconds.

TABLE I

SUMMARY OF GRARR AND SECOR PASSES

PASS NO.	DATE	TIME	MAXIMUM ELEVATION ANGLE				
			HOMEFL	FTWART	GREENV	HERDN	ROSRAN
665	1/1/66	08^h	64.3^o	N/A	80.7^o	32.5^o	51.8^o
676	1/2/66	06^h	27.5^o	38.0^o	28.4^o	68.0^o	43.3^o
677	1/2/66	08^h	48.3^o	40.8^o	69.6^o	25.3^o	40.2^o
700	1/4/66	06^h	N/A	55.4^o	33.7^o	70.2^o	62.7^o

Pass 700 over ROSRAN was from the C channel transponder, the other three passes were from the A channel.

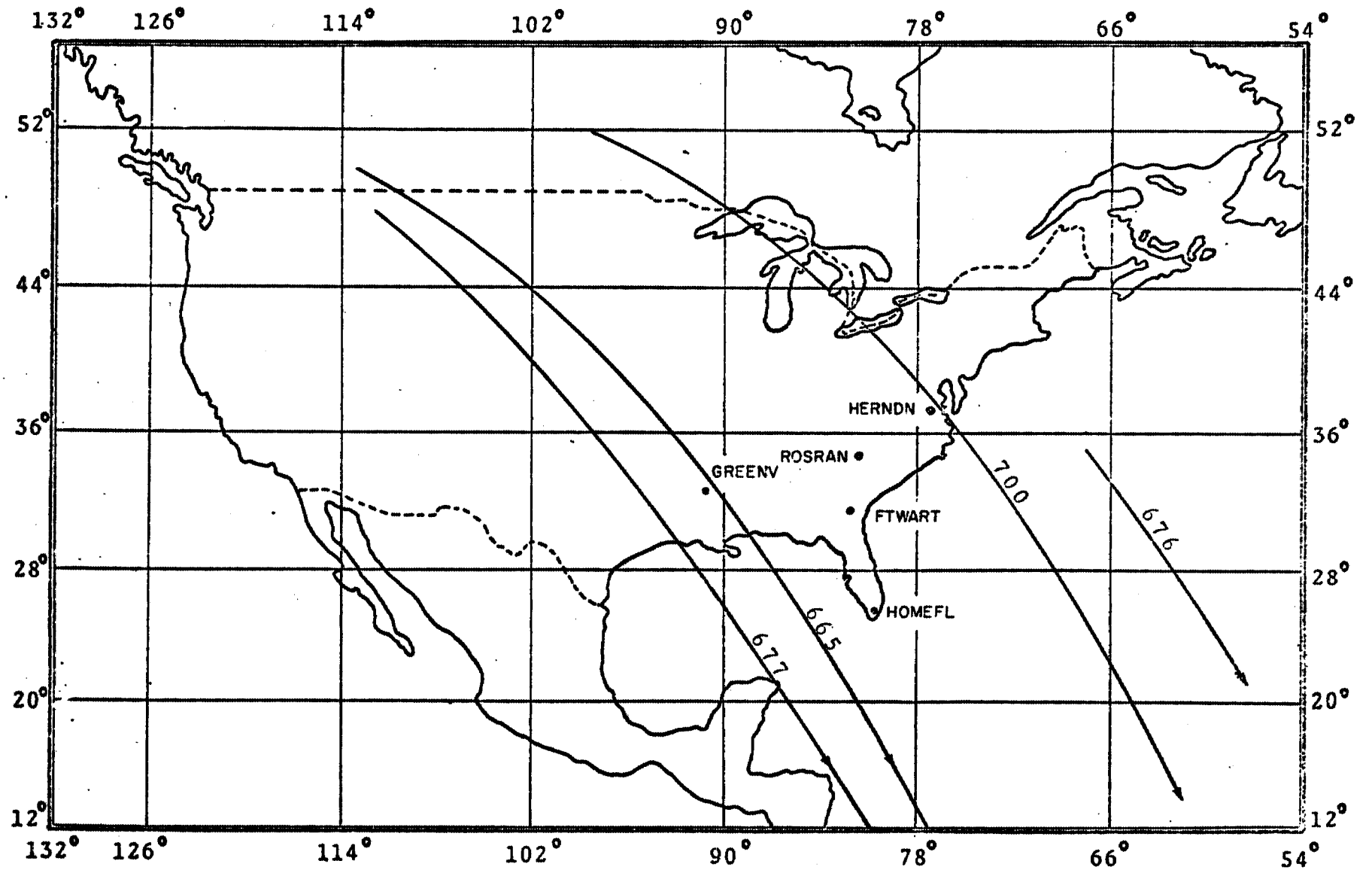

Figure 1

SECOR PASSES

1.1 Intercomparison with Long Arc Orbital Solutions

The reference orbits used for this evaluation were estimated from optical data using the orbit determination program NONAME.[2] The optical data used are flash sequence data and some passive observations made from five major geodetic optical tracking networks. The networks and camera types consisted of the SAO Baker-Nunn, the GSFC STADAN and SPEOPT MOTS 40" and 24", the USAF PC-1000, and the U.S.C. and G.S. BC-4.

The following earth and force models were used in this evaluation:

- SAO C5 Standard Earth [Appendix A-4]
- SAO M1 Gravity Model [Appendix A-3]
- Perturbations due to solar and lunar gravity [Appendix A-3]
- Perturbations due to solar radiation pressure [Appendix A-2]

Six reference orbits were fitted to data sets from the period analyzed, five of the orbits were fitted to long arcs (greater than six revolutions) and the other was fitted to a medium arc (1/4 to 6 revolutions). The orbital solutions were fitted to overlapping data sets in order to assess the effects any errors in the orbital solutions were having

---

[2] "Interim Status Report on Program Development and GEOS-A Data Analysis (NAS 5-9756-44A,55,71)" Wolf Research and Development Corporation

on the evaluation. Summaries of the orbital solutions and root mean squares of fit are given in Tables II and III. A more complete description of the data sets is given in Appendix A-1.

TABLE II

SUMMARY OF ORBITAL SOLUTIONS

Solution No.	Approximate Arc Length	Time of 1st Measurement	Time of Final Measurement
1	5-1/2 days	12/31/65 01 hr.	01/05/66 06 hr.
2	2-1/2 days	01/01/66 01 hr.	01/03/66 08 hr.
3	2-1/2 days	01/03/66 01 hr.	01/05/66 06 hr.
4	2 days	01/02/66 06 hr.	01/04/66 06 hr.
5	1 day	01/02/66 06 hr.	01/03/66 08 hr.
6	2 hrs.	01/02/66 06 hr.	01/02/66 08 hr.

TABLE III

ROOT MEAN SQUARES ABOUT THE ORBITAL SOLUTIONS

Orbital Sol^{n}	No. of Obs.	Rms. of Fit (Secs. of Arc)
1	1057	3.08
2	631	2.58
3	532	2.74
4	644	2.45
5	444	2.33
6	236	2.17

1.2 Intercomparison with Short Arc Orbital Solutions

Several intercomparisons for the evaluation of the SECOR range measurements have been conducted using short arc orbital solutions and intervisible techniques. These are:

(1) Short arc orbital solutions (up to 15 minutes duration) determined from optical observations.[4]

(2) Short arc orbital solutions determined from SECOR and GRARR range measurements.[1]

(3) Comparison of SECOR range measurements with those determined from intervisible optical observations.[4]

The GRARR data used in the above analyses was not subjected to any smoothing.

---

(4) Unpublished
Berbert et al.

2.0 EVALUATION OF THE RANGE MEASUREMENTS

The SECOR and GRARR range measurements were corrected for refraction [Appendix A-2] and the GRARR measurements were in addition corrected for transponder delay and known cable bias at Rosman[3] [Appendix A-2]. The GRARR measurements evaluated in this report have been smoothed over two minute intervals using a sixth order polynomial. For the purposes of this evaluation, no observations taken when the elevation of the satellite from the station was less than 20^{o} have been used.

The following error model was fitted to the range residuals:

$$\Delta R = \Delta B + \Delta t \dot{R}$$

where

ΔR = Observed range minus calculated range,

ΔB = error in the zero-set value of the range

Δt = error in the timing.

This model was fitted to the range residuals from each station for each pass separately using the method of least squares to solve for the unknown parameters ΔB and Δt.

---

(3) "Evaluation of the Goddard Range and Range Rate System at Rosman by Intercomparison with GEOS-I Long Arc Orbital Solutions", NASA Report X-

2.1 Results from the Long Arc Orbital Solutions

The zero-set, timing and random error estimates obtained from the 5 1/2 day reference orbit are summarized in Tables IV-VI, and the range residuals from this orbit are summarized in Figures 2-5. These results indicate that although the random error estimates for the SECOR and GRARR systems are comparable (an average of $\sim 3_m$ for SECOR and GRARR A channel), the SECOR system displays significantly larger and less stable zero-set biases than the GRARR system A channel. Similarly the estimates of the timing errors are uniformly larger for the SECOR system than for the GRARR system.

The estimates obtained from the five overlapping reference orbits are summarized in Tables VII-IX, in general these results agree reasonably well with the estimates obtained from the 5 1/2 day arc. The only estimates that show appreciable variation when estimated from different orbital solutions are some of the extrapolated zero-set error estimates.

TABLE IV

SUMMARY OF ZERO-SET ERROR ESTIMATES (METERS)

PASS NO.	Station				
	HOMEFL	FTWART	GREENV	HERNDN	ROSRAN
665	36.6	N/A	60.1**	43.1	- 2.0
676	20.9	8.3	29.7	- 3.7	2.3
677	17.0	-1.8	33.5	3.5	0.2
700	N/A	9.7**	46.9**	11.3**	20.6*

TABLE V

SUMMARY OF TIMING ERROR ESTIMATES (MILLISECS)

PASS NO.	Station				
	HOMEFL	FTWART	GREENV	HERNDN	ROSRAN
665	0.2	N/A	- 6.4	3.8	1.0
676	- 8.1	-3.2	-12.3	-3.2	-6.3
677	- 2.4	1.6	- 3.6	2.6	-0.2
700	N/A	-2.7	-12.9	-3.2	-5.4*

TABLE VI

SUMMARY OF RANDOM ERROR ESTIMATES (METERS)

PASS NO.	Station				
	HOMEFL	FTWART	GREENV	HERNDN	ROSRAN
665	3.0	N/A	2.0	1.1	4.5
676	1.5	5.1	2.6	3.1	2.9
677	1.6	6.3	2.2	1.0	3.2
700	N/A	2.9	1.2	2.0	5.8*

*This pass is a C channel pass; the other three are from the A channel.

**These are extrapolated estimates since the station did not track until the satellite was moving away from the station.

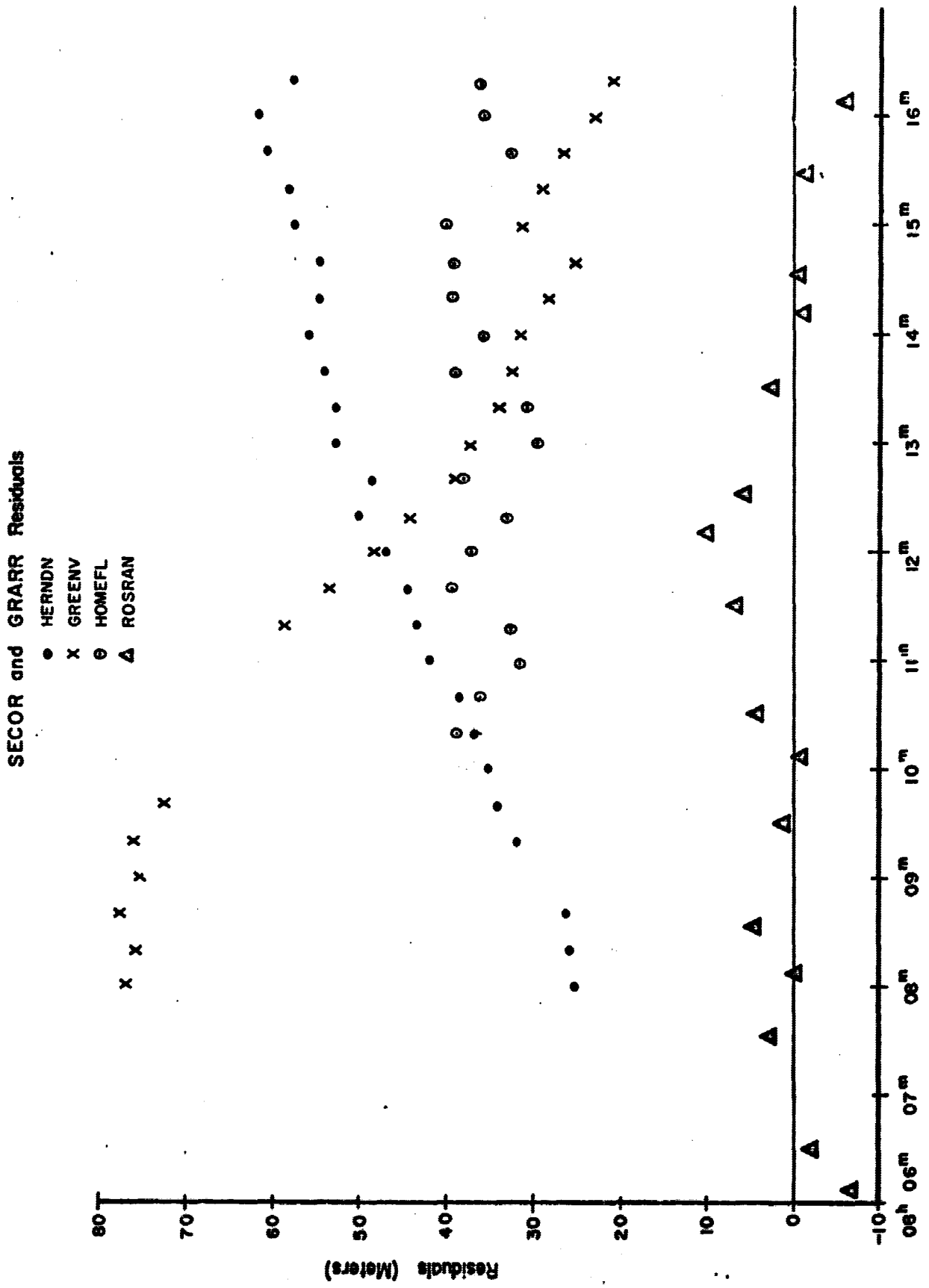
SECOR and GRARR Residuals
HERNDN
GREENV
HOMEFL
ROSRAN
Residuals (Meters)
80
70
60
50
40
30
20
10
0
-10
08h 06m
07m
08m
09m
10m
11m
12m
13m
14m
15m
16m
JAN. 1 08hr

Figure 2

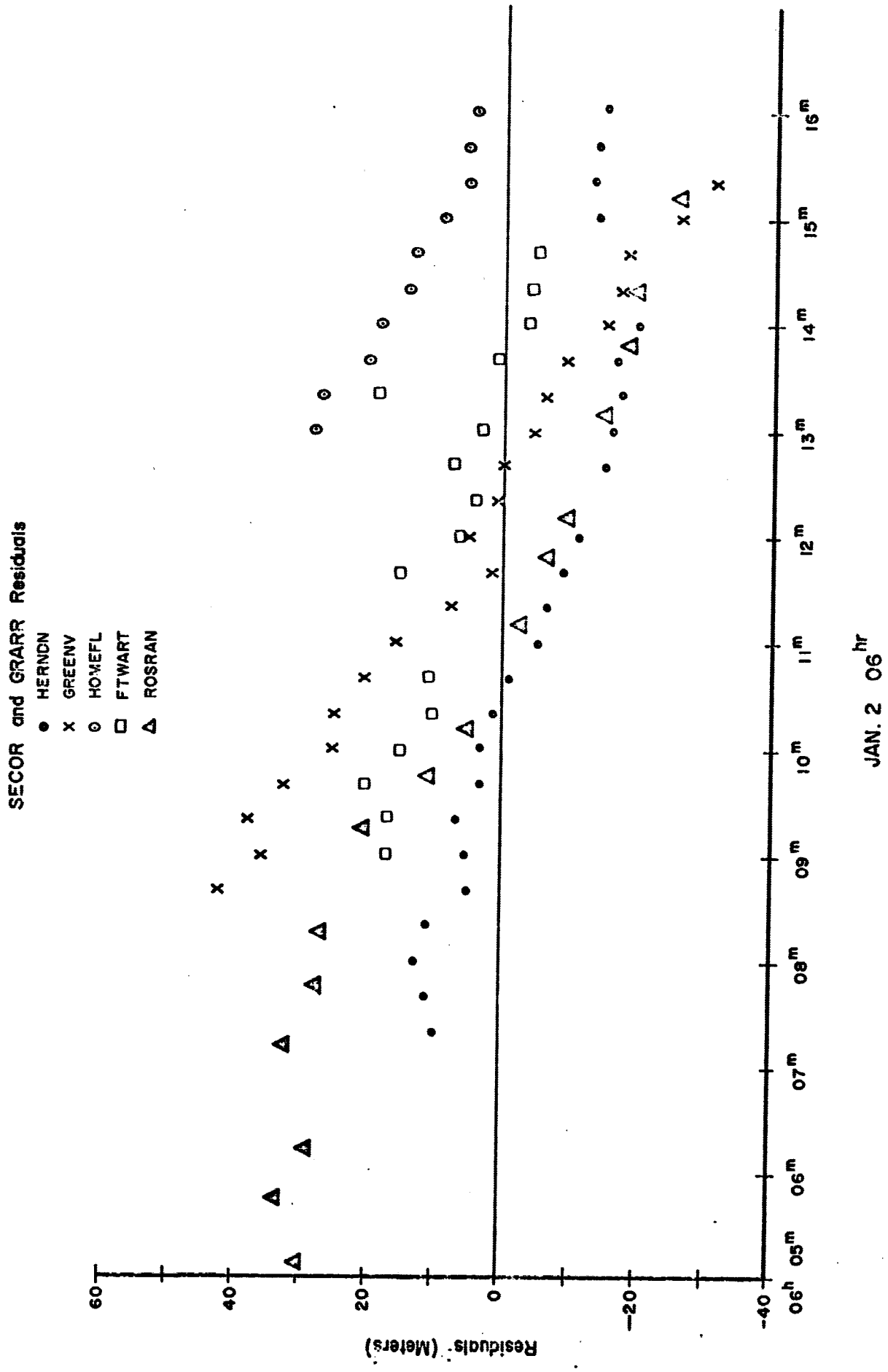
SECOR and GRARR Residuals
HERNDN
GREENV
HOWEFL
FTWART
ROSRAN
Residuals (Meters)
60
40
20
0
-20
-40
06h 05m
06m
07m
08m
09m
10m
11m
12m
13m
14m
15m
16m
JAN. 2 06hr

Figure 3

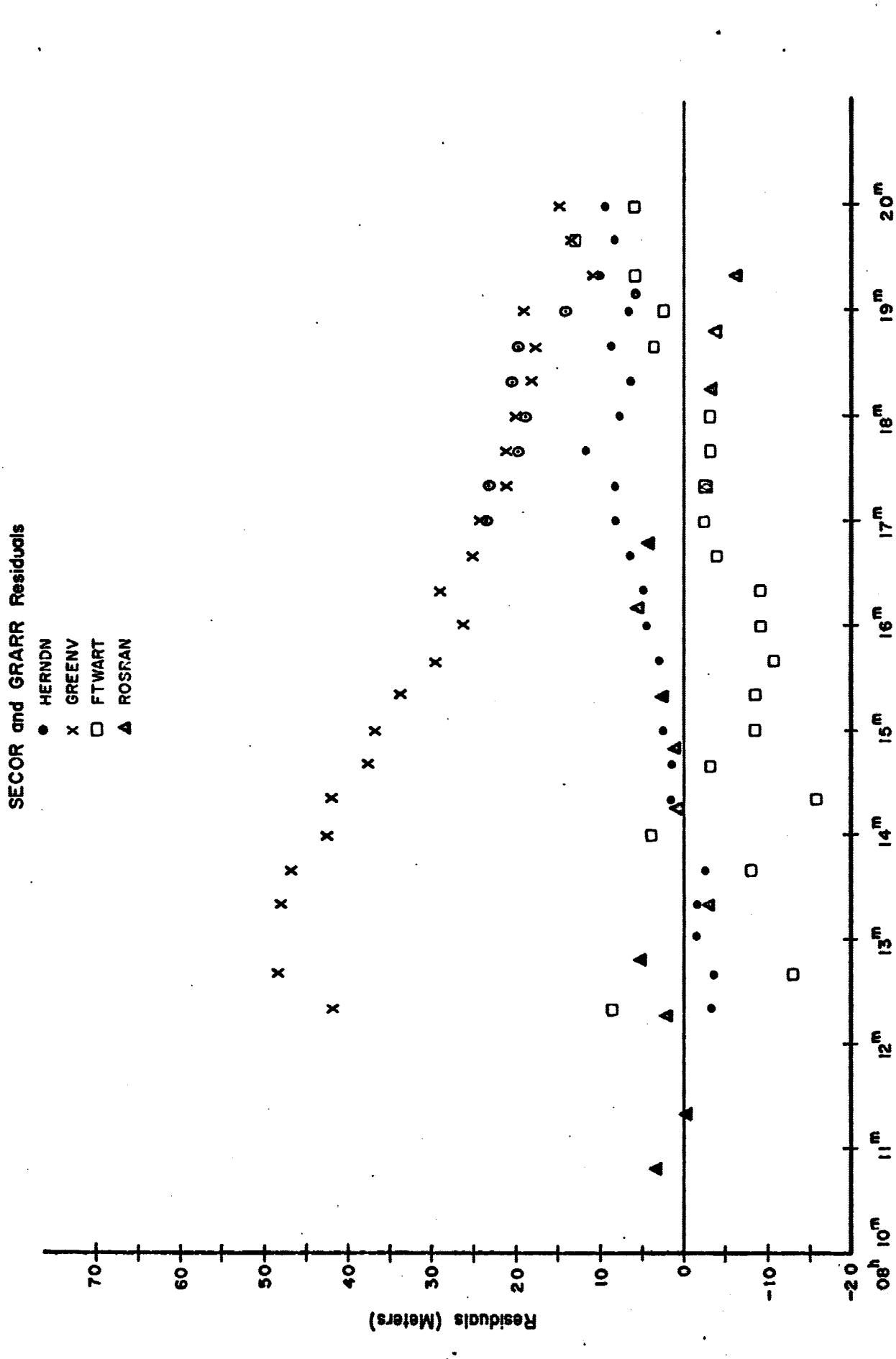
SECOR and GRARR Residuals
HERNDN
GREENV
FTWART
ROSRAN
Residuals (Meters)
70
60
50
40
30
20
10
0
-10
-20
08h 10m
11m
12m
13m
14m
15m
16m
17m
18m
19m
20m
JAN. 2 08hr

Figure 4

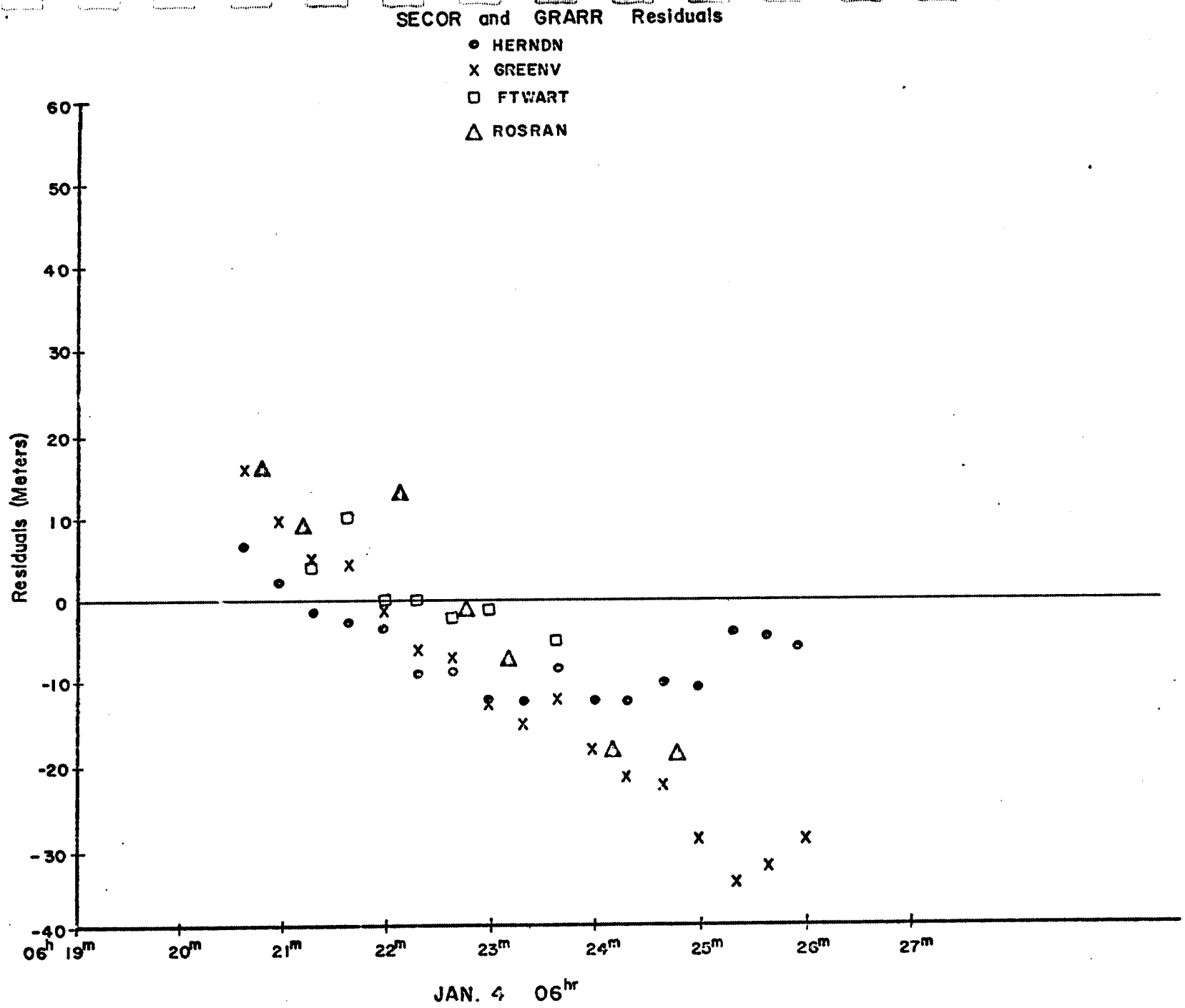
SECOR and GRARR Residuals
HERNDN
GREENV
FTWART
ROSRAN
Residuals (Meters)
60
50
40
30
20
10
0
-10
-20
-30
-40
06h 19m
20m
21m
22m
23m
24m
25m
26m
27m
JAN. 4 06hr

Figure 5

TABLE VII

SUMMARY OF ZERO-SET ERRORS FOR OVERLAPPING ARCS

Station: HOMEFL

PASS NO.	ORBITAL SOLUTION				
	2	3	4	5	6
665	39.1	---	---	---	---
676	25.8	---	21.0	21.0	22.6
677	19.3	---	27.3	27.3	22.5
700	N/A	N/A	N/A	---	---

Station: FTWART

PASS NO.	ORBITAL SOLUTION				
	2	3	4	5	6
665	N/A	---	---	---	---
676	13.3	---	10.0	10.0	11.1
677	- 0.1	---	6.6	6.6	3.1
700	---	2.0	13.8	---	---

TABLE VII

SUMMARY OF ZERO-SET ERRORS FOR OVERLAPPING ARCS

Station: GREENV

PASS NO.	ORBITAL SOLUTION				
	2	3	4	5	6
665	59.0	---	---	---	---
676	35.5	---	32.5	32.5	33.8
677	36.4	---	39.8	39.8	37.3
700	---	36.3	51.4	---	---

Station: HERNDN

PASS NO.	ORBITAL SOLUTION				
	2	3	4	5	6
665	43.0	---	---	---	---
676	0.8	---	- 0.1	- 0.1	- 0.1
677	4.8	---	12.0	12.0	8.6
700	---	7.6	19.8	---	---

TABLE VII

SUMMARY OF ZERO-SET ERRORS FOR OVERLAPPING ARCS

Station: ROSRAN

PASS NO.	ORBITAL SOLUTION				
	2	3	4	5	6
665	- 2.8	---	---	---	---
676	6.6	---	2.7	4.2	5.2
677	1.4	---	6.0	7.4	4.4
700	---	15.8	21.5	---	---

TABLE VIII

SUMMARY OF TIMING ERRORS FOR OVERLAPPING ARCS

Station: HOMEFL

PASS NO.	ORBITAL SOLUTION				
	2	3	4	5	6
665	1.0	---	---	---	---
676	- 8.2	---	- 9.0	- 9.0	- 5.3
677	- 2.3	---	- 2.3	- 2.3	- 4.2
700	---	N/A	N/A	---	---

Station: FTWART

PASS NO.	ORBITAL SOLUTION				
	2	3	4	5	6
665	N/A	---	---	---	---
676	- 2.8	---	- 3.7	- 3.7	- 0.1
677	1.7	---	1.6	1.6	- 0.2
700	---	- 2.3	- 2.1	---	---

TABLE VIII

SUMMARY OF TIMING ERRORS FOR OVERLAPPING ARCS

Station: GREENV

PASS NO.	ORBITAL SOLUTION				
	2	3	4	5	6
665	- 4.7	---	---	---	---
676	-12.1	---	-12.9	-12.9	- 9.5
677	- 3.6	---	- 4.0	- 4.0	- 5.6
700	---	-12.0	-12.6	---	---

Station: HERNDN

PASS NO.	ORBITAL SOLUTION				
	2	3	4	5	6
665	5.4	---	---	---	---
676	- 2.8	---	- 3.4	- 3.4	0.0
677	2.8	---	3.0	3.0	1.0
700	---	- 2.9	- 3.0	---	---

TABLE VIII

SUMMARY OF TIMING ERRORS FOR OVERLAPPING ARCS

Station: ROSRAN

PASS NO.	ORBITAL SOLUTION				
	2	3	4	5	6
665	0.9	---	---	---	
676	- 6.1	---	- 6.4	- 6.9	- 3.5
677	- 0.4	---	- 0.1	- 0.3	- 2.3
700	---	- 4.8	- 6.5	---	

TABLE IX

SUMMARY OF RANDOM ERRORS FOR OVERLAPPING ARCS

Station: HOMEFL

PASS NO.	ORBITAL SOLUTION				
	2	3	4	5	6
665	3.1	---	---	---	---
676	1.4	---	1.5	1.5	1.5
677	1.6	---	1.7	1.7	1.6
700	---	N/A	N/A	---	---

Station: FTWART

PASS NO.	ORBITAL SOLUTION				
	2	3	4	5	6
665	N/A	---	---	---	---
676	5.3	---	5.2	5.2	5.2
677	6.0	---	5.6	5.6	5.9
700	---	2.8	2.8	---	---

TABLE IX

SUMMARY OF RANDOM ERRORS FOR OVERLAPPING ARCS

Station: GREENV

PASS NO.	ORBITAL SOLUTION				
	2	3	4	5	6
665	3.2	---	---	---	---
676	2.6	---	2.6	2.6	2.6
677	2.5	---	2.9	2.9	2.5
700	---	1.1	1.2	---	---

Station: HERNDN

PASS NO.	ORBITAL SOLUTION				
	2	3	4	5	6
665	1.8	---	---	---	---
676	2.5	---	2.5	2.5	2.7
677	0.9	---	0.8	0.8	0.9
700	---	2.2	1.8	---	---

TABLE IX

SUMMARY OF RANDOM ERRORS FOR OVERLAPPING ARCS

Station: ROSRAN

PASS NO.	ORBITAL SOLUTION				
	2	3	4	5	6
665	5.2	---	---	---	---
676	3.0	---	2.9	3.0	2.9
677	3.5	---	3.8	4.0	3.5
700	---	4.7	6.4	---	---

2.2 Results from Short Arc Orbital Solutions

A number of short arc and geometric intercomparisons using optical data as a reference were performed by Berbert et al.[4] These results are generally in agreement with the long arc optical evaluation of the SECOR system.

The zero-set, timing and random error estimates obtained using short arc orbital solutions determined from SECOR and GRARR range measurements are summarized in Tables X-XII. These are found to be in gross disagreement with those obtained in the present analysis. This disagreement is in part due to the lack of synchronization between the SECOR stations and any universal time system. In addition, the magnitude of the SECOR biases found using optical reference data would preclude the use of these range measurements to determine the reference orbits.

Table X

Summary of Zero-Set Error Estimates (meters)

Pass No.	Station				
	HOMEFL	FTWART	GREENV	HERNDN	ROSRAN
665	-4.	N/A	17	-13	-17
676	8.	-11	-2	9	-8
677	5	-5	10	-3	-13
700	N/A	2	-3	2	-4*

Table XI

Summary of Random Error Estimates (meters)

Pass No.	Station				
	HOMEFL	FTWART	GREENV	HERNDN	ROSRAN
665	3.2	N/A	3.5	2.1	11.3
676	1.7	2.7	3.4	1.8	11.9
677	2.4	1.9	2.7	2.3	10.9
700	N/A	1.7	4.6	2.4	14.1*

Table XII

Summary of Timing Differences for Rosman Relative to SECOR Master Station at Herndon

Pass No.	Timing Differences (milliseconds)
665	+0.4
676	+1.0
677	-1.6
700	+0.9

3.0 CONCLUSIONS

There are significant discrepancies between the results obtained from the long arc optical reference orbits and those from the short arc SECOR reference orbits. Whereas the SECOR zero-set errors ranged from +17 to -13 meters as determined from a SECOR reference orbit, these same errors had values ranging from +60 to -6 meters when referenced to an optical orbit. Significantly, the GRARR A channel zero-set errors which ranged from -8 to -17 meters when evaluated with a SECOR orbit were between +2 and -2 meters in the optical solution.

The results of the present analysis indicate that the SECOR system has the larger zero-set and timing errors, and these remain of some concern. It is possible that some of this error may be due to other sources such as survey. It should be noted that, at the time these data were obtained, the SECOR data was being referenced to a station clock which was not carefully synchronized to WWV, since this was not necessary for the normal SECOR operation. In any case, further investigation including expanded error models and other data sets are likely to be necessary in order to identify the sources of these errors.

4.0 REFERENCES

1. "Evaluation of Range Accuracy for the Goddard Range and Range Rate System at Rosman"
   NASA Report X-514-66-513 John Berbert, Robert Reich, and John Stevenson.

2. "Interim Status Report on Program Development and GEOS-A Data Analysis (NAS 5-9756-44A,55,71)"
   Wolf Research and Development Corporation.

3. "Evaluation of the Goddard Range and Range Rate System at Rosman by Intercomparison with GEOS-I Long Arc Orbital Solutions"
   NASA Report X- F. J. Lerch, J. G. Marsh, and B. O'Neill.

4. Berbert, et al.

APPENDIX A-1

Summary of Data Sets and Orbital Solutions

1.1 OPTICAL DATA

The optically determined reference orbits that are used as standards in this report were determined from right ascension and declination measurements taken with STADAN and SPEOPT MOTS 40" and 24" cameras, SAO Baker-Nunn and Geodetic 36" cameras, USAF PC-1000 cameras and United States Coast and Geodetic Survey BC-4 cameras. The locations of some of these cameras are shown in Figures 1 and 2. These figures serve to illustrate that the majority of the observations were taken in North America.

Observations from two periods in January 1966 were used. The two periods were:

1. December 31, 1965 to January 5, 1966
2. January 11 to January 17, 1966

The complete data sets that were used from each period are summarized in Tables I and II, and Figures 3 and 4. Tables I and II summarize the observations by tracking station, and Figures 3 and 4 indicate the data coverage by time.

Six overlapping orbits were estimated using subsets of data from Period 1, and four overlapping orbits were estimated using the data from Period 2. These orbital solutions are summarized in Tables III - V and Figures 5 and 6. The lengths of the arcs in these solutions range from two hours to approximately 5-1/2 days in length, and root mean squares about the orbital solutions are given in Table VI.

Figure 1

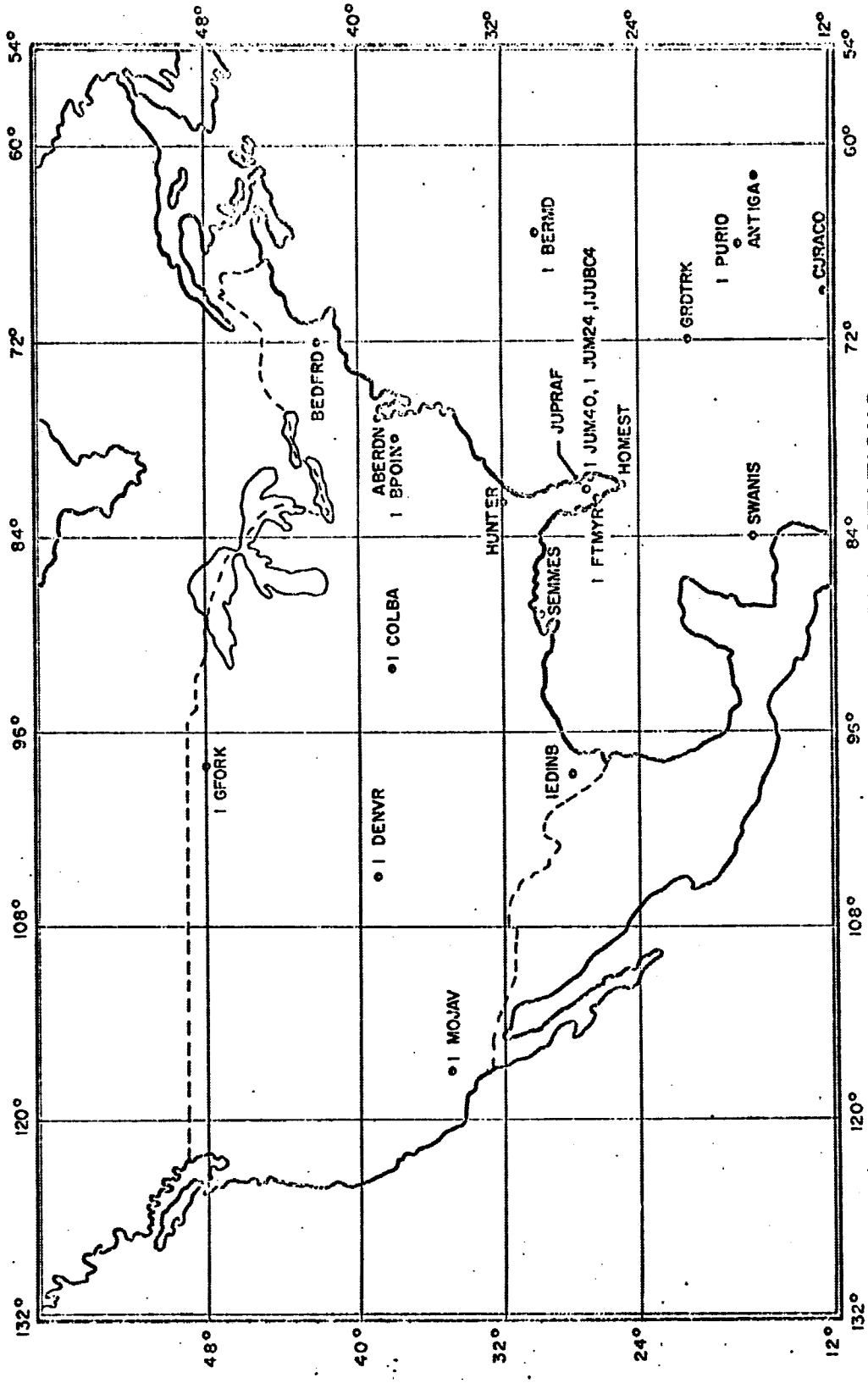
STADAN, SPEOPT AND USAF CAMERA STATIONS
BEDFRD
ABERDN
BPOIN
COLBA
DENVR
GFORK
MOJAV
HUNTR
SEMMES
IEDINB
FTMYR
JUPRAF
JUM40, JUM24, JJUBC4
HOMEST
BERMD
GRDTRK
PURIO
ANTIGA
CURACO
SWANIS
54°
60°
72°
84°
96°
108°
120°
132°
48°
40°
32°
24°
12°

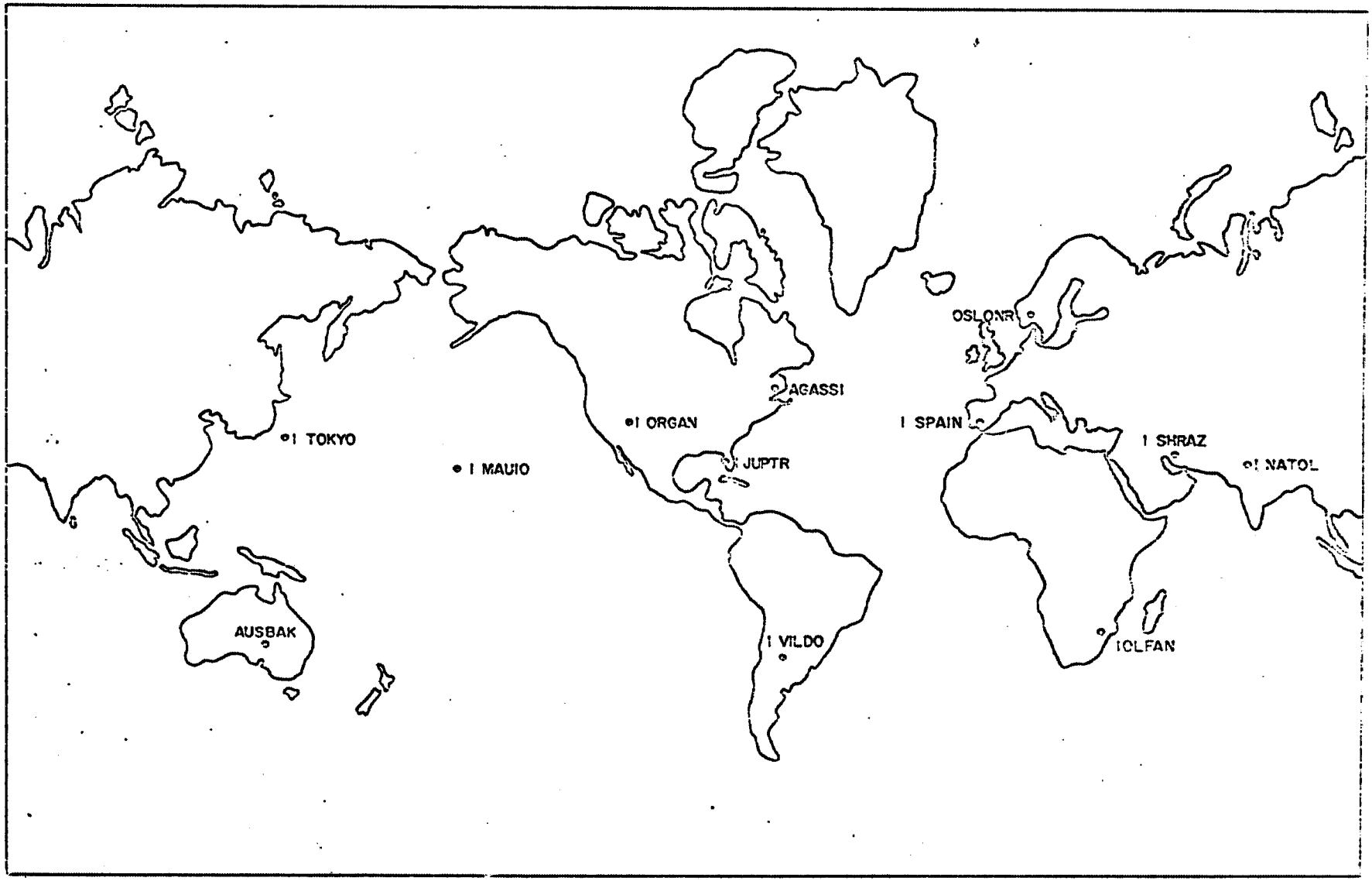

SAO BAKER-NUNN STATIONS

Figure 2

TABLE I

SUMMARY OF OPTICAL MEASUREMENTS BY STATION

FOR PERIOD 1

NETWORK	STATION	CAMERA TYPE	NO. OF OBSERVATIONS
SAO	1ORGAN	BAKER-NUNN	2
	1JUPTR	BAKER-NUNN	26
	1NATOL	BAKER-NUNN	8
	OSLONR	BAKER-NUNN	4
	AUSBAK	BAKER-NUNN	4
	1SHRAZ	BAKER-NUNN	2
	1SPAIN	BAKER-NUNN	6
	1TOKYO	BAKER-NUNN	12
	1VILDO	BAKER-NUNN	2
	1MAUIO	BAKER-NUNN	2
	AGASSI	Geodetic 36"	10
	TOTAL:		78
SPEOPT	1COLBA	MOTS 40"	164
	1JUM40	MOTS 40"	22
	1BERMD	MOTS 40"	84
	1PURIO	MOTS 40"	14
	1DENVR	MOTS 40"	70
	1JUM24	MOTS 24"	26
	TOTAL:		380
STADAN	1FTMYR	MOTS 40"	82
	1BPOIN	MOTS 40"	53
	1GFORK	MOTS 40"	26
	1MOJAV	MOTS 40"	25
	TOTAL:		186
USAF	HUNTER	PC-1000	59
	SWANIS	PC-1000	14
	GRDTRK	PC-1000	7
	ANTIGA	PC-1000	26
	SEMMES	PC-1000	60
	CURACO	PC-1000	40
	HOMEST	PC-1000	94
	JUPRAF	PC-1000	17
	BEDFRD	PC-1000	22
	ABERDN	PC-1000	74
	TOTAL:		413

TOTAL OF ALL OBSERVATIONS = 1057

TABLE II

SUMMARY OF OPTICAL MEASUREMENTS BY STATION FOR PERIOD 2

NETWORK	STATION	CAMERA TYPE	NO. OF OBSERVATIONS
SAO	1OLFAN	BAKER-NUNN	6
	1TOKYO	BAKER-NUNN	4
	1JUPTR	BAKER-NUNN	84
	1VILDO	BAKER-NUNN	8
	AUSBAK	BAKER-NUNN	8
	AGASSI	Geodetic 36"	63
	OSLONR	BAKER-NUNN	1
	TOTAL		174
SPEOPT	1EDINB	MOTS 40	109
	1COLBA	MOTS 40	92
	1BERMD	MOTS 40	10
	1PURIO	MOTS 40	34
	1GSFCP	MOTS 40	40
	1DENVR	MOTS 40	82
	1JUM24	MOTS F24	62
	1JUM40	MOTS F40	70
	1JUBC4	BC4	65
	TOTAL		654
STADAN	1BPOIN	MOTS 40	41
	1FTMYR	MOTS 40	168
	1MOJAV	MOTS 40	87
	1COLEG	MOTS 40	30
	1GFORK	MOTS 40	74
	1ROSMA	MOTS 40	34
	TOTAL		434
USAF	ANTIGA	PC-1000	52
	BEDFRD	PC-1000	85
	SEMMES	PC-1000	60
	GRDTRK	PC-1000	74
	CURACO	PC-1000	21
	TRNDAD	PC-1000	21
	HUNTER	PC-1000	12
	JUPRAF	PC-1000	73
	ABERDN	PC-1000	74
	HOMEST	PC-1000	108
	TOTAL		580
US C&GS	TIMINS	BC4	14

TOTAL OF ALL OBSERVATIONS = 1856

Figure 3

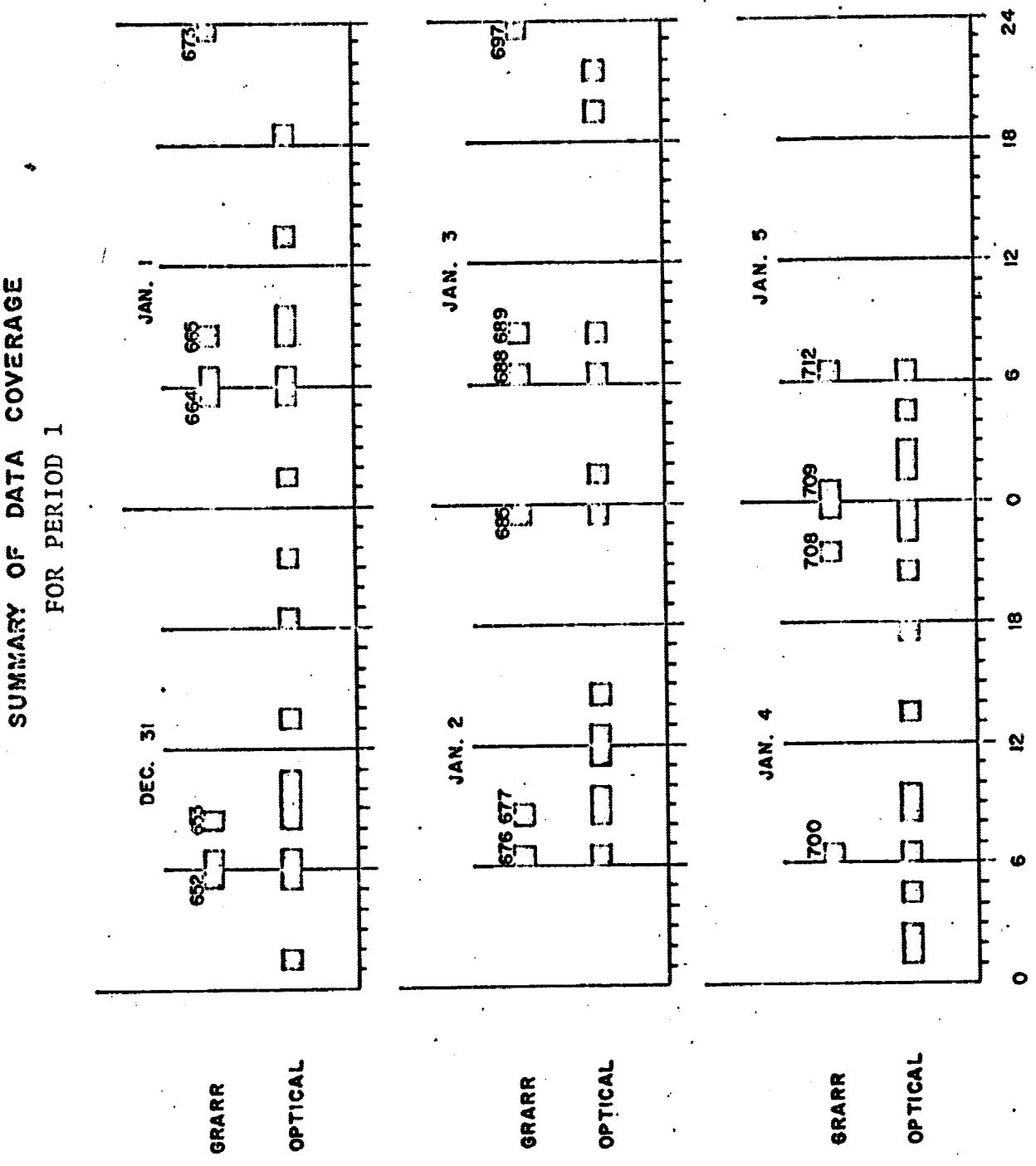
SUMMARY OF DATA COVERAGE
FOR PERIOD 1
DEC. 31
JAN. 1
JAN. 2
JAN. 3
JAN. 4
JAN. 5
652
653
664
665
673
676
677
685
688
689
697
700
708
709
712
0
6
12
18
24
HOURS G.M.T.
GRARR
OPTICAL
GRARR
OPTICAL
GRARR
OPTICAL

TABLE III

Summary of Orbital Solutions

Period 1

Solution No.	Approximate Arc Length	Time of 1st Measurement	Time of final Measurement
1	5-1/2 days	12/31/65 01 hr	01/05/66 06 hr
2	2-1/2 days	01/01/66 01 hr	01/03/66 08 hr
3	2-1/2 days	01/03/66 01 hr	01/05/66 06 hr
4	2 days	01/02/66 01 hr	01/04/66 06 hr
5	1 day	01/02/66 06 hr	01/03/66 08 hr
6	2 hrs	01/02/66 06 hr	01/02/66 08 hr

Period 2

1	4 days	01/11/66 01 hr	01/15/66 05 hr
2	3 days	01/12/66 03 hr	01/15/66 05 hr
3	2 days	01/13/66 05 hr	01/15/66 05 hr
4	2 days	01/15/66 04 hr	01/17/66 05 hr

TABLE IV

Subsets of Optical Measurements used in Orbital Solutions from Period 1

		No. of Observations				
Network	Station	Arc 2	Arc 3	Arc 4	Arc 5	Arc 6
SAO	1ORGAN		2			
	1JUPTR	26		26	26	26
	1NATOL	4	2	2	2	
	OSLONR		4			
	AUSBAK	2				
	1SHRAZ	2		2	2	
	1SPAIN		4	4		
	1TOKYO	6	2	4	4	
	1VILDO		2			
	AGASSI		10			
	TOTAL	40	26	38	34	26
SPEOPT	1COLBA	71	164	136	71	
	1JUM40	16		16	16	16
	1BERMD	64	40	50	36	10
	1PURIO		14			
	1DENVR	42	14	28	14	14
	1JUM24	21		21	21	21
	TOTAL	212	232	251	158	61
STADAN	1FTMYR	82	42	54	54	12
	1BPOIN		46	26		
	1GFORK	26	9	9	9	
	1MOJAV	25		25	25	25
	TOTAL	133	97	113	91	37
USAF	HUNTER	59	14	47	47	23
	SWANIS	14	14	14	14	
	GRDTRK		7	7		
	ANTIGA	12	14	14		
	SEMMES	50		36	36	36
	CURACO	26	28	40	26	12
	HOMEST	66	28	38	24	24
	JUPRAF	17		17	17	17
	BEDFRD		22	14		
	ABERDN		50	14		
	TOTAL	244	177	241	164	112
GRAND TOTAL		631	532	644	444	236

TABLE V

Subsets of Optical Measurements Used in Orbital Solution from Period 2

Network	Station	No. of Observations			
		Arc 1	Arc 2	Arc 3	Arc 4
SAO	1OLFAN	6	4		
	1TOKYO	4	2	2	
	1JUPTR				84
	1VILDO	8	6	6	2
	AUSBAK	6	4	4	2
	AGASSI	63	46	12	12
	OSLONR				1
	TOTAL	87	62	24	101
SPEOPT	1EDINB	72	48	20	65
	1COLBA	92	92	92	38
	1BERMD				10
	1PURIO	20	14	14	14
	1GSFCP	40	40	26	
	1DENVR	56	56	56	26
	1JUM24	22	22	22	54
	1JUM40	28	28	28	56
	1JUBC4	38	38	38	41
	TOTAL	368	338	296	304
STADAN	1BPOIN	37	37	18	8
	1FTMYR	103	103	75	78
	1MOJAV	52	52	52	42
	1COLEG	17	17	17	13
	1GFORK	40	14	14	34
	1ROSMA	22			12
	TOTAL	271	223	176	187
USAF	ANTIGA	38	83	24	24
	BEDFRD	58	58	26	27
	SEMMES	50	26		10
	GRDTRK	46	34	34	38
	CURACO	21	21	21	10
	TRNDAD	11	11		10
	HUNTER	12			
	JUPRAF	38	38	38	53
	ABERDN	68	42	14	20
	HOMEST	51	51	51	69
	TOTAL	393	319	208	261
USC&GS	TIMINS	14	14		
GRAND TOTAL		1133	956	704	853

TABLE VI

Root Mean Squares about the Orbital Solutions

Period 1

Orbital Sol^{n}	No. of Obs.	Rms of fit (secs. of arc)
1	1057	3.08
2	631	2.58
3	532	2.74
4	644	2.45
5	444	2.33
6	236	2.17

Period 2

1	1133	3.16
2	956	2.94
3	704	2.80
4	853	2.80

Figure 5

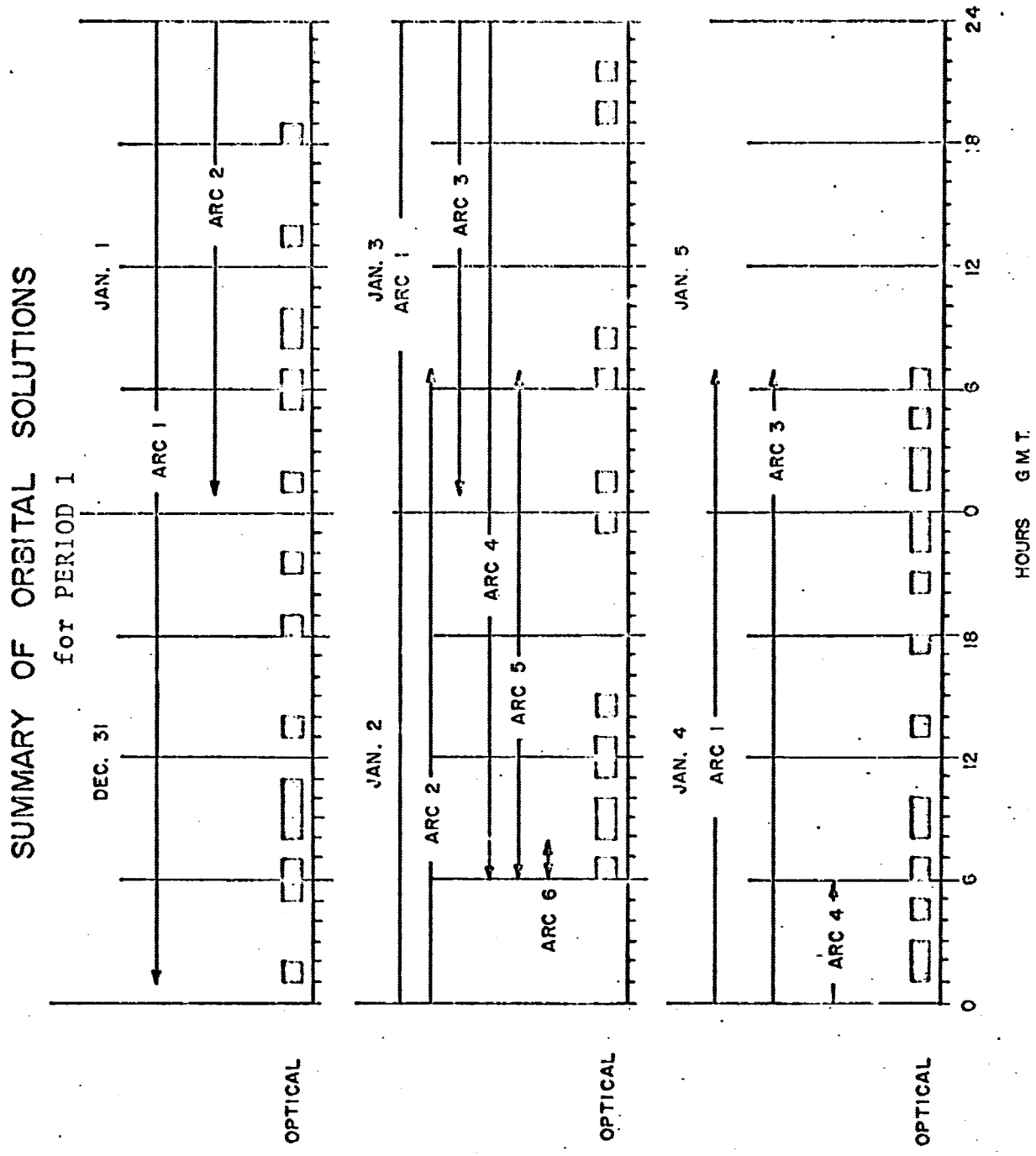
SUMMARY OF ORBITAL SOLUTIONS
for PERIOD 1
DEC. 31
JAN. 1
ARC 1
ARC 2
OPTICAL
JAN. 2
ARC 2
ARC 4
ARC 5
ARC 6
JAN. 3
ARC 1
ARC 3
OPTICAL
JAN. 4
ARC 1
ARC 4
JAN. 5
ARC 3
OPTICAL
0
6
12
18
24
HOURS G M T.

SUMMARY OF ORBITAL SOLUTIONS
for PERIOD 2

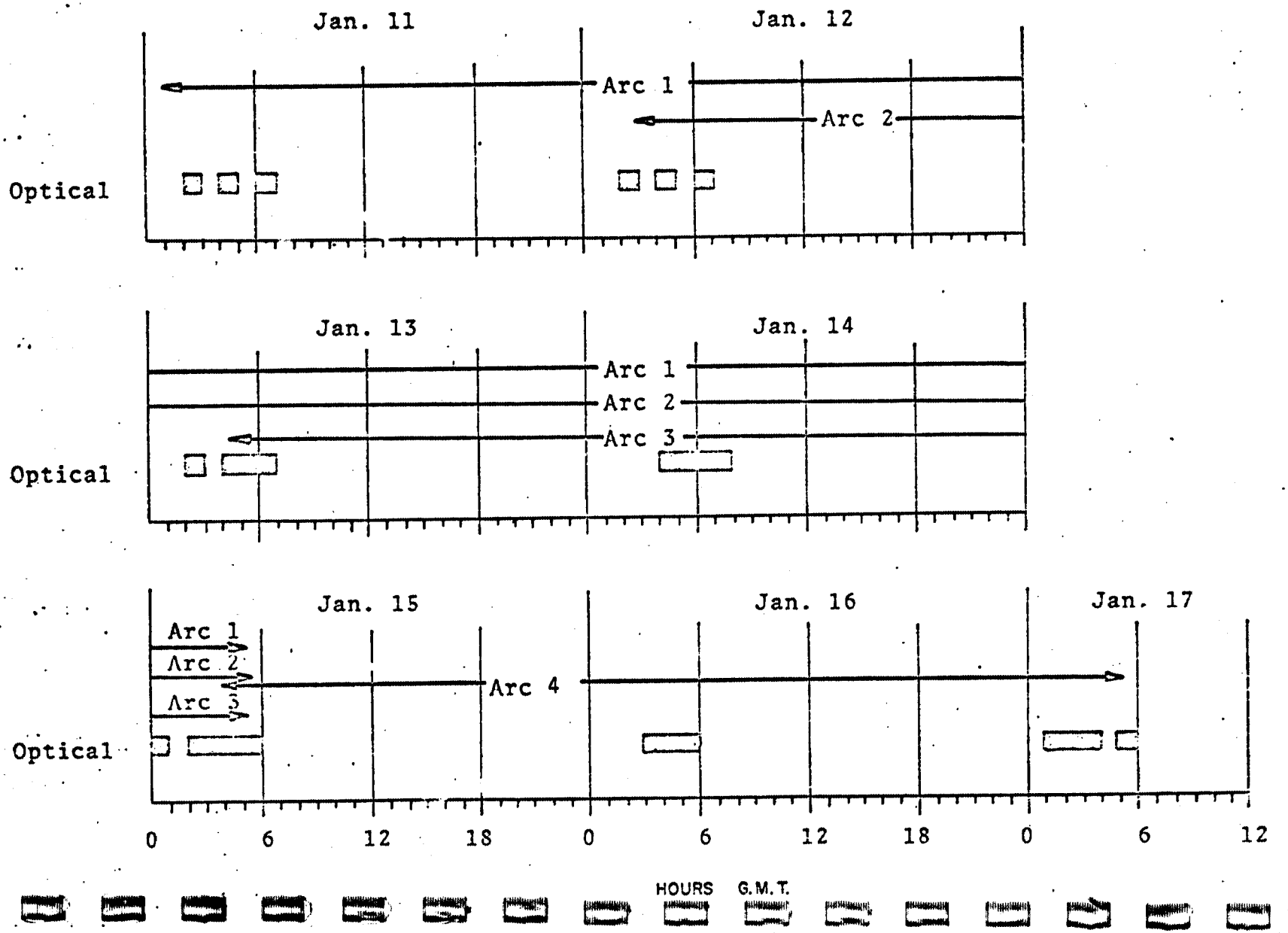

Figure 6

1.2 GRARR Data

The Goddard Range and Range Rate (GRARR) system was designed as a high-precision tracking system able to accurately determine the range and radial velocity of a spacecraft by measuring phase shift and Doppler. Each station uses an S-band and a VHF system. Only the S-band system was used in this evaluation.

The GRARR observations used in this evaluation had been smoothed using a sixth order polynomial smoothing program. The data was smoothed over two minute periods and smoothed values were obtained at 32 second intervals within these periods.

TABLE VII

SUMMARY OF GRARR AND SECOR PASSES

PASS NO.	DATE	TIME	MAXIMUM ELEVATION ANGLE				
			HOMEFL	FTWART	GREENV	HERDN	ROSRAN
665	1/1/66	08^h	64.3^o	N/A	80.7^o	32.5^o	51.8^o
676	1/2/66	06^h	27.5^o	38.0^o	28.4^o	68.0^o	43.3^o
677	1/2/66	08^h	48.3^o	40.8^o	69.6^o	25.3^o	40.2^o
700	1/4/66	06^h	N/A	55.4^o	33.7^o	70.2^o	62.7^o

Pass 700 over ROSRAN was from the C channel transponder, the other three passes were from the A channel.

1.3 SECOR Data

The SECOR system which is operated by the Army Map Service, operates on the principle of "trilateration". Three or four ground stations make range observations, which are in effect simultaneous, by means of a transponder in the satellite. A representation of the geometry of the four "quad" passes analyzed is given in Figure 7.

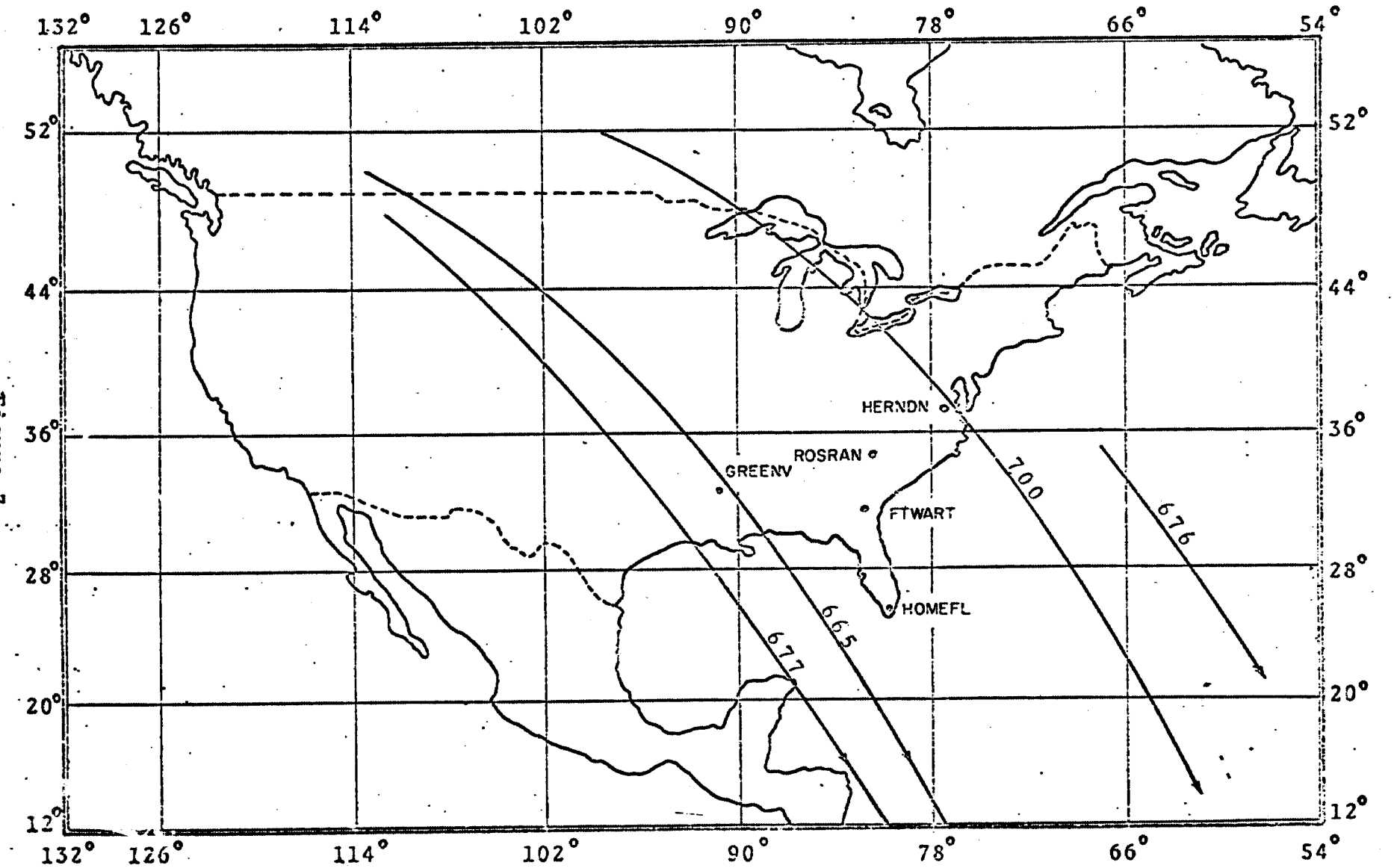

Figure 7

SECOR PASSES

From Period No. 1

APPENDIX A-2

Preprocessing of Observations

2.1 Preprocessing of Optical Data

The first step in the processing of optical observations is usually performed by the observing source. This consists of developing a plate or film, identifying the image or images of the satellite and the images of several reference stars whose right ascensions and declinations are well known. The initial measurements of both satellite images and reference stars consist of linear rectangular coordinates. From the knowledge of the spherical coordinates of the reference stars, the right ascensions and declinations of the satellite images may be calculated. These coordinates as received by the preprocessor may be referred to the mean equator and equinox of date, true equator and equinox of date, or mean equator and equinox of some standard epoch.

The preprocessor then transforms these observations to a common coordinate system. Currently, the preprocessor transforms all right ascensions and declinations to the true equator and equinox of the epoch of the elements being processed. If the observations were originally referred to the mean equator and equinox of a particular epoch, it

is only necessary to precess from that epoch to the epoch of the elements. However, if they were referred to the true equator and equinox of a particular epoch, it is necessary first to transform them to the mean equator and equinox of that same epoch and then precess to the epoch of the elements.

Finally, a transformation must be made from the mean equator and equinox of the epoch of the elements to the true equator and equinox of the epoch of the elements.

2.2 Nutation

The transformations from the true equator and equinox of date to the mean equator and equinox of date is

$$Y = NX$$

where

$$Y = \begin{bmatrix} \cos \delta_m & \cos \alpha_m \\ \cos \delta_m & \sin \alpha_m \\ \sin \delta_m & \end{bmatrix}$$

$$X = \begin{bmatrix} \cos \delta_T & \cos \alpha_T \\ \cos \delta_T & \sin \sigma_T \\ \sin \delta_T & \end{bmatrix}$$

$$N = \begin{bmatrix} 1 & +\Delta\psi\cos\varepsilon_m & +\Delta\psi\sin\varepsilon_m \\ -\Delta\psi\cos\varepsilon_m & 1 & +\Delta\varepsilon \\ -\Delta\psi\sin\varepsilon_m & -\Delta\varepsilon & 1 \end{bmatrix}$$

where

α_m, δ_m = right ascension and declination referred to mean equator and equinox of date

α_T, δ_T = right ascension and declination referred to true equator and equinox of date

ε_m = mean obliquity of date

$\Delta\psi$ = nutation in longitude

$\Delta\varepsilon$ = nutation in obliquity

The inverse transformation is simply:

$$X = N^{-1}X = N^{T}X$$

2.3 Precession

The transformation from the mean equator and equinox of 1950.0 to the mean equator and equinox of an arbitrary epoch t1 is

$$Y = PX$$

where

$$Y = \begin{bmatrix} \cos\delta_{t1} & \cos\alpha_{t1} \\ \cos\delta_{t1} & \sin\alpha_{t1} \\ \sin\delta_{t1} & \end{bmatrix}$$

$$X = \begin{bmatrix} \cos\delta_{1950.0} & \cos\alpha_{1950.0} \\ \cos\delta_{1950.0} & \sin\alpha_{1950.0} \\ \sin\delta_{1950.0} & \end{bmatrix}$$

$$P = \begin{bmatrix} (\cos\zeta\cos\theta\cos\zeta-\sin\zeta\sin\zeta)(-\cos\zeta\cos\theta\sin\zeta-\sin\zeta\cos\zeta)(-\cos\zeta\sin\theta) \\ (\sin\zeta\cos\theta\cos\zeta+\cos\zeta\sin\zeta)(-\sin\zeta\cos\theta\sin\zeta+\cos\zeta\cos\zeta)(-\sin\zeta\sin\theta) \\ (\sin\theta\cos\zeta) \qquad (-\sin\theta\sin\zeta) \qquad (\cos\theta) \end{bmatrix}$$

The inverse transformation is

$$X = P^{-1}Y = P^{T}Y$$

Since the expression for z, θ, ζ are tied to 1950.0 as an epoch, the precession between 2 different epochs, neither of which is 1950.0, must be performed in two steps, using 1950.0 as an intermediary epoch.

2.4 Preprocessing of STADAN/GRARR Observations

The complete analysis and derivations of the various preprocessing corrections made to Goddard range and range rate observations are contained in the following references.

Ref. 1: "Tropospheric Refraction Corrections and their Residual Errors", C. Martin, C. Carroll, 1964.

Ref. 2: "NASA-GSFC Final Report on GRARR/GEOS-A Data Validation", John H. Berbert, Robert Reich.

Ref. 3: "Final Report on Ionospheric Correction to Tracking Parameters", J. J. Freeman Associates.

Ref. 4: "Description of the GRARR Data Processing Program for the CDC-160A", E. R. Watkins, D. H. Rose, GSFC.

The range and range rate corrections, ΔR and $\Delta \dot{R}$, are to be added algebraically to the measured values of range, R_m, and range rate, $\dot{R}_m$.

1. Tropospheric and Ionospheric (Ref. 1)

$$\Delta R_T + R_I = - \frac{k}{\sin E} \text{ meters}$$

where a nominal value of k = 3 is currently used.

E = elevation of satellite

2. Transponder Dealy (Ref. 2)

$$\Delta R_{DA} = -3.32 \times 10^{-4} \dot{R}_m - 7.18 \times 10^{-18} \dot{R}_m^2 \text{ meters}$$

$$\Delta R_{DC} = +5.22 \times 10^{-4} \dot{R}_m + 8.34 \times 10^{-8} \dot{R}_m^2 + 4.42 \times 10^{-12} \dot{R}^3 + 1.82 \times 10^{-15} \dot{R}^4 \text{ meters}$$

for A and C channels respectively.

3. Station Bias

ΔR = 9.7 meters at ROSRAN

2.5 Preprocessing of AMS SECOR Data

Refraction[1]

The same refraction model is used in preprocessing SECOR range data as is used for Goddard STADAN range data with appropriate allowances for the frequency differences.

---

(1) "Advanced Techniques for the Reduction of Geodetic SECOR Observations"
Prepared for U.S. Army GIMRADA Contract No. DA-44-009-AMC-93X(X), Duane C. Brown.

APPENDIX A-3

Force Models used in NONAME

3.1 Force Models

The data reduction program in its present form incorporates four force models. These are:

1. The earth gravitational field
2. The solar and lunar gravitational perturbations
3. Solar radiation pressure
4. Atmospheric drag

The program is designed such that the gravitational coefficients and pertinent physical characteristics of satellites, such as reflectivity, cross-sectional area mass, and drag coefficient can be simply changed through card input or block data statement.

3.2 The Earth's Gravitational Field

The formulation of the geopotential used is:

$$u = \frac{GM}{r}\left\{1 + \sum_{n=2}^{k}\sum_{m=0}^{n}\left(\frac{a}{r}\right)^n P_n^m(\sin\phi)[C_{nm}\cos m\lambda + S_{nm}\sin m\lambda]\right\} \quad (1)$$

where

G	is the universal gravitational constant
M	is the mass of the earth
r	is the geocentric satellite distance
a	is the earth's mean equatorial radius
ϕ	is the sub-satellite latitude
λ	is the sub-satellite east longitude
$P_m^n(\sin\phi)$	is the associated spherical harmonic of degree n and order m.

The design of the potential function requires that denormalized gravitational coefficiences $C_{n,m}$ and $S_{n,m}$ be used. The program is presently capable of accepting coefficients up to (20,20) or any sub-set of these.

The denormalized gravitational coefficiences determined by SAO are listed in table 2. These coefficients have been used extensively in NONAME for the reduction of optical data. The same data have been reduced by NONAME using various other gravity models. An intercomparison of the results is being prepared for publication in the near future.

The transformation of the geopotential in earth-fixed coordinates (r,ϕ,λ) to gravitational accelerations in inertial coordinates (x,y,z) is accomplished as follows:

$$\ddot{x}_\bullet = \frac{\partial u}{\partial r}\frac{\partial r}{\partial x} + \frac{\partial u}{\partial \phi}\frac{\partial \phi}{\partial x} + \frac{\partial u}{\partial \lambda}\frac{\partial \lambda}{\partial x}\,;\ \ddot{y}_\bullet\,,\ \ddot{z}_\bullet \qquad (2)$$

TABLE 2

SAO DENORMALIZED COEFFICIENTS M-1

$C(2,0) = -1082.645 \cdot 10^{-6}$		$C(5,4) = -0.206 \cdot 10^{-8}$	
$S(2,0) = 0$		$S(5,4) = +0.498 \cdot 10^{-9}$	
$C(2,2) = +1.536 \cdot 10^{-6}$		$C(5,5) = +0.384 \cdot 10^{-9}$	
$S(2,2) = -0.872 \cdot 10^{-6}$		$S(5,5) = -0.146 \cdot 10^{-8}$	
$C(3,0) = +2.546 \cdot 10^{-6}$		$C(6,0) = -0.646 \cdot 10^{-6}$	
$S(3,0) = 0$		$S(6,0) = 0$	
$C(3,1) = +2.091 \cdot 10^{-6}$		$C(6,1) = -0.370 \cdot 10^{-7}$	
$S(3,1) = +0.287 \cdot 10^{-6}$		$S(6,1) = -0.212 \cdot 10^{-7}$	
$C(3,2) = +0.251 \cdot 10^{-6}$		$C(6,2) = +0.858 \cdot 10^{-8}$	
$S(3,2) = -0.184 \cdot 10^{-6}$		$S(6,2) = -0.455 \cdot 10^{-7}$	
$C(3,3) = +0.782 \cdot 10^{-7}$		$C(6,3) = -0.112 \cdot 10^{-8}$	
$S(3,3) = +0.226 \cdot 10^{-6}$		$S(6,3) = +0.643 \cdot 10^{-9}$	
$C(4,0) = +1.649 \cdot 10^{-6}$		$C(6,4) = -0.167 \cdot 10^{-9}$	
$S(4,0) = 0$		$S(6,4) = -0.196 \cdot 10^{-8}$	
$C(4,1) = -0.543 \cdot 10^{-6}$		$C(6,5) = -0.253 \cdot 10^{-9}$	
$S(4,1) = -0.445 \cdot 10^{-6}$		$S(6,5) = -0.370 \cdot 10^{-9}$	
$C(4,2) = +0.738 \cdot 10^{-7}$		$C(6,6) = -0.932 \cdot 10^{-11}$	
$S(4,2) = +0.148 \cdot 10^{-6}$		$S(6,6) = -0.361 \cdot 10^{-10}$	
$C(4,3) = +0.509 \cdot 10^{-7}$		$C(7,0) = +0.333 \cdot 10^{-6}$	
$S(4,3) = -0.113 \cdot 10^{-7}$		$S(7,0) = 0$	
$C(4,4) = -0.112 \cdot 10^{-8}$		$C(7,1) = +0.144 \cdot 10^{-6}$	
$S(4,4) = +0.486 \cdot 10^{-8}$		$S(7,1) + +0.114 \cdot 10^{-6}$	
$C(5,0) = +0.210 \cdot 10^{-6}$		$C(7,2) = +0.362 \cdot 10^{-7}$	
$S(5,0) = 0$		$S(7,2) = +0.162 \cdot 10^{-7}$	
$C(5,1) = -0.677 \cdot 10^{-7}$		$C(7,3) = +0.352 \cdot 10^{-8}$	
$S(5,1) = -0.882 \cdot 10^{-7}$		$S(7,3) = +0.254 \cdot 10^{-9}$	
$C(5,2) = +0.102 \cdot 10^{-6}$		$C(7,4) = -0.323 \cdot 10^{-9}$	
$S(5,2) = -0.375 \cdot 10^{-7}$		$S(7,4) = -0.217 \cdot 10^{-9}$	
$C(5,3) = -0.172 \cdot 10^{-7}$		$C(7,5) = +0.269 \cdot 10^{-10}$	
$S(5,3) = +0.231 \cdot 10^{-9}$		$S(7,5) = +0.191 \cdot 10^{-10}$	

TABLE 2 (Cont'd)

C(7,6)	$-0.145 \cdot 10^{-10}$	C(10,01)	$+0.649 \cdot 10^{-7}$
S(7,6)	$+0.437 \cdot 10^{-11}$	S(10,01)	$-0.779 \cdot 10^{-7}$
C(7,7)	$+0.102 \cdot 10^{-11}$	C(10,02)	$-0.624 \cdot 10^{-8}$
S(7,7)	$+0.178 \cdot 10^{-11}$	S(10,02)	$-0.250 \cdot 10^{-8}$
C(8,0)	$+0.270 \cdot 10^{-6}$	C(10,03)	$-0.379 \cdot 10^{-9}$
S(8,0)	0	S(10,03)	$+0.175 \cdot 10^{-9}$
C(8,1)	$-0.515 \cdot 10^{-7}$	C(10,04)	$-0.436 \cdot 10^{-10}$
S(8,1)	$+0.447 \cdot 10^{-7}$	S(10,04)	$-0.654 \cdot 10^{-10}$
C(8,2)	$+0.214 \cdot 10^{-8}$	C(11,0)	$-0.302 \cdot 10^{-6}$
S(8,2)	$+0.320 \cdot 10^{-8}$	S(11,0)	0
C(8,3)	$-0.374 \cdot 10^{-9}$	C(11,01)	$-0.313 \cdot 10^{-7}$
S(8,3)	$+0.404 \cdot 10^{-10}$	S(11,01)	$+0.885 \cdot 10^{-8}$
C(8,4)	$-0.277 \cdot 10^{-9}$	C(12,0)	$+0.357 \cdot 10^{-6}$
S(8,4)	$-0.157 \cdot 10^{-10}$	S(12,0)	0
C(8,5)	$-0.959 \cdot 10^{-11}$	C(12,01)	$-0.923 \cdot 10^{-7}$
S(8,5)	$+0.214 \cdot 10^{-10}$	S(12,01)	$-0.402 \cdot 10^{-7}$
C(8,6)	$-0.475 \cdot 10^{-12}$	C(12,02)	$-0.470 \cdot 10^{-8}$
S(8,6)	$+0.888 \cdot 10^{-11}$	S(12,02)	$-0.233 \cdot 10^{-9}$
C(8,7)	$-0.444 \cdot 10^{-13}$	C(12,12)	$-0.278 \cdot 10^{-18}$
S(8,7)	$+0.158 \cdot 10^{-12}$	S(12,12)	$+0.718 \cdot 10^{-20}$
C(8,8)	$-0.316 \cdot 10^{-12}$	C(13,0)	$+0.114 \cdot 10^{-6}$
S(8,8)	$+0.130 \cdot 10^{-12}$	S(13,0)	0
C(9,0)	$+0.532 \cdot 10^{-7}$	C(13,12)	$-0.126 \cdot 10^{-18}$
S(9,0)	0	S(13,12)	$+0.117 \cdot 10^{-18}$
C(9,1)	$+0.760 \cdot 10^{-7}$	C(13,13)	$-0.216 \cdot 10^{-19}$
S(9,1)	$+0.780 \cdot 10^{-8}$	S(13 13)	$+0.282 \cdot 10^{-19}$
C(9,2)	$-0.277 \cdot 10^{-9}$	C(14,0)	$-0.179 \cdot 10^{-6}$
S(9,2)	$+0.242 \cdot 10^{-8}$	S(14,0)	0
C(10,0)	$+0.541 \cdot 10^{-7}$	C(14,01)	$-0.788 \cdot 10^{-8}$
S(10,0)	0	S(14,01)	$+0.280 \cdot 10^{-8}$

TABLE 2 (Cont'd)

C(14,11)	=	$+0.947 \cdot 10^{-21}$
S(14,11)	=	$-0.473 \cdot 10^{-21}$
C(14,12)	=	$+0.140 \cdot 10^{-20}$
S(14,12)	=	$-0.132 \cdot 10^{-19}$
C(14,14)	=	$-0.193 \cdot 10^{-21}$
S(14,14)	=	$-0.414 \cdot 10^{-22}$
C(15,09)	=	$-0.241 \cdot 10^{-18}$
S(15,09)	=	$-0.483 \cdot 10^{-18}$
C(15,12)	=	$-0.138 \cdot 10^{-19}$
S(15,12)	=	$-0.190 \cdot 10^{-20}$
C(15,13)	=	$-0.117 \cdot 10^{-20}$
S(15,13)	=	$-0.927 \cdot 10^{-21}$
C(15,14)	=	$+0.114 \cdot 10^{-22}$
S(15,14)	=	$-0.558 \cdot 10^{-22}$

where the subscript "⊕" denotes accelerations due to the earth's field.

3.3 Solar and Lunar Gravitational Perturbations

The perturbations caused by a third body, e.g., the sun or moon, on a satellite orbit are treated by defining a disturbing function R[1] which can be treated as the potential function U. For the solar perturbation $R_\odot$ takes the form

$$R_\odot = \frac{GMm_\odot}{r_\odot}\left[\left(1 - \frac{2r}{r_\odot}S + \frac{r^2}{r_\odot^2}\right)^{-1/2} - \frac{r}{r_\odot}\right] \qquad (3)$$

where $S = \cos(r, r_\odot)$

$m_\odot$ is the mass of the sun in earth masses

$r_\odot$ is the geocentric distance to the sun

r is the geocentric distance to the satellite

G is the universal gravitational constant

M is the mass of the earth

The acceleration of the satellite due to the sun is then

$$\ddot{x}_\odot = \frac{\partial R_\odot}{\partial r}\frac{\partial r}{\partial x}\ ;\ \ddot{y}_\odot,\ \ddot{z}_\odot \qquad (4)$$

---

[1] Kozai, Y, Smithsonian Astrophysical Observatory Special Report 22, pp. 7-10.

The lunar perturbations are found from equation (3) by substituting the lunar mass and distance for those of the sun.

The lunar and solar ephermerides are computed internal to the program. These positions are computed at ten equal intervals over each five day period and least squares fit to a fourth order polynomial in time about the midpoint of the five day period. The positions of these bodies are then determined at each data point by evaluating the polynomial at the observation time.

3.4 Solar Radiation Pressure

The acceleration acting on a satellite due to solar radiation pressure is formulated as follows [2].

$$\ddot{x}_{RAD} = -\frac{AP_{\odot}}{m} \gamma\nu \, L_x; \; \ddot{y}_{RAD}, \; \ddot{z}_{RAD} \qquad (5)$$

where

- L is the inertial unit vector from the geocenter to the sun and whose components are L_x, L_y, L_z.
- A is the cross sectional area of the satellite
- m is the satellite mass
- γ is a factor depending on the reflective characteristics of the satellite

[2] H. Koelle, Handbook of Astronautical Engineering, pp. 8-33, McGraw-Hill, 1961.

ν is the eclipse factor such that:

$$\nu = \begin{cases} 0 \text{ when satellite is in earth's shadow} \\ 1 \text{ when satellite is illuminated by the sun} \end{cases}$$

P_s is the solar radiation pressure in the vicinity of the earth,

$$4.5 \times 10^{-6} \ \frac{\text{Newton}}{m^2}$$

At present, it is assumed that the satellite is specularly reflecting with reflectivity, ρ, and thus

$$\gamma = (1 + \rho). \tag{6}$$

The vector $\hat{L}$ and the eclipse factor are determined from the solar ephemeris subroutine previously described, the satellite ephemeris, and involve the approximation of a cylindrical earth shadow.

3.5 Atmospheric Drag

The atmospheric decelerations are computed as follows:

$$\ddot{x}_{DRAG} = -\frac{\rho C_D A v v_x}{2m} \ ; \ \ddot{y}_{DRAG}, \ \ddot{z}_{DRAG} \tag{7}$$

where

ρ is the ambient atmospheric density

C_D is the satellite drag coefficient

A is the projected area of the satellite on a plane perpendicular to direction of motion

m is the satellite mass.

The velocity vector $\vec{v}$ given in inertial coordinates by

$$\vec{v} = v_x\hat{i} + v_y\hat{j} + v_z\hat{k} \tag{8}$$

can be chosen to be either the velocity relative to the atmosphere which implies that the atmosphere rotates with the earth or the inertial velocity which assumes that the atmosphere is static. Presently, the former assumption is made.

The density, ρ, is computed from the 1962 U.S. Standard Atmosphere.

APPENDIX A-4
Station Position Transformations

4.1 Station Position Transformations

The analysis of "long arc" passes of the GEOS-A satellite requires that the various tracking station *a priori* positions be available on a uniform world geodetic system in order that the results not be biased by interdatum uncertainties. The world geodetic system selected for these analyses is the SAO Standard Earth (C-5 datum).

A priori estimates of the tracking station positions and their uncertainties relative to the geo-center (earth's center of mass) are derived from the knowledge of the following:

a. Baker-Nunn camera station positions on the original datums.

b. Baker-Nunn camera station positions on the SAO C-5 datum.

c. The positions of the various tracking sites in their original datums.

d. Intra-datum survey connections between the Baker-Nunn sites and the various tracking sites.

e. Empirical formulae for the estimation of surface survey uncertainties between the Baker-Nunn sites and the tracking sites.

The method used to effect this transformation is simple and straight forward and has been checked to ascertain its compatibility with the more rigorous and arduous transformation formulae commonly used to compute datum shifts. It should be noted that this method can be used only when the type of information that has been calculated for the Baker-Nunn sites is available. That is to say, one must have available the positions of the control stations (Baker-Nunn sites) in the original datum and in the new reference system, and a direct survey tie between the control stations and the tracking stations which are to be transformed.

4.2 SAO Standard Earth Reference System

The reference system used in the derivation of the a priori positional information is the SAO Standard Earth as described in [1]. The ellipsoidal parameters are a_e = 6,378,165 meters and f = 1/298.25. This system is the best available geocentric (earth's center of mass) terrestrial system. The Z axis is oriented in the direction of the mean pole of 1900-1905 and the X axis in the direction of the mean observatory. Since the definition of UT-1 was based on the U. S. Naval Observatory's time determination the X axis is directed toward the meridian 75^{o}-03'-55".94 East of the U. S. Naval Observatory.

The uncertainty related to this system is defined

(by [1] to be about ±10 meters for the origin (geocentricity), 0".2 for the direction of the axes, and a few parts per million in scale. The scale actually depends on the adopted value for GM which in this instance is $3.986032 \times 10^{20} cm^3 sec^{-2}$. The absolute coordinates of the Baker-Nunn stations are given to an accuracy of ±15 to 20 meters. The fact that this system is oriented to the mean pole of 1900-1905 must be taken into consideration when station positions as derived from the tracking data are obtained. Unless corrections for polar motion are applied, the positions derived from the tracking data will be based on the instantaneous pole at the time of observation.

4.3 Coordinate Transformations

All of the Baker-Nunn camera stations are connected to individual major geodetic datums and their coordinates in these datums are known. The coordinates of the Baker-Nunn camera stations on the SAO Standard Earth are also known, having been derived by SAO through the reduction of approximately 35,000 satellite observations with wide orbital variety. The coordinates of the Baker-Nunn camera stations are given in both the ellipsoidal and three-dimensional cartesian coordinate systems. For ease and simplicity of calculation, we have elected to use the cartesian coordinates to obtain our transformations. By comparing the original datum coordinates with the derived mass-centered coordinates, one derives the "datum shift" for the particular datum. The "datum shift" is simply the total transformation to be applied to the original datum coordinates to obtain the new mass-centered coordinates. Once the

"datum shift" has been derived for the Baker-Nunn station this shift is then applied in a weighting scheme to derive the SAO Standard Earth coordinates for tracking stations that have positions given in the same original datum as the Baker-Nunn and are connected to the Baker-Nunn station through conventional surface surveys. A weighting scheme (which is described below) is used since the Baker-Nunn stations were allowed to adjust independently and subsequently where more than one Baker-Nunn station was located on a single datum, the individual stations show slightly different "datum shifts".

As an example of the single station case, consider Baker-Nunn camera station 9005, TOKYO. Its coordinates on the Tokyo (JAP) datum are:

X: -3,946,554 (meters)

Y: +3,365,774 (meters)

Z: +3,698,151 (meters)

Its geocentric (mass centered) coordinates on the SAO Standard Earth are:

X_g: -3,946,703 (meters)

Y_g: +3,366,291 (meters)

Z_g: +3,698,849 (meters)

The transformation to be applied to tracking stations on the Tokyo datum is therefore:

$$X_g - X = \Delta X = -149 \text{ meters}$$

$$Y_g - Y = \Delta Y = +517 \text{ meters}$$

$$Z_g - Z = \Delta Z = +698 \text{ meters}$$

The ΔX, ΔY, ΔZ is applied to the tracking station coordinates on Tokyo datum. This in effect then furnishes an a priori estimate of the coordinates of the tracking station in the SAO Standard Earth reference system.

As mentioned above, the coordinates of the Baker-Nunn camera stations are furnished in both the ellipsoidal and three-dimensional cartesian coordinate systems. However, the coordinates of the various tracking stations may be given in ellipsoidal coordinates only, thereby requiring the calculation of the three-dimensional cartesian coordinates. This is done using the following standard formulation:

$$X = (\nu + h + N) \cos \phi \cos \lambda$$

$$Y = (\nu + h + N) \cos \phi \sin \lambda$$

$$Z = [(1 - e^2)\nu + h + N] \sin \phi$$

where:

ϕ = geodetic latitude

λ = geodetic longitude

$\nu = a_e/(1 - e^2 \sin^2\phi)^{1/2}$

a_e = semi major axis of reference ellipsoid

e^2 = eccentricity squared of reference ellipsoid

h = height of station above the geoid (mean sea level elevation)

N = height of the geoid above or below the spheroid.

In the case where the tracking station information only contains mean sea level elevations, the geoid height is derived from geoid contour charts for the particular reference spheroid. These charts are based on gravitational coefficients derived from satellite observations.

Having derived the a priori estimates of the tracking station positions on the SAO Standard Earth we now derive estimates of the uncertainties of these positions relative to the earth's center of mass.

4.4 A Priori Uncertainty Derivation

In order to derive a priori estimates of the uncertainty in the tracking station positions, use is made of an empirical formula derived by Lansing Simmons, USC & GS, to describe the accuracy of first order triangulation. The formula states that the relative accuracy between two points connected by conventional first-order triangulation (1 part in 25,000) is approximately:

$$1/20{,}000\sqrt[3]{M},$$

where M is distance between the two stations in statute miles. As an example consider two stations 1000 miles apart, and connected by standard triangulation. The proportional accuracy would therefore be 1 part in 200,000 or approximately 26.4 ft. This means that the relative uncertainty between the two stations caused by the surface survey errors is approximately 26 ft. or 8 meters. Accepting the stated accuracy of the Baker-Nunn stations relative to the center mass as $\pm$ 20 meters, one can then take the root sum square of the uncertainty in the Baker-Nunn station relative to the center of mass and the surface survey uncertainty between the Baker-Nunn and the tracking station as derived by the Simmons formula as a conservative estimate of the uncertainty of the tracking station relative to the center of mass. The formula then becomes:

$$\sigma_g = \sqrt{\sigma_s^2 + 20^2}$$

where

σ_g = uncertainty of the tracking station relative to the center of mass.

σ_s = survey uncertainty as computed by Simmons formula.

4.5 Weighting Scheme for Multi-Station Connections

In the case where a tracking station is located on a datum which contains more than one Baker-Nunn station, we use a weighted average of the geocentric coordinates of the tracking station derived from the general formula

$$P = \left(\frac{W_1}{W_1+W_2\ldots W_n}\right) P_1 + \left(\frac{W_2}{W_1+W_2\ldots W_n}\right) P_2$$

$$+ \ldots \left(\frac{W_n}{W_1+W_2\ldots W_n}\right) P_n$$

where:

P is the weighted position

$W_1 \ldots W_n$ are the weights

P_1 is the station position derived from Baker-Nunn Station 1

P_2 is the station position derived from Baker-Nunn Station 2

P_n is the station position derived from Baker-Nunn Station n

The weights used are inversely proportional to the distances between the Baker-Nunn stations and the tracking station to be transformed. This weighting scheme allows us to take into consideration the varying shifts of the Baker-Nunn stations while placing proper emphasis on the contribution of individual stations upon the transformation. As an example, consider the case where the tracking station is located close to one of the Baker-Nunn stations in the datum. One can rightfully expect that the tracking station would shift approximately the same amount and in the same direction as the co-located Baker-Nunn and that the effect of the other Baker-Nunn stations would be minimal. In the case where the tracking station were located equidistant from several Baker-Nunn stations one would assume equal contribution to the transformation from each of the Baker-Nunn shifts.

While the above weighting scheme is apparently quite adequate, investigations are continuing into other weighting schemes. Foremost of these is the computation of the weights (W_n) as being inversely proportional to the square of the distances between the Baker-Nunn stations and tracking station to be transformed. Another procedure being investigated is the distance cut-off, whereby a very distant Baker-Nunn coordinate shift will have essentially no effect on the station to be transformed. This cut-off distance is being presently considered in the range of 5000 km.

The transformed station coordinates derived using these weighting schemes are being compared in separate NO-NAME data reduction runs. Identical observational data are being reduced in each run, and the observational residuals are being compared.

4.6 Isolated Datums

An ellipsoidal transformation is performed for a tracking station on an isolated datum such as the Tananarive datum. For these station positions, the ΔU, ΔV, and ΔW shifts are unknown and considered to be zero. The shifts are computed as follows:

$$\Delta N = (a\,\Delta f + f\,\Delta a)\sin^2\phi - \Delta a$$

$$\Delta\phi = 206265[(a\,\Delta f + f\,\Delta a)\sin 2\phi]/R_m$$

$$R_m = \frac{a(1-e^2)}{[(1-e^2\sin^2\phi)^{1/2}]^{3/2}}$$

where

a = 6378165. meters

f = 1/298.25

Δa = 6378165. minus original survey ellipsoid value of a.

Δf = 1/298.25 minus original survey ellipsoid value of F.

ϕ = Latitude of tracker in original system

e^2 = $2f - f^2$

REFRACTION CORRECTION INTERCOMPARISONS

Geodetic Investigation at GSFC

by

Horace C. Parker

Radio Corporation of America Service Company
9430 Lanham-Severn Road
Scabrook, Maryland 20801

under
NASA CONTRACT NO. NAS 5-9756

13 December 1967

PAGES 370 & 372 BLANK

REFRACTION CORRECTION INTERCOMPARISONS

The GEOS Geodetic tracking systems do not have a standard set of refraction formulas. Different groups using the same data employ different mathematical models of the atmosphere or different approximations to the same model. Atmospheric refraction profile measurements just prior to a tracking operation, then ray tracing by means of a digital computer is the best method of predicting the effects of the atmosphere upon radiowave propagation. The method used by the GEOS Geodetic tracking systems is to obtain an estimate of the atmosphere refraction profile for the troposhpere, from a mathematical model based on the surface refractivity measurements taken just prior to tracking, and for the effects of the ionosphere on radiowave propagation an average state of the ionosphere is assumed.

The primary purpose of this paper is to compute values from the different formulas, so that the differences can be determined. Range and range rate refraction error values versus the elevation angles were computed from formulas obtained from the following GSFC developed programs:

1. The Differential Correction Program
2. The Freeman Recommendations
3. The NONAME Program
4. The Laser system by both the GSFC developed program and the SAO developed program
5. The GDAP Program

The following assumptions were made to aid calculations in this preliminary study:

N_s, The tropospheric surface index of refraction = 252×10^{-6}

N_i, The ionosphere index of refraction typical for 2GHZ = 3.941×10^{-6}

h_i, The height of the F_2 layer of the ionosphere = 400K meters

h =, The height of the satellite above the surface of the earth = 1333 KM

This particular set of values allows for comparison with those equations, where the atmosphere models are a constant.

The refraction comparisons are presented as follows:

Range tropospheric in figure 3

Range ionospheric in figure 4

Range rate tropospheric in figure 5

Range rate ionospheric in figure 6

Total range in figure 7

Total range rate in figure 8

In summary; Table 1 lists the maximum differences between models at 30° elevation, and in all cases as the elevation increases the differences decrease.

R_T	R_I	$\dot{R}_T$	$\dot{R}_I$	R_{total}	$\dot{R}_{total}$
.8 meters	.62 meters	.003 m/sec.	.008 m/sec.	1.4 meters	.01 m/sec.

TABLE 1

Maximum Differences Between Models at 30° Elevation

A continuation of this study will be made to include angle correction differences while varying the troposphere surface index of refraction, Ionosphere index of refraction, and the height of the F_2 layer of ionosphere.

REFRACTION CORRECTION INTERCOMPARISONS

The refraction correction equations for the GEOS geodetic tracking systems are not standardized. Different groups using the same data employ different correction equations. Some of these equations are compared to determine the resulting differences in the methods of making refraction corrections.

GSFC Differential Correction Program

The Advanced Orbit Programming Branch, Data System Division's Differential Correction Program has the following refraction formulas, obtained from "F 116- $\ell, m, \rho, \dot{\rho}$ Corrector for Ionosphere Refraction", by Isabella J. Cole. Dated: November, 1965. The $\Delta\rho$ and $\Delta\dot{\rho}$ formulas have not been utilized to date.

(1) $\Delta R = -C_5 \cos E - C_8 / (1 - C_6 \cos^2 E)^{\frac{1}{2}}$ * ** $E \leq 10^\circ$

(2) $\Delta R = -(C_4 / \sin E) - C_8 / \sin E$ * ** $E > 10^\circ$

(3) $\Delta \dot{R} = \left[\dot{r} N_1 e^{\gamma} e^{u} / (1 - C_6^2 \cos^2 E)\right]$ ** $+ \left[C_5 \dot{E} \sin E \cos E / (C_3)^{\frac{3}{2}}\right]$ * $+ \left[C_8 \sin E \cos E \dot{E} C_6^2 / (1 - C_6^2 \cos^2 E)^{\frac{3}{2}}\right]$ ** $E \leq 10^\circ$

(4) $\Delta \dot{R} = \left[\dot{r} N_1 e^{\gamma} e^{u} / \sin E\right]$ ** $+ \left[C_4 \dot{E} \cos E / \sin^2 E\right]$ * $+ \left[C_8 \cos E \dot{E} / \sin^2 E\right]$ ** $E > 10^\circ$

(5) $C_1 = 8750$ Meters

(6) $C_2 = .999614$

(7) $C_3 = 1 - C_2^2 \cos^2 E$

(8) $C_4 = C_1 A_s$

(9) $C_5 = C_1 C_2 A_s$

(10) $C_6 = Re/(Re + h_1)$

(11) $C_8 = N_1 H_{DC} e^{\gamma}$

(12) $H_{DC} = \frac{4}{3}\left[30 \text{ km} - .2(h_1 - 200\text{km})\right]$

(13) $u = (h_1 - h)/ H_{DC}$

* = Tropospheric ** = Ionosphere

(14) $\gamma = 1-e^{u}$

h= Height of the satellite above the surface

h_i= Height of the F_2 layer of the ionosphere

R_e= 6378166 Meters = earth radius

e= 6.28318531

$N_i = \frac{1}{2}\left(\frac{M_o}{f_s}\right)^2$ = Index of refraction for ionosphere

A_s= Tropospheric index of refraction at the surface = N_s

f_s= Satellite transmitting frequency

M_o= Maximum usable frequency at zero kilometers

The above formulas have been simplified by assuming that the earth is a spheroid.

R/$\dot{R}$ Freeman Recommendations

The following formulas were recommended for use in making tropospheric and ionosperic refraction corrections by the memorandum, "Interim GRARR Corrections at GSFC" from John H. Berbert to the Working Committee on the Statistical Combination of Satellite Observational Data, dated 15 May, 1967. The refraction model was formulated by J.J. Freeman Associates Inc., in "Final Report on Ionospheric Correction to Tracking Parameters", NASA contract NAS5-9782.

(15) $\Delta R = \frac{-1}{\sin E}\left[\int_o^h N dh - \frac{\cot^2 E}{R_e}\int_o^h N h dh\right]$

(16) $\Delta \dot{R} = \frac{\dot{E}\cos E}{\sin^2 E}\left[\int_o^h N dh + \left\{(1-3/\sin^2 E)/R_e\right\}\int_o^h N h dh\right]$

For GEOS-A, which is well above the ionosphere, the height of the target,h, can be assumed to be infinity, giving the following evaluation of equations (15) and (16) for an exponential reference atmosphere and the atomosphere is spherically symetric.

(17) $$\Delta R = -\underbrace{\frac{C_9}{\sin E}\left[1-\frac{\cot^2 E}{D_1}\right]}_{*} - \underbrace{\left[\frac{D_3}{\sin E}\right.}_{**}\left.(1-D_2\cot^2 E)\right]$$

(18) $$\dot{\Delta R} = \underbrace{\frac{C_9 \dot{E}\cos E}{\sin^2 E}\left[1+(1-\frac{3}{\sin^2 E})/D_1\right]}_{*} + \underbrace{\frac{D_3 \dot{E}\cos E}{\sin^2 E}\left[1+D_2\left(1-\frac{3}{\sin^2 E}\right)\right]}_{**}$$

(19) $$C_9 = \frac{N_s}{C_e}$$

(20) $$D_1 = C_e R_e$$

(21) $$D_2 = \frac{H_f + h_i}{R_e}$$

(22) $$D_3 = N_i H_f e$$

(23) $$H_f = \frac{5}{3}\left[30KM + .2\,(h_i - 200KM)\right]$$

(24) $$C_e = -\ln\left(1 + \frac{7.32}{N_s} e^{.005577 N_s}\right)$$

$N_s = A_s$ = Troporpheric index of refraction at the surface

Freeman states that these formula are entirely adequate for $E > 30^\circ$, but for $E < 30^\circ$ equations (15) and (16) should be evaluated by numerical integration.

$R/\dot{R}$ GSFC GDAP Program

From "A Users Guide for GEOS Data Adjustment Program" by Joe J. Lynn of D. Brown Associates. Dated September 1, refraction formulas are as follows:

(25) $$\Delta R = \underbrace{\frac{-2N_s\,(H_o)}{\sin E + (\sin^2 E + .00452)^{\frac{1}{2}}}}_{*} - \underbrace{\frac{4H_o N_i}{(1-a^2\cos^2 E)^{\frac{1}{2}} + \left[(1-a^2\cos^2 E) - a^2(1-b)\cos^2 E\right]^{\frac{1}{2}}}}_{**}$$

(26) $$\dot{\Delta R} = \underbrace{\frac{2H_o N_s \dot{E}\cos E}{\sin E\,(\sin^2 E + .00452)^{\frac{1}{2}} + \sin^2 E}}_{*} + \underbrace{\quad}_{**}$$ Dual Frequency

(27) $$a = \frac{R_e}{R_e + h_i - 3H_G}$$

* = Tropospheric
** = Ionoshpere

(28) $$b = \frac{25H_G}{3(R_e+h_i - 3h_G)}$$

H_o = Scale height (nominal 7200 Meters)

H_G = Scale height of ionoshpere (Nominal 50000 Meters)

R/$\dot{R}$ GSFC NONAME Program

The "Interim Status Report on Program Development and GEOS-A Data Analysis" prepared by The Applied Sciences Department Wolf Research and Development Corporation gives the following formulas for total refraction correction.

(29) $$\Delta R = - \frac{K}{\sin E} \quad \text{Meters}$$

(30) $$\Delta \dot{R} = \frac{K\dot{E}\,\mathrm{Cos}E}{\sin^2 E} \quad \text{Meters / second}$$

$K = 3$

R - SAO and GSFC LASER

The Laser refraction correction formula is obtained from "An Analysis of the GSFC Laser Ranging Data" by S. J. Moss and W.T. Wells, also from "A Ruby- Laser System for Satellite Ranging" by C.G. Lehr, L.A. Maestre and P.H. Anderson. Dated: October 16, 1967.

(31) $$\Delta R = \frac{-2.1}{\sin E}$$

Assumptions for Intercomparisons

The earth is assumed to be spherical and stationary to obtain the approximate magnitude for each of the refraction formulas listed. In addition a circular orbit with an overhead pass is assumed; therefore, $\frac{dE}{dt}$ is determined from the geometry of Figure 1.

(32) $$\dot{E} = \frac{-\omega \cos E \sin(E+\omega t)}{\sin \omega t} = \frac{-\omega r(r-R_e \cos\omega t)}{r^2 + R_e^2 - 2rR_e \cos\omega t}$$

(33) $$E = \sin^{-1}\left[-\frac{R_e - r\cos\omega t}{\left[r(r-R_e\cos\omega t) + R_e(R_e - r\cos\omega t)\right]^{1/2}}\right]$$

$$r = R_e + h$$

$$T = T_c\left(\frac{R_e + h}{R_e}\right)^{3/2}$$

T_c = 5060.82 seconds

$\omega = 2\pi / T$

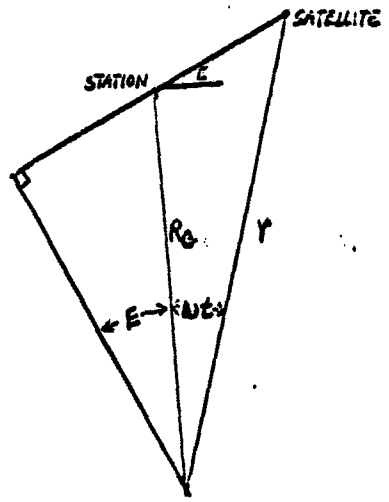

FIGURE 1

To futher simplify the calculation the following values were assumed: Values more representive of a standard atmosphere will be Investigated.

h_i = 400 K Meters

$N_i = 3.941 \times 10^{-6}$

$A_s = N_s = 252 \times 10^{-6}$

h = 1333333 Meters

Substituting these values into equations (1) through (33) gives the following set of equations that were used to develope Figures 2 through 8.

Range Refraction Corrections for Troposphere

(34) $\Delta R_T = -2.20415 \cos E \quad E \leq 10^\circ$ D.C.

(35) $\Delta R_T = -2.205 / \sin E \quad E > 10^\circ$ D.C.

(36) $\Delta R_T = -2\,(1 - \cot^2 E / 803.648916) / \sin E$ Freeman

(37) $\Delta R = -2.1 / \sin E$ Laser

(38) $\Delta R_T = -3.6288 / \left[\sin E + (\sin^2 E + .00452)^{\frac{1}{2}}\right]$ GDAP

Range Refraction Corrections for Ionosphere

(39) $\Delta R_I = -1/(1- .885455 \cos^2 E)^{\frac{1}{2}}$ $E \leq 10^0$ D.C.

(40) $\Delta R_I = -1 / \sin E$ $E > 10^0$ D.C.

(41) $\Delta R_I = -1.2498 (1- .081 \cot^2 E) / \sin E$ Freeman

(42) $\Delta R_I = -1.5764 / \left[(1- .92599 \cos^2 E)^{\frac{1}{2}} + (1- .86778 \cos^2 E)^{\frac{1}{2}}\right]$ GDAP

Range Tate Refraction Corrections for Troposphere

(43) $\Delta \dot{R}_T = 2.2033 \dot{E} \sin E \cos E / (1- .999228 \cos^2 E)^{\frac{3}{2}}$ $E \leq 10^0$ D.C.

(44) $\Delta \dot{R}_T = 2.205 \dot{E} \cos E / \sin^2 E$ $E > 10^0$ D.C.

(45) $\Delta \dot{R}_T = 2\dot{E}\cos E \left[1+(1-3/\sin^2 E)/803.648916\right] /\sin^2 E$ Freeman

(46) $\Delta \dot{R}_T = 3.6288 \cos E \dot{E} / \left[\sin E (\sin^2 E + .00452)^{\frac{1}{2}} + \sin^2 E\right]$ GDAP

Range Rate Refraction Corrections for Ionosphere

(47) $\Delta \dot{R}_I = \sin E \cos E \dot{E} \left[.88545/(1-.885455 \cos^2 E)^{\frac{3}{2}}\right]$ $E \leq 10^0$ D.C.

(48) $\Delta \dot{R}_I = \cos E \dot{E}/\sin^2 E$ $E > 10^0$ D.C.

(49) $\Delta \dot{R}_I = 1.2498 \cos E \dot{E} \left[1+ .082 (1-3/\sin^2 E)\right] /\sin^2 E$ Freeman

Range and Range Rate Total Refraction Corrections

(50) $\Delta R_{total} = -3/\sin E$ NONAME

(51) $\Delta \dot{R}_{total} = 3\cos E \dot{E} / \sin^2 E$ NONAME

If in equations (15) and (16) the integerals $\int_0^h N dh$ were deleted then equations (36), (41), (45), and (49) would be;

(36a) $\Delta R_T = -2/\sin E$

(41a) $\Delta R_I = -1.2498 / \sin E$

(45a) $\Delta \dot{R}_T = 2\dot{E} \cos E / \sin^2 E$

(49a) $\Delta \dot{R}_I = 1.2498\dot{E} \cos E / \sin^2 E$

and for the weather conditions and satellite height assumed there is little difference between the formulas for $E > 10^\circ$.

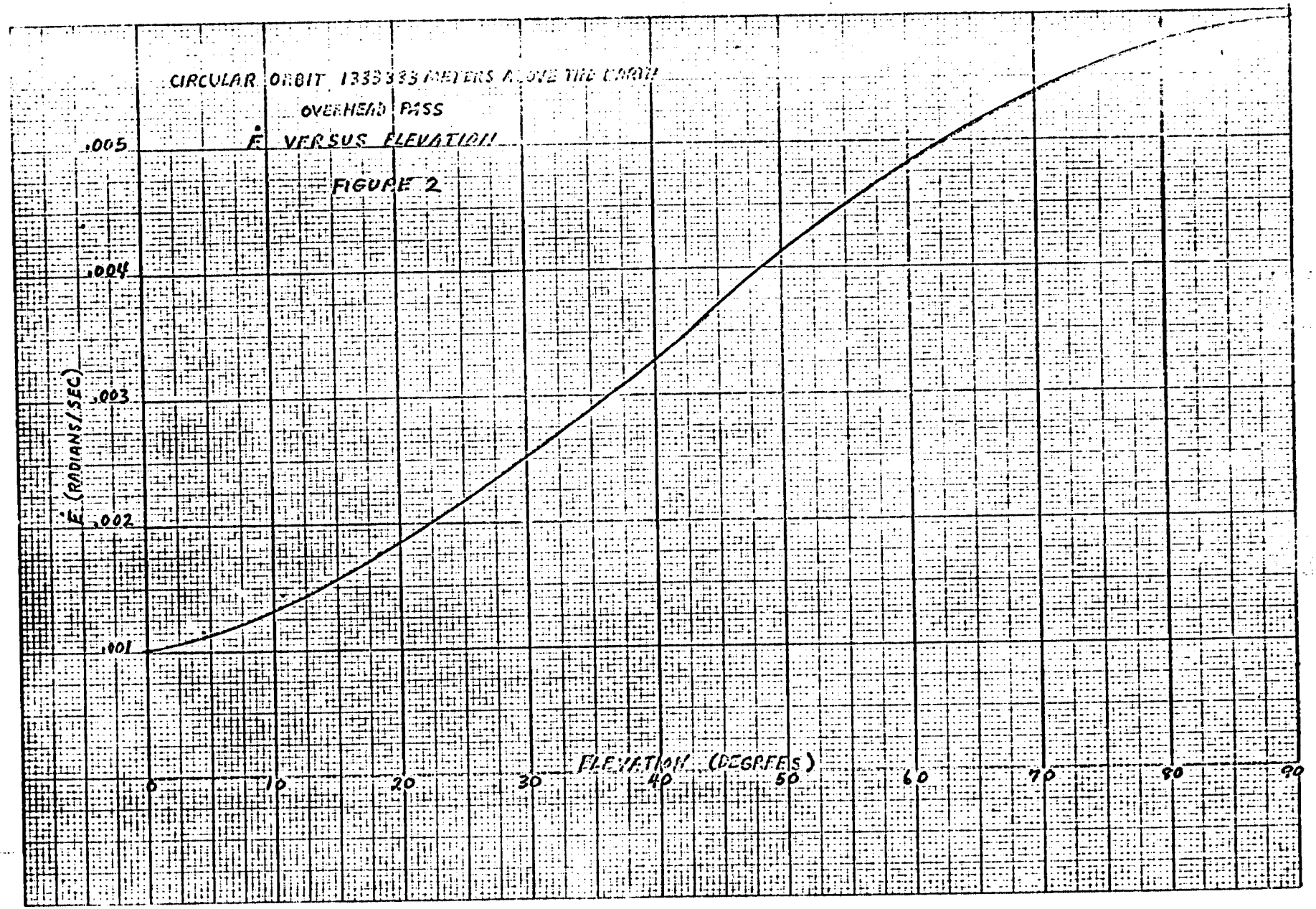

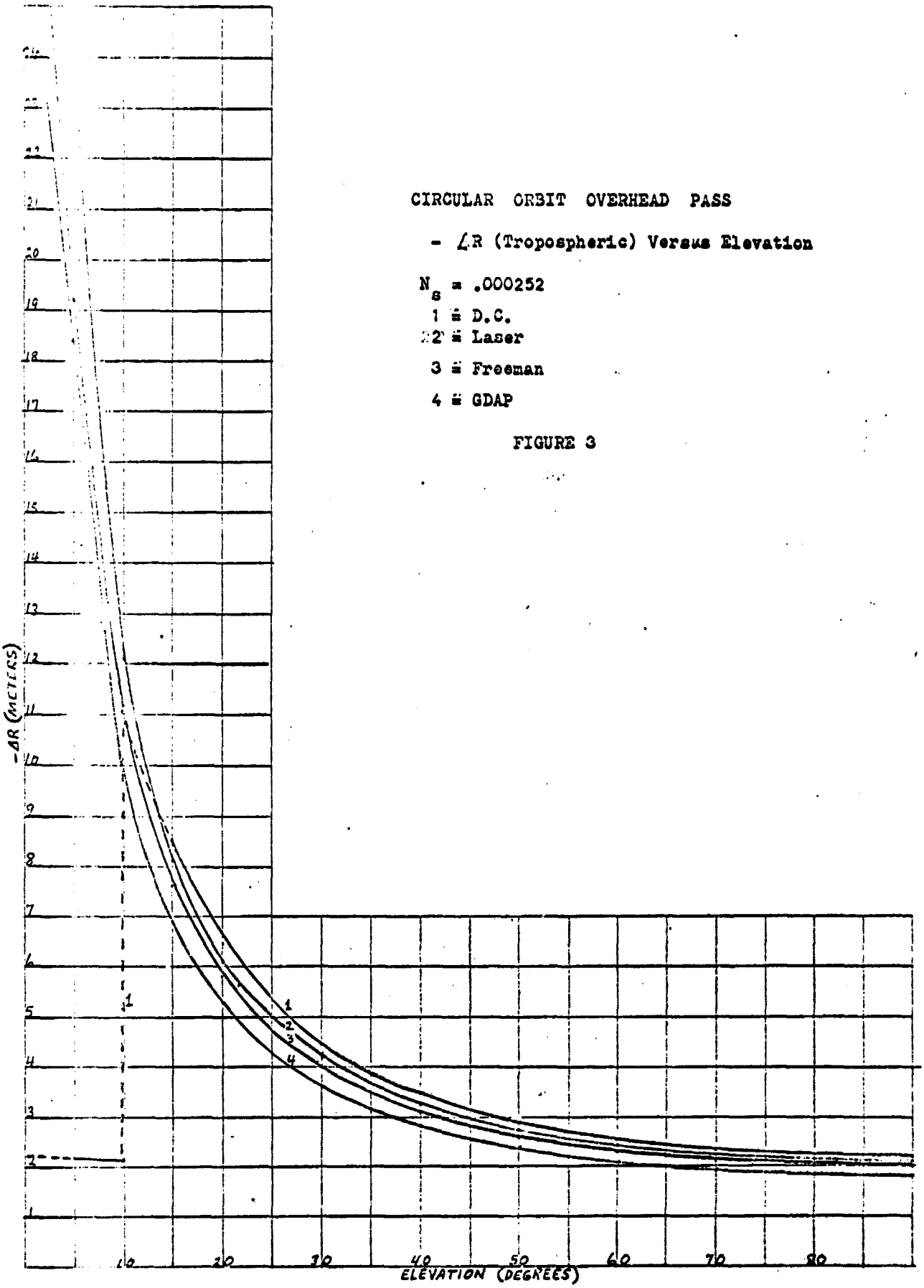

CIRCULAR ORBIT OVERHEAD PASS

- ΔR (Tropospheric) Versus Elevation

N_s = .000252

1 ≙ D.C.

2 ≙ Laser

3 ≙ Freeman

4 ≙ GDAP

FIGURE 3

CIRCULAR ORBIT OVERHEAD PASS

-ΔR (Ionosphere) Versus Elevation

N_1 = .000003941

h_1 = 400000 Meters

1 = D.C.

3 = Freeman

4 = GDAP

FIGURE 4

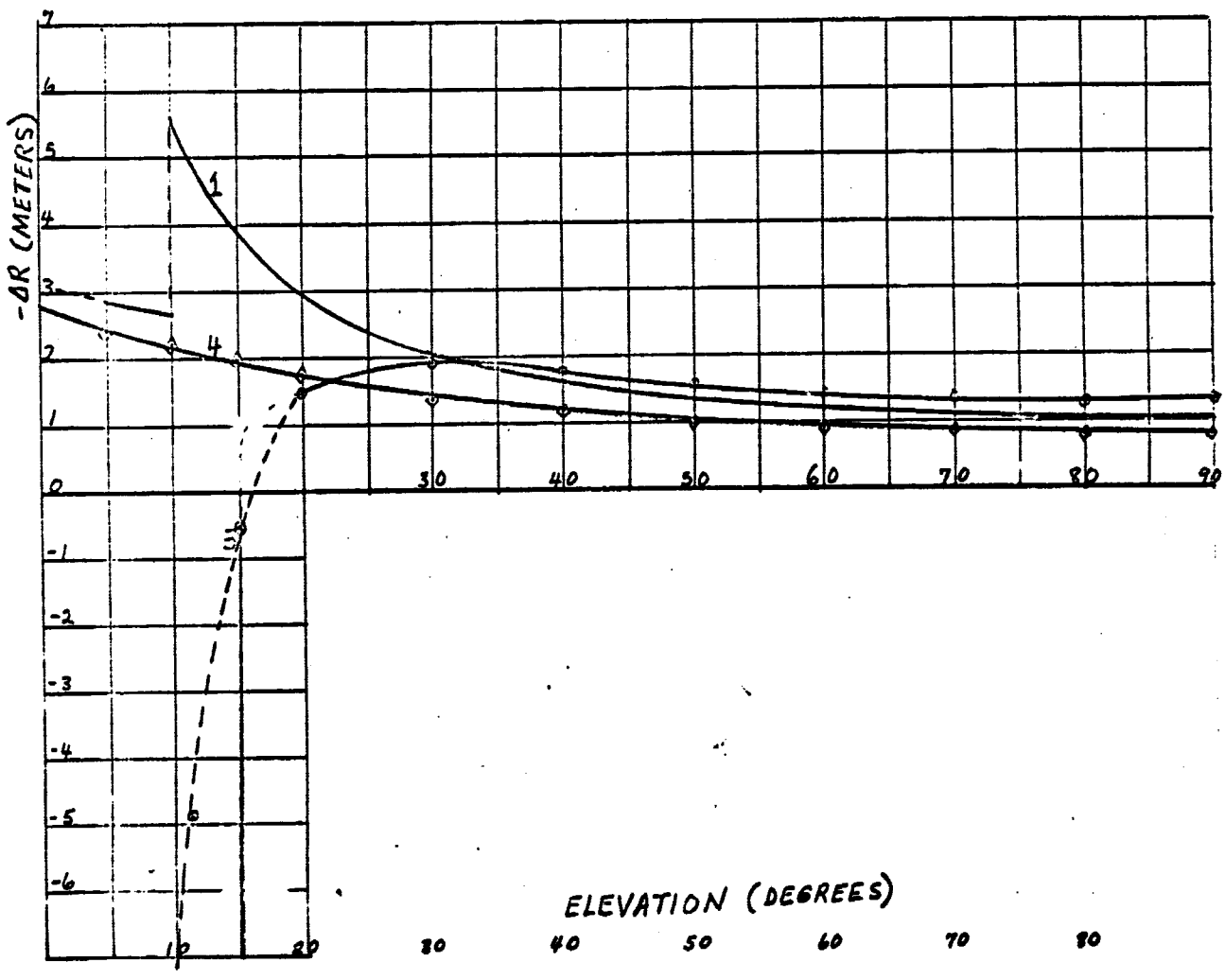

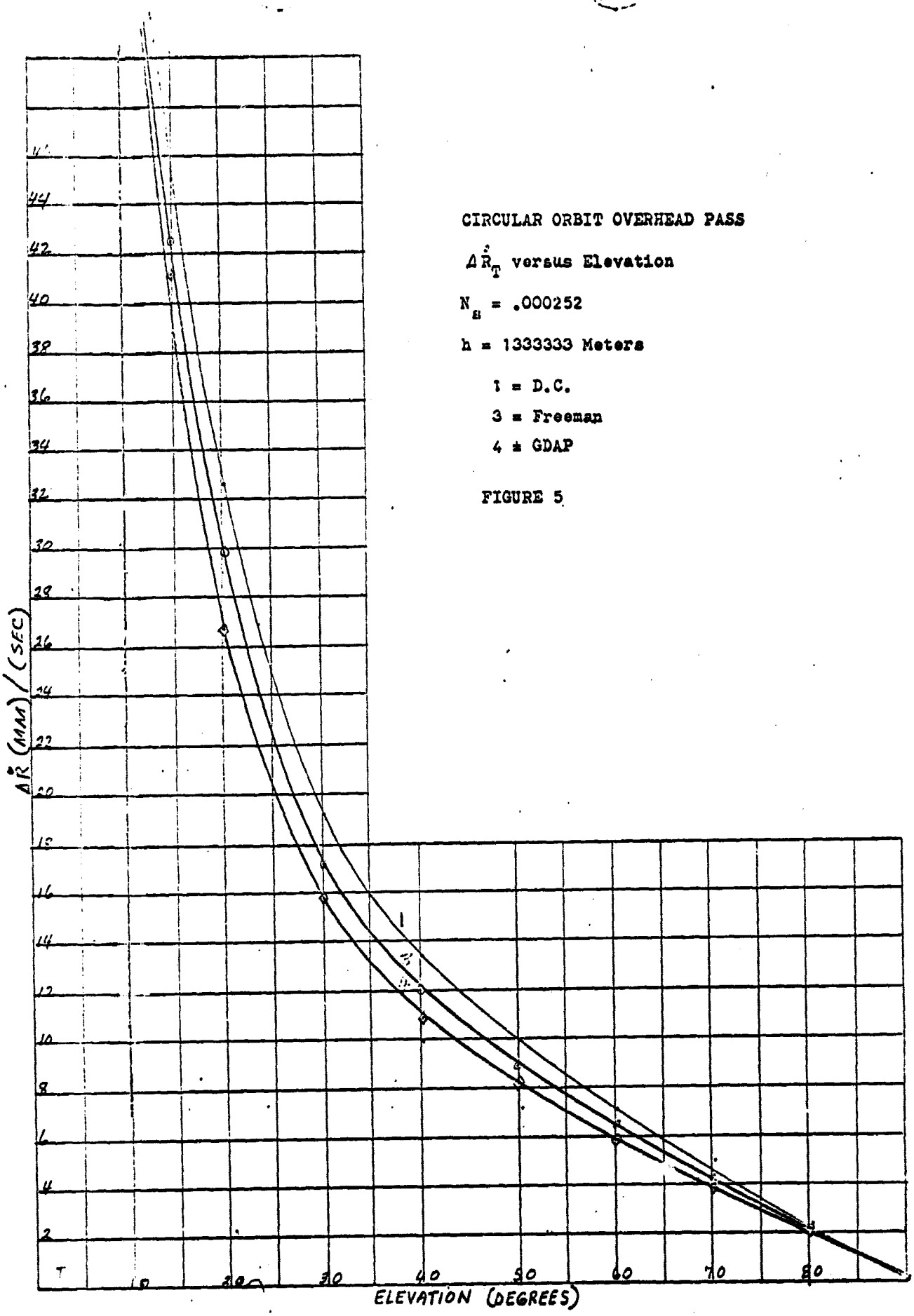

CIRCULAR ORBIT OVERHEAD PASS

$\Delta \dot{R}_T$ versus Elevation

N_s = .000252

h = 1333333 Meters

1 = D.C.

3 = Freeman

4 = GDAP

FIGURE 5

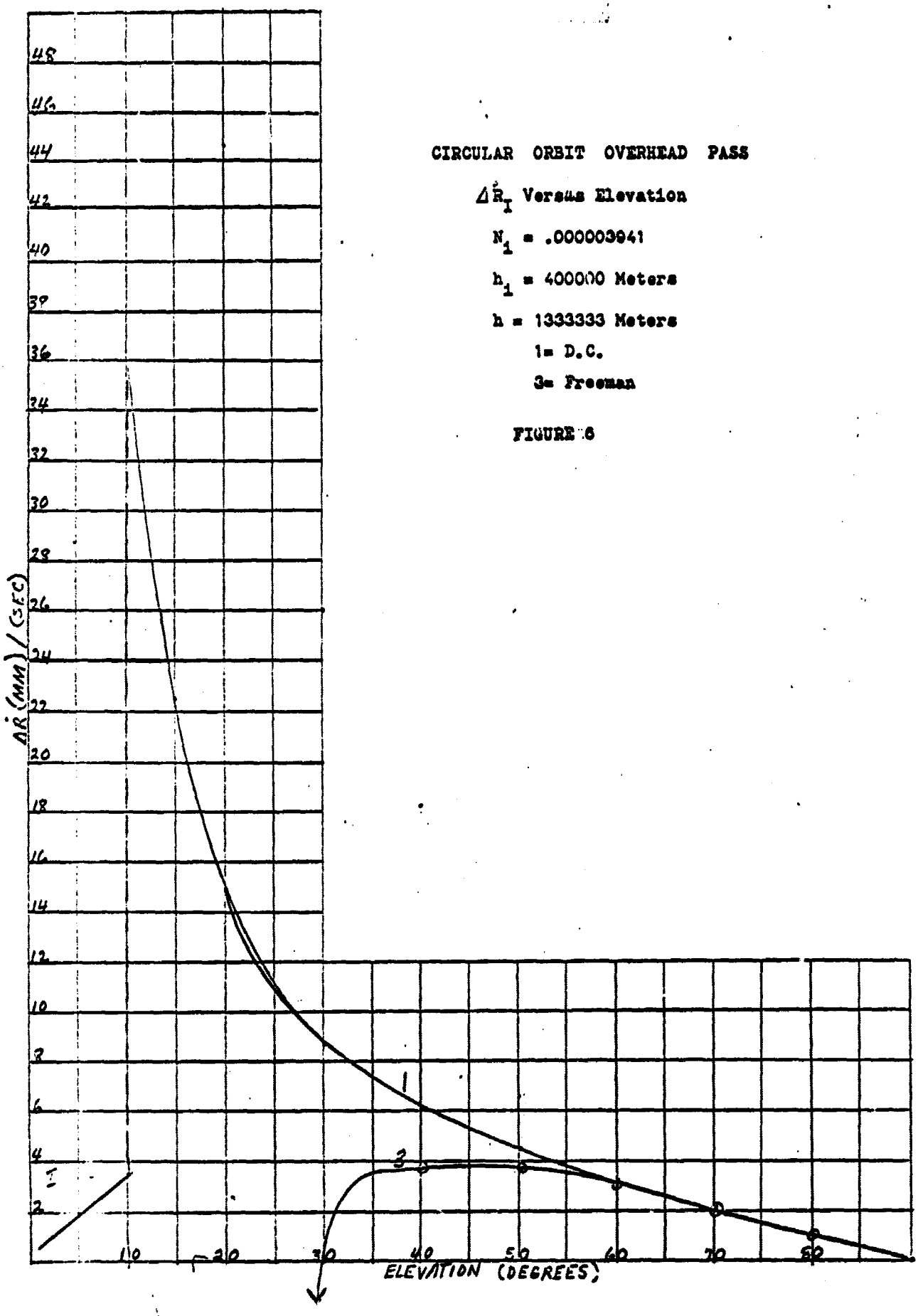

CIRCULAR ORBIT OVERHEAD PASS

$\Delta \dot{R}_I$ Versus Elevation

N_1 = .000003941

h_1 = 400000 Meters

h = 1333333 Meters

1= D.C.

3= Freeman

FIGURE 6

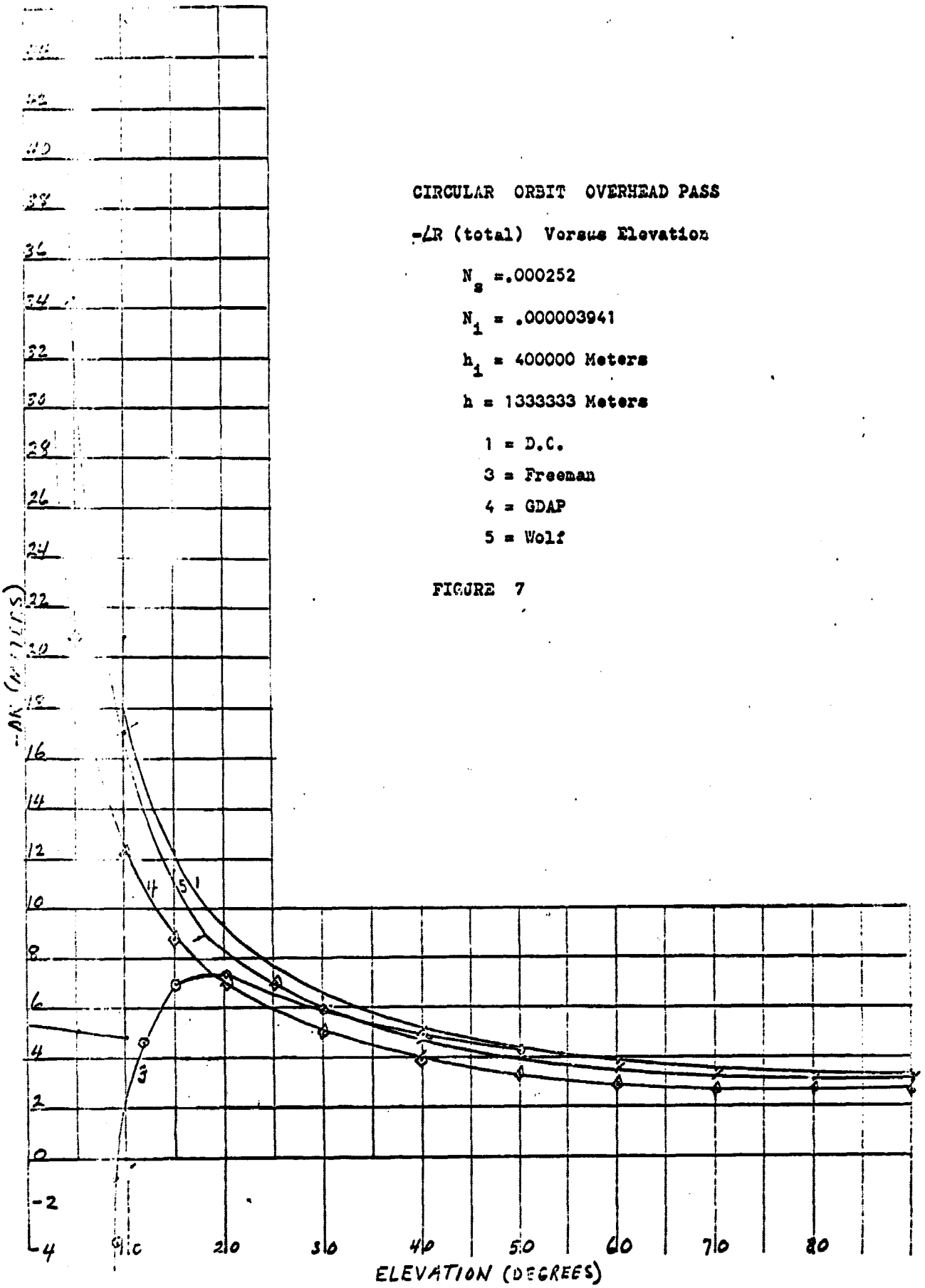

CIRCULAR ORBIT OVERHEAD PASS

$-\Delta R$ (total) Versus Elevation

N_s = .000252

N_i = .000003941

h_i = 400000 Meters

h = 1333333 Meters

1 = D.C.

3 = Freeman

4 = GDAP

5 = Wolf

FIGURE 7

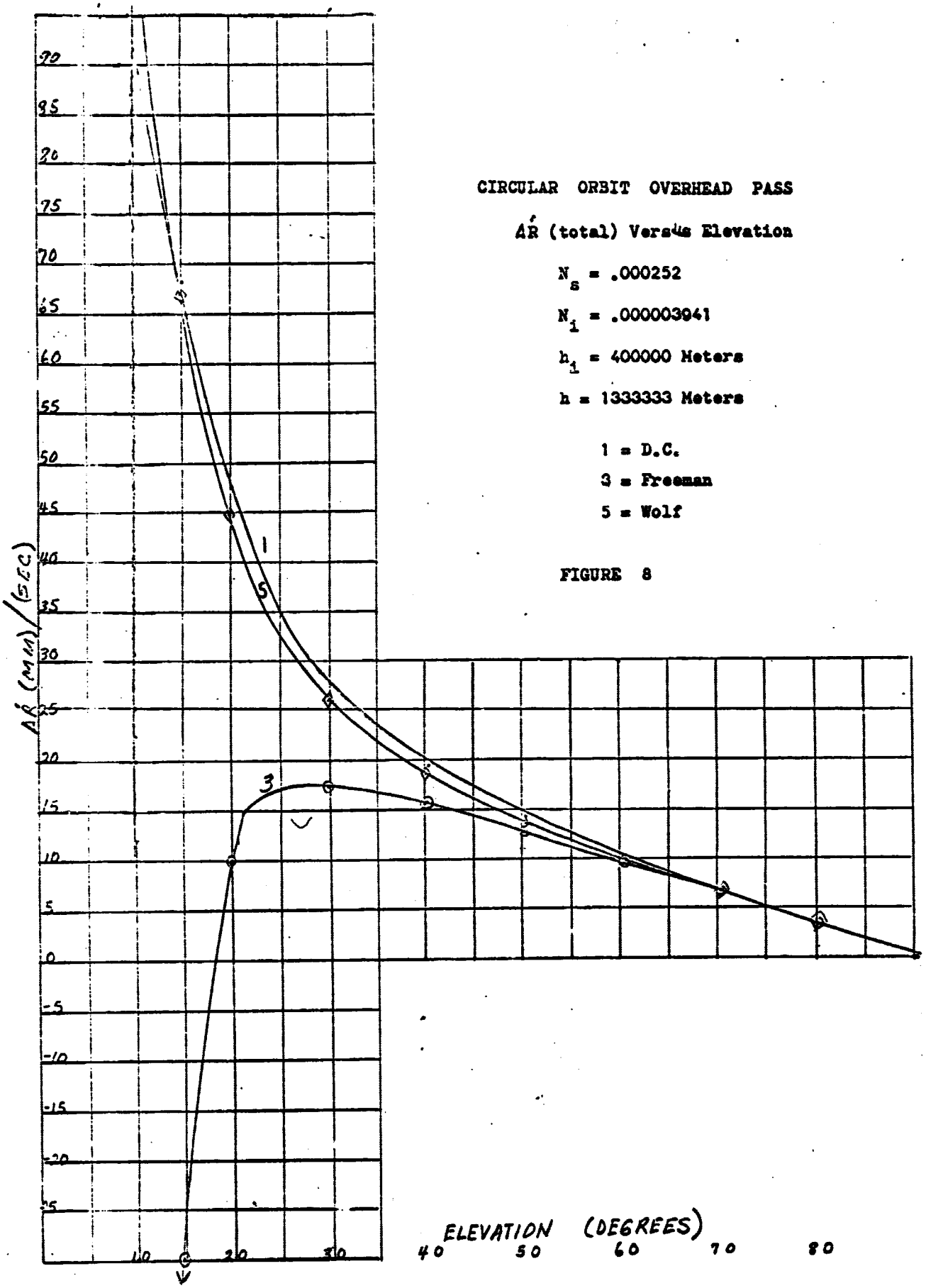

CIRCULAR ORBIT OVERHEAD PASS

$\dot{\Delta R}$ (total) Versus Elevation

N_s = .000252

N_i = .000003941

h_i = 400000 Meters

h = 1333333 Meters

1 = D.C.

3 = Freeman

5 = Wolf

FIGURE 8